



**Frequency Control for Microgrids  
using Enhanced  
STATCOM and Supercapacitor Energy  
Storage**

**Alex Taiwo Agbedahunsi, B.Eng.**

**Thesis submitted to the University of Nottingham for**

**the degree of Doctor of Philosophy**

**May, 2013**

# ABSTRACT

The face of electricity generation, transmission and distribution is changing due to economic, technology and environmental incentives. Recently, interactive and intelligent electricity grid structures which consist of interconnected small/medium sized generators, power electronic technologies and energy storage elements have been developed to address the major shortcomings of the traditional electricity grid structure. Microgrids are key elements of these emerging grid structures. Although microgrids are accepted as possible solutions to power quality and power stability issues in ac power systems, the uncertainty in the ability of microgrids to cope with severe fluctuating load and fault conditions is a major concern in the operation of these new grid structures. This project was aimed at improving frequency control within a microgrid. Four objectives were identified and addressed to meet this aim.

- I. A weak microgrid network using an emulated internal combustion engine generator and associated loads was modelled. The emulation of a diesel generating set was achieved with a vector controlled induction motor driving a synchronous generator. The diesel engine emulation was achieved by incorporating a single delay into the speed control loop of the vector controlled induction motor. The modelled microgrid network is a very useful tool for the development of novel control schemes for frequency control within a microgrid.
- II. Simulation studies were carried out to investigate how a weak power system can be strengthened through the use of enhanced STATCOM and Supercapacitor energy storage. This assisted in understanding the limitations and performances of the novel algorithms proposed for frequency control improvement.

## Abstract

- III. Novel open and closed loop control algorithms for frequency control within a microgrid were proposed. The advantage of the open loop control scheme is its simplicity but the functionality of the control action is limited with the knowledge of the diesel engine transfer function and load current being important requirements. A closed loop control scheme was employed to address the limitations of the open loop control scheme.
- IV. A laboratory prototype of the microgrid network was developed and used in validating the novel control schemes proposed.

The thesis describes the novel algorithms for frequency control using an intelligent STAtic COMpensator (STATCOM) and SuperCapacitor Energy Storage System (SCESS). The benefits and effectiveness of the proposed algorithms are given in the simulation and experimental results.

# Acknowledgement

I would like to express my deepest and sincere gratitude to my supervisor Prof Mark Sumner for his guidance, patience and invaluable support throughout the course of this research. I would also like to thank Dr Li Zhang and Prof Dave Thomas for sparing their time to act as my examiners.

Thanks to all the members of the PEMC group at the University of Nottingham for providing a pleasant environment to work in. Special thanks to Emmanuel Amankwah, Dr Alessandro Costabeber, Dr Alan Watson, Dr Ed Christopher, Anthony Aigbomian, Dr Saul Lopez, Dr Wesam Rohouma, Dr Ji Chao, Dr Milijana Odavic, Francis Effah, Oe Sung, Matt Copper, Mohammed Waseem and Paul Moss for their support, valuable discussions and technical assistance throughout the different stages of this research.

Special thanks to my family, My Sisters, Matilda, Anne and Flora, My Brothers, Adeolu and Adeniyi, My lovelies, Niall and Siobhan for a lifetime of support and encouragement. I would also like to specially thank Dr and Mrs Alaba Akande for taking me as one of theirs and giving me the opportunity to study in the U.K.

I owe the greatest debt of gratitude to my Parents Prof and Mrs Agbedahunsi for providing me with a loving, stable and stimulating upbringing and for supporting me in many ways throughout the course of my doctoral research programme. For this and countless reasons I will forever be grateful.

Finally, I want to thank the lord Jesus for giving me the ability to undertake and complete this work.

## List of Contents

### **Table of Contents**

ABSTRACT.....	i
Acknowledgement .....	iii
Chapter 1.....	1
Introduction .....	1
1.1 Traditional structure for distribution of electrical power .....	1
1.2 Distributed Generation .....	4
1.2.1 DG Plants .....	4
1.2.2 Impacts of DG.....	6
1.3 Project Objectives .....	10
1.4 Thesis Overview.....	11
Chapter 2.....	13
2.1 Introduction .....	13
2.2 Smart grid and Microgrid concept .....	14
2.3 Energy storage technologies.....	18
2.3.1 Flywheel energy storage .....	20
2.3.2 Superconducting magnetic energy storage .....	21
2.3.3 Pumped hydro energy storage.....	22
2.3.4 Compressed air energy storage .....	22
2.3.5 Fuel cells .....	23
2.3.6 Battery energy storage .....	24
2.3.7 Supercapacitor energy storage .....	25
2.4 The role of power electronics in emerging electricity grid structures	
	28

## List of Contents

2.5	Conclusion.....	34
Chapter 3.....		36
3.1	Introduction .....	36
3.2	Grid connected converters.....	37
3.2.1	Two –level three phase VSC.....	38
3.2.2	Control schemes for grid connected converters.....	40
3.2.3	Grid current control.....	44
3.3	STATCOM.....	46
3.3.1	Principle of operation.....	48
3.3.2	Control design.....	48
3.4	SuperCapacitor Energy Storage System .....	56
3.4.1	Operation.....	57
3.4.2	Control Strategies.....	60
3.5	STATCOM with SCESS.....	63
3.5.1	STATCOM only mode .....	65
3.5.2	STATCOM with SCESS boost mode .....	65
3.5.3	STATCOM with SCESS buck mode.....	65
3.6	Simulation Study.....	66
3.6.1	Simulation without the STATCOM.....	68
3.6.2	Simulation of the system with the STATCOM.....	70
3.6.3	Simulation of the system with the combined STATCOM and SCESS	72
3.7	Conclusion.....	76
Chapter 4.....		78
4.1	Diesel generating sets.....	78
4.2	Internal Combustion Engines .....	80

## List of Contents

4.3	Diesel engine model .....	81
4.4	Emulation of a diesel engine using a vector controlled induction motor	83
4.4.1	Vector control theory .....	83
4.4.2	Dynamic emulation of a diesel engine.....	85
4.4.3	Speed controller design.....	88
4.5	Analysis of instability and origin of frequency variation.....	91
4.6	Response of diesel generating sets to load transients.....	94
4.7	Weak grid model .....	99
4.7.1	Simplified grid model .....	100
4.8	Conclusion.....	107
Chapter 5	.....	110
5.1	Introduction .....	110
5.2	Quantification of the energy required for the frequency compensation	111
5.3	Open loop energy management scheme.....	119
5.4	Proposed closed loop energy management scheme .....	121
5.5	Simulation studies .....	126
5.5.1	Simulation without the proposed closed loop energy management scheme (load application) .....	129
5.5.2	Simulation with the proposed closed loop energy management scheme (load application).....	133
5.5.3	Simulation without the proposed closed loop energy management scheme (load removal) .....	139
5.5.4	Simulation with the proposed closed loop energy management scheme (load removal).....	143
5.6	Conclusion.....	148

## List of Contents

Chapter 6.....	149
6.1 Introduction .....	149
6.2 Experimental rig.....	150
6.2.1 Design considerations .....	153
6.2.2 STATCOM and SCESS.....	154
6.2.3 Emulated diesel generating set.....	155
6.2.4 Current mirror and Gate drive circuit .....	157
6.3 Control platform.....	160
6.4 Data acquisition.....	161
6.4.1 Voltage and Current measurements .....	163
6.4.2 Speed measurement .....	164
6.4.3 Data multiplexer.....	165
6.4.4 Trip Handling.....	167
6.5 Conclusion.....	168
Chapter 7.....	169
7.1 Introduction .....	169
7.2 Effects of active power load change on a microgrid network.....	171
7.3 Operation of STATCOM and SCESS.....	177
7.4 Frequency control improvement using the real power capability of STATCOM and SCESS .....	182
7.5 Conclusion.....	187
Chapter 8.....	188
8.1 Future work .....	191
8.2 Publications resulting from the project .....	192
Appendix A.....	193
A.1 Co-ordinates Transformation .....	193

## List of Contents

Appendix B .....	197
B.1 Power flow control .....	197
8.2.1 Power flow between converter and grid .....	200
Appendix C .....	204
C.1 Introduction .....	204
C.2 State equation for buck mode equation .....	205
C.3 State equation for boost mode equation .....	208
Appendix D .....	212
References .....	218

## List of Figures

### **List of Figures**

Figure 1-1: The traditional electricity grid structure.....	2
Figure 1-2: A power distribution network incorporating DG .....	8
Figure 2-1: Microgrid Structure [8, 32] .....	16
Figure 2-2: Positioning of energy storage options [51] .....	28
Figure 3-1: Two-level grid connected converter .....	39
Figure 3-2: Scalar control strategy.....	41
Figure 3-3: Vector control strategy .....	42
Figure 3-4: Power circuit diagram of a STATCOM .....	47
Figure 3-5: Control structure of a STATCOM in the rotating d-q reference frame .....	49
Figure 3-6: Closed loop block diagram for the current control .....	52
Figure 3-7: Equivalent circuit diagram of the STATCOM in the d-q reference frame .....	53
Figure 3-8: Closed loop block diagram for the voltage control.....	55
Figure 3-9: The power circuit diagram of the SCESS .....	57
Figure 3-10: SCESS buck mode circuit .....	58
Figure 3-11: SCESS boost mode circuit .....	59
Figure 3-12: Current mode control structure .....	60
Figure 3-13: Buck mode control block diagram .....	61
Figure 3-14: Boost mode control block diagram .....	62
Figure 3-15: The power circuit diagram of the STATCOM with SCESS.....	63
Figure 3-16: Control structure of STATCOM with SCESS .....	64
Figure 3-17: Power circuit diagram of the simulated system .....	66
Figure 3-18: PCC voltage, step load current, supply current, support current and DC-link voltage without STATCOM support.....	68
Figure 3-19: $ V_{pcc} $ of the system without STATCOM support.....	69
Figure 3-20: PCC voltage, step load current, supply current, support current and DC-link voltage with STATCOM support.....	70
Figure 3-21: $ V_{pcc} $ of the system with STATCOM support .....	71

## List of Figures

Figure 3-22: PCC voltage, step load current, supply current, support current and DC-link voltage with combined STATCOM and SCESS .....	72
Figure 3-23: $ V_{pcc} $ of the system with the combined STATCOM and SCESS .....	73
Figure 3-24: d and q components of the support currents (simulation of the system with STATCOM only).....	75
Figure 3-25: d and q components of the support currents (simulation of the system with combined STATCOM and SCESS) .....	75
Figure 4-1: Block diagram of a diesel generating set .....	79
Figure 4-2: A typical diesel engine speed loop.....	81
Figure 4-3: Definition of field oriented co-ordinates.....	84
Figure 4-4: Emulation of a diesel generating set .....	86
Figure 4-5: IM control architecture.....	86
Figure 4-6: IM speed control loop .....	88
Figure 4-7: Closed-loop Bode diagram for the speed control system .....	90
Figure 4-8: Closed -loop step response diagram.....	90
Figure 4-9: Diesel engine speed control loop .....	94
Figure 4-10: Response of generator to load application and removal .....	98
Figure 4-11: The power circuit diagram of the modelled grid.....	100
Figure 4-12: Generator, Load and STATCOM currents without real power support.....	103
Figure 4-13: Rotor speed response without real power support .....	104
Figure 4-14: Time diagram describing energy management scheme .....	105
Figure 4-15: Generator, Load and STATCOM currents with real power support.....	106
Figure 4-16: Rotor speed response with real power support .....	107
Figure 5-1: Time diagram describing the energy management scheme .....	112
Figure 5-2: Prime mover's speed control loop.....	114
Figure 5-3: Representation of the speed regulator and engine response .....	114
Figure 5-4: Single line diagram of a simplified microgrid set-up .....	118
Figure 5-5: Response of the prime mover to a large load step transient.....	119
Figure 5-6: Modified speed control loop .....	120

## List of Figures

Figure 5-7: closed loop algorithm control block diagram .....	122
Figure 5-8: Proposed closed loop control architecture .....	123
Figure 5-9: Flow chart describing the proposed closed loop algorithm .....	124
Figure 5-10: Time diagram depicting how minimum speed variation was achieved with the closed loop energy management scheme.....	125
Figure 5-11: Power circuit diagram of the simulated system .....	126
Figure 5-12: Load currents, generator currents and STATCOM+SCESS currents during simulation without the proposed closed loop algorithm.....	130
Figure 5-13: Voltage measured at the point of common coupling .....	130
Figure 5-14: Real power current demand (without the proposed closed loop algorithm).....	131
Figure 5-15: Engine torque output (without the proposed closed loop algorithm).....	131
Figure 5-16: Speed response of the prime mover to an active power load step demand during simulation without the proposed control algorithm.....	132
Figure 5-17: Electrical frequency response to an active power load step demand during simulation without the proposed control algorithm.....	132
Figure 5-18: Active load power step.....	134
Figure 5-19: Load currents, generator currents and STATCOM+SCESS currents during simulation with the proposed control algorithm.....	134
Figure 5-20: Phase voltage measured at the point of common coupling.....	135
Figure 5-21: Real power current demand (with the proposed closed loop algorithm).....	136
Figure 5-22: Engine torque output (with the proposed closed loop algorithm) .....	136
Figure 5-23: Speed response of the prime mover during the simulation with the proposed control algorithm .....	137
Figure 5-24: Electrical frequency response during the simulation with the proposed control algorithm .....	137
Figure 5-25: Zoomed response of the prime mover (without and with the proposed closed loop algorithm).....	138

## List of Figures

Figure 5-26: Zoomed electrical frequency response (without and with the proposed closed loop algorithm).....	138
Figure 5-27: Load currents, generator currents and STATCOM+SCESS currents during simulation without the proposed control algorithm.....	140
Figure 5-28: Real power current demand (without the proposed closed loop algorithm).....	141
Figure 5-29: Engine torque output (without the proposed closed loop algorithm).....	141
Figure 5-30: Speed response of the prime mover to an active power load step demand during simulation without the proposed control algorithm.....	142
Figure 5-31: Electrical frequency response to an active power load step demand during simulation without the proposed control algorithm.....	142
Figure 5-32: Load currents, generator currents and STATCOM+SCESS currents during simulation with the proposed control algorithm.....	144
Figure 5-33: Real power current demand (with the proposed closed loop algorithm).....	145
Figure 5-34: Engine torque output (with the proposed closed loop algorithm).....	146
Figure 5-35: Speed response of the prime mover during the simulation with the proposed control algorithm.....	146
Figure 5-36: Electrical frequency response during the simulation with the proposed control algorithm.....	147
Figure 6-1: Overall layout of the experimental rig.....	151
Figure 6-2: Control architecture of the emulated diesel generating set.....	156
Figure 6-3: Current mirror circuit.....	158
Figure 6-4: Gate drive circuit.....	159
Figure 6-5: Functional block diagram of the data acquisition and pulse generation process.....	161
Figure 6-6: Voltage measurement circuit.....	163
Figure 6-7: current measurement circuit.....	164
Figure 6-8: Input circuitry of the incremental encoder interface.....	165
Figure 6-9: Data multiplexer circuit.....	166

## List of Figures

Figure 7-1: Single line diagram of the experimental rig.....	170
Figure 7-2: Response of the speed controller to a step change of 100 RPM.	171
Figure 7-3: Torque reference during speed step change .....	172
Figure 7-4: Generator 3-phase voltages whilst prime mover is rotating at 1500RPM .....	172
Figure 7-5: Current flowing across light load.....	173
Figure 7-6: Main load currents during active power load change .....	174
Figure 7-7: Generator currents during active power load change.....	174
Figure 7-8: Mechanical speed response during active power load step.....	175
Figure 7-9: Electrical frequency response during active power load step .....	175
Figure 7-10: Torque response during active power load step.....	176
Figure 7-11: Response of the d-axis current controller to a step change of 6A .....	177
Figure 7-12: $V_{pcc}$ , $V_{dc-link}$ and STATCOM support currents of the system when the STATCOM was energized.....	178
Figure 7-13: Phase “A” voltage and current when combined STATCOM and SCESS inject reactive power .....	179
Figure 7-14: Data Captured for STATCOM operating at 110Vrms, 400VDCLink with an $I_q$ demand of 6A (x-axis 10ms/div) .....	179
Figure 7-15: $V_{pcc}$ , $V_{dc-link}$ and STATCOM support currents of the system during real power injection from STATCOM and SCESS to the ac grid.....	180
Figure 7-16: Phase “A” voltage and current when combined STATCOM and SCESS inject real power .....	181
Figure 7-17: Data captured for STATCOM and SCESS operating at 110Vrms, 400VDCLink, 140Vsc and $I_d$ demand of 6A (x-axis 10ms/div) .....	181
Figure 7-18: STATCOM D-axis current reference generated by the transient management controller during active power load step .....	183
Figure 7-19: Three phase real power current injected by the combined STATCOM and SCESS during the active power load step.....	184
Figure 7-20: Mechanical speed response in RPM during active power load step with STATCOM -SCESS support.....	184
Figure 7-21: $V_{pcc}$ , $V_{dc-link}$ measured during the active power load step .....	185

## List of Figures

Figure 7-22: Comparison of the mechanical response of the prime mover with and without the closed loop energy management scheme. ....	186
Figure 7-23: Comparison of the electrical frequency with and without the closed loop energy management scheme. ....	186
Figure A-1: Definition of rotating reference frame .....	195
Figure B-1: Equivalent single phase power flow diagram.....	198
Figure B-2: Equivalent single phase circuit depicting power exchange between the grid and the converter .....	200
Figure B-3: The possible flow of power between the grid and the converter	202
Figure C-1: The power circuit diagram of the SCESS .....	205
Figure C-2: SCESS buck mode circuit .....	205
Figure C-3: Inductor current waveform during one sampling period.....	206
Figure C-4: Buck mode control block diagram .....	207
Figure C-5: SCESS boost mode circuit .....	209
Figure C-6: Boost mode control block diagram .....	209
Figure D-1: Overall experimental rig structure .....	214
Figure D-2: Induction motor coupled to Synchronous generator .....	215
Figure D-3: Eurotherm 620 series drive used for the vector control operation of the induction motor.....	215
Figure D-4: DC/AC Inverter.....	216
Figure D-5: DC/DC converter used as an interface between the DC-link and the Supercapacitor modules .....	216
Figure D-6: Ten series connected Supercapacitor modules rated at 9.5 F, 20V .....	217
Figure D-7: Load Banks.....	217

List of Tables

**List of Tables**

Table 2-1: Comparison of various energy storage devices [36] .....	27
Table 3-1: Simulation parameters .....	67
Table 4-1: Magnetic MA 133 KF1 plate data.....	87
Table 4-2: Speed loop system parameters. ....	89
Table 5-1: Simulation parameters .....	128
Table 6-1: Experimental rig parameters .....	153

# Chapter 1

## Traditional Electricity Grid Structures

---

### Introduction

#### 1.1 Traditional structure for distribution of electrical power

The present day electricity transmission and distribution structure is a product of rapid urbanization and infrastructure developments in various parts of the world over the past 130 years. Since its inception, the power industry has operated with clear demarcations between its generation, transmission and distribution subsystems [1].

## Chapter 1: Traditional Electricity Grid Structures

Figure 1-1 shows the traditional structure which is a hierarchical system in which power plants at the top of the chain ensure power is delivered to the customers' loads at the bottom of the chain.

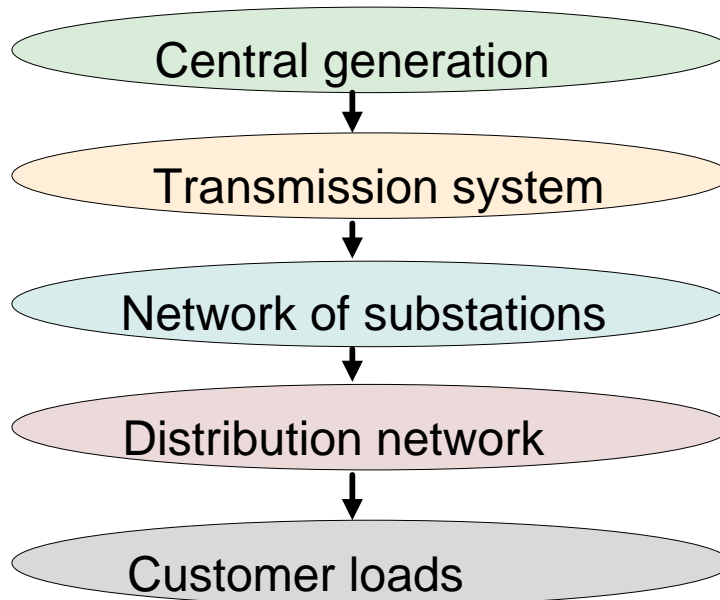


Figure 1-1: The traditional electricity grid structure

Today's electrical power generation plants convert about 35% of fuel energy to electricity [1, 2]. The other 65% is dissipated as heat without recovery. Approximately 20% of the generation capacity exists to meet peak demand which lasts for 5% of the time [2].

Hydro, thermal and nuclear power generation are the three major types of power plants currently being used. The friendly environmental impact of hydro power plants makes them a preferred generation technology. However, they cause significant environmental and societal disturbance during construction. Most fossil fuel supplies are located in limited areas on the earth. The extraction and transportation of fossil fuels to other areas is costly. The depletion of fossil fuel stocks threatens the security and sustainability of future electric energy. Fossil fuel thermal plants bring operating pollution problems that are difficult to ignore. Nuclear power plants with existing technology are soon to be retired and they are not being replaced at a significant rate [3]. The

## Chapter 1: Traditional Electricity Grid Structures

construction of hydro, thermal and nuclear power plants are time consuming and very expensive. In today's competitive energy market, only a few corporations are capable of spending such amounts of money with a pay-back period measured in decades.

Environmental concerns mandate that thermal and nuclear power plants must be located far away from cities. This requires the construction of large complex and expensive power transmission lines that cause ecological and environmental problems.

The Kyoto protocol is an international agreement negotiated in December 1997. The objective of the Kyoto protocol is the "stabilization of greenhouse gas (CO<sub>2</sub>, NO<sub>x</sub>, SO<sub>x</sub> etc.) in the atmosphere at a level that would prevent dangerous anthropogenic interference with the climate system" [4]. The United Kingdom is a signatory to the Kyoto protocol. The energy policy of the United Kingdom fully endorses the reduction of carbon dioxide emissions. To achieve this, the government has set a target that 20% of the generated electrical energy will be produced from renewable energy sources by 2020 [5]. In the United Kingdom, the 2008 climate change act requires an 80% in reduction of emissions by 2050 compared with 1990 levels [6].

The current trends in electricity generation show that most of the United Kingdom's electricity was generated by gas (39%), coal (33%) and nuclear (20%) [7]. Thirty large power plants meet the majority of electrical demand which is approximately 40GW at a typical point in time and 60GW at peak periods.

The face of electricity generation, transmission and distribution is changing due to economic, technology and environmental incentives [2, 8]. The rapid growth in electrical energy demand puts the transmission system under greater stress every year resulting in the system operation closer to its limits. The basic solution to this problem is to construct more transmission lines which is very difficult especially with this increasingly rapid growth in consumer demands. The other alternative is to use the existing systems in a more

## Chapter 1: Traditional Electricity Grid Structures

effective way. These difficulties necessitate the re-thinking or even re-designing of the traditional electricity structure.

Centralized power plants are giving way to smaller Distributed Generation (DG). These emerging technologies have lower emissions and the potential to negate the cost advantage of the expansion of centralized power plants.

### **1.2 Distributed Generation**

Distributed Generation (DG) in distribution systems reduces the physical and electrical distance between generation and loads. The proximity of sources to loads contributes to enhancement of the voltage profile, reduction of distribution and transmission bottlenecks, lower losses and cancellation of investments in new transmission and large scale generation systems [2, 9]. Any electric power production technology that is integrated within the distribution network can be classified as DG. DG units can either be grid connected or independent of the grid. DG has the capability of interacting with the power system and becoming an “active” distribution network.

#### **1.2.1 DG Plants**

There are several types of DG plants connected to distribution networks. DG technologies can be categorized into renewable and non-renewable technologies.

##### **1.2.1.1 Renewable Energy Plants**

Wind, solar, geothermal and ocean technologies are all forms of renewable energy DG plants. The location of these plants is determined by the placement of primary renewable energy sources. The output of wind power plants is proportional to the wind speed which varies from one location to another. Hence wind turbines must be located in areas where wind resource is

## Chapter 1: Traditional Electricity Grid Structures

available. The location of wind power plants is usually away from residential areas which can make it difficult to connect to the distribution network and sometimes these results in considerable amount of investment.

Renewable energy sources are inexhaustible, non-polluting, diverse in resources and available almost everywhere. The construction of renewable DG units is fast and cheap in comparison to central power plants and this choice limits the greenhouse gas (GHG) emissions. However, the intermittent nature of renewable energy source results in a reduction of reliability and stability of the distribution system.

### **1.2.1.2 Non Renewable Energy Plants**

Internal combustion engines, combined cycle engines, combustion turbines, micro turbines and fuel cells are all non-renewable forms of DG production technologies. At present, the predominant DG technology is internal combustion engines driving standard electric generators. Majority of those units were installed to serve as back- up generators for sensitive loads (such as hospitals airports and hotels) for which long duration energy supply failures would be catastrophic [3].

Energy production increase can be achieved by using back up internal combustion engine generator but such utilization of engine generators creates location specific environmental issues as well as potential utility interconnection issues. Transient events such as faults in a distribution network or overloading conditions may cause a variation of the generator shaft speed and consequently the system frequency. The lower capital cost and availability of diesel makes internal combustion engine driven generators the most economical and most commonly installed DG facilities today.

## **1.2.2 Impacts of DG**

The restructuring of the traditional electricity structure has induced a significant penetration of DG technologies into the power distribution system. The introduction of DG can impact on flow of power and voltage conditions. These impacts can either be positive or negative. The positive impacts are generally called “system support benefits” and they include improvement of system reliability, minimizing the network power losses and deferral of transmission and distribution upgrades [10]. Nevertheless there are also some negative impacts caused by the installation of DG. The technical impacts of DG on a power distribution network will be described briefly.

### **1.2.2.1 Network fault level change**

The deployment of DG in a distribution network will change the characteristics of the distribution network, turning it into an active network like the transmission network which reverses the flow of power and injects extra current to a fault [11, 12].

All forms of DG impart some increase to fault level. This is because almost all DG employ rotating machines as the generator. Both induction and synchronous generators can contribute additional current that increases the fault level of distribution systems. Fault level change may hinder the development of DG due to the impact it has on the protection system. There is a potential for the rise in the protection cost if all the related protection equipment has to be updated to match the fault level. Fault level contribution can be limited by inserting an appropriate impedance, reactor or transformer between the DG and the network. However this results in increased losses and voltage change [13].

### **1.2.2.2 Network voltage change**

The responsibility of every distribution utility is to supply its customer at a voltage within specified limits. The voltage profiles used differ from country to country but the principle of operation of radial feeder remains the same [13].

Distribution networks are traditionally arranged in the form of a radial system. Voltage regulation practice is based on radial power flow. The flow of power from the generator to the load is unidirectional. Voltage drop across the impedance along the radial line can cause poor voltage profiles especially at the most remote bus. Voltage variation across a radial network can be minimized by installing a DG directly into the network. However the installation of DG will cause bidirectional power flow along the radial line which can result in the variation of the network voltage levels and complications for protection systems [10, 14].

The incompatibility of DG with the radial power flow based voltage regulations used in most distribution networks can cause a variation in the network voltage. To determine if the installation of a DG in a distribution network will cause a significant impact on the voltage variation, the size and location of the DG and the impedance characteristic of the DG must be properly considered[10].

### **1.2.2.3 Power Quality**

DG can either decrease or increase the quality of power distributed. The transients caused by DG and the nature of DG if it relies on renewable energy sources may cause power quality problems. DG may cause noticeable voltage flicker. The current transients caused by DG during connection and disconnection from the network may lead to a high magnitude transient

## Chapter 1: Traditional Electricity Grid Structures

voltage in the network [3, 10, 13, 15]. Voltage flicker can be reduced by placing constraints on when and how often DG operators may start and change the output of DG systems.

The majority of the DG technologies use some form of power electronic device in the distribution network interface. The type and severity of harmonics introduced by these power electronic devices will depend on the power converter technology and interconnection configuration. Most of the new inverter designs are based on IGBTs that use pulse width modulation to generate the injected sine wave. These newer inverters are capable of generating a very clean output. Coordinated voltage control can be used to improve power quality.

### 1.2.2.4 System stability

The consideration for system stability tends not to be of great significance if the objective of the DG is solely to generate power from new renewable energy sources. However if the DG is installed for the provision of power system support, the security of the DG is very important for the stability of the system[13].

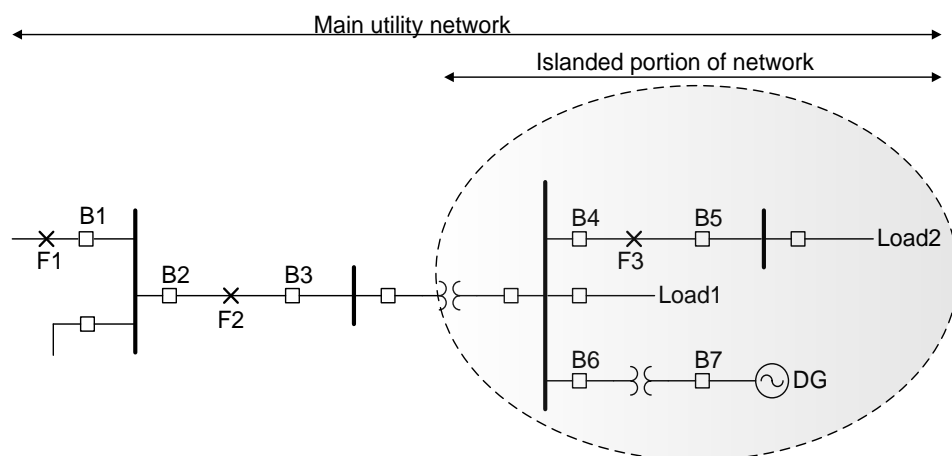


Figure 1-2: A power distribution network incorporating DG

## Chapter 1: Traditional Electricity Grid Structures

Figure 1-2 shows a power utility system that incorporates DG into the network. The impact of network faults at various sections of the utility will be considered.

If a network fault occurs at F1 which is not related to the DG, Circuit breaker B1 will separate the faulted section from the system. This event may cause a variation of the voltage magnitude which results in the nuisance tripping of the protection system of the DG[13].

If a network fault occurs at F2, the faulted section will be separated and cleared by B2 and/or B3. If the output of the DG is able to match the real and reactive power demand of the loads (load 1 and load2) precisely then the distribution network load operation is not interrupted. The operation of the DG in this situation, where there is no voltage or frequency reference is called “ISLANDING” or loss of main mode [13, 16-18]. It is not desirable for a DG to island under present regulations with any part of the utility because this can lead to safety and power quality problems that will affect the network and the load [10, 13, 17, 19]. The re-connection of B2 and B3 after fault clearance without synchronisation can result in severe failure. Although under current legislations “ISLANDING” is not allowed, the continuous penetration of DG in power distribution systems will result in a situation where “ISLANDING” becomes an inevitable situation. Therefore, the technical and regulatory challenges for protection of DG need to be met to cover this eventuality.

Voltage and frequency relays are used as a means of anti-islanding protection. At the beginning of islanding the frequency will change as the loads are transferred to the DG; the imbalance in power between the load and the supply can cause a sudden change of frequency [20]. A special protection relay called “rate of change of frequency” (ROCOF) relay is used to monitor the change of frequency and prevent the DG from operating in an island mode [20-22].

## Chapter 1: Traditional Electricity Grid Structures

Load transient events can lead to the unnecessary tripping of the relay due to the sensitivity of the ROCOF relay. For example a temporary fault at F3 will result in loss of B4 and B5. The reconnection of B4 and B5 while load2 is still demanding full power will cause a short term transient mismatch of power within the network. This results in a reduction in the system frequency as the generator slows down (changing kinetic energy to electrical energy to meet the new load requirements). The change of system frequency may be detected by the ROCOF relay protection, causing a nuisance tripping of B7. This unnecessary tripping reduces the security and stability of the system.

### **1.3 Project Objectives**

The uncertainty in the ability of power distribution systems which incorporate distributed generation to cope with fault conditions is a major concern in the operation of ac power systems. It is a common occurrence for these types of systems to trip due to load changes rather than real fault conditions.

Power electronic converters using fast switching semiconductors and high speed real time controllers are capable of implementing integrated, advanced and complex algorithms making them a good choice for deployment in power distribution systems [23]. The penetration of power electronic converters in power distribution systems has made it possible to expand their use to enable greater stability both under severe fluctuating loads and under fault conditions. Their applications include interfacing of renewable energy sources, interfacing of energy storage devices and provision of power quality improvement e.g. STATic COMPensators (STATCOM).

The aim of this thesis is to investigate the use of a STATCOM device with incorporated energy storage technology to see if significant improvement to power system stability can be achieved. In [24, 25] a solution to enhance the performance of a STATCOM by adding Supercapacitor energy storage to the dc-link of the STATCOM was proposed. The proposed STATCOM with Supercapacitor energy storage system (SCESS) offered a superior ability to

## Chapter 1: Traditional Electricity Grid Structures

compensate for both real and reactive power that can be useful for the short period stressed conditions in an ac power system.

A theoretical exploration of the operation of a weak grid is presented. A novel control method for power matching under severe fluctuating loads is proposed. Simulation work is carried out to demonstrate the frequency improvement capability of the STATCOM plus SCESS within a specific system scenario to support the proposed idea. Finally, experimental test results are presented to validate the proposed control method.

The main objectives of this project can be summarised as below;

- I. To model a weak microgrid network using an emulated internal combustion engine generator.
- II. To investigate how a weak power system can be strengthened through the use of enhanced STATCOM and Supercapacitor energy storage.
- III. To develop novel control algorithms for frequency control improvement in a weak power system.
- IV. To demonstrate the benefits of the enhanced STATCOM plus SCESS in providing frequency control improvement in weak power systems.

### **1.4 Thesis Overview**

Chapter 2 examines the existing literature for microgrid configuration including the control and regulations within this reduced scale power system. The smart grid concept is described briefly. A brief review of the energy storage system technology is presented. An overview of the role of power electronic technologies in transmission and distribution systems is then given.

Chapter 3 reviews the details of the conventional STATCOM including its operation and design. The vector control strategy for the STATCOM is presented. The Supercapacitor energy storage system and its control techniques are described briefly. Finally a simulation study to demonstrate the

## Chapter 1: Traditional Electricity Grid Structures

real and reactive power compensation capabilities of the STATCOM plus SCESS is presented.

Chapter 4 presents the modelling of a weak microgrid. An internal combustion engine driven generator is introduced. The simplified diesel engine model is clearly described. The emulation of a diesel generating set using a vector controlled induction motor is presented. Analysis of instability within a microgrid and origin of frequency variation during load power transients is discussed with mathematical support. Finally optimum response of a diesel generating set to large load transients is presented with an introduction of novel control schemes for energy management.

Chapter 5 describes the novel control methods for frequency control within a microgrid. The open and closed loop control schemes are explained in detail. Simulation studies demonstrating the frequency control improvement capability of the STATCOM plus SCESS using the proposed schemes are explained.

Chapter 6 describes the experimental setup and associated control platform. Details of the experimental rig are described section by section. Practical circuit diagrams are explained fully.

Chapter 7 presents the experimental results obtained during the experimental validation of the proposed control schemes. The usefulness of the schemes in terms of frequency control improvement within a microgrid is verified.

Chapter 8 summarizes the conclusion for the whole project and recommendations for future work.

# Chapter 2

## Emerging Electricity Grid Structures

---

### 2.1 Introduction

Existing/traditional grid structures were established to support generation using large centralised power plants with energy delivery provided by a network of transmission and distribution lines. Existing grid structures have reached an age where they need to be replaced. A viable option is the creation of a more efficient and flexible grid structure that incorporates low level of carbon footprints and increase the role of electricity in the energy market[26].

In this chapter, emerging/next generation electricity grid structures are described in detail. The general structure of their key elements such as smart grids and microgrids are introduced. An overview of the various energy

storage technologies is presented. Finally, the role of power electronics in emerging electricity grid structures is discussed in detail.

## **2.2 Smart grid and Microgrid concept**

Deregulation and competitive electricity markets for electricity structure have changed the organizational structures of the electricity supply industry as well as the operation of electric power systems. Emerging electricity grid structures known as the smart/intelligent grids are expected to address the major shortcomings of the existing /traditional grid structure [27, 28].

Given the fact that the roots of power system issues are typically found in the electrical distribution system, it is imperative to start the overhaul of the existing grid from the bottom of the existing grid chain i.e. the distribution subsystem. However, one may argue that given the size and value of the existing grid assets, the emergence of the smart grid concept will more likely follow an evolutionary process rather than a drastic overhaul. The smart grid will therefore materialize through strategic implants of distributed control and monitoring systems[1].These smart grid implants will facilitate distributed generation and cogeneration of energy. They will also provide for the integration of alternative sources of energy and management of carbon footprints.

In view of the aforementioned, the smart grid paradigm provides a general platform to describe the collection of all technologies, concepts, topologies and approaches that allow the hierarchies of the traditional electricity grid structure (generation , transmission and distribution) to be replaced with an end-to-end intelligent and fully integrated environment[1]. Smart grid is characterized by a two-way flow of electricity and information to create an automated and widely distributed energy delivery network that enables integration, effective cooperation and information interchange among the many interconnected elements of the electric power grid [29, 30].

## Chapter 2: Emerging Electricity Grid structures

Emerging electricity grid structures will require the transformation of the traditional/existing electricity transmission and distribution grid into an interactive and unified power supply network. The transformation of the existing structure arose as the production, brokerage and sale of electricity became competitive functions within a unified electricity market [31]. Distributed generation (DG) plays a key role in the emerging electricity grid structure. As the demand for more and better quality electric power increases, DG can provide alternatives for reliable and cost effective premium power for homes and businesses.

The greatest potential power for DG is displacing power supplied through centralized power generation. On-site power generation minimises the transmission and distribution losses as well as transmission and distribution cost, a significant part of the total electricity cost. The application of individual distributed generators can cause as many problems as it may solve. To realize the potential of distributed generation, a system approach which views generation and associated loads as a subsystem or microgrid has to be taken [2, 8, 32].

The microgrid concept assumes a cluster of loads and microsources operating as a single controllable system that provides power to its local area [8, 32]. Microgrids offer solutions to implementing distributed energy resources such as diesel generators, wind turbines, photovoltaic cells etc. at or near the point of load. This decreases the stress on the electrical transmission system and offers a significant increase in power system reliability as power can be generated locally. From a grid perspective, the microgrid concept is attractive because it recognizes the reality that the traditional grid structure is old and has to change[8]. Microgrids may or may not be connected to the main distribution grid that is maintained and operated by the distribution network operators (DNO) [33].Microgrids can also provide premium power through the ability to smoothly move from dispatched power mode while connected to the main utility grid to load tracking while in island mode [32]. The microgrid concept is made possible by the recent advances in reliable small scale

## Chapter 2: Emerging Electricity Grid structures

generators, power electronics and digital controllers. The majority of the present day microsources are power electronics based. As a result, they can provide the required flexibility to ensure controlled operation as a single system.

A basic microgrid architecture is shown in Figure 2-1[8, 32]. The electrical system is assumed to be radial with three feeders-A, B and C and a collection of loads.

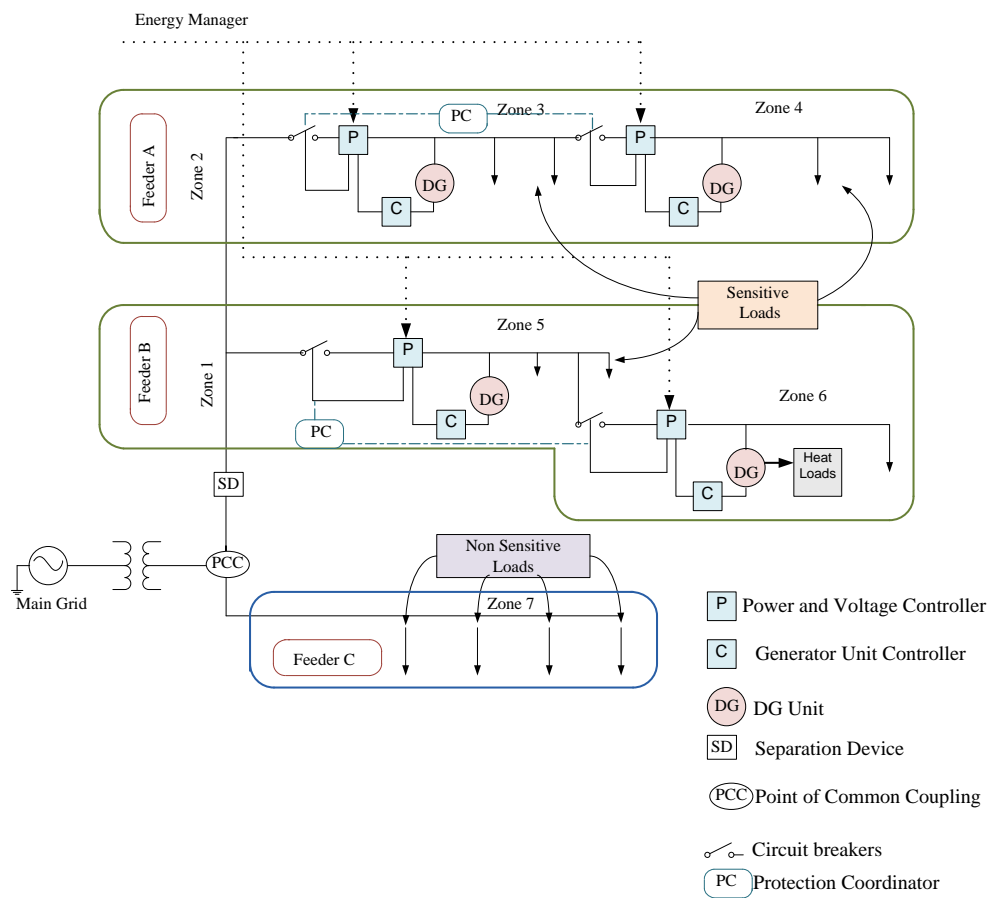


Figure 2-1: Microgrid Structure [8, 32]

The architecture consists of a point of common coupling (PCC), separation device (SD), power and voltage controllers (P), generator unit controllers (C), distributed generation units (DG) circuit breakers and an energy manager.

The main grid is separated from the microgrid at the point of common coupling (PCC). The separation device (SD) disconnects all the sensitive loads

## Chapter 2: Emerging Electricity Grid structures

from the main grid once the quality of power delivered from the utility starts to deteriorate.

The Power and Voltage controller (P) regulates the feeder power flow at a level prescribed by the Energy Manager. The Generator unit controller (C) provides the power and voltage regulation at each DG unit during disturbances and load changes [32].

In Figure 2-1, there are distributed generators on feeders A and B but none on feeder C. Feeders A and B have sensitive loads while feeder C has non-sensitive loads. When a disturbance occurs at the main utility grid, feeders A and B can island by using the separation device to minimize the disturbance to the sensitive load. Islanding can only occur if enough local generation is present to meet the demands of the sensitive loads. The non-sensitive loads on feeder C are left to ride through the disturbance. This eliminates the nuisance tripping of the non-sensitive loads when the microgrid islands to protect the sensitive load.

The protection system (PC) of a microgrid requires unique solutions which can provide required functionalities. The protection system must respond to both system and microgrid faults. For a fault on the utility grid, the main protection system will quickly isolate the sensitive load portion of the microgrid. For a fault within the portion of the microgrid that can be islanded, the protection system will isolate the smallest possible section of the radial feeder to eliminate the fault [32].

A lot of research has been carried out on the microgrid concept. The findings are described in literature such as [2, 8, 32]. System behaviour when several microsources are connected to form a microgrid is complicated and unpredictable. In order to understand the behaviour of a microgrid with several microsources, key issues such as microgrid control, stability and protection have to be considered in detail.

## Chapter 2: Emerging Electricity Grid structures

Microgrid control is mainly concerned with energy and power management between load power demand and power supply. This energy/power management scheme must be maintained to keep system frequency constant. A microgrid with many small generators is inherently a weak system. Generation equipment are usually equipped with some form of regulator to control the generated power in accordance with the load demand. For example, local synchronous generators employ the use of an automatic voltage regulator (AVR) and a governor to control the reactive and real power respectively. These regulation systems have slow dynamic response time during transient events [34, 35]. Control delays in these regulation systems can cause problems such as variation of system frequency in small independent microgrids. Frequency control is usually an important issue within a microgrid. Machines in such a system must be able to respond quickly during transient events in order to ensure power balance at all times. This means rapid detection of frequency change and fast accurate control of load power generation. Inverters can be used to control frequency since the inverter frequency can be controlled independently from the load. The presence of energy storage can help achieve the requested balance between generated power and load power during transient events.

In the next section, a brief overview of the various electrical energy storage technologies is presented.

### **2.3 Energy storage technologies**

Economic, environmental, technical and governmental regulation constraints have inhibited power generation and transmission facilities from meeting the continuous growth in electric power demand. The continuous real time balancing of supply and load demand including losses is a prerequisite for successful operation of an ac power grid. Over the past decade, the application of renewable energy in existing power grid to meet these growth demands has

## Chapter 2: Emerging Electricity Grid structures

increased at a rapid rate. However, the intermittent nature of renewable energy sources is a major concern when system stability and reliability is critical.

Energy storage technologies when properly designed and integrated provide the ability to store electrical energy at times of low demand or when generation cost is low. While energy storage technologies do not represent energy sources, they provide environmental, economic and energy diverse advantages to the system. These include reducing the risks of power outages, power quality improvement, matching electricity supply to load, reducing investment cost for building additional generation reserves and enabling renewable energy technologies [36]. Energy storage technologies can potentially improve power system stability by providing frequency and voltage regulation benefits during power system disturbances. Energy storage facilities can also inject bulk energy to restrict peak demands on the power facilities to maintain a stable and working grid. Electrical energy in an ac system cannot be stored electrically. However, energy can be stored by converting the ac electricity and storing it as electromagnetic energy, electrochemical energy, and kinetic energy or as potential energy [37].

A number of energy storage technologies currently exist. Power rating, energy rating, charging and discharging characteristics and efficiency are important factors considered when selecting the energy storage to be employed in a specific power system. Based on discharge time and storage capacity, energy storage technologies can be classified into three categories: short-term (few seconds or minutes), medium-term (minutes or hours) and long-term (many hours to days). Short-term energy storage technologies are usually applied to improve power quality, particularly to maintain voltage and frequency stability during transients. Medium-term energy storage technologies are deployed to contribute to grid congestion management. Long-term energy storage technologies are usually deployed to match supply and demand over 24 hours or longer.

A brief overview of different types of energy storage devices with the potential to improve power system performance are discussed in the next section.

### **2.3.1 Flywheel energy storage**

Energy is stored mechanically in form of kinetic energy in the rotating mass of a rapidly spinning flywheel. The stored energy (E) depends on the moment of inertia (j) and the square of the rotational velocity ( $\omega$ ) of the flywheel as shown in Equation (2-1).

$$E = \frac{1}{2} j\omega^2 \quad (2-1)$$

A motor–generator set is required to convert electrical energy to kinetic energy and vice versa. Energy is stored when the motor-generator set acts as a motor. Electrical energy is converted to kinetic energy by accelerating the flywheel to a higher speed during the charging process. The motor-generator set acts as a generator during the discharging process. Kinetic energy is converted back to electrical energy by decelerating the flywheel. In most cases, a power converter is used to drive the flywheel to provide wide operating range. Details of the flywheel energy storage system are described in [36-40].

Flywheel energy storage has been considered for several power system applications such as stability enhancement and peak shaving. Flywheels have been used for applications that require short discharge time such as frequency and voltage stabilization. Power capacity of flywheel energy storage is less than 100kW and the energy capacity is less than 100kWh. The advantages of flywheel energy storage include high efficient energy storage and relative long life. Rotational losses, increase in maintenance cost and possibility of the rotor

breaking loose due to high speed operation of flywheels are some of the disadvantages of the flywheel[37].

### **2.3.2 Superconducting magnetic energy storage**

Superconducting magnetic energy storage converts the ac current from a power system into dc current flowing in the superconducting coil and stores the energy in the magnetic field. The inductively stored energy (E) is given in Equation (2-2).

$$E = \frac{1}{2}LI^2 \quad (2-2)$$

where L is inductance of the coil and I is the dc current flowing through the coil. Energy is stored according to the current circulating through the superconducting coil and the energy stored can be released to the ac system when required. Details of the superconducting magnetic energy storage can be found in [36, 37, 41].

Superconducting magnetic energy storage is employed in applications that require fast response time such as power quality improvement, dynamic and transient stability improvement and voltage levelling; hence it can be classified as short term response energy storage device. Power capacity of superconducting magnetic energy storage ranges between 0.3MW-3MW and its energy capacity is less than 250kWhr.

Superconducting magnetic energy storage is highly efficient and reliable. A refrigeration system is necessary to maintain the superconductivity of the coil due to the sensitive nature of the coil to temperature changes. The interactions of the current flowing in the magnetic coils produce a force that may be problematic. An auxiliary system is required to support the magnetic force. Cost of refrigeration, protection and control equipment are some of the failings of the Superconducting magnetic energy storage.

### **2.3.3 Pumped hydro energy storage**

Pumped hydro energy storage stores energy in the form of water pumped from a lower reservoir to a higher elevation reservoir thus giving it potential energy. Energy is usually stored during period of low generation cost. Stored energy will be converted to electrical energy by releasing the elevated water to a lower reservoir through hydro turbines. This process will normally take place when generation cost is high and/or when the load demand exceeds the supply [42, 43].

Pumped hydro energy storage has been commercially implemented for load balancing for over 80 years. In comparison to other forms of energy storage, pumped hydro energy storage supplies the highest amount of electrical energy. Pumped hydro energy storage can be classified as long term response energy storage and it is used for applications that require power to be supplied for hours and days. Power capacity of pumped hydro energy storage is about 2GW and its energy capacity is less than 24GWhr. However, its dependence on associated geography can reduce the efficiency of the energy storage [42].

### **2.3.4 Compressed air energy storage**

Compressed air energy storage stores energy in the form of compressed air by using a compressor. Energy is stored by converting electrical energy to potential energy. Electricity is used to run compressors that push air at high pressure into underground reservoirs. Compressed air is stored in reservoirs such as naturally occurring caverns, mine caverns or artificially rock reservoirs [44]. Compressed air is used together with natural gas to power a turbine generator in order to generate electrical energy during the discharge process.

## Chapter 2: Emerging Electricity Grid structures

Compressed air energy storage systems require a reversible turbine that allows the operation of the turbine during the charging and the discharge process. They are long term energy storage devices that can supply power for days and are commonly used in applications that require provision of backup power e.g. during long blackouts [36]. Compressed air energy storage systems have power capacity of 100-300MW and energy capacity of 0.4-7GWhr

### **2.3.5 Fuel cells**

Fuel cell is an electrochemical device that converts a source fuel e.g. hydrogen into electrical energy by oxidizing the fuel. Fuel cell has the potential to store higher energy per kilogram of weight than that stored in batteries.

The method of production and storage of hydrogen are important factors considered when fuel cells are employed. Hydrogen can be produced from non- renewable and renewable energy sources. Liquefaction, compression of hydrogen gas, absorption in metal hydrides and adsorption in carbon nanotubes are examples of hydrogen storage techniques currently employed.

Safety concerns are raised when liquefaction and hydrogen storage by high pressure compression are the storage techniques employed. The absorption of hydrogen in metal hydrides offers a safe way of storing hydrogen but the downside of this method is the slow kinetics and high temperature requirements during the release of stored hydrogen [45].

Carbon is known to adsorb significant quantity of hydrogen due to its molecular characteristics. Its high surface area enables it to store a relatively large amount of hydrogen. This characteristic makes the adsorption of hydrogen in carbon nanotubes a promising technology for hydrogen storage.

## Chapter 2: Emerging Electricity Grid structures

Alkaline fuel cells, methanol fuel cells and PEM (proton exchange membrane) fuel cells are examples of fuel cells that have been developed. Alkaline fuel cells give high power but they use a poisonous electrolyte. Methanol fuel cells generate high power in a safe environment but at a high cost. PEM fuel cells are easy and safe to handle. Their solid plastic membrane can tolerate a modest pressure differential across the cell, making for easy pressurization which increases energy density and reduces cost.

Fuel cells are used as distributed power sources in power systems due to their low emission, high energy conversion and fast response to transients. Energy capacity of fuel cells is less than 200MWhr. However, fuel cells are seen as energy conversion devices rather than energy storage devices due to the nature of the charging process (hydrogen storage process)[46].

### **2.3.6 Battery energy storage**

A battery is an electrochemical device that stores electrical energy in the form of chemical energy. It has two electrodes immersed separately in an electrolyte. Batteries are charged when a potential applied to the terminal cause an internal chemical reaction in the electrolyte [37]. During the charging process, electrical energy transferred to the battery is electrochemically absorbed and stored. The stored energy is discharged when a load is connected to the terminals of the battery. During the discharge process, the internal chemical reaction is reversed.

Battery energy storage systems have recently emerged as one of the more promising near term storage technologies for power applications. Current battery technologies include nickel metal hydride battery, alkaline battery nickel cadmium battery, lead acid battery, sodium sulphur battery and redox flow battery. Details of battery energy storage systems can be found in [36, 37].

## Chapter 2: Emerging Electricity Grid structures

Lead-acid batteries are designed for applications that require large energy storage and fast charge/discharge rates. They represent a low cost option for applications that require large storage capabilities. However, low energy density and limited cycle life are some of the limitations of lead acid batteries. Sodium –sulphur battery was developed with the aim of improving the energy density of batteries. The energy density of a sodium sulphur battery is four times greater than that of a lead acid battery [47]. Sodium-sulphur battery develops a very high resistance which causes battery failure during the charging process. Redox flow batteries are commonly used in large energy storage facilities. Electrolytes are pumped into electrodes circulating from each other. The whole system generates a considerable noise which originates from the circulating and cooling systems. The maintenance cost due to the circulating and cooling systems and environmental impact due to the noise are some of the limitations of the redox flow battery.

Battery energy storage systems are medium term energy storage devices used in power system applications such as area regulation, spinning reserve and power factor correction [36, 37]. Their characteristics include high energy densities, high cycling capabilities and high reliability. These characteristics give them the edge over other types of energy storage systems. However, their use in power system applications has been limited because of their maintenance cost and short lifetime.

### **2.3.7 Supercapacitor energy storage**

Supercapacitors are electrochemical double layer capacitors that store energy in an electric field (like a parallel plate capacitor) by means of separating positive and negative ions in the electrolyte. Their electrodes are specially made from highly porous materials which allow more ions to be separated in the cell [48, 49].

## Chapter 2: Emerging Electricity Grid structures

The stored energy (E) is given in Equation (2-3), where C is the capacitance and V is the voltage across the plates.

$$E = \frac{1}{2}CV^2 \quad (2-3)$$

A supercapacitor is charged when a DC voltage is applied to the supercapacitor terminals. To produce an electric field that is distributed between the two terminals, current collectors are attached directly to the positive and negative terminals. The electrodes are attached to the current collectors. When a voltage is applied to the terminals, the voltage potential will distribute over the electrodes and thus activate the electrodes. Electrolytic ions under the influence of the electric field provided by the activated electrodes are then drawn to the opposite polarity i.e. positive ions travel and attach to the negative porous electrodes and the negative ions travel and attach to the positive porous electrodes. This action results in energy being stored in the form of an electric field between the electrodes and the ions. The activated electrodes are isolated from each other with a separator through which the ions can travel through. Supercapacitors are discharged by reversing the process and the energy stored in the electric field are converted into electrical energy. Supercapacitors are called electrochemical double layer capacitor because of the two layers of electric field that appears in the cell.

Supercapacitors are classified as short term response devices and are suitable for burst power applications that require fast response and short duration e.g. voltage and frequency stabilization. Supercapacitors have typical power capacity which is less than 250kW. In comparison to batteries, supercapacitors have a much faster charge and discharge rate, higher power density and a longer life cycle [36, 37].

A comparison of various energy storage devices in terms of power capacity, energy capacity and discharge duration is shown in Table 2-1.

## Chapter 2: Emerging Electricity Grid structures

Device	Power capacity	Energy capacity	Discharge duration
Flywheel	<100kW	<100kWhr	Sec/Min
SMES	0.3-3MW	<250kWhr	Sec/Min
Pumped hydro	<2GW	<24GWhr	Days
Compressed air	100-300MW	0.4-7GWhr	Days
Fuel cells	<20MW	<200MWhr	Min/Hours
Batteries	<20MW	<200MWhr	Min/Hours
Supercapacitors	<250kW	<3MWhr	Sec/Min

Table 2-1: Comparison of various energy storage devices [36]

Energy storage technologies provide an added degree of freedom to a microgrid by allowing time-shifting between the generation and use of energy. The theoretical capabilities of energy storage technologies connected to a microgrid are unit placement, spinning reserve, load-levelling from grid, source-levelling for intermittent sources, peak shaving and frequency regulation [50]. Figure 2-2 shows the applications of various energy storage options in ac power systems.

## Chapter 2: Emerging Electricity Grid structures

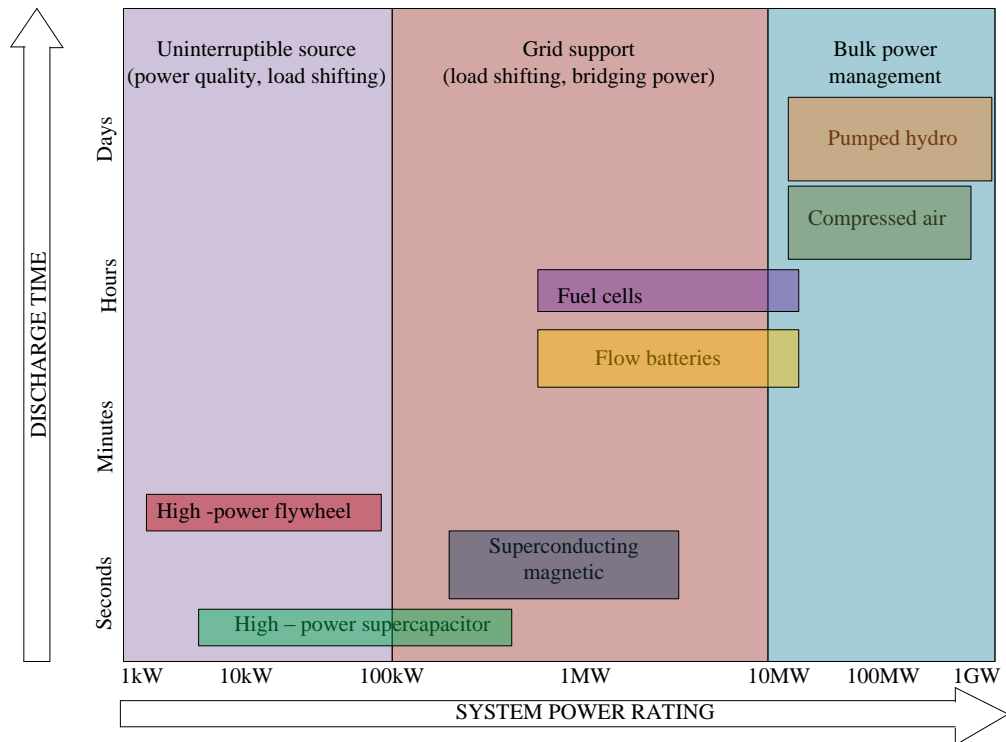


Figure 2-2: Positioning of energy storage options [51]

### 2.4 The role of power electronics in emerging electricity grid structures

In the late 19<sup>th</sup> century, problems like voltage and frequency deviation during load changes and power transfer limitations were observed due to reactive and active power unbalances. Today, these problems have higher impact on reliability and security of electrical power systems [52]. It is a real challenge to ensure that transmission and distribution systems are flexible enough to meet new and less predictable supply and demand condition in emerging electricity markets[53].

Transmission and Distribution (T&D) lines are the electrical medium used to transport electricity from the generation sites to load centres. In T&D systems, the lines are characterized by the distributed reactance (series inductance and

## Chapter 2: Emerging Electricity Grid structures

shunt capacitance) which is generally associated with the flow of reactive power. The flow of reactive power along the lines during loading may cause a change in the voltage profile. This may result in a large variation of the voltage at the load buses and can eventually lead to power quality problems such as voltage instability. Voltage instability may cause low performance of associated loads and equipment failure. Transient events such as faults, load switching and other disturbances can cause a change in the flow of active power in the system. The sudden change in the flow of active power will cause a generator or group of generators to accelerate or decelerate from its /their steady state speed. This will result in a variation of the system frequency and power oscillation. Variation of the system frequency may lead to loss of synchronism and even in some cases may cause cascaded failure of the system.

In the past, permanently connected reactance and mechanically switched shunt capacitors (MSC) and mechanically switched reactors (MSR) were used to ensure that the voltage profile along the T&D lines is within the prescribed range [54]. MSC and MSR were used for loads that vary from hour to hour. For applications that require handling of fast changes in reactive power, synchronous condensers (rotating synchronous machine without a prime mover and turbine) were installed.

In recent times, advances in the development of high power semi –conductors and power electronics technology have made possible the development of fast compensators without mechanical movement for applications in electrical power systems.

Power electronics technology covers a very wide spectrum of power ratings and applications (from watts to Giga watts). Its applications for T&D systems tend to be amongst the very highest in terms of voltage and power ratings [55]. Power electronics technology provides an opportunity for enhanced value of T&D in terms of loading capability, reliability, availability and flexibility of

## Chapter 2: Emerging Electricity Grid structures

electrical power systems [56]. Power electronics technology has been applied to T&D systems in a number of ways over the past thirty years. Its applications range from providing continuous variable and dynamic reactive power compensation to providing high voltage direct current (HVDC) power transmission [57].

Power flow in electrical power system is usually uncontrolled and is governed by Kirchoff's and Ohm's laws. The uncontrollable power flows may result in bottlenecks such as generator outages, line tripping, voltage instability and system blackouts [53]. Power electronics technology such as FACTS and HVDC systems can provide voltage regulation, power flow management and elimination of the aforementioned bottlenecks. Some T&D applications of power electronics technology such as HVDC systems have been available for many decades. FACTS systems such as STATCOM are available in high voltage (HV) markets and are starting to penetrate the distribution (medium voltage (MV) and low voltage (LV)) markets [55]. The application of power electronics technology in emerging electricity grids are driven mainly by challenges imposed by key players in the unified electricity market (DG and microgrids).

The highest power ratings of any power electronics technology application are those associated with power transmission by high voltage direct current (HVDC). HVDC systems are re-emerging as very important technology for large scale bulk power transfer over long distances particularly in emerging economies such as China, India and Brazil [55]. HVDC systems have been used in niche power transmission applications for more than fifty years. They have the advantage of allowing additional power to be injected into a network without increasing the fault level. In the past, all HVDC systems employed a thyristor based "line commutated" technology. This technology has the capability of only turning on its switching elements. HVDC systems based on line commutated converter technology have a long and successful history. It is worth mentioning that line commutated converters have some technical

## Chapter 2: Emerging Electricity Grid structures

restrictions. The fact that the commutation within the converter driven by ac voltages requires the connected ac system to be in proper condition is a major limitation [58]. Power electronics technology with self-commutated converters such as the Voltage source converter (VSC) can overcome this limitation. VSC technology does not require any driving system voltage. It can build up three-phase ac voltage via the dc-voltage (black start capability). The voltage source converter (VSC) HVDC technology with the capability of turning on and turning off its switching elements is finding its way into power transmission applications. VSC technology started to appear in HVDC applications in 1997 [55]. The converter is self-commutated because the semiconductors have the capability of turning on and turning off their switching elements. High power devices such as GTO (Gate Turn off) thyristors, IGCT (Insulated Gate Commutated Thyristors), IEGT (Injection Enhancement Gate Transistor) can be employed as the switching device but the most commonly used device is the IGBT (Insulated Gate Bipolar transistor). A major problem faced in classical line commutated HVDC technology and the VSC HVDC technology is the extrapolation of high voltage from the low rated voltage of the switching devices. To achieve the required voltage rating required for VSC HVDC applications, large number of IGBTs can be connected in series, multi-level circuits and modular multi-level converter circuits described in [59, 60] can also be employed.

Power electronics technology provides an opportunity for enhanced value of transmission in terms of flexibility of ac transmission. Flexible AC Transmission System (FACTS) can be defined as an alternating circuit system that incorporates power electronic based controllers and other static controllers to enhance controllability and increase power transfer capability [56]. FACTS technology can provide stability, voltage control and network loading control. A significant feature of FACTS technology is its high speed response. As with HVDC technology, FACTS controllers are also based on line commutated and self-commutated technologies. FACTS controllers are categorized according to their voltage and current injection characteristics with T&D systems.

## Chapter 2: Emerging Electricity Grid structures

According to their injection characteristics, there are three types of FACTS controllers. The first type is series connected FACTS controllers. They are characterised by injecting voltage in series to the T&D system. Examples of series type FACT controllers are Thyristor Controlled Series Capacitor (TCSC), Static Synchronous Series Compensator (SSSC) and GTO Controlled Series Capacitor (GCSC) [56]. TCSC injects voltage that is proportional to the current due to its variable capacitive impedance while SSSC directly injects variable voltage of either polarity in quadrature with the current. GCSC on the other hand offers greater control of capacitive impedance due to its turn-off characteristics. Series type FACT controllers are more suitable for power flow control.

The second type is shunt connected FACT controllers. They are characterized by injecting current in shunt/parallel to the T&D system. Examples of shunt type FACT controllers are conventional thyristor based Static Var Compensator (SVC) and IGBT based STatic COMpensator (STATCOM) [56]. SVC can be a combination of Thyristor Switched Reactor (TSR), Thyristor Controlled Reactor (TCR), Thyristor Controlled Reactor (TCR) Thyristor Switched Capacitor (TSC) and a Fixed Capacitor (FC). SVC operates with the same principle as the MSC and MSR. It generates /absorbs reactive power, but the precise control of the firing angle of a thyristor switch gives the SVC the ability to provide reactive power continuously and sufficient speed response to handle fast changes [54]. Reactive power generated by means of SVC is based on using thyristors as control elements to vary the reactive power produced by the passive power components (capacitors and reactor banks). However, recent developments in the field of power electronics has made it possible to improve the size and cost requirements of static var generators [61, 62]. A static var generator based on only small DC-link capacitor has emerged in recent times. STATCOM is a recently developed var generator. It consists of a dc-to-ac voltage source converter (VSC), a small dc-link capacitor and a coupling reactor. STATCOM generates reactive power if the voltage produced by the VSC is higher than the

## Chapter 2: Emerging Electricity Grid structures

utility voltage of the system it is connected to. Conversely, it absorbs reactive power if the voltage produced by the VSC is less than the utility voltage it is connected to [61-63]. STATCOM has a faster response time for reactive power compensation in comparison to other var generators [64, 65]. It can be incorporated with energy storage systems in order to improve its power system stability capabilities [66]. The control of a STATCOM is based on the production of a sinusoidal voltage with respect to the system voltage. As a result, both the magnitude and phase of the voltage can be adjusted rapidly. SVC is controlled by varying the conduction period of the thyristor to adjust the susceptance of the capacitor and reactor. This may react with the system impedance to cause severe resonance. As a result, the speed of the SVC controller is limited in order to reduce the resonance effect when applying the SVC to transient event compensation [67]. Current is a function of line voltage in SVC. Hence its reactive power is a function of square of the line voltage. Thus when the dynamic voltage is 70%, the injected reactive power is 49%, just when more power might be needed. The STATCOM on the other hand injects current of either polarity and will inject appropriate power needed for reactive power compensation. Shunt type FACTS controllers are applied to systems that require control of reactive power and voltage.

The third type of FACTS controllers is a combination of voltage injection in series and current injection in shunt. Examples of series-shunt FACT controllers are Thyristor Controlled Phase Angle Controller (TCPA) and Unified Power Flow Controller (UPFC). TCPA injects variable voltage in quadrature with the line to ground voltage. UPFC is a combination of SSSC and STATCOM. It injects variable voltage in series, with variable angle with respect to current [56]. The shunt controller not only supplies required active power for the series element, it can also supply variable reactive power in shunt. As a result, UPFC can dynamically control active and reactive power flow as well as the line voltage. UPFC has similar control capability to the newly developed VSC HVDC system which can control both the independent

## Chapter 2: Emerging Electricity Grid structures

active and reactive power flows of a transmission line and the voltage of a local bus [53].

In general, T&D systems must be economical as well as meet the requirements for system security, reliability and sufficient capacity to meet the demands of the customers in emerging electricity grid structures [56]. FACTS and HVDC technology can be considered as important tools used in the transformation of the traditional/existing electricity transmission and distribution grid into an interactive and unified power supply network. HVDC and FACTS technology will also provide the essential features to avoid the envisaged problems of emerging electricity grid structures.

## **2.5 Conclusion**

In emerging electricity grid structures, a large number of small and medium sized generators, power electronics technologies and energy storage elements will be interconnected through a fully interactive and intelligent electricity grid structure. The primary objectives of emerging electricity grid structures are enhancing the overall performance of electric power systems, facilitating electricity trading, reacting quickly to disturbances to minimise their impact and prevent power systems against black outs and restoring power systems to normal operating mode after disturbances.

It is well accepted that power electronics technology is a key enabling element in emerging electricity grid structures. FACTS and HVDC technology together with advanced communication and control technologies will help achieve the objectives of emerging electricity grid structures.

In order to fully employ the capabilities of FACTS technology, the use of energy storage integrated with FACTS will be a viable option in providing multi-functional controls for enhanced microgrid operation. The superior

## Chapter 2: Emerging Electricity Grid structures

performance of the STATCOM in comparison to other var generators makes it a preferable choice for transient event compensation. Supercapacitors are classified as short term response devices and are suitable for burst power applications that require fast response and short duration e.g. voltage and frequency stabilization within a microgrid.

Based on the gaps in literature, the work carried out in this research investigated the use of a STATCOM and supercapacitor energy storage system in providing frequency control improvement within a microgrid. In the next chapter, the principle of operation and control of a STATCOM integrated with supercapacitor energy storage system is discussed in detail.

## **Chapter 3**

# **STATCOM with SuperCapacitor Energy Storage System**

---

### **3.1 Introduction**

The control of active power and reactive power exchange between grid connected converters and the utility grid is an important factor when considering the operation of ac power systems that employ distributed generation. The call for a sustainable society with renewable and distributed resources has driven the implementation of power electronic technology into ac power systems. Recently a power electronic converter called the static var compensator (STATCOM) has been employed to provide reactive power support to the ac power system [25]. Active power support cannot be provided with the standard STATCOM due to the limited energy stored in the dc-link capacitor, nonetheless the real power capabilities of the STATCOM can be

## Chapter 3: STATCOM with SuperCapacitor Energy Storage System

enhanced by the addition of energy storage to the dc-link. The exchange of active power and reactive power can be controlled by adjusting the amplitude and phase of the converter output voltage.

In this chapter, the operation and control schemes for grid connected power converters are described in section 3.2. The operation and control of a voltage source converter (VSC) based STATCOM are presented in section 3.3. The operation and control of a supercapacitor energy storage system (SCESS) are presented in section 3.4. The operation of the STATCOM with SCESS is described in section 3.5. A simulation study highlighting the reactive and real power capabilities of the STATCOM with SCESS is presented in section 3.6. Finally the conclusions are presented in section 3.7.

### **3.2 Grid connected converters**

Power electronic converters have been predominantly employed in domestic and industrial applications. However, due to advancements in power semiconductor and microelectronics technologies, their application in power systems has gained more attention in recent times. Thus power electronic converters are increasingly employed in power conditioning, compensation and power filtering applications [68].

Power electronic converters employed in power systems can be categorized into voltage source converters (VSC) and current source converters (CSC). In a VSC the dc-side is a DC-link voltage. CSC derives its terminal power from a current source e.g. a reactor. In comparison, a magnetized reactor is much lossier than a charged capacitor. The Voltage Source Converter (VSC) has several advantages over the Current Source Converter (CSC). Examples are unrestricted flow of reactive power in VSC and independent active and reactive power conversion [69, 70].

Based on the number of synthesized output voltage levels, VSCs can generally be categorized into two-level converters and multilevel converters. In recent times there has been a move towards increasing the voltage compatibility of IGBT voltage source converters. Diode-clamped multilevel converter [71, 72], flying-capacitor multilevel converter [73, 74], cascaded converter [75, 76] and mixed level hybrid cell converters [77] are examples of multilevel converter topologies introduced to achieve this. These converter topologies allow recent semiconductor devices to be utilized in higher voltage applications without incurring voltage-sharing problems. However, in order to have multilevel converters operate safely and reliably, their complex configurations require more complicated control techniques. Therefore, for simplicity and economic reason, the two-level PWM converter has been chosen in this work. The switching technique used is based on the standard sine wave PWM modulation. Switching techniques are required for the purpose of synthesizing a close-approximation to a sinusoidal voltage.

### **3.2.1 Two –level three phase VSC**

Figure 3-1 shows the schematic diagram of a two-level voltage source converter (VSC) connected to the AC grid. The converter is called the two-level VSC since each of its AC-side terminals can assume either of the voltage levels  $+V_{DC}/2$  and  $-V_{DC}/2$ . Two switching devices are connected in series in each phase leg (six switches in total). The two switches in the phase-leg are operated in a complementary way. Thus, only one switch is turned on at any point in time. A small time delay (lockout/dead time) is usually included in the switching pattern to prevent failure if both switches are on at the same time.

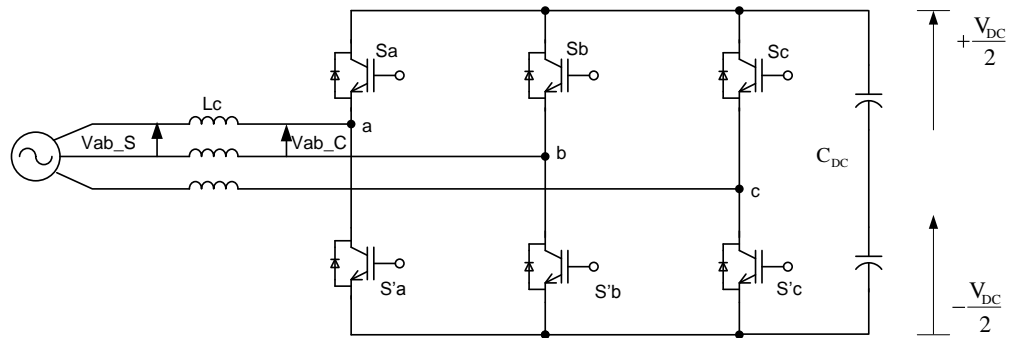


Figure 3-1: Two-level grid connected converter

Pulse width modulation (PWM) switching technique can be used to turn on and turn off the switching devices in the converter configuration. The width of the switching signals (pulses) is modulated according to the control input signals. The PWM signals are generated by comparing the three phase sinusoidal signals which are  $120^\circ$  out of phase, with a repetitive switching-frequency triangular waveform.

When the upper switch  $S_a$  is turned on, the 'a' terminal is connected to  $+V_{DC}/2$  resulting in a phase voltage equal to  $+V_{DC}/2$ . The other phases are connected in the same way but with a phase delay of  $120^\circ$  as in a three phase AC system. Conversely when the lower switch  $S'a$  is turned on, the 'a' terminal is connected to the  $-V_{DC}/2$  resulting in a phase voltage equal to  $-V_{DC}/2$ . The phase voltages indicate that there are two levels in the voltage waveforms. The turn on and turn off of the upper and lower switches result in a series of square wave pulses of different width. The difference in the width of the pulses represents the magnitude of the voltage that is related to the sinusoidal control signal.

Most grid side converters adopt the VSC topology with a current controller to regulate the current injected into the grid. The control schemes for grid connected converters are discussed in the next section.

## **3.2.2 Control schemes for grid connected converters**

Control issues related to the use of grid connected converters are mainly the control of the DC voltage and the control of the AC power. The AC power can be controlled with the aim of either feeding the main grid or feeding stand – alone loads or a microgrid [78].

The DC voltage can be subjected to transient conditions due to change of power. DC voltage control is necessary to compensate for voltage variations during power changes. DC voltage control is achieved through the control of the power exchanged by the converter with the grid. This is achieved by injecting/absorbing power to/from the grid, thus changing the value of the reference for the AC current loop. The control of the DC voltage through the AC current can result in the identification of two loops, an outer DC voltage loop and an internal current loop. The internal loop is designed to achieve short settling times while the outer loop is designed to achieve optimum regulation and stability.

A commonly adopted approach for the control of AC power is the control of power in a stationary or rotating reference frame [78, 79]. These strategies are discussed below.

### **3.2.2.1 Scalar control**

The general idea of the scalar control strategy is to have the controller operate in the stationary a-b-c reference frame as described in [80-82]. The block diagram of a current controlled voltage source inverter in the stationary a-b-c reference frame is shown in Figure 3-2. An outer loop is required to control

### Chapter 3: STATCOM with SuperCapacitor Energy Storage System

the DC voltage to a value greater than the peak AC line voltage such that it behaves as a boost converter.

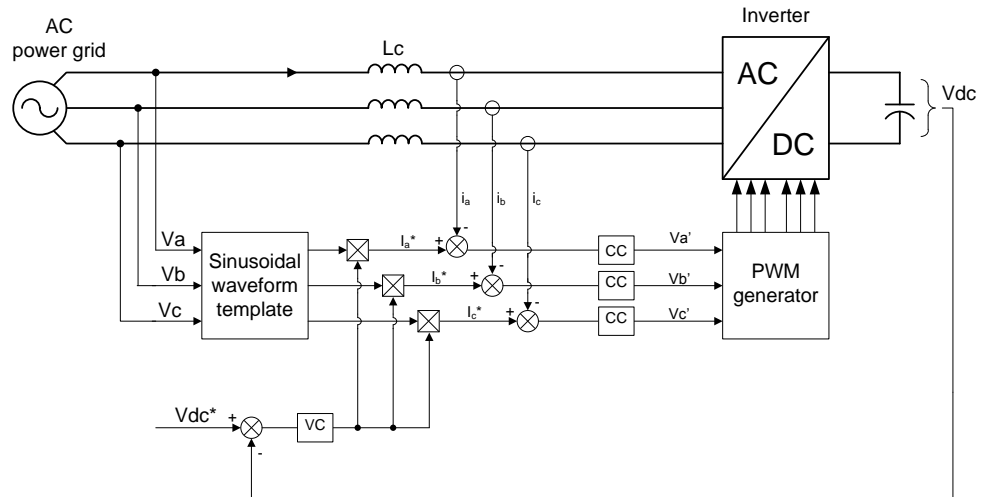


Figure 3-2: Scalar control strategy

The output of the DC voltage controller (VC) produces a demand for the current control which is used to vary the magnitude of the controlled current. The voltages at the point of common coupling ( $V_a$ ,  $V_b$ , and  $V_c$ ) are measured and fed into a unity amplitude sinusoidal waveform template. The sinusoidal waveform template is in phase with the grid phase voltage. The output of the DC voltage controller is then multiplied by the sinusoidal waveform template outputs. The results are used as the reference currents ( $I_a^*$ ,  $I_b^*$ ,  $I_c^*$ ) which are compared with the measured currents ( $I_a$ ,  $I_b$ ,  $I_c$ ). Three individual current controllers (CC) are used, one for each phase, to generate the voltage demands  $V_a'$ ,  $V_b'$  and  $V_c'$ , which are then passed to the PWM generator. The desired voltage at the front-end is generated according to the controlled PWM signal. The advantage of this scheme is its simplicity which means it can be implemented with an analogue circuit, thereby improving the speed response of the control scheme as there are no sampling or processing delays. The main disadvantage is an inherent tracking error resulting from the controller trying to follow a constantly changing reference value. This problem can be resolved

with a high switching frequency and high current controller bandwidth. However at high power levels, the switching frequency and the current controller bandwidth will be constrained and the current errors due to the inherent tracking delay will become significant.

### 3.2.2.2 Vector control

To overcome the problems associated with the scalar control strategy, a control scheme based on the dynamic equations of a grid connected converter as described in [79, 83-90] can be employed. A block diagram of the vector control strategy is shown in Figure 3-3.

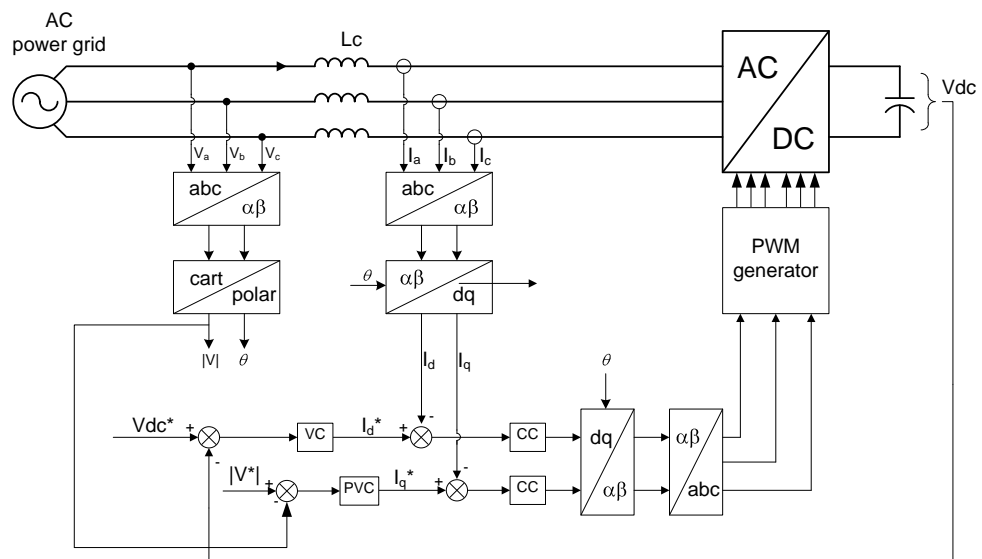


Figure 3-3: Vector control strategy

The instantaneous grid voltages and currents in the three-phase a-b-c-stationary frame are measured and transformed into the two-phase  $\alpha$ - $\beta$  stationary frame by using the  $\alpha$ - $\beta$  transformation (described in Appendix A). The rotating angle,  $\theta$ , of the grid voltage is obtained from the transformed voltages  $V_\alpha$  and  $V_\beta$ . The angle is used as the reference angle for the transformations in order to synchronize the transformed signals with the grid voltage. The voltages and currents in the  $\alpha$ - $\beta$  can further be transformed into

### Chapter 3: STATCOM with SuperCapacitor Energy Storage System

two DC signal components in the d-q rotating frame which rotates at the AC grid voltage frequency.

As far as the control system is concerned, the grid voltage now appears as a constant DC disturbance which is much more easily compensated than the sinusoidal varying value in the stationary frame previously discussed. If the d-axis voltage is aligned with the vector of the grid voltage, the d and q-axis components account for the active power and reactive power current respectively.

The DC voltage is kept constant by the DC voltage controller (VC). The output of the DC voltage controller gives the active power reference ( $I_d^*$ ). The PCC (point of common coupling) voltage is kept constant by the PCC voltage controller (PVC). The output of the PCC voltage controller is the reactive power reference ( $I_q^*$ ). The reference demands ( $I_d^*$  and  $I_q^*$ ) are compared with the measured and transformed currents ( $I_d$  and  $I_q$ ). Two current controllers are used, one for each axis, to generate the voltage demands  $V_d'$  and  $V_q'$  which are transformed to  $V_a'$ ,  $V_b'$  and  $V_c'$ , which are then passed to the PWM generator to produce the associated voltages at the ac terminals of the converter.

The disadvantage of this system in comparison to the scalar control strategy is the added complexity which generally requires a digital controller to be applied. However, the vector control strategy enables the system to remove steady state errors. The vector control strategy also provides fast independent control of the d and q axis components which lead to the direct control of the active and reactive power.

Grid current is usually controlled in order to control active and reactive power exchange. The basic current control techniques employed in grid connected converters are reviewed in the next section.

### **3.2.3 Grid current control**

Current controlled converters have the advantages of high accuracy control of instantaneous current, peak current protection, overload rejection and very good dynamics [91]. They exhibit better safety, better stability and faster response. There are various possible strategies and structures for controlling the current in voltage source converters. These can be divided into two main groups, namely linear and non-linear controllers.

#### **3.2.3.1 Linear current controllers**

Linear current controllers have separate current control blocks and voltage modulation (PWM) blocks. Their structure enables them to exploit the advantages of modulators such as sinusoidal PWM and space vector modulation where constant switching frequency with a well-defined harmonic spectrum is employed. PI-Based controllers and deadbeat controllers are examples of linear current controllers [78].

Classical PI control is commonly used for current-controlled grid connected converters. This approach exhibits two major drawbacks: The inability of the PI controller to track a sinusoidal reference without steady state error and a poor rejection capability. This is due to the poor performance of the integral action when the disturbance is a periodic signal. As discussed in the previous section (vector control), this limitation can be solved by implementing the PI control in a d-q rotating frame. The performance of a PI controller implemented in the rotating d-q frame can be improved by using cross coupling terms ( $\omega L$ ) and /or feed-forward grid voltage [92, 93]. The feed-forward grid voltage is used to improve the dynamics of the controller during grid voltage fluctuations. The cross-coupling terms are used to control the flow of active and reactive power through the active and reactive current

components. Details of the design of the PI controllers are discussed in section 3.3.

Deadbeat controller belongs to the family of predictive controllers [94-97]. It is widely employed for sinusoidal current regulation due to its high dynamic response. Deadbeat controller has a very high bandwidth which is good for tracking sinusoidal signals. It is widely used for current error compensation. The principle of deadbeat controller is to calculate the derivative of the controlled variable in order to predict the effect of the control action. The main disadvantage of the deadbeat controller is its inherent sensitivity to model and parameter mismatches which can generate tracking error and stability problems [78, 98, 99].

### **3.2.3.2 Non-linear current controllers**

Nonlinear current controllers can produce the switching signals required to control grid connected converters directly. They are employed in applications where the PWM modulators are negligible. Examples of non-linear current controllers are hysteresis controller [100, 101], neural network controllers [102] and fuzzy logic controllers [103]. Non-linear current controllers have excellent control response. With the exception of hysteresis controller, these controllers are difficult to implement in practical systems.

Hysteresis control is simple and robust. The output of the hysteresis comparator is the state of the switches in the power converter. In the case of a two-level three phase grid connected converter, three hysteresis controllers are required (one for each leg of the converter). Three-phase output currents of the inverter are detected and compared with a corresponding phase current references individually. The switching signals are produced when the error exceeds an assigned tolerance band.

### Chapter 3: STATCOM with SuperCapacitor Energy Storage System

Hysteresis control is insensitive to system parameters changes but it has unsatisfactory features as described in [104]. The main disadvantage of hysteresis control is the varying switching frequency it generates for the power converter. A number of proposals have been put forward to overcome variable switching frequency. A fixed modulation frequency has been achieved by varying the width of the hysteresis band as a function of instantaneous output voltage [105]. This is achieved with the use of a feed forward action or a phase locked loop [106, 107]. Depending on the method used the complexity of the controller can be increased significantly, hence the advantage of the simplicity of the hysteresis controller is lost.

The hysteresis controller has arguably the best performance of all the available controllers. However, its performance is significantly affected by switching frequency constraints enforced at high power levels. Amongst the linear controllers, the classical PI control implemented in the d-q rotating frame shows the most promise due to its excellent control performance and less dependence on plant parameters. Therefore, the PI based control implemented in the d-q rotating frame has been adopted for the control of grid current in this work.

In the next section the operation and control of a voltage source converter based STATCOM is described in full detail.

## **3.3 STATCOM**

STATCOM is a member of the Flexible AC transmission systems (FACTS) family that is connected in shunt with ac power systems. STATCOM has played an important role in the power industry since the 1980s. STATCOM provides many advantages, in particular the fast response time and superior voltage support capability. STATCOM is used for dynamic voltage control to

### Chapter 3: STATCOM with SuperCapacitor Energy Storage System

suppress short term voltage fluctuations because its dynamic performance far exceeds other var compensators [108-111].

STATCOM is a DC-AC voltage source converter with an energy storage unit, usually a DC capacitor. Power electronic switches are used to derive an approximately sinusoidal output voltage from a DC source. The power circuit diagram of a VSC-based STATCOM is illustrated in Figure 3-4 where six IGBTs with its anti-parallel diodes and a DC-link capacitor are used to produce the three-phase voltage. The STATCOM is coupled to the ac power grid via coupling inductors  $L_c$ . The coupling inductors are also used to filter out the current harmonic components that are generated by the pulsating output voltage of the power converter.

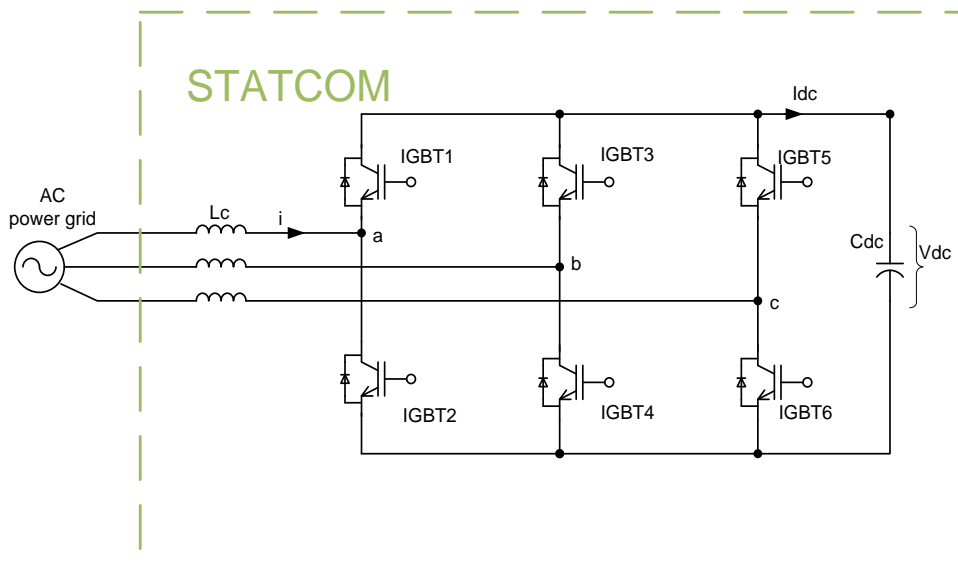


Figure 3-4: Power circuit diagram of a STATCOM

### **3.3.1 Principle of operation**

The exchange of active and reactive power between the STATCOM and the ac power grid can be controlled by adjusting the phase and amplitude of the converter output voltage. As described in Appendix B (power flow control), the STATCOM can be operated in the capacitive mode (inject reactive power) by controlling the amplitude of the converter voltage to be greater ac power grid voltage. In contrast, the magnitude of the converter voltage is controlled to be less than that of the ac power grid voltage in order to absorb reactive power or operate the STATCOM in the inductive mode. The converter operation is associated with internal losses caused by non-ideal power semiconductor devices and passive components. Without any proper control, the capacitor voltage will be discharged to compensate for these losses. The capacitor voltage is regulated by introducing a small phase shift between the converter voltage and the ac power grid voltage.

### **3.3.2 Control design**

As mentioned in section 3.2.2.2, the vector control strategy provides fast independent control of the d and q axis components which lead to the direct control of the active and reactive power. The vector control strategy as described in [83-90] has been adopted to achieve instantaneous power control in this project. The overall control structure for the STATCOM in the rotating d-q reference frame is shown in Figure 3-5.

### Chapter 3: STATCOM with SuperCapacitor Energy Storage System

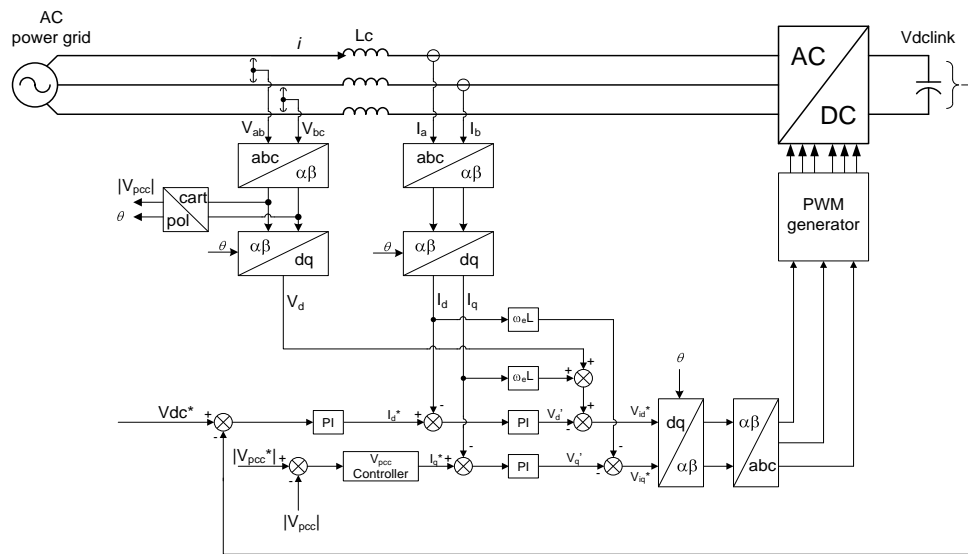


Figure 3-5: Control structure of a STATCOM in the rotating d-q reference frame

Three main control loops were designed for the STATCOM- the inner current control loop and the outer DC-link voltage control and PCC voltage control loops. The controller structure is cascaded because the output of the DC-link voltage controller and PCC voltage controller are used to manipulate the reference value of the current control. Typically the inner current loops are ten times faster than the outer loop. The current control loop will be employed to control  $I_d$  and  $I_q$  according to the desired active and reactive power demand. The current controller will determine the demand values used for the calculation of the PWM reference voltages. The DC-link voltage control loop regulates the DC-link voltage during the operation of the STATCOM in order to allow the current control to operate in the linear region. The DC-link voltage controller also sets the reference for the active power current to flow between the converter and the ac power grid. The PCC voltage controller regulates the voltage at the point of common coupling by setting the reference for the reactive power current to flow between the converter and the ac power grid.

### 3.3.2.1 Current control design

The plant for the current control loop design can be derived from the dynamic equations of the STATCOM. The dynamic equations are defined as follows [112].

$$\begin{aligned}V_a &= Ri_a + L \frac{di_a}{dt} + V_{sa} \\V_b &= Ri_b + L \frac{di_b}{dt} + V_{sb} \\V_c &= Ri_c + L \frac{di_c}{dt} + V_{sc}\end{aligned}\quad (3-1)$$

Applying the d-q transformation described in appendix A to Equation (3-1), gives:

$$\begin{aligned}V_d &= Ri_d + L \frac{di_d}{dt} - \omega_e Li_q + V_{sd} \\V_q &= Ri_q + L \frac{di_q}{dt} + \omega_e Li_d + V_{sq}\end{aligned}\quad (3-2)$$

Where:

$V_d$ = Supply voltage: d-axis component

$V_q$ = Supply voltage: q-axis component

$i_d$  = Line current: d-axis component

$i_q$ = Line current: q-axis component

$V_{sd}$ =STATCOM output voltage: d-axis component

$V_{sq}$ =STATCOM output voltage: q-axis component

$R$ =Total resistance per phase

### Chapter 3: STATCOM with SuperCapacitor Energy Storage System

$L$ =Total inductance per phase

$\omega$  =Angular frequency of the rotating reference frame

If the d-axis of the reference frame is aligned to the grid voltage vector, Equation (3-2) can be written as:

$$\begin{aligned} V_d &= Ri_d + L \frac{di_d}{dt} - \omega_e Li_q + V_{sd} \\ 0 &= Ri_q + L \frac{di_q}{dt} + \omega_e Li_d + V_{sq} \end{aligned} \quad (3-3)$$

To control the d and q axis currents, the STATCOM has to produce associated output voltages according to the reference voltage signals determined from Equation (3-3). The associated output voltages are given as:

$$\begin{aligned} V_{sd}^* &= -V_d' + (\omega_e Li_q + V_d) \\ V_{sq}^* &= -V_q' - (\omega_e Li_d) \end{aligned} \quad (3-4)$$

Noting that,

$$\begin{aligned} V_d' &= Ri_d + L \frac{di_d}{dt} \\ V_q' &= Ri_q + L \frac{di_q}{dt} \end{aligned} \quad (3-5)$$

Equation (3-5) is given in the s –domain as:

$$\begin{aligned} V_d'(s) &= Ri_d(s) + sLi_d(s) \\ V_q'(s) &= Ri_q(s) + sLi_q(s) \end{aligned} \quad (3-6)$$

The current controller will determine the voltage demand values  $V_d'$  and  $V_q'$  which are used to calculate the PWM reference voltages in Equation (3-4).

The plant  $G_p(s)$  for the current loop design control can be derived as follows:

$$G_p(s) = \frac{i_d(s)}{v_d(s)} = \frac{i_q(s)}{v_q(s)} = \frac{1}{sL + R} \quad (3-7)$$

### Chapter 3: STATCOM with SuperCapacitor Energy Storage System

A coupling reactor  $L_c = 10\text{mH}$  with  $R = 0.1\Omega$  was used in the design of the PI controller for the current control loop. The block diagram of the current control loop is shown in Figure 3-6, where  $I$  represents the d-axis and q-axis current ( $I_d$  and  $I_q$ ) and  $V'$  represents the voltage reference  $V_d'$  and  $V_q'$ . An anti-aliasing filter with a cut-off frequency of 1500Hz is used to remove the high frequency switching noise. A 5 kHz switching frequency is used and this is also used as the sampling frequency.

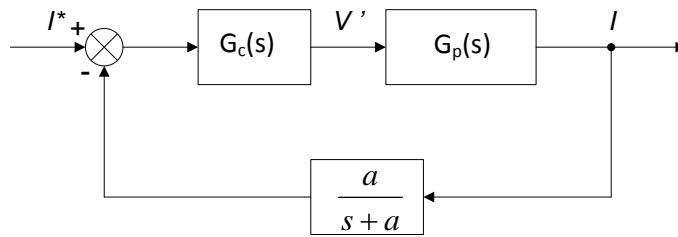


Figure 3-6: Closed loop block diagram for the current control

A standard control design procedure can be carried out with the block diagram. The control loop was designed with the MATLAB SISO tool box with a damping ratio of 0.7 and a closed loop bandwidth of 110Hz. The resulting current controller  $G_c(s)$  is given in Equation (3-8).

$$G_c(s) = 4.87 \left( \frac{s + 256}{s} \right) \quad (3-8)$$

For digital control, the controller transfer function in s-domain as in Equation (3-8) is converted using MATLAB bilinear (Tustin) approximation with a sampling time of 200μseconds. The controller in the z-domain is given in Equation (3-9).

$$G_c(z) = 4.99 \frac{(z - 0.953)}{z - 1} \quad (3-9)$$

### 3.3.2.2 DC-link voltage control design

The equivalent circuit of the STATCOM in the d-q reference frame is shown in Figure 3-7.

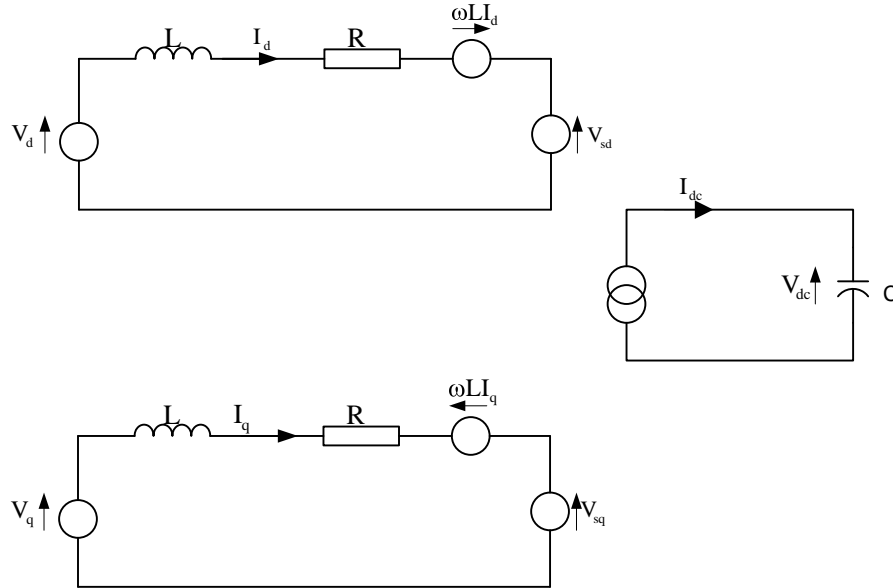


Figure 3-7: Equivalent circuit diagram of the STATCOM in the d-q reference frame

The value of the DC-link voltage is dependent on the instantaneous power flowing between the grid and the converter. The supply and the six switching devices of the STATCOM are considered to be a current source to the DC-link capacitor and  $I_{dc}$  is the current flowing from the current source.

Assuming all the losses (line resistance losses, DC-link losses and switching losses) are neglected, the current flowing from the current source is given as:

$$I_{dc} = 3 \frac{V_d I_d + V_q I_q}{V_{dc}} = C \frac{dV_{dc}}{dt} \quad (3-10)$$

As mentioned earlier, if the d-axis of the reference frame is aligned with the supply voltage vector,  $V_q$  is zero and  $V_d$  is a constant. Equation (3-10) can be re written as:

### Chapter 3: STATCOM with SuperCapacitor Energy Storage System

$$I_{dc} = 3 \frac{V_d I_d}{V_{dc}} = C \frac{dV_{dc}}{dt} \quad (3-11)$$

The modulation index (m) is a ratio relating the supply voltage to the DC-link voltage.

$$m = \frac{2\sqrt{2} * V_d}{V_{dc}} \quad (3-12)$$
$$V_d = \frac{m * V_{dc}}{2\sqrt{2}}$$

Substituting Equation (3-12) into Equation (3-11)

$$I_{dc} = 3 \frac{m * V_{dc} * I_d}{2\sqrt{2} * V_{dc}} = C \frac{dV_{dc}}{dt} \quad (3-13)$$
$$I_{dc} = 3 \frac{m * I_d}{2\sqrt{2}} = C \frac{dV_{dc}}{dt}$$

Equation (3-13) is given in the s –domain as:

$$I_{dc} = \frac{3 * m}{2\sqrt{2}} * I_d(s) = sC V_{dc}(s) \quad (3-14)$$

The plant  $G_p(s)$  for the voltage loop design control can be derived as follows:

$$G_p(s) = \frac{V_{dc}(s)}{I_d(s)} = \frac{3m}{2\sqrt{2} * sC} \quad (3-15)$$

The block diagram of the DC-link voltage control loop is shown in Figure 3-8. An anti-aliasing filter with a cut-off frequency of 120 Hz is used to remove the high frequency switching noise. The cut-off frequency is chosen with a compromise between the speed of the dynamic response of the controller and the filtering of high frequency switching noise. A capacitor with  $C=1000\mu\text{F}$  was used in the design of the PI controller for the voltage control loop.

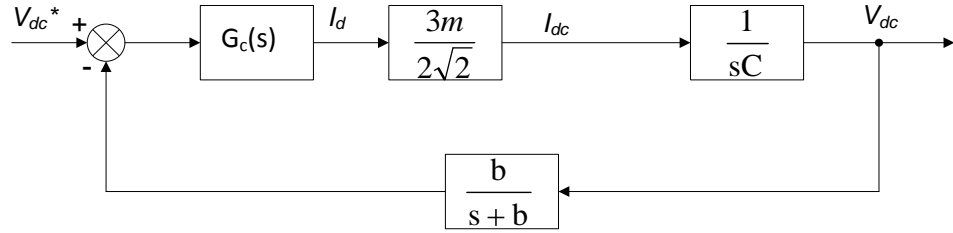


Figure 3-8: Closed loop block diagram for the voltage control

A standard control design procedure can be carried out with the block diagram. The control loop was designed with the MATLAB SISO tool box with a damping ratio of 0.7 and a closed loop bandwidth of 10Hz. The resulting DC-link voltage controller  $G_c(s)$  is given in Equation (3-16).

$$G_c(s) = 0.041 \left( \frac{s + 20}{s} \right) \quad (3-16)$$

For digital control, the controller transfer function in s-domain as in Equation (3-16) is converted using MATLAB bilinear (Tustin) approximation with a sampling time of 200μseconds. The controller in the z –domain is given in Equation (3-17)

$$G_c(z) = 0.041 \frac{(z - 0.996)}{z - 1} \quad (3-17)$$

As mentioned earlier, the conventional STATCOM can be used to compensate for reactive power dynamically in an AC power system. However, its real power compensating capability is limited due to the small amount of energy stored in the DC-link capacitor. The performance of the STATCOM can be enhanced by integrating an energy storage system into the STATCOM.

In the next section, the operation and control of the energy storage technology employed in enhancing the performance of the STATCOM is described.

### **3.4 SuperCapacitor Energy Storage System**

As described in section 3.3, the real power capabilities of the standard STATCOM is limited due to the limited energy stored in its conventional DC-link capacitor. The integration of supercapacitor as the main energy storage will enhance the performance and real power capabilities of the STATCOM. However, connecting the supercapacitor directly to the DC-link of the STATCOM will affect the performance of the STATCOM during real power injection.

During real power injection, the supercapacitor will discharge energy and as a result the supercapacitor voltage will drop. Consequently the DC-link voltage will drop when energy is injected to the ac power grid. If the DC-link voltage drops to a level lower than the ac-side line-line peak voltage value, the operation of the STATCOM will be stopped. It is imperative to keep the DC-link voltage constant when energy is exported to the grid.

To keep the DC-link voltage constant, a bi-directional dc-to-dc converter is interfaced between the DC-link of the STATCOM and the supercapacitor. The transfer of energy from the supercapacitor to the ac power grid and from the ac power grid to the supercapacitor can be regulated by controlling the dc-to-dc-converter. The bi-directional flow of power between the supercapacitor and the DC-link capacitor is controlled through an inductor.

The DC-link capacitor, dc-to-dc converter, inductor and the supercapacitor make-up the SuperCapacitor Energy Storage System (SCESS). The power circuit diagram of the SCESS is shown in Figure 3-9.

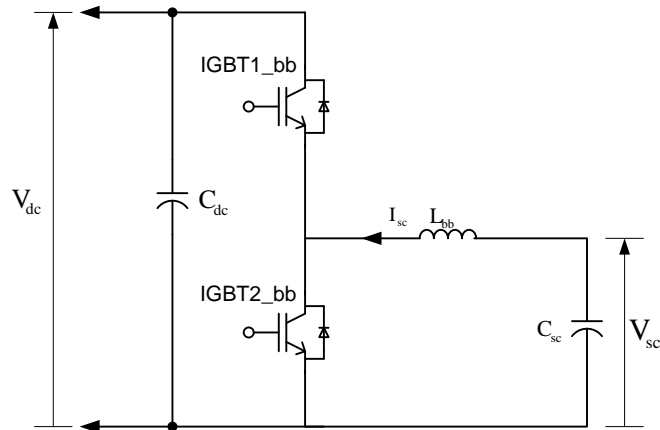


Figure 3-9: The power circuit diagram of the SCESS

In Figure 3-9,  $C_{dc}$  is an electrolytic capacitor. The dc-to-dc converter employs two IGBTs with anti-parallel diode  $D$  as its switching devices. The Inductor  $L_{bb}$  is used to control the bi-directional flow of power between the DC-link and the supercapacitor.  $C_{sc}$  is the supercapacitor unit. It consists of ten series connected supercapacitor modules. Each supercapacitor module is rated at 95F 20V 19kJ

### 3.4.1 Operation

As mentioned earlier, the transfer of energy from the supercapacitor to the ac power grid and from the ac power grid to the supercapacitor can be regulated by controlling the dc-to-dc- converter. This is achieved by operating the dc-to-dc converter in two modes. Energy is transferred from the supercapacitor to the ac power grid when the dc-to-dc converter operates in the boost mode while energy is transferred from the ac power grid to the supercapacitor when the dc-to-dc converter operates in the buck mode.

### 3.4.1.1 Buck operation (Charging of the supercapacitor)

The transfer of energy from the grid to the supercapacitor is regulated by turning on and turning off IGBT1\_bb. According to the power circuit diagram shown in Figure 3-10,

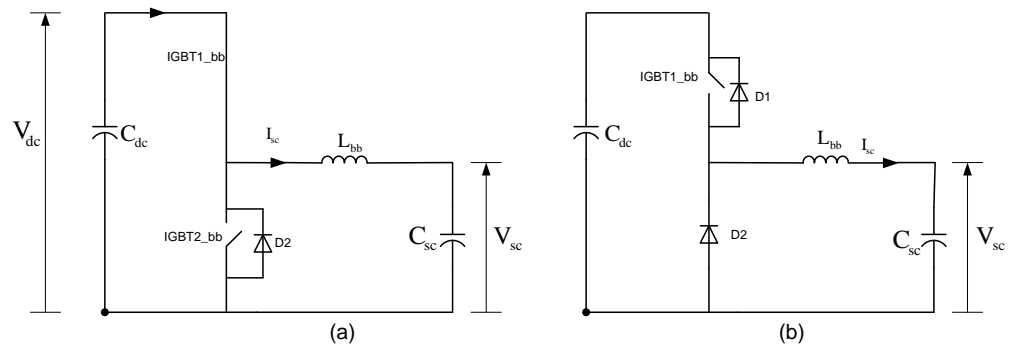


Figure 3-10: SCESS buck mode circuit

When IGBT1\_bb is turned on as shown in (a), the energy from the grid is transferred from the DC-link capacitor ( $C_{dc}$ ) to the buck-boost inductor ( $L_{bb}$ ) with the flow of  $I_{sc}$ . The energy is stored in the inductor as magnetic energy. When IGBT1\_bb is turned off as shown in (b), the induced back emf across  $L_{bb}$  causes D2 to conduct allowing  $L_{bb}$  to release the stored energy to the supercapacitor ( $C_{sc}$ ). The transfer of energy from the DC-link to the supercapacitor is controlled through the duty cycle of IGBT1\_bb. The supercapacitor voltage is regulated in this mode. However, if the supercapacitor voltage reaches the maximum limit, the charging process will stop.

### 3.4.1.2 Boost operation (utilising energy stored)

The transfer of energy from the supercapacitor to the power grid is regulated by turning on and turning off IGBT2\_bb. According to the power circuit diagram in Figure 3-11,

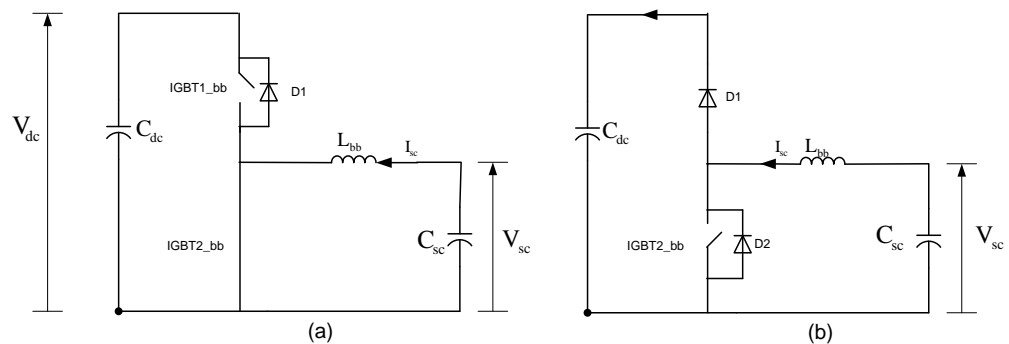


Figure 3-11: SCESS boost mode circuit

When IGBT2\_bb is turned on as shown in (a), the energy stored in the supercapacitor ( $C_{sc}$ ) is transferred to the buck-boost inductor ( $L_{bb}$ ) with the flow of  $I_{sc}$ . When IGBT2\_bb is turned off as shown in (b), the induced back emf across  $L_{bb}$  causes D1 to conduct allowing  $L_{bb}$  to release the stored magnetic energy to the DC-link capacitor and consequently the grid. The transfer of energy from the supercapacitor to the DC-link can be controlled through the duty cycle of IGBT2\_bb. The optimum point where the stored energy can be extracted from the supercapacitor is at a duty ratio of 0.5. During the boost mode of operation, the DC-link voltage is kept constant at its rated voltage. This is applicable during real power injection where constancy of the DC-link voltage is essential.

The supercapacitor voltage will drop to 0V if all the stored energy is utilised. This will affect the stability and efficiency of the operation of the dc-to-dc converter. A threshold needs to be set to ensure stable operation of the dc-dc converter. A reasonable minimum value for the supercapacitor voltage is 50% of the maximum value if 75% of the energy is to be utilised.

### 3.4.2 Control Strategies

Two control strategies can be employed for the control of the dc-to-dc converter. They are voltage mode control and current mode control.

In the voltage mode control, the amount of energy to be stored or utilised is controlled by the voltage error signals. During the buck operation, the supercapacitor voltage error is used to generate the gating signal required to control the switching device. During the boost operation, the DC-link voltage error is used to generate the signal for the switching device. As mentioned earlier, the amount of energy exchanged between the supercapacitor and DC-link capacitor is dependent on the inductor current. This control strategy does not control the inductor current directly. It is essential to implement a control strategy that can control the inductor current directly. The current control strategy offers the possibility of controlling the inductor current directly. The control structure of the current mode control is shown in Figure 3-12

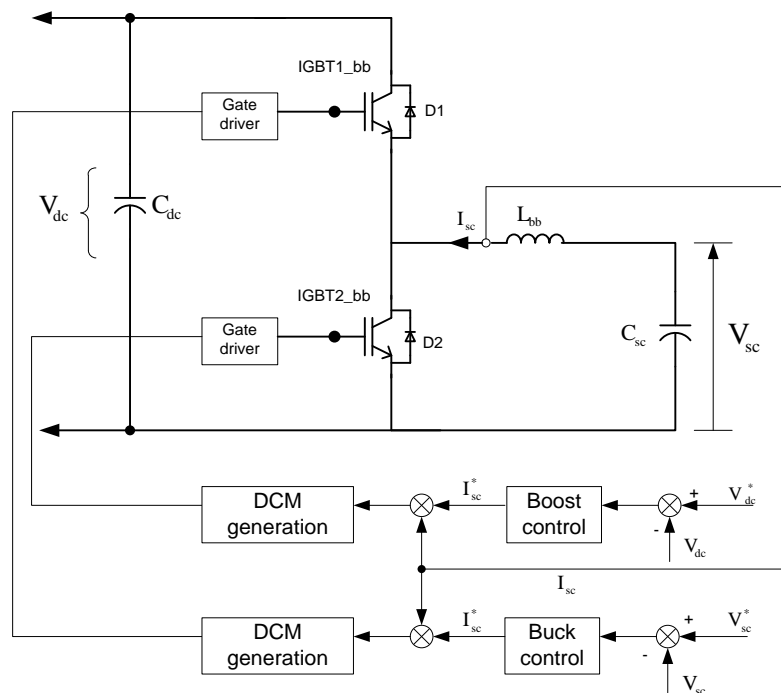


Figure 3-12: Current mode control structure

In the current mode control, the amount of energy to be stored or utilised is controlled by the current error signals. During the buck operation, the supercapacitor voltage error is used to provide the reference value for the inductor current ( $I_{sc}^*$ ). During the boost operation, the DC-link voltage error is used to set the reference value for the inductor current. The inductor current errors are then used to generate the gating signals required to control the switching devices. The current mode control strategy provides fast direct control over the energy transferred between the supercapacitor and the DC-link capacitor.

### 3.4.2.1 Buck mode control design

The buck mode control block diagram is shown in Figure 3-13. The outer loop controls the supercapacitor voltage while the inner loop uses state equations to calculate the duty cycle.

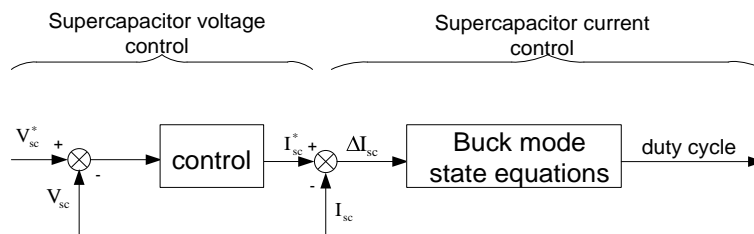


Figure 3-13: Buck mode control block diagram

The inner loop controls the supercapacitor current according to the reference from the supercapacitor voltage control. The outer loop gives a reference for the desired buck current. The duty cycle for the buck converter operation is calculated by using Equation (3-19) as a form of predictive control.

$$d_{\text{buck}} = \frac{L\Delta I + V_{sc}}{V_{\text{dclink}}} \quad (3-19)$$

### 3.4.2.2 Boost mode control design

The boost mode control block diagram is illustrated in Figure 3-14. The outer loop controls the DC-link voltage while the inner loop controls the inductor current required for the boost mode operation.

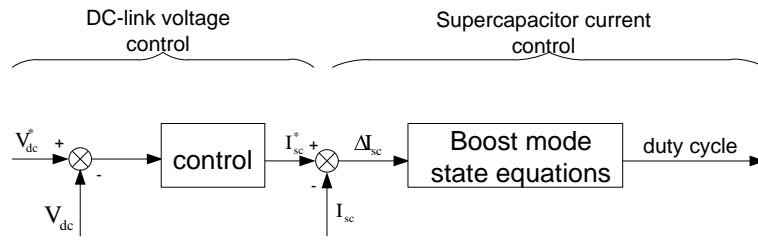


Figure 3-14: Boost mode control block diagram

The inner loop controls the supercapacitor current according to the reference from the DC-link voltage control until the supercapacitor voltage reaches a minimum value. The duty cycle for the boost converter is calculated by using Equation (3-20) as a form of predictive control.

$$d_{\text{boost}} = \frac{L\Delta I - V_{\text{sc}}}{V_{\text{dclink}}} + 1 \quad (3-20)$$

where,

$V_{\text{sc}}$  is the supercapacitor voltage, V.

$V_{\text{dclink}}$  is the dc link voltage, V.

$\Delta I$  is the change in the inductor current, A.

$L$  is the boost inductor, H.

The derivation of the buck and boost mode state equations are discussed in detail in Appendix C.

### 3.5 STATCOM with SCESS

The integration of supercapacitor energy storage system with the STATCOM provides solutions to problems of transient and dynamic instability within an ac power network. The power circuit diagram of the STATCOM with SCESS is illustrated in Figure 3-15.

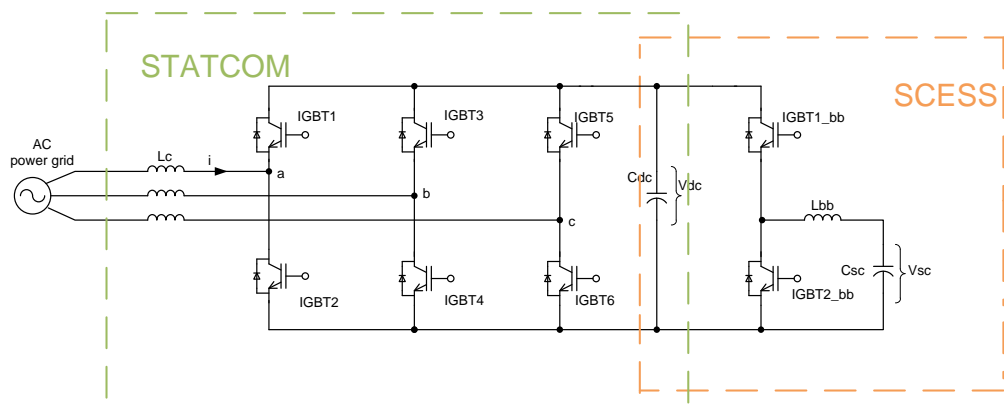


Figure 3-15: The power circuit diagram of the STATCOM with SCESS

The control structure of the STATCOM with SCESS is a combination of the STATCOM control described in section 3.3.2 and the control of the SCESS described in section 3.4.2. The overall control structure of the STATCOM with SCESS is shown in Figure 3-16. The operation and control of STATCOM with SCESS can be classified into three main modes- STATCOM only mode, STATCOM with SCESS boost mode and STATCOM with SCESS buck mode.

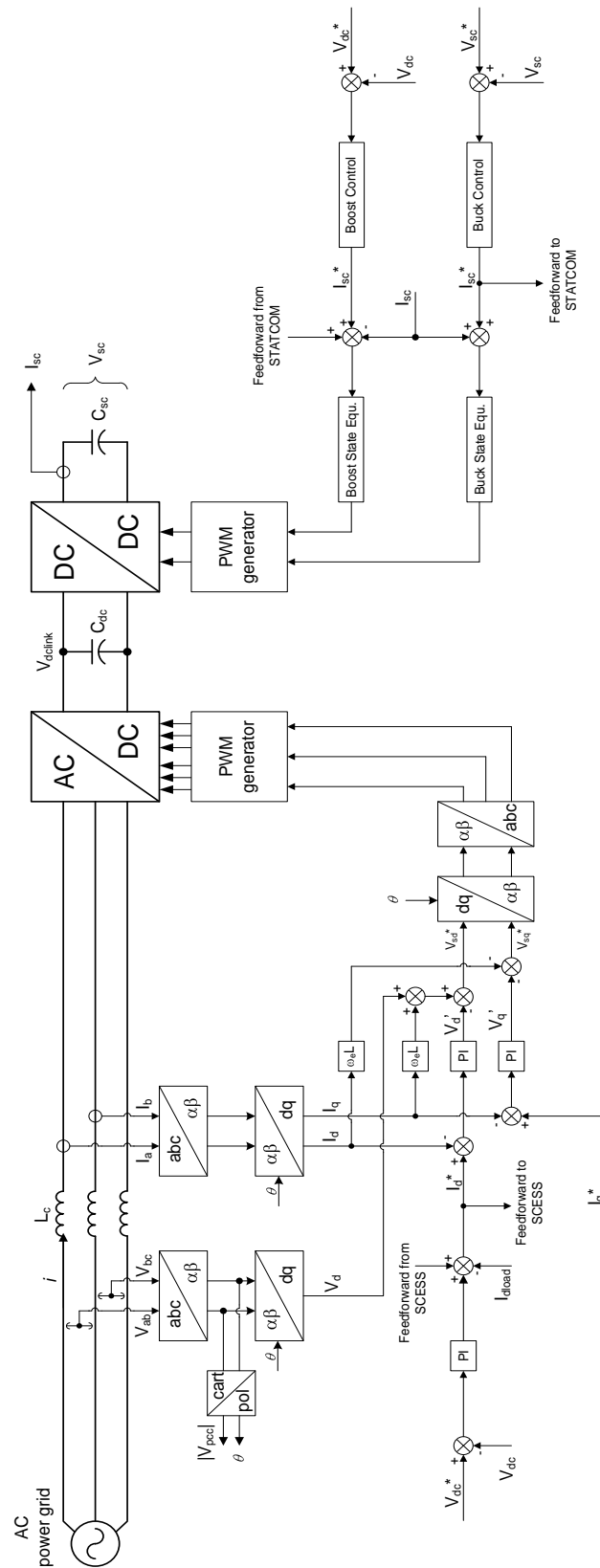


Figure 3-16: Control structure of STATCOM with SCESS

### **3.5.1 STATCOM only mode**

In this mode, The STATCOM exhibits its reactive power compensation capabilities. Reactive power control is achieved by controlling the magnitude of the STATCOM's output voltage. During the injection of reactive power, the DC-link voltage is kept constant by drawing real power from the ac power grid. The constancy of the DC-link voltage is regulated by the DC-link voltage controller.

### **3.5.2 STATCOM with SCESS boost mode**

In this mode, the STATCOM with SCESS exhibits its real and reactive power compensation capabilities. The STATCOM's DC-link voltage control is disabled to prevent the DC-link voltage of the SCESS and the DC-link control of the STATCOM from opposing each other. As a result, only the SCESS's DC-link voltage control is enabled to regulate the transfer of energy from the supercapacitor to the DC-link. The SCESS DC-link control also keeps the DC-link voltage constant at its demand level. The amount of energy to be transferred from the supercapacitor modules to the ac grid during a system disturbance is quantified as a feedforward current measurement from the grid event.

### **3.5.3 STATCOM with SCESS buck mode**

In this mode, real power is drawn from the grid via the operation of the DC-link voltage controller of the STATCOM. The DC-link voltage control also regulates the DC-link voltage. Power is transferred from the ac power grid to the DC-link. The transfer of power from the DC-link to the supercapacitor modules is regulated by the SCESS's supercapacitor voltage control. The amount of power to be absorbed from the ac grid is quantified as the

feedforward current used in the STATCOM current control. The feedforward current can be obtained from the supercapacitor charge current.

### 3.6 Simulation Study

A case study scenario with the power circuit diagram shown in Figure 3-17 is simulated to show the reactive and real power capabilities of the STATCOM with SCESS.

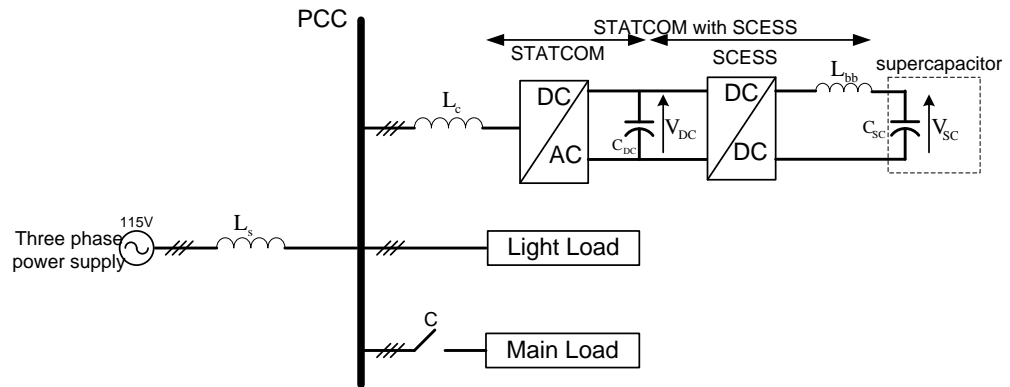


Figure 3-17: Power circuit diagram of the simulated system

The focus of the study is to verify that the STATCOM with SCESS can provide reactive and real power support to an ac power grid during system disturbances. A simulation based on the power circuit diagram shown in Figure 3-17 was devised using MATLAB/ Simulink software package and all the power circuit component models can be found in the sim power system blockset.

The main components of a STATCOM with SCESS are the STATCOM and the supercapacitor based energy storage system (SCESS). A STATCOM consists of a coupling inductor ( $L_c$ ), a voltage source DC-AC inverter and a DC-link capacitor ( $C_{DC}$ ) usually an electrolytic capacitor. The SCESS consists of the supercapacitor ( $C_{SC}$ ), a buck-boost inductor ( $L_{bb}$ ) and a bi-directional DC-DC buck-boost converter. An additional inductor ( $L_s$ ) is connected

### Chapter 3: STATCOM with SuperCapacitor Energy Storage System

between the supply and the point of common coupling (PCC) in order to highlight the voltage drop due to the load current. The light load represents the quiescent system load. The main load causes a sudden change in the load current which consequently results in a voltage drop at the PCC and a change in real power demand.

Table 3-1 summarizes the circuit parameters used in the simulation study.

Symbol	Description	Nominal value
$V_s$	Grid voltage	115 V
$f$	Grid frequency	50Hz
$L_s$	Supply inductance	5mH
$L_c$	Coupling inductance	10mH
$L_{bb}$	Buck-boost inductance	10mH
$V_{DC}$	DC-link voltage	400V
$V_{SC}$	Supercapacitor voltage	200V
$C_{SC}$	Supercapacitor value	9.5F
$C_{DC}$	DC-link capacitor value	1000 $\mu$ F
$T_{step}$	Main load step change time	1 sec

Table 3-1: Simulation parameters

## Chapter 3: STATCOM with SuperCapacitor Energy Storage System

Three scenarios are considered in the simulation study. The first scenario is the simulation of the system without the STATCOM. The second scenario is the simulation of the system with the STATCOM. The third scenario is the simulation of the system with the combined STATCOM and SCESS.

### 3.6.1 Simulation without the STATCOM

To show the reactive power capabilities of the STATCOM, it is worthwhile to carry out a simulation of the power circuit diagram shown in Figure 3-17 without the STATCOM. The results obtained from the simulation are shown in Figure 3-18 and Figure 3-19.

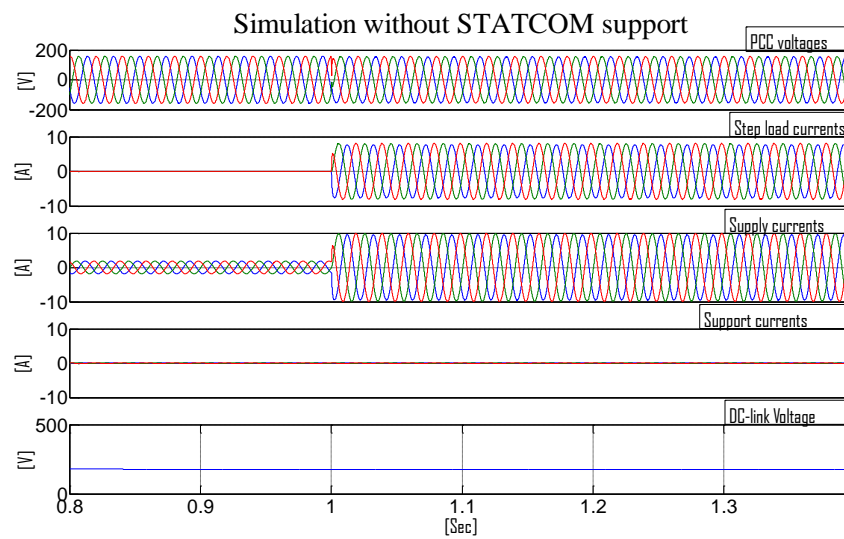


Figure 3-18: PCC voltage, step load current, supply current, support current and DC-link voltage without STATCOM support.

### Chapter 3: STATCOM with SuperCapacitor Energy Storage System

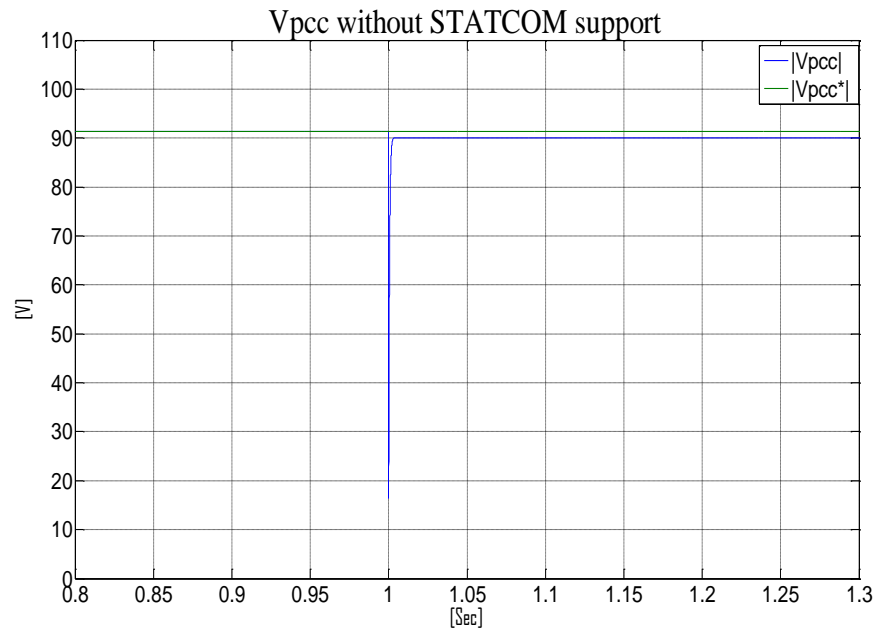


Figure 3-19:|Vpcc| of the system without STATCOM support

In Figure 3-18, a supply current of approximately 1.8A as shown in third trace is seen to flow across the light load from the start of the simulation until time  $t=1$  sec. At  $t=1$ sec, the main load is turned on by closing the contactor (c). A sudden change in the supply current (from 1.8A to 10A) can be seen in the third trace. A step load current of approximately 8A can be seen on the second trace. The DC-link voltage remains at 200V as no power is drawn from the DC-link.

The voltage at the point of common coupling ( $V_{pcc}$ ) drops as shown in the top trace of Figure 3-18. Its magnitude can be clearly seen in Figure 3-19. The drop in  $V_{pcc}$  suggest that there is a voltage drop across the system line inductance ( $L_s$ ) relating to the load current drawn from the 3-phase power supply.

### 3.6.2 Simulation of the system with the STATCOM

The reactive power capabilities of the STATCOM will be demonstrated by carrying out a simulation of the power circuit diagram shown in Figure 3-17 with a STATCOM connected to the PCC.

The simulation results are shown in Figure 3-20 and Figure 3-21 .

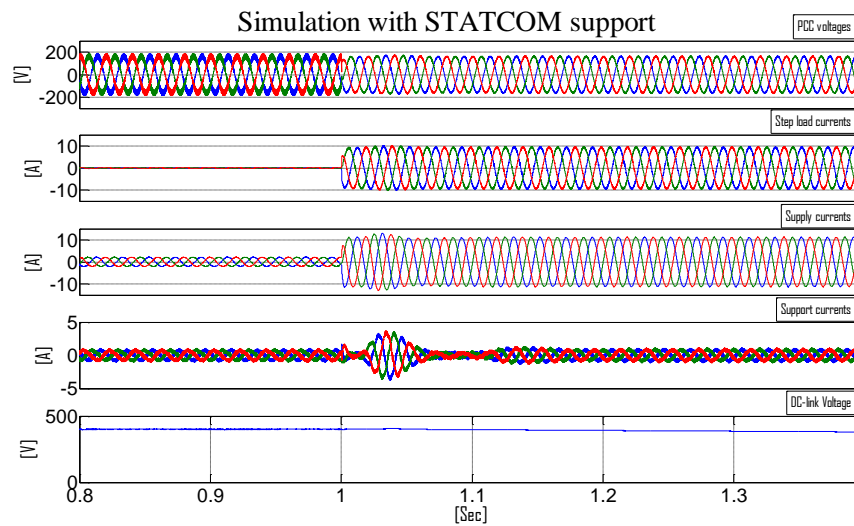


Figure 3-20: PCC voltage, step load current, supply current, support current and DC-link voltage with STATCOM support

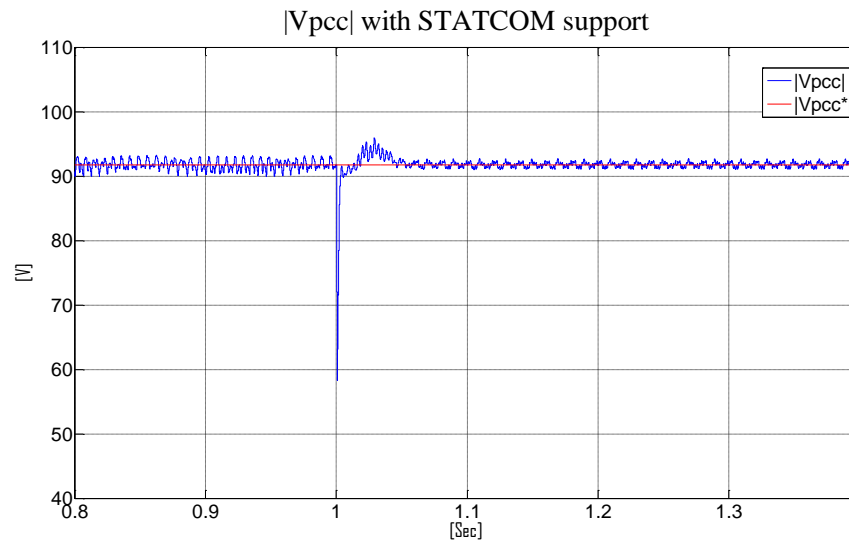


Figure 3-21:|Vpcc| of the system with STATCOM support

The STATCOM is connected to the system at  $t = 0.5$ sec. As a result, the DC-link voltage shown in the bottom trace of Figure 3-20 is regulated reasonably to the demand value of 400V. A noticeable support current can be seen in the 4<sup>th</sup> trace of Figure 3-20. This support current is the reactive power generated by the STATCOM. A comparison of the magnitude of the PCC voltage obtained from the simulation of the system without the STATCOM (Figure 3-19) and simulation of the system with the STATCOM (Figure 3-21) shows that the PCC voltage is regulated when the STATCOM is connected to the system.

It can also be seen from the third trace of Figure 3-20 that the real power demand by the load is supplied solely by the 3-phase power supply. If the supply was a generating set, the prime mover will not be able to react to the load change quickly and this will result in the variation in the speed and frequency of the supply.

The aforementioned verifies that the conventional STATCOM can only provide reactive power support to an ac power system. However, the STATCOM can provide both real and reactive power by adding a SCESS to the STATCOM.

### 3.6.3 Simulation of the system with the combined STATCOM and SCESS

The real and reactive power capabilities of the STATCOM with the SCESS will be demonstrated by carrying out a simulation of the power circuit diagram shown in Figure 3-17 with a STATCOM combined with SCESS connected to the PCC. The results from the simulation will be compared with the system described in section 3.6.2 (Simulation of system with the STATCOM only).

The simulation results from the STATCOM combined with SCESS are shown in Figure 3-22 and Figure 3-23.

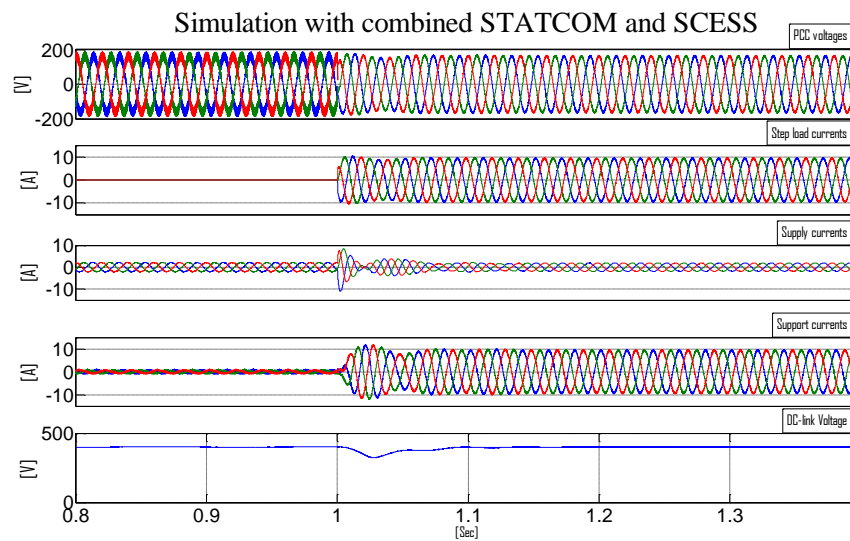


Figure 3-22: PCC voltage, step load current, supply current, support current and DC-link voltage with combined STATCOM and SCESS

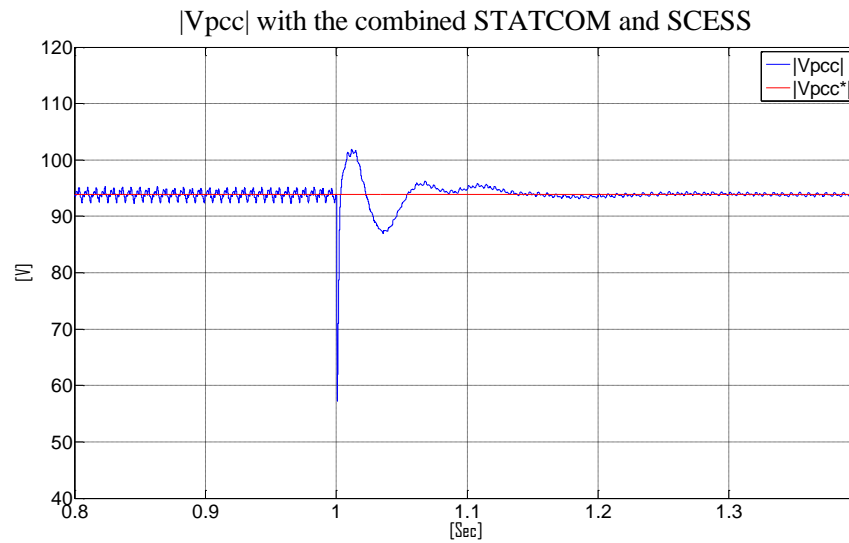


Figure 3-23:  $|V_{pcc}|$  of the system with the combined STATCOM and SCESS

As shown in Figure 3-22 , the system operates as a conventional STATCOM from the start of the simulation until  $t=1\text{sec}$ . A supply current of approximately 1.8A as shown in third trace of Figure 3-22 is seen to flow across the light load from the start of the simulation until time  $t=1\text{sec}$ . The DC-link voltage shown in the bottom trace of Figure 3-22 is regulated reasonably to the demand value of 400V.

At  $t=1\text{sec}$ , the main load is turned on by closing the contactor (c). A sudden step change in the main load current can be seen in the second trace of Figure 3-22. The main load current is measured and transformed to d-q components. The measured main load current is then used to trigger the STATCOM with SCESS. At the instance of the load change, a supply current of 9A as shown in the third trace of Figure 3-22 is seen between  $t= 1\text{sec}$  and  $t=1.03\text{sec}$  (settling time of the current control). The three phase supply provides the real power demand by the main load briefly until the support current from the STATCOM with SCESS unit takes full control. The DC-link voltage drops at the beginning of the load change and it is then regulated by the SCESS boost mode controller to the demand value of 400V.

### Chapter 3: STATCOM with SuperCapacitor Energy Storage System

The magnitude of the voltage at the point of common coupling ( $V_{pcc}$ ) is kept constant by the reactive power compensation from the STATCOM as shown in Figure 3-23. However, in comparison to Figure 3-21 the system response during the load change is worse. Although reactive power compensation was still achieved, the poor system response is due to the drop in DC-link voltage when the DC-link voltage controller is disabled and the boost controller is employed in regulating the DC-link voltage. The real power capabilities of the STATCOM with SCESS can be verified clearly by comparing the third and fourth traces of Figure 3-20 (simulation with STATCOM only) and Figure 3-22 (simulation of the system with the combined STATCOM and SCESS).

In Figure 3-20, the real power demanded by the main load is provided solely by the three phase supply as shown in the third trace (supply currents). The support currents shown in the fourth trace are the reactive currents provided by the STATCOM to keep the voltage constant during the load transient. In Figure 3-22, the supply currents seen on the third trace are small currents due to the light load connected to the system. The real power demanded by the main load is provided by the combined STATCOM and SCESS as shown in the fourth trace (support current). In order to supply the real power demanded by the main load, the STATCOM takes energy from the DC link until the SCESS starts to operate in the boost operating mode. The exportation of energy from the DC link results in a drop in the DC link voltage as shown in the bottom trace of Figure 3-22. This consequently causes an overshoot with some oscillations on the PCC voltage shown in Figure 3-23 and the d and q components of the support currents shown in Figure 3-25

The reactive power capabilities of the conventional STATCOM and the reactive and real power capabilities of the combined STATCOM and SCESS can also be verified by comparing the d and q components of the support currents shown in the third trace of Figure 3-20 and Figure 3-22.

### Chapter 3: STATCOM with SuperCapacitor Energy Storage System

The d and q components of the support currents for the simulation with the STATCOM only and the simulation with the combined STATCOM and SCESS are shown in Figure 3-24 and Figure 3-25 respectively.

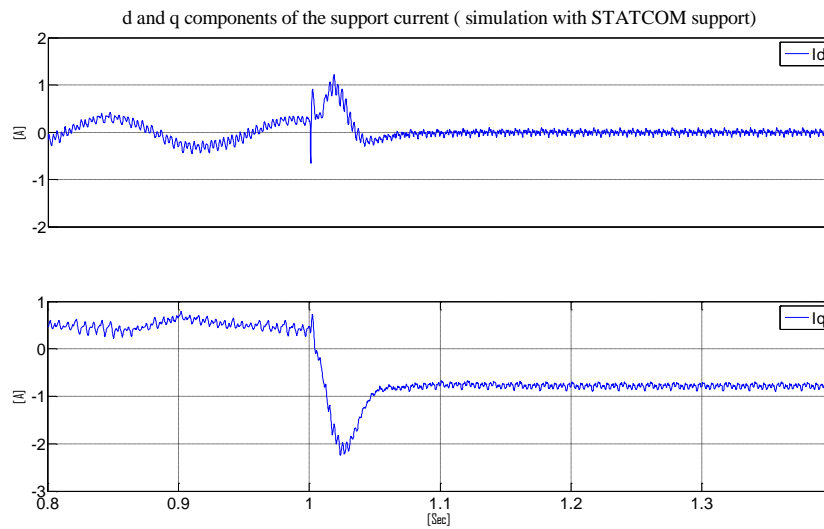


Figure 3-24: d and q components of the support currents (simulation of the system with STATCOM only)

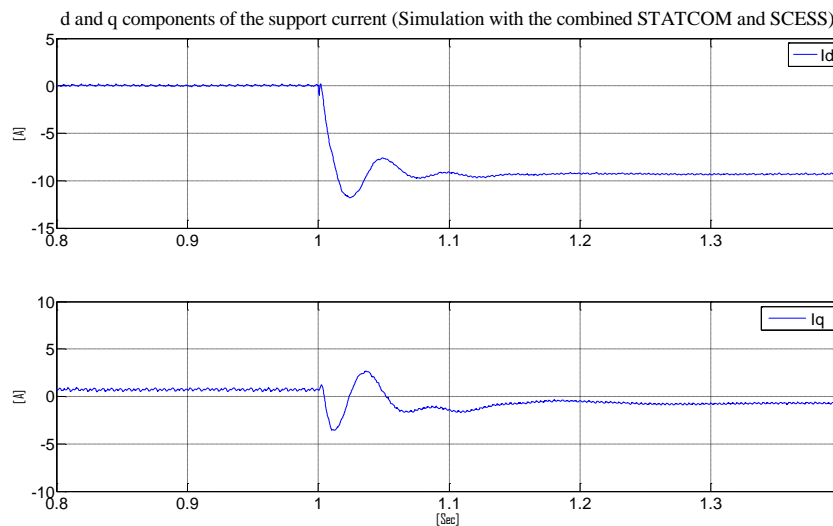


Figure 3-25: d and q components of the support currents (simulation of the system with combined STATCOM and SCESS)

### Chapter 3: STATCOM with SuperCapacitor Energy Storage System

In Figure 3-24, it can be clearly seen that a reactive power current ( $I_q$ ) of approximately -1A as shown in the second trace was injected to regulate the PCC voltage when the main load was connected to the system. The d-axis current ( $I_d$ ) is approximately zero as shown in the top trace. As expected the conventional STATCOM can only provide reactive power but not real power.

In Figure 3-25, it can be clearly seen that a real power current ( $I_d$ ) of approximately -10A as shown in the top trace was injected to meet the real power demanded by the main load when the main load was connected to the system. The negative  $I_d$  current indicates that real power is being transferred to the ac power grid to support the main load. The q-axis current ( $I_q$ ) is approximately -1A as shown in the bottom trace. The current is the reactive power current used for the voltage compensation at the point of common coupling.

## **3.7 Conclusion**

In this chapter, the role of grid connected converters in the enhancement of power system stability has been explored.

Reactive power compensation can be provided by static compensators (STATCOM). STATCOM employs a voltage source converter (VSC) which internally generates capacitive/inductive reactive power. The operation and control of a VSC based STATCOM has been explained. The control of the STATCOM based on the vector control strategy which provides fast independent control of active and reactive power was presented.

The real power capability of the conventional STATCOM is limited due to the limited energy stored in its DC-link capacitor. The performance of the STATCOM was enhanced by integrating a supercapacitor energy storage

### Chapter 3: STATCOM with SuperCapacitor Energy Storage System

system (SCESS) into the STATCOM. The operation and control of the STATCOM with SCESS has also been explained.

A simulation study highlighting the real and reactive power capabilities of the STATCOM with SCESS has been explained in detail. The simulation study verified that the STATCOM with SCESS can rapidly absorb/inject stored energy from/to the grid. The real power capabilities of the STATCOM with SCESS can be employed in power burst application such as frequency stabilization studies where rapid discharge of stored energy is required to compensate for frequency variation due to the slow response of generators.

In the next chapter, the origin of frequency variation and analysis of instability within an ac power system will be discussed. A simulation study showing the potential of the STATCOM with SCESS in enhancing power system stability will be explained in detail.

## Chapter 4

# Modelling of a weak grid

---

### 4.1 Diesel generating sets

Diesel generating sets (diesel gen-sets) consist of a diesel engine coupled to a synchronous machine. They are mainly used in power applications that have isolated power source requirements or in scenarios where sudden demands for back-up power are expected[113]. The most demanding application of gen-sets is when they provide a back-up power supply. The high efficiency and reliability of diesel engines have established their position in a wide range of industrial applications such as commercial vehicles, ships and electric power generators.

Modern gen-sets with high power density will have a lower inertia in comparison to traditional gen-sets. Since a gen-set's transient speed response



## **4.2 Internal Combustion Engines**

The purpose of internal combustion engines is the production of mechanical power from the chemical and thermal energy contained in the fuel. Energy is released by burning or oxidizing the fuel inside the engine [115, 116]. Internal combustion engines can be classified according to the type of fuel and the method of ignition. They can be broadly classified into spark ignition or gasoline engines and compression ignition or diesel engines based systems. In spark ignition engines, the air and fuel are usually mixed together in the intake system prior to entry to the engine cylinder, using a carburettor or a fuel injection system. The ignition of the compressed air fuel mixture is achieved by using a spark produced electronically. In compression ignition engines, air alone is inducted into the cylinder. The fuel will then be injected into the engine cylinder just before the combustion process is required to start. The liquid fuel evaporates and fuel vapour then mixes with air to within combustible proportions. The air temperature (800K) and pressure (4MPa) at this point will be above the fuel's ignition point therefore after a short delay period, spontaneous ignition of the fuel air mixture will initiate the combustion process [116]. Torque control is achieved by varying the amount of fuel injected in each cycle.

The majority of internal combustion engines operate on what is known as the four-stroke cycle. Each cylinder requires four strokes of its piston (two revolutions of the crankshaft) to complete the sequence of events which produce one power stroke. The entire cycle can be divided into four principal phases as the name suggests:

- Intake stroke
- Compression stroke
- Expansion stroke
- Exhaust stroke

During the intake stroke, the intake valve will be opened and fresh air will occupy the cylinder volume as the piston moves downward. In the compression stroke, the air in the cylinder is compressed by the piston moving

upwards. In this phase, both the intake and exhaust valves are closed. The compression process causes the temperature inside the cylinder to rise and when it is high enough to self-ignite the fuel; the injection of fuel into the cylinder will begin. After an ignition delay the fuel ignites. The fuel ignition causes the release of heat which expands the gases inside the chamber (expansion stroke). The rise in pressure forces the piston to move downward and provide the power for operating the engine. During the exhaust stroke, the upward motion of the piston forces the exhaust gases out of the cylinder via the exhaust valve which is opened.

### 4.3 Diesel engine model

An engine model that quantifies the major delays and relates the input fuel demand to the average torque that can be produced at the shaft can be used to represent the dynamic model of a diesel engine. An important feature of the diesel engine is the existence of a dead time between the actuator for fuel injection and the production of mechanical torque. The dead time is usually a function of operating conditions and engine speed. There are many methods already proposed for modelling a diesel gen-set. In this work, a similar approach to the simulation of diesel engines described in [117-121] has been adopted. For this application with narrow range of speed operation, a constant time delay is justifiable. The model of a typical diesel driven engine is shown in Figure 4-2.

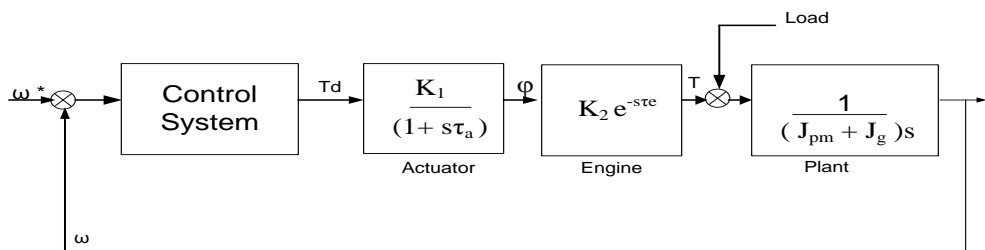


Figure 4-2: A typical diesel engine speed loop

#### Chapter 4: Modelling of a weak grid

It can be observed that the diesel engine model consists of four blocks which are:

- Control system ;
- Actuator ;
- Engine ;
- Plant.

The “control system” block represents the speed controller. This can be a conventional PI controller or a PID controller. The block computes the torque demand according to the error between the actual and desired engine speed and this can be translated to a fuel demand, as fuel controls output torque.

The “actuator” block represents the governor system of the diesel engine. The block precisely controls the fuel rack position  $T_d$  (throttle position) which in turn determines the amount of fuel ( $\phi$ ) to be injected into the combustion chamber. The block can be represented by a first order phase lag function which is characterized by a gain  $K_1$  and a time constant  $T_a$  [119].

The “engine” block represents the combustion system of the diesel engine. The injected fuel is ignited by the compressed hot air in the combustion chamber causing the movement of the piston during the power strokes. The movement of the piston drives the crankshaft and the mechanical torque ( $T$ ) is produced. The block is represented by a gain  $K_2$  and a dead time  $\tau_e$  that represents the time for fuel to burn and the generation of torque (combustion delay).

The “plant” block represents the approximation of the combined dynamic effect of the engine inertia and the generator’s inertia. They are represented as  $J_{pm}$  and  $J_g$  respectively.

## **4.4 Emulation of a diesel engine using a vector controlled induction motor**

The majority of generator models currently in use have been developed for use in power system stability studies such as those used in [114]. The order of complexity of the plant is reduced to ease the computational effort required to simulate a large network in power system stability models. This is especially due to the mechanical response of the prime mover. The reduction in the complexity of the model is based on the assumption that the frequency response is typically less pronounced and slower than the voltage response. An inherent feature of diesel engines is their low inertia structure [114, 119]. The low inertia makes diesel engines more susceptible to frequency variations during transient events.

It is not a practical option to have a diesel engine within the current laboratory set-up; however an emulation strategy of a diesel engine can be a viable alternative. The purpose of the emulation is to reproduce the dynamic response of a diesel generating set by using a vector controlled induction motor as the prime mover. For the research project, this was achieved experimentally by using a commercial electrical drive. In this section, the vector control theory will be explained briefly. Focus will be laid on the control of the induction motor (IM) only. The details and dynamic equations of the induction motor model can be found in literature [122, 123].

### **4.4.1 Vector control theory**

Vector control has become a powerful and frequently adopted technique in recent years. The implementation of vector control techniques has enabled induction motor drives to be used for high dynamic performance applications. Vector controlled induction motor drives have been developed to contend with dc drives for high performance applications[124]. The advantages of induction motors over traditional dc motors include simpler and cheaper mechanical

## Chapter 4: Modelling of a weak grid

structure and easy maintenance. The complicated control issues associated with adjustable speed drive applications of induction motor drives are solved by recent developments in the theory of field oriented control or vector control [125]. Vector control theory provides independent control between torque and flux in a similar way to the decoupled control of active and reactive power in the STATCOM.

Figure 4-3 shows the definition of the field oriented co-ordinate. The d-axis is coincident with the rotor flux ( $\psi_r$ ) and the q-axis is quadrature with it. The q-axis current component accounts for the IM torque current and the d-axis current accounts for the field producing current.  $i_{sq}$  and  $i_{sd}$  are called the torque and field producing currents only if the d-co-ordinate axis lies on  $\psi_r$ .

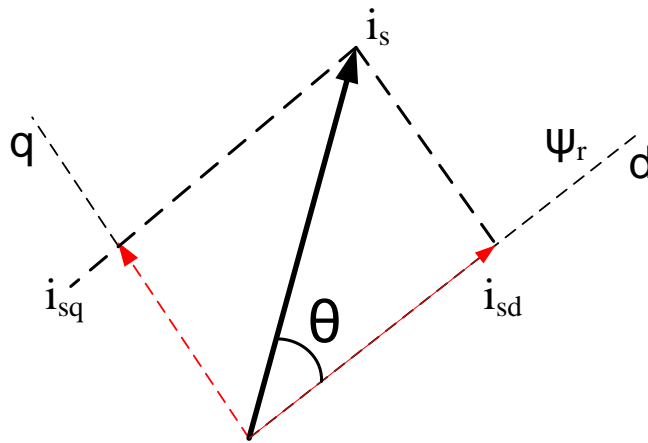


Figure 4-3: Definition of field oriented co-ordinates

$\psi_r$  is the rotor flux vector of IM and  $i_s$  is the stator current of the IM

The IM machine torque is

$$T = k (i_s * \psi_r) = k |i_s| |\psi_r| \sin \theta \quad (4-1)$$

When the d-axis of the co-ordinating reference frame lies on  $\psi_r$ , then the system is said to be field orientated (on the rotor flux).

Thus equation (4-1) can be rewritten as

## Chapter 4: Modelling of a weak grid

$$T = k |i_s| |\psi_r| \sin \theta = k(i_s \sin \theta) \psi_r = k i_{sq} \psi_{rd} \quad (4-2)$$

If,

$$\psi_{rd} = L_o i_{mrd} \quad (4-3)$$

$$T = k L_o i_{sq} i_{mrd} \quad (4-4)$$

If

$$k = \frac{3}{2} \left(\frac{P}{2}\right) \frac{L_o}{L_r} \quad (4-5)$$

Where,

P is the number of pole pairs

$L_o$  is the Magnetising inductance, (H)

$L_r$  is the Rotor inductance, (H)

$i_{mrd}$  is the magnetising current, (A)

Equation (4-4) can be rewritten as

$$T = \frac{3}{2} \left(\frac{P}{2}\right) \frac{L_o^2}{L_r} i_{sq} i_{mrd} \quad (4-6)$$

Vector control provides fast independent control in the induction motor and the induction motor machine torque in Equation (4-6) can be considered to be an ideal torque current.

### **4.4.2 Dynamic emulation of a diesel engine**

The instantaneous torque produced by a diesel engine usually depends on the thermodynamic processes taking place within the cylinder as well as the mechanical linkages that connect the cylinder to the crankshaft [126, 127]. In this research, focus will be placed on the use of a diesel engine to provide the input mechanical torque to the generator. The block diagram of the emulated system is shown in Figure 4-4.



#### Chapter 4: Modelling of a weak grid

A 22kW eurotherm commercial drive implementing field oriented control was employed as the drive to run the IM. In this research work, the drive was considered ideal and the running operation was set by following the instructions in the datasheet. An auto tuning procedure defines the internal DQ current control parameters and the required magnetizing current reference.

A 16kW two pole pair induction motor was used in this work. Details of the induction motor can be found in Table 4-1.

<b>Parameter</b>	<b>Value</b>
Nominal Speed	1500 RPM
Nominal Power	16 kW
Nominal Torque	102 Nm
Nominal Voltage	340V <sub>RMS</sub> line to line
Nominal Current	34 A
Magnetizing Current	16A
Nominal frequency	51.5Hz
Maximum speed	7000RPM
Phase resistance	0.1721Ω
Leakage inductance	3.025mH
Magnetic inductance	32.31mH
Rotor resistance	0.153Ω

Table 4-1: Magnetic MA 133 KF1 plate data.

### 4.4.3 Speed controller design

A block diagram of the prime mover's speed control is shown in Figure 4-6

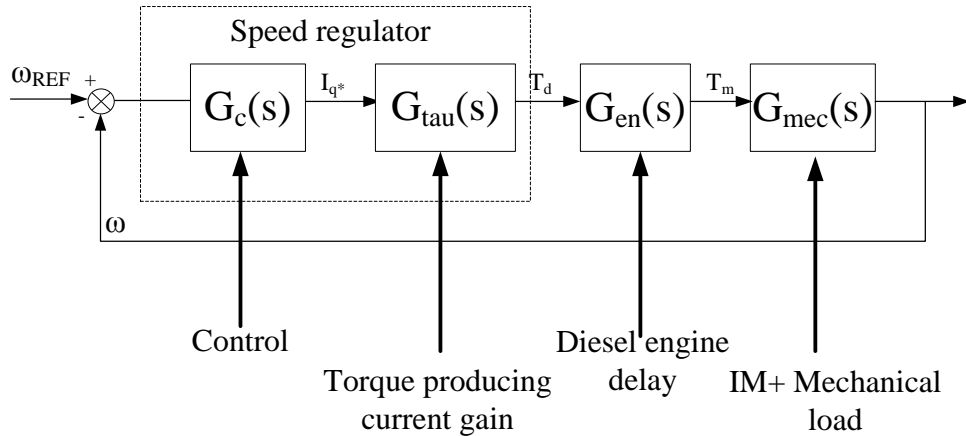


Figure 4-6: IM speed control loop

The ‘control’ block represents the actual speed controller which detects a speed error and creates an actuation signal accordingly. This can be a conventional PI controller or a PID controller. The “current gain” block converts the Q current produced by the speed control block into a torque value. The diesel engine has been represented by an “engine delay” block which would include delays to account for the operation of the throttle, the ignition time and the combustion delays associated with a diesel engine [117-120]. As mentioned earlier, the diesel engine is emulated with a vector controlled induction motor drive which acts as a “perfect” torque controller. A single delay is incorporated into its control to represent the main feature of the diesel generating set- the combustion delay.

The speed regulator sets the equivalent torque/throttle demand (q current demand) requested for the drive. This reference is then passed through a first order transfer function emulating the diesel engine delay. The output of the engine delay block is effectively the torque producing current that is sent to the IM drive. It is assumed that the inertia of the IM is comparable to a diesel engine.

#### Chapter 4: Modelling of a weak grid

The set of parameter values used in the control design are listed in Table 4-2.

Parameter	Value
Speed reference	1500 RPM
Mechanical inertia $J_m$	0.2 kg*m <sup>2</sup>
Mechanical Friction $B_m$	0.05 Nms/rad
Maximum power	8kW
Magnetizing current $I_d$	14.4A
Speed control sample frequency	250Hz
Diesel throttle to torque delay cut-off frequency(first order transfer function)	5Hz
Speed loop bandwidth	1.5Hz
Speed loop phase margin	60°

Table 4-2: Speed loop system parameters.

The control loop was designed using the MATLAB SISO (single input single output) toolbox [128] with the system parameters shown in Table 4-2. The resulting speed controller transfer function is given in equation (4-7).

$$G_c(s) = 1.351 \frac{(s + 3.7)}{s} \quad (4-7)$$

For digital control, the controller transfer function in s-domain as in equation (4-7) is converted using MATLAB bilinear (Tustin) approximation with a sampling time of 4ms. The controller in the z –domain is given in equation (4-8)

$$G_c(z) = 1.36 \frac{(z - 0.986)}{z - 1} \quad (4-8)$$

The Bode diagram and the corresponding response to a step demand are shown in Figure 4-7 and Figure 4-8 respectively.

## Chapter 4: Modelling of a weak grid

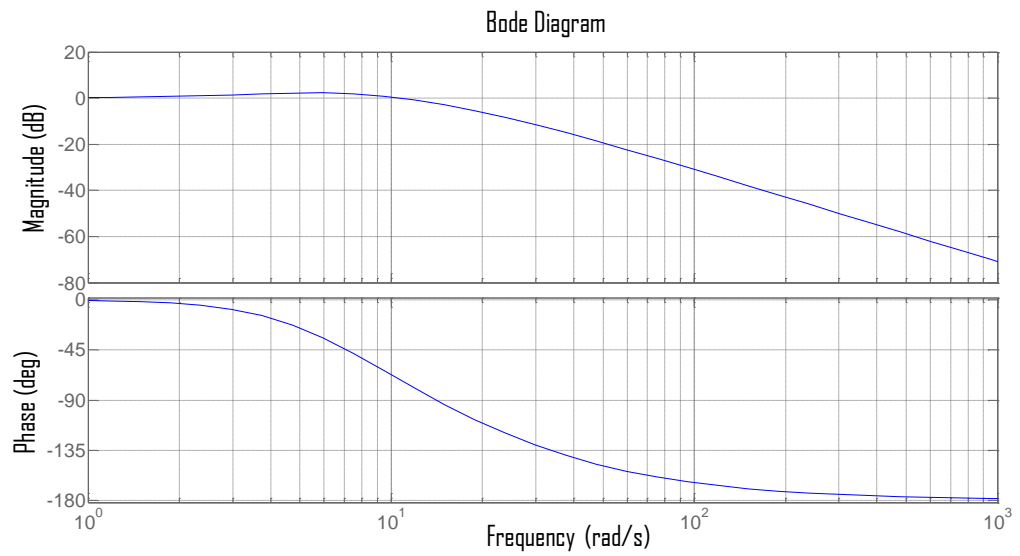


Figure 4-7: Closed-loop Bode diagram for the speed control system

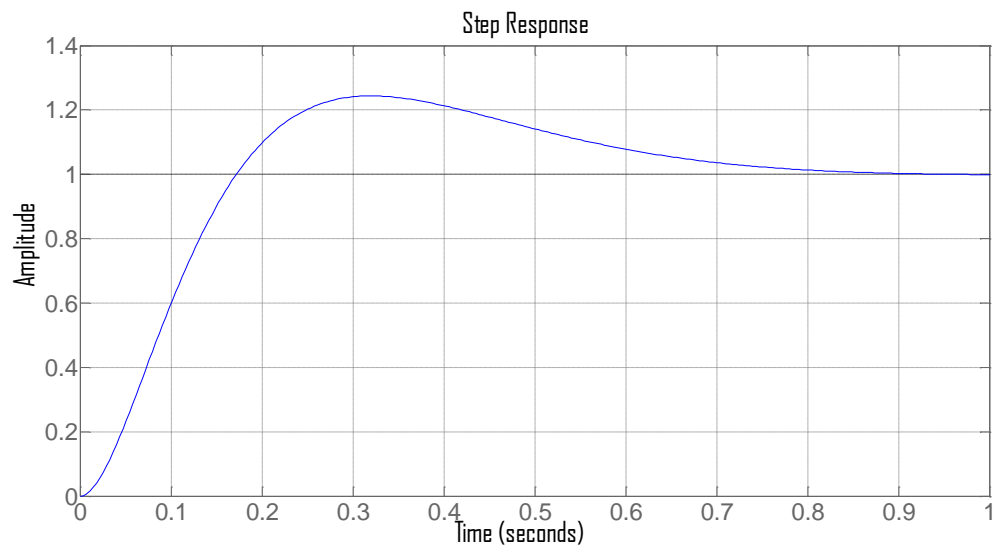


Figure 4-8: Closed-loop step response diagram

## 4.5 Analysis of instability and origin of frequency variation

The provision of reliable and uninterrupted services to the load is the main priority of an ac power system. An ac power system must be able to supply energy to meet the demand in the presence of system disturbances. An ac power system operating under this condition is called a stable system. Power system stability is the property of a power system that enables it to remain in a state of operating equilibrium under normal operating conditions and to regain an acceptable state of equilibrium after being subjected to a disturbance [129, 130].

Instability in an ac power system may be manifested in many different ways depending on the system configuration and operating mode. In the analysis of instability in an ac power system, it is important to understand the nature of conversion of mechanical input power of a generator to useful electrical power output and the behaviour of generators when subjected to transient disturbances. The response of the output power to the input demand is directly related to the response of the prime mover. During transient events, the balance between the input power and output power can be seen in the simplified relationship of the mechanical torque and electrical torque described by the rotational inertia equations (4-9), (4-10) and (4-11).

Assuming that the losses are ignored,

$$T_a = T_m - T_e \quad (4-9)$$

Where

$T_a$  is the accelerating torque, N·m

$T_m$  is the input mechanical generator torque, N·m

$T_e$  is the output electrical torque, N·m

## Chapter 4: Modelling of a weak grid

At the input, the generator shaft rotates according to the rotational inertia of the masses attached to the shaft. Equation (4-9) can be re-written as shown in Equation (4-10) in order to relate the mechanical speed with the produced torque.

$$T_a = J \frac{\partial \omega}{\partial t} = T_m - T_e \quad (4-10)$$

Where

- J is the moment of inertia of generator and turbine,  $\text{kg}\cdot\text{m}^2$
- $\omega$  is the angular velocity of the rotor,  $\text{rad/s}$
- t is time, s.

At the output, neglecting the losses, the generator terminals give the electrical power. Recalling that the product of torque T and the angular velocity  $\omega$  is the shaft power P in watts. Equation (4-11) can be rewritten as

$$J\omega \frac{\partial \omega}{\partial t} = M \frac{\partial \omega}{\partial t} = P_m - P_e \quad (4-11)$$

Where

- $P_m$  is the generator mechanical input power, W
- $P_e$  is the electrical output power, W
- M is the inertia constant, J·s.

According to Equation (4-9), the input mechanical torque applied to the shaft of the prime mover is equal to the output electrical torque caused by the electrical output of the generator during normal operating conditions i.e.  $T_m = T_e$ . In this mode the generator rotates at a constant speed and the net

#### Chapter 4: Modelling of a weak grid

torque is zero. Consequently the electrical output power has a constant frequency.

However, when the power system is subjected to transient disturbances, there will be an immediate imbalance between the power generated and the load demand i.e.  $T_m \neq T_e$ . This imbalance will result in a change in the generator shaft speed and therefore a change in the frequency of the electrical power generated which can affect the system stability. During the disturbance, the sudden change in electrical loading will not be matched by the output of the prime mover. The generator control, particularly the governor which controls the power output from the prime mover, has a slow response so it will not be able to respond to the load change. The generator can only supply the additional load by slowing down and releasing stored kinetic energy. If this happens only over a short period of time, the governor can react and the system can resume stable operation. As the governor slowly responds the system speed will increase back to its set point value. If during the transient, the frequency or the rate of change of frequency exceeds operational boundaries, the generator may trip causing system failure.

According to Equation (4-11) the mismatch of power indicates the variation in the generator speed. For example in the event of a fault (loss of load) occurring in the system the electrical power  $P_e$  is less than the mechanical input power  $P_m$  and this will result in a positive  $\Delta P$  that will increase the speed and frequency. Conversely a sudden increase of the load will result in a negative  $\Delta P$  that will reduce the speed of the generator.

## 4.6 Response of diesel generating sets to load transients.

The disturbance response of a diesel generating set is the reaction of the generator to the application and removal of real power load. A typical diesel generator control system consists of an automatic voltage regulator (AVR) and a governor. The AVR provides voltage control when the generator is operating as an island and reactive power control when operating in parallel with the utility supply. The governor controls the speed of the engine while operating as an island and real power control when operating in parallel with the utility supply [131].

As mentioned in section 4.5, the frequency variation during load transients is due to the slow dynamic response of the prime mover's speed control loop. A block diagram of the prime mover's speed control is shown in Figure 4-9.

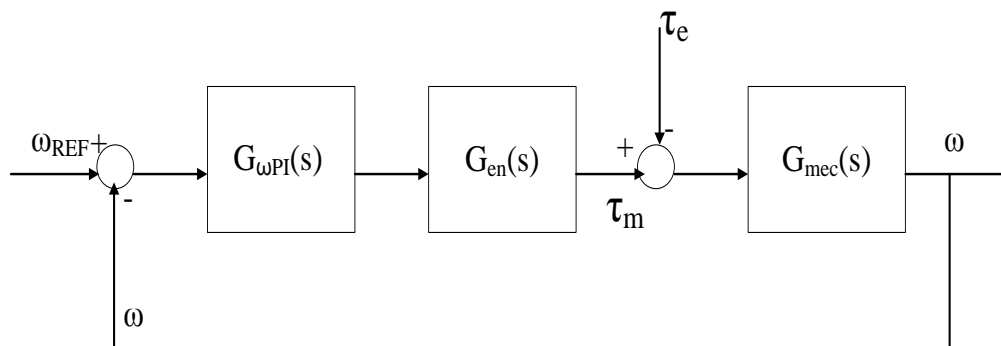


Figure 4-9: Diesel engine speed control loop

$G_{\omega PI}(s)$  represents the speed regulator's transfer function,  $G_{en}(s)$  represents the diesel engine's throttle to torque transfer function,  $G_{mec}(s)$  represents the inertia of the coupled system i.e. prime mover and synchronous generator,  $\tau_m$  represents the input mechanical shaft torque provided by the emulated diesel engine and  $\tau_e$  represents the electrical loading on the generator (disturbance in the regulation loop).

## Chapter 4: Modelling of a weak grid

The transfer functions in Figure 4-9 are:

$$G_{\omega PI}(s) = K_{P\omega} + \frac{K_{I\omega}}{s} = \frac{K_{I\omega}}{s} \left(1 + \frac{sK_{P\omega}}{K_{I\omega}}\right) = \frac{K_{I\omega}}{s} (1 + T_{I\omega}s)$$

$$\frac{K_{P\omega}}{K_{I\omega}} = T_{I\omega}$$

$$G_{en}(s) = \frac{1}{1 + \tau_{en}s}$$

$$G_{mec}(s) = \frac{1}{B + Js} \quad (4-12)$$

The disturbance transfer function is:

$$\frac{\omega(s)}{\tau_e(s)} = - \frac{G_{mec}(s)}{1 + G_{mec}(s)G_{en}(s)G_{\omega PI}(s)} \quad (4-13)$$

Substituting equation (4-12) into equation (4-13) gives;

$$\frac{\omega(s)}{\tau_e(s)} = - \frac{\frac{1}{B + Js}}{1 + \left(\frac{1}{B + Js}\right)\left(\frac{1}{1 + \tau_{en}s}\right)\left(\frac{K_{I\omega}}{s}(1 + T_{I\omega}s)\right)}$$

$$\frac{\omega(s)}{\tau_e(s)} = - \frac{\frac{1}{B + Js}}{1 + \left(\frac{K_{I\omega}(1 + T_{I\omega}s)}{(B + Js)(1 + \tau_{en}s)s}\right)}$$

$$\frac{\omega(s)}{\tau_e(s)} = - \frac{\frac{1}{B + Js}}{\left(\frac{(B + Js)(1 + \tau_{en}s)s + K_{I\omega}(1 + T_{I\omega}s)}{(B + Js)(1 + \tau_{en}s)s}\right)}$$

$$\frac{\omega(s)}{\tau_e(s)} = - \frac{1}{B + Js} \times \frac{(B + Js)(1 + \tau_{en}s)s}{(B + Js)(1 + \tau_{en}s)s + K_{I\omega}(1 + T_{I\omega}s)}$$

$$\frac{\omega(s)}{\tau_e(s)} = - \frac{(1 + \tau_{en}s)s}{(B + Js)(1 + \tau_{en}s)s + K_{I\omega}(1 + T_{I\omega}s)} \quad (4-14)$$

#### Chapter 4: Modelling of a weak grid

A simplified expression can be derived assuming the PI controller's time constant is equal to the engine's time constant i.e.  $T_{I\omega} = \tau_{en}$ . With this assumption equation (4-14) becomes;

$$\begin{aligned}\frac{\omega(s)}{\tau_e(s)} &= -\frac{(1 + T_{I\omega}s)s}{(B + Js)(1 + T_{I\omega}s)s + K_{I\omega}(1 + T_{I\omega}s)} \\ \frac{\omega(s)}{\tau_e(s)} &= -\frac{s}{(B + Js)s + K_{I\omega}} \\ \frac{\omega(s)}{\tau_e(s)} &= -\frac{s}{Js^2 + Bs + K_{I\omega}} \\ \frac{\omega(s)}{\tau_e(s)} &= -\frac{1}{J} \frac{s}{s^2 + \frac{B}{J}s + \frac{K_{I\omega}}{J}}\end{aligned}\tag{4-15}$$

Assuming the disturbance was a step change in the real power demand;

$$\tau_e(s) = \frac{A}{s}\tag{4-16}$$

The response to a step change with amplitude A will be:

$$\omega(s) = -\frac{A}{J} \frac{1}{s^2 + \frac{B}{J}s + \frac{K_{I\omega}}{J}}\tag{4-17}$$

Using the quadratic formula  $as^2 + bs + c = 0$ , the roots of the equation are;

$$\frac{-b \pm \sqrt{b^2 - 4ac}}{2a} = \frac{b(-1 \pm \sqrt{1 - \frac{4ac}{b^2}})}{2a}$$

From equation (4-17);

$$a = 1, b = \frac{B}{J}, c = \frac{K_{I\omega}}{J}$$

The poles of  $\omega(s)$  are;

Chapter 4: Modelling of a weak grid

$$p_{1,2} = \frac{\frac{B}{J}(-1 \pm \sqrt{1 - \frac{4K_{I\omega}J}{B^2}})}{2} \quad (4-18)$$

$$p_1 = \frac{B}{2J} \left( -1 + \sqrt{1 - \frac{4K_{I\omega}J}{B^2}} \right)$$

$$p_2 = \frac{B}{2J} \left( -1 - \sqrt{1 - \frac{4K_{I\omega}J}{B^2}} \right)$$

Assuming the PI controller was designed to give a non-oscillatory response, the poles will be real therefore;

$$\frac{4K_{I\omega}}{B^2} < 1 \quad (4-19)$$

Equation (4-17) can be rewritten as;

$$\omega(s) = -\frac{A}{J(p_1 - p_2)} \left( \frac{1}{s - p_1} - \frac{1}{s - p_2} \right) \quad (4-20)$$

To obtain the speed function in the time domain, the inverse Laplace transform of equation (4-20) will yield;

$$\begin{aligned} \omega(t) = & -\frac{A}{J(p_1 - p_2)} (\exp(p_1 t) - \exp(p_2 t)) = \\ & -\frac{A}{B\sqrt{1 - \frac{4K_{I\omega}J}{B^2}}} \left( \exp\left(\frac{B}{2J} \left(-1 + \sqrt{1 - \frac{4K_{I\omega}J}{B^2}}\right) t\right) - \exp\left(\frac{B}{2J} \left(-1 - \sqrt{1 - \frac{4K_{I\omega}J}{B^2}}\right) t\right) \right) \end{aligned} \quad (4-21)$$

Equation (4-21) represents the speed response due to the load torque disturbance. It can be observed from equation (4-21) that a positive load step change ( $A > 0$ ) will result in a negative function i.e. reduction in the generator

## Chapter 4: Modelling of a weak grid

speed. Conversely a negative load step change will result in a positive function i.e. increase in the generator speed.

Figure 4-10 shows the disturbance response with the application and removal of a resistive load of 4kW. A simulation study based on the disturbance response of an 8kW diesel generating set to the application and removal of a 4kW load was carried out.

In the event of a fault occurring in the system which causes a sudden loss of load, during the transient period the removal of the load will result in a positive accelerating torque (speed and frequency increase). On the other hand, a sudden increase of load demand will result in a negative net torque or decelerating torque that immediately reduces the speed of the generator.

This is shown in Figure 4-10 where the lower trace represents the removal of load from the generator and the upper trace represents the application of load to the generator.

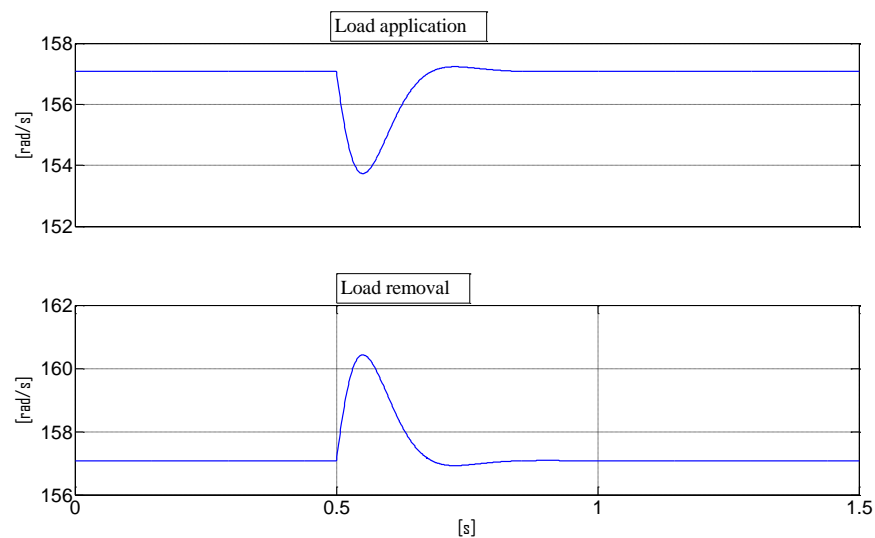


Figure 4-10: Response of generator to load application and removal

An inherent feature of diesel engines is their low inertia structure. Kundur defined an ac power system as being weak if it has (a) a low mechanical inertia and /or (b) high impedance.[130] A weak network is one where

## Chapter 4: Modelling of a weak grid

changes in real and reactive power flows into or out of the network cause significant changes in voltage and /or frequency within the network. Grid code requirements can be used to determine the strength of a grid. Studies have shown that even if generic grid code requirements can be defined, detailed and challenging network analysis have to be made for every power distribution system that employ DG wherein information about type of DG unit installed is taken into consideration. For a grid network to be considered “STIFF (not WEAK)”, the voltage range must be  $\pm 10\%$  of the nominal voltage and the frequency range must be  $\pm 5\%$  of the nominal frequency [132]. The grid code requirements seem disproportionately high, but it should be noted that the grid code requirements vary for different countries.

The significant change in frequency due to change in real power flow has been shown in Figure 4-10. It can be concluded that diesel generating sets exhibit the characteristics of a weak network. In the next section, the microgrid model considered in this work is described. An energy management scheme to improve system behaviour is also introduced.

### **4.7 Weak grid model**

Weak grids are usually found in remote places where the feeders are long and operated at a medium voltage level [133]. The grids in these places are usually designed for relatively small loads. When the design load is exceeded, the voltage and /or frequency level will be below the allowed minimum i.e. the capacity of the grid will exceed operational boundaries. The generator may trip when it exceeds its operating boundaries and this can result in system failure.

The load shedding phenomenon is employed in countries with reduced utility power production and distribution capacity (e.g., South East Asia or Africa). In such weak grid markets power outages tend to happen one or several times a day.

### 4.7.1 Simplified grid model

The model considered in this work is shown in Figure 4-11.

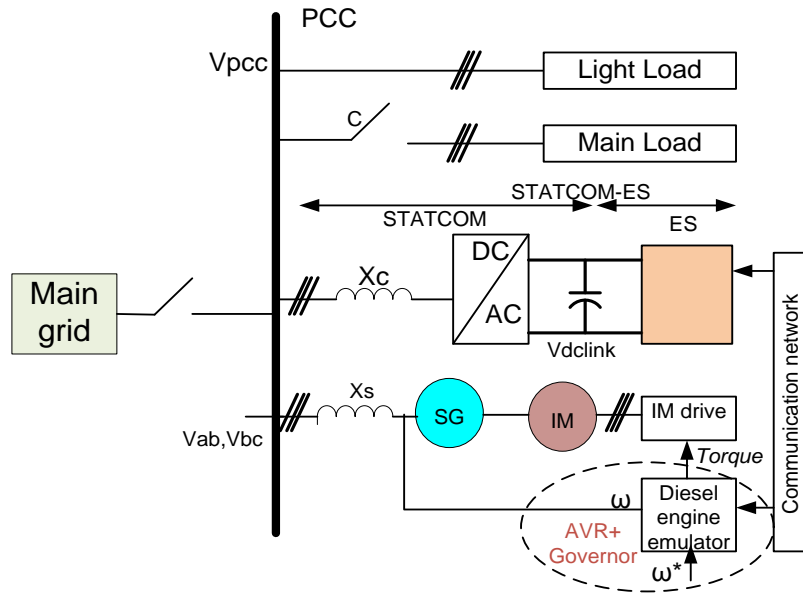


Figure 4-11: The power circuit diagram of the modelled grid

The microgrid can be synchronized to the main grid, but it usually operates as an island fed solely by the local synchronous generator (SG) which provides all of the power needed by the load in steady state operation. There is a potential for the microgrid to exhibit the characteristics of a weak grid when it operates in this mode.

The system consists of a diesel generating set supplying a load. The diesel generating set comprises of a prime mover (diesel engine) and a synchronous generator. The diesel engine was emulated with a vector controlled induction motor as described in section 4.4. The synchronous generator (SG) is equipped with a governor and an automatic voltage regulator (AVR) which combines to give it a slow dynamic response.  $X_s$  represents the equivalent line impedance in series with the internal impedance of the synchronous generator. The STATCOM consists of a three phase voltage source PWM Inverter and a DC link capacitor and it is connected to the supply via a coupling inductance  $X_c$ . Energy storage is added to the STATCOM to provide real power support

#### Chapter 4: Modelling of a weak grid

during transient events. The light load represents the quiescent system load. The main load causes a sudden change in the demand for real power. The system also incorporates a communication between the STATCOM-ES system and the governor of the local generator. Coordinated communication helps to maintain requirements for power matching during transient events, for example a sudden change in the demand for real power.

A case study scenario with the power circuit shown in Figure 4-11 is simulated with and without real power support from the STATCOM –ES system. The focus of the study was to analyse the response of the governor to the new load and to demonstrate the potential of the coordinated control of the governor and the STATCOM-ES system in improving system control.

A simulation based on the power circuit diagram was devised using MATLAB. The generator was represented by a controlled voltage source. The STATCOM consist of a three phase voltage PWM inverter using six IGBTs, a three phase coupling inductor and a dc link capacitor. The energy storage was simplified as an ideal voltage source connected to the DC link in this preliminary study. The light load is rated at 0.8kW and the main load is rated at 3.2kW.

The basic aim of the governor and AVR is to increase or decrease the power output of the prime mover and the magnitude of the terminal voltage of the distributed synchronous generator when there is a change in the flow of real and reactive power within the system. During normal operating condition, the generator will run at its rated speed. An overload condition will cause an imbalance between the load demand and the power supplied.

When a load step is applied by closing the contactor (c) in Figure 4-11, if the load is of comparable rating to the generator, the sudden change in loading condition will not be matched by the output of the prime mover. The generator control, particularly the governor has a slow response so it will not be able to respond to the load change. The prime mover and the generator will initially slow down and the frequency of the system voltage will reduce. The frequency

dip is unacceptable. The requirements for power matching can be maintained by employing a STATCOM-ES system. STATCOM-ES system is a short-term, fast response system used to fill the gap in the power requirements during overload conditions. In the next section, the governor response to the new load and an open loop control of the STATCOM-ES system which provides dynamic power matching will be discussed.

### **4.7.1.1 A generator supplying a system with a sudden change in load without real power support**

As shown in the power circuit diagram the generator initially supplies a light load. Figure 4-12 and Figure 4-13 show the results obtained when the generator supplied power to a system with a sudden change in load without real power support.

At time  $t=1s$  the main load is switched on resulting in a load step being imposed on the system. A sudden load current change from 2A to approximately 10A can be clearly seen in the middle trace of Figure 4-12. This load demand will be supplied only by the generator; the sudden change of the generator current also appears in the top trace of Figure 4-12 with the same trend as of the load current. The bottom trace of Figure 4-12 shows that in this operation mode there is no support current from the STATCOM unit.

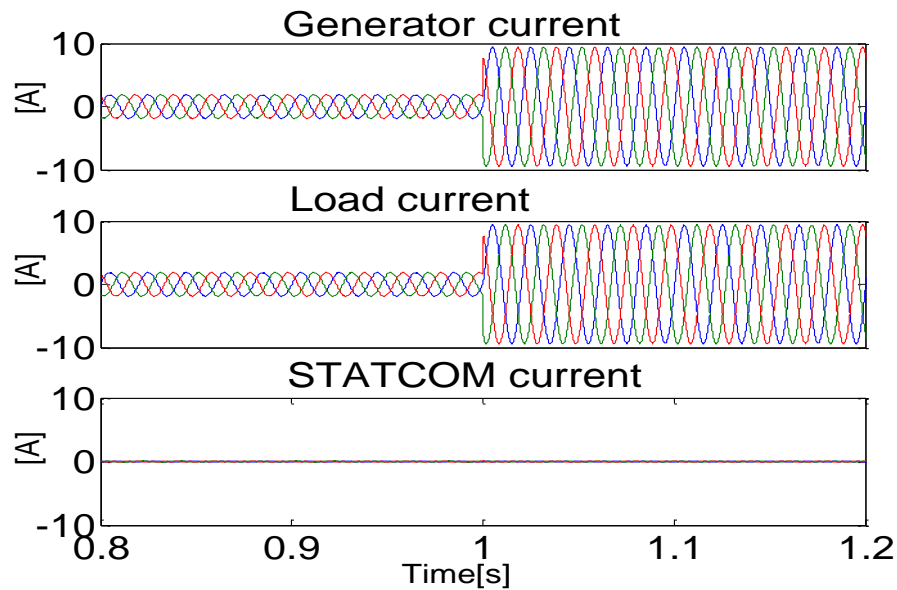


Figure 4-12: Generator, Load and STATCOM currents without real power support

When the load step is imposed, the generator can only respond to the power demand by slowing down and releasing only a small amount of stored kinetic energy. Without real power support from the STATCOM-ES system, there will be a deviation in the rotor speed of the generator as shown in Figure 4-13

Before the load impact, there is no change in the generator's rotor speed meaning that the generator's speed is constant at the synchronous speed. However with the impact of the sudden load change as shown in Figure 4-13 the rotor speed deviates over the period  $t=1s$  and  $t=1.1s$ . This shows a frequency drop of less than 0.5 Hz during that period. From  $t=1.1s$  onward, the generator governor control responds to this change by modulating the appropriate mechanical input power to the generator in order to match the electrical power at its output terminals. The rotor speed then gradually increases until the mechanical and electrical power are equal (at approximately  $t= 1.4s$ ).

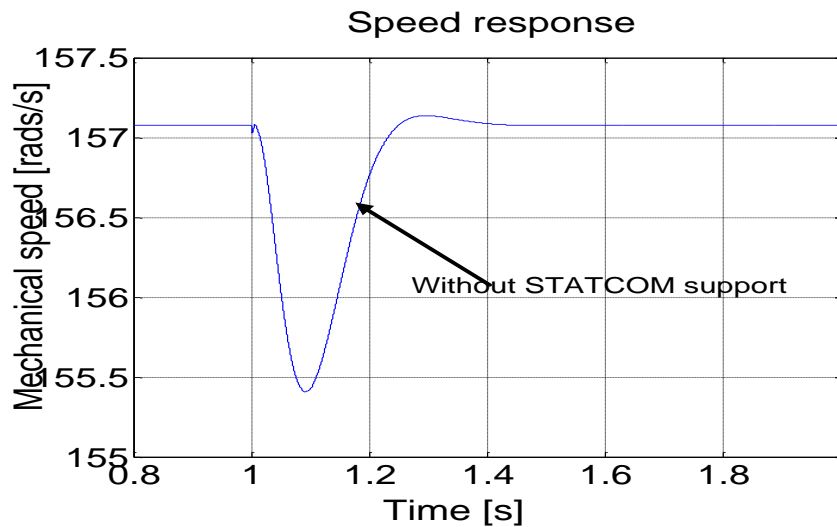


Figure 4-13: Rotor speed response without real power support

### 4.7.1.2 Energy management with STATCOM-ES system

Frequency excursions experienced during sudden load changes can directly cause instability which induces generators to pull out of synchronism with the power system. In the presence of generators with slow dynamic responses, energy storage systems can be used to improve the stability of a power system by providing supplemental temporary power. Energy storage coupled to a STATCOM can be used to feed the sudden change in load whilst the slow governor of the prime mover reacts to the sudden load change as shown in Figure 4-13. The STATCOM–ES system can only carry out this role if its dynamic response is much faster than the speed of the governor.

The immediate power imbalance between the generation and consumption of power during transient events can cause unnecessary or nuisance tripping of generators by rate of change of frequency (ROCOF) relay. ROCOF relay events can induce cascade power system shutdown. It is imperative to minimise frequency excursions during transient events to help prevent nuisance tripping of generators. This can be achieved by implementing an energy management scheme such that power generation and consumption are

## Chapter 4: Modelling of a weak grid

matched before, during and after transient events. A time diagram describing the operation of the energy management scheme is shown in

Figure 4-14.

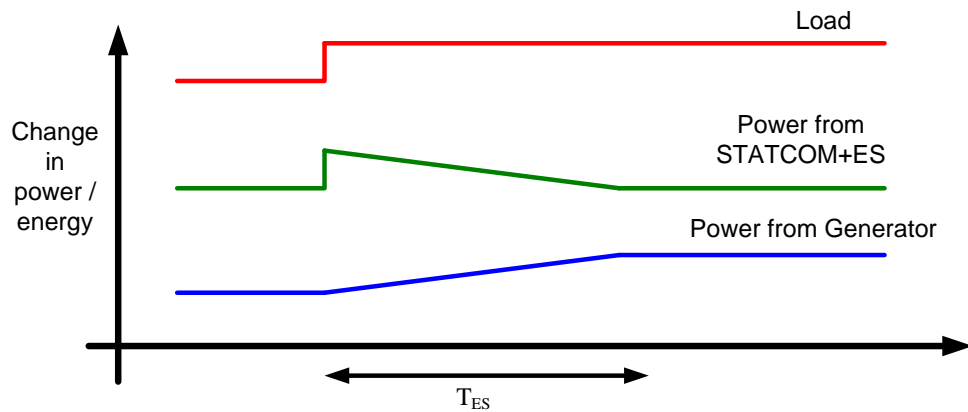


Figure 4-14: Time diagram describing energy management scheme

In Figure 4-14, the top waveform is the step change in the electrical load. The middle waveform is an ideally created power profile to demonstrate the potential improvement to frequency stability by using the STATCOM-ES unit. The governor response has been approximated as a ramp function. The bottom waveform is the mechanical generator power. It can also be seen that the real power demand by the load is jointly supplied by the STATCOM-ES unit and the generator. The energy management scheme was achieved by implementing the combined control of the governor and the STATCOM\_ES in an open loop. A realistic control scheme for energy management will be described in detail in chapter 5.

Figure 4-15 and Figure 4-16 show the result obtained following the implementation of the energy matching scheme. It can be clearly seen from the third trace of Figure 4-15 that the real power demand by the load is supplied by the STATCOM-ES while the generator is trying to react to the load change hence there will not be a need for the generator to slow down to release stored kinetic energy.

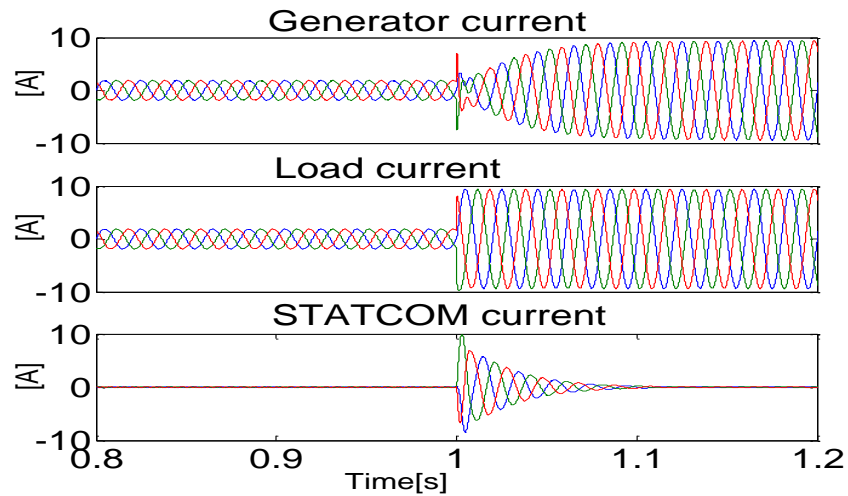


Figure 4-15: Generator, Load and STATCOM currents with real power support

From  $t=1s$ , the same sudden change in the main load current from 2A to 10A as described previously is seen in the middle trace of Figure 4-15. To minimise the impact on the generator, at the beginning of this transient condition, the load is supplied partly by the rapid real power injection produced from the STATCOM unit.

The STATCOM-ES unit and the speed controller of the prime mover must work in a coordinated manner. When the STATCOM-ES unit detects a change in load, it supplies the additional power to the load. However it also needs to communicate with the generator controller. It does this by requesting maximum control input to the governor dynamics block. The time  $T_{ES}$  required for the mechanical torque to change from the value required before the load change, to the value required after the load change can be calculated. This time is used for the control of the STATCOM-ES i.e. it is the time taken to bring the STATCOM-ES output from its initial value to 0. Over the period  $T_{ES}$ , the additional electrical power required for the new load is transferred from the STATCOM-ES to the generator with minimal variation in speed.

According to the limit in the amount of stored energy in the STATCOM unit, the rapid support current is designed to inject real power to the load with magnitude equal to the maximum load current at the beginning then reducing

## Chapter 4: Modelling of a weak grid

constantly to zero at  $t=1.1\text{s}$  as shown in the bottom trace of Figure 4-15. As a consequence, at the beginning of the load impact, the generator current increases constantly with the support current from the STATCOM-ES unit until reaching the maximum current at time  $t=1.1\text{s}$  (when the support current becomes zero) as shown in the top trace of Figure 4-15.

With the support power from the STATCOM-ES unit, the impact on the generator due to a sudden change in the loading condition is reasonably reduced (also the degree of the imbalance between the power generated and load demand is reduced). The rotor speed variation is therefore minimised as illustrated in Figure 4-16. This also indicates that the frequency variation during the load impact will be minimised.

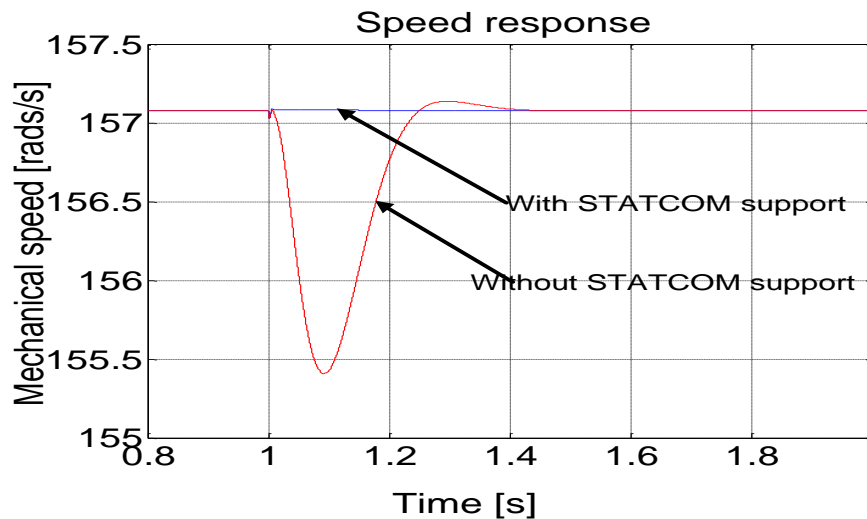


Figure 4-16: Rotor speed response with real power support

## 4.8 Conclusion

In this chapter, the characteristics of an internal combustion engine driven synchronous generator was described and the key features which dominate the transient response were identified so that an emulation of a diesel generating set was achieved with a vector controlled induction motor driving a

#### Chapter 4: Modelling of a weak grid

synchronous generator. The diesel engine emulation was achieved by incorporating a single delay into the speed control loop of the vector controlled induction motor.

It is imperative to carry out a stability analysis on ac power systems that employ distributed generation (DG) due to the unnecessary or nuisance tripping of DG by rate of change of frequency (ROCOF) relays. Although DG has introduced benefits to ac power systems, the impact of load changes on the stability of power systems that employ DG has been highlighted in this chapter. Large load steps can cause instabilities such as frequency excursions beyond acceptable limits in a microgrid network or weak systems. The immediate power imbalance between the generation and consumption caused by large load steps can cause unnecessary or nuisance tripping of generators by ROCOF relays. Therefore, it is essential to minimise frequency excursions in order to improve system stability.

An energy management scheme that can improve the response of generators during load transients has been proposed. The case study investigated in this chapter confirms the proposed idea. The results clearly show that the proposed energy management scheme can help improve system stability. The energy management scheme was achieved by implementing the combined control of the governor and the STATCOM\_ES in an open loop. The combined control action was only employed during the load transient. During normal operation, the governor's PI regulator was used to regulate the speed. The shape of the total torque disturbance is modified by the real power support from the STATCOM-ES unit. The proposed open loop control algorithm has its limitations. These limitations include knowledge of the load current, diesel engine transfer function and use of infinite energy storage. In real applications, the energy storage is limited e.g. supercapacitors.

#### Chapter 4: Modelling of a weak grid

In the next chapter, the open loop compensation scheme will be described in detail and a closed loop compensation scheme which addresses the aforementioned limitations is presented. .

## Chapter 5

# Frequency control improvement within a microgrid

---

### 5.1 Introduction

Frequency stability within a synchronous generator fed microgrid can be improved by using the combined STATCOM and SCESS described in chapter 3 to support the generator during load change transients. As shown in chapter 4, the frequency variation under active power load steps is due to the slow dynamic response of the prime mover (diesel engine). This is due to the inability of the prime mover to cope with the fast active power load variations.

Frequency variation is unacceptable for utilities that require tight frequency regulation e.g. microgrids. For this reason, the international regulation for

## Chapter 5: Frequency control improvement within a microgrid

power generation and distribution (IEEE1547) [134] was imposed to govern frequency variation within certain limits. When the limits are exceeded by a distributed generator, the generator will be disconnected from the grid. The disconnection of a generator from the grid may cause a chain reaction of events which can consequently lead to black outs when the disconnection appears to other generators connected to the grid as another load step variation.

In this chapter, the concept of frequency control improvement is discussed by using the energy management scheme introduced in chapter 4. The quantification of the energy required for the frequency compensation is presented in section 5.2. The open loop energy management scheme introduced in chapter 4 is described in detail in section 5.3. An optimum control algorithm based on a closed loop energy management scheme is described in section 5.4. A simulation study showing how improvements to frequency stability can be achieved with the proposed closed loop energy management scheme is presented in section 5.5. Finally the conclusions are presented in section 5.6.

### **5.2 Quantification of the energy required for the frequency compensation**

As mentioned in chapter 4, the immediate power imbalance between the generation and consumption of power during transient events can be minimised by implementing an energy management scheme such that power generation and consumption are matched at all times.

An energy source is required for the implementation of the energy management scheme. An infinite energy storage device incorporated with a STATCOM can potentially compensate for all the load power demand. However, the use of an infinite energy source is unrealistic in terms of size

## Chapter 5: Frequency control improvement within a microgrid

and cost of energy required as real power injection is only required whilst the slow prime mover is trying to react to the active power load variation. In this research a limited energy storage device called a supercapacitor energy storage system (SCESS) combined with a STATCOM as described in chapter 3 is used for the energy management scheme.

In view of the aforementioned, it is imperative to quantify the amount of energy required for the frequency compensation during load active power steps as the active power injection from the STATCOM has to be a time-limited power profile.

A time diagram based on the energy management scheme introduced in chapter 4 is shown in Figure 5-1.

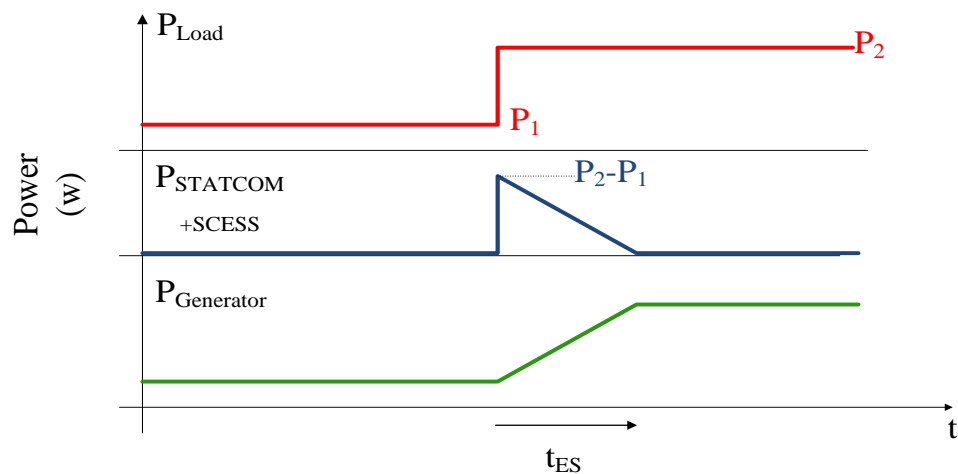


Figure 5-1: Time diagram describing the energy management scheme

The top waveform is the step change in the electrical load power. The middle waveform is a time-limited power profile depicting the active power injection from the combined STATCOM and SCESS. The bottom waveform is the mechanical generator power. The time  $t_{ES}$  required for the mechanical torque to change from the value required before the load change, to the value required after the load change can be calculated. The worst case for this situation is

## Chapter 5: Frequency control improvement within a microgrid

when the system changes from an unloaded condition (P1) to a fully loaded condition (P2) and vice versa.

A key factor in the implementation of the energy management scheme is the coordinated communication between the combined STATCOM and SCESS and the local generator. The coordinated communication between the combined STATCOM and SCESS and the local generator is divided into three stages which are:

- Detection of the load change
- Triggering of combined STATCOM and SCESS to inject enough power to match new load
- Application of maximum torque demand until prime mover output power matches new load condition.

The load change is detected through the direct measurement of the load current during the load impact or the change in the mechanical speed of the prime mover. The time limited power profile of the combined STATCOM and SCESS used for the open loop energy management scheme introduced in chapter 4 is calculated based on the knowledge of the load current and the time  $t_{ES}$ .

In order to calculate  $t_{ES}$ , it is worthwhile reviewing the response of the speed control loop of the prime mover shown in Figure 5-2. The time  $t_{ES}$  is calculated by analysing the speed controller output and the prime mover torque output shown in Figure 5-3.

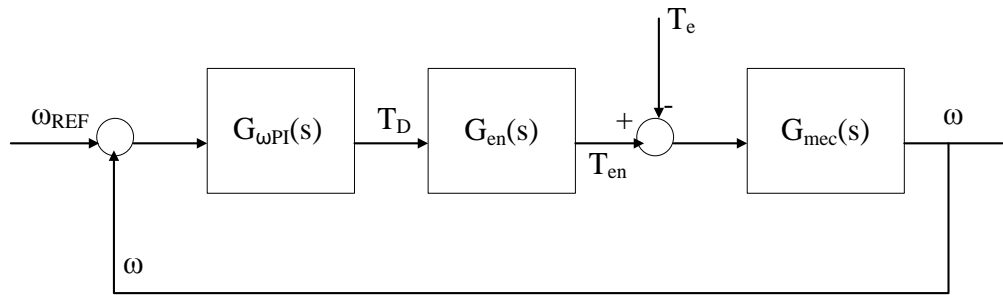


Figure 5-2: Prime mover's speed control loop

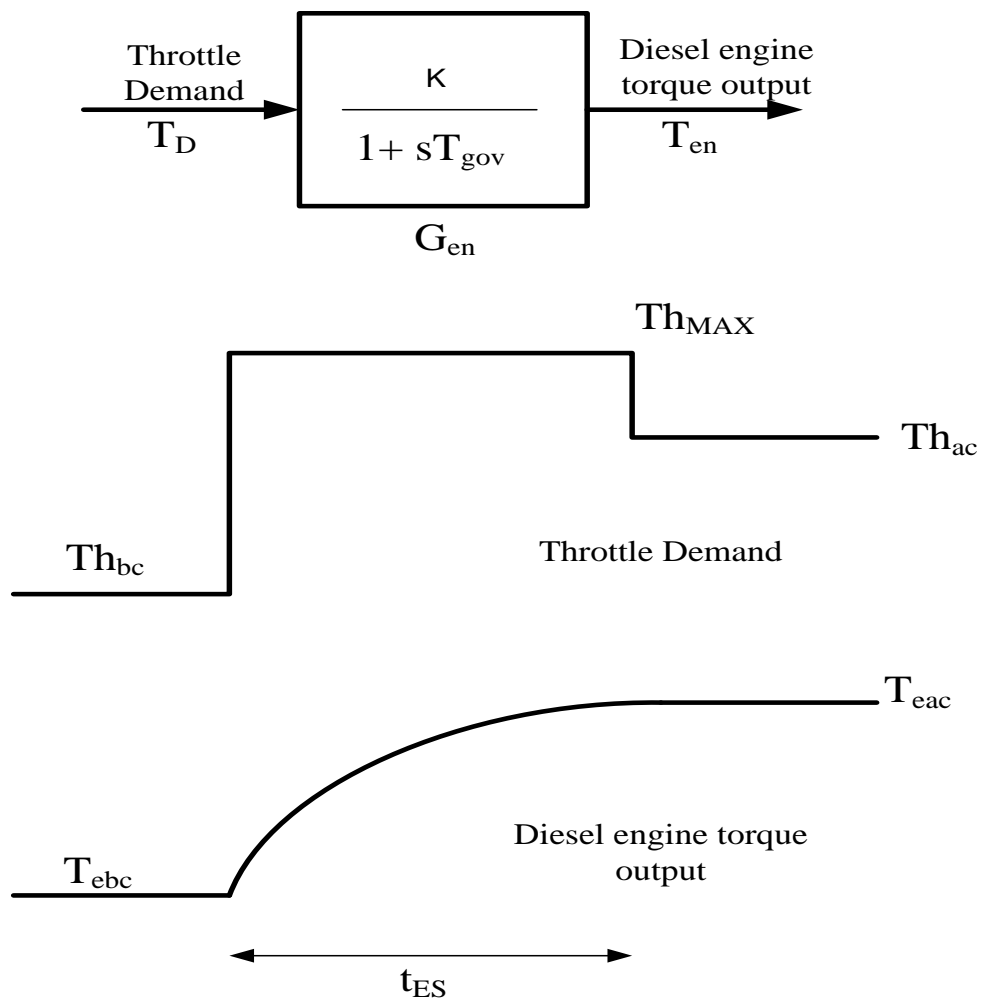


Figure 5-3: Representation of the speed regulator and engine response

The throttle-torque transfer function from Figure 5-3 introduced in chapter 4 is given as:

Chapter 5: Frequency control improvement within a microgrid

$$T_D(s) \left( \frac{K}{1 + sT_{GOV}} \right) = T_{EN}(s) \quad (5-1)$$

$$\frac{T_{EN}(s)}{T_D(s)} = \left( \frac{K}{1 + sT_{GOV}} \right) = \left( \frac{K/T_{GOV}}{1/T_{GOV} + s} \right) \quad (5-2)$$

Since  $T_D(s)$  is a unit step response, applying an inverse Laplace transform to Equation (5-2) gives,

$$\begin{aligned} T_{EN}(t) &= T_D(t)(1 - e^{-at}) \\ a &= 1/T_{GOV} \quad \text{and} \\ t &= t_{ES} \end{aligned} \quad (5-3)$$

From Figure 5-3,

$$T_{EN}(t) = T_{eac} - KTh_{MAX} = -KTh_{MAX} + T_{eac} \quad (5-4)$$

$$T_D(t) = KTh_{MAX} - T_{ebc} \quad (5-5)$$

$$\begin{aligned} \frac{T_{EN}(t)}{T_D(t)} &= (1 - e^{-at}) \\ \left( \frac{-KTh_{MAX} - T_{eac}}{KTh_{MAX} - T_{ebc}} \right) &= (1 - e^{-at}) \end{aligned} \quad (5-6)$$

$$-\left( \frac{KTh_{MAX} - T_{eac}}{KTh_{MAX} - T_{ebc}} \right) - 1 = -e^{-at} \quad (5-7)$$

Applying a logarithmic function to both sides of Equation (5-7) yields,

$$-\log\left( \frac{KTh_{MAX} - T_{eac}}{KTh_{MAX} - T_{ebc}} + 1 \right) = at \quad (5-8)$$

Chapter 5: Frequency control improvement within a microgrid

$$-\log\left(\frac{KTh_{MAX} - T_{eac}}{KTh_{MAX} - T_{ebc}}\right) = at \quad (5-9)$$

The time  $t_{ES}$  is obtained as:

$$t_{ES} = \left( -\log\left(\frac{KTh_{MAX} - T_{eac}}{KTh_{MAX} - T_{ebc}}\right) / a \right) \quad (5-10)$$

$$t_{ES} = -\log\left(\frac{KTh_{MAX} - T_{eac}}{KTh_{MAX} - T_{ebc}}\right) \times T_{GOV} \quad (5-11)$$

The concept of compensating for kinetic energy with an energy storage device is known as “VIRTUAL INERTIA”. Results from the swing equation can be used to determine the amount of power required from the energy storage device during transient periods to assist low inertia DG units in maintaining transient stability.

$$P_a = P_{MECH} - P_{LOAD} \pm P_{STATCOM} \quad (5-12)$$

With the assumption that the input mechanical power is constant for transient study:  $\Delta P_{STATCOM} = \Delta P_{LOAD}$  . (5-13)

With the knowledge of the load current and the time  $t_{ES}$ , the energy required for the frequency compensation can be quantified. The minimum amount of energy required if the combined STATCOM and SCESS were to be used for the frequency compensation is obtained from the integration of the time-limited power profile shown in Figure 5-1;

## Chapter 5: Frequency control improvement within a microgrid

$$E_{\text{REQUIRED\_MIN}} = \int \Delta P_{\text{STATCOM}} dt$$

where

$$\Delta P_{\text{STATCOM}} = \Delta P_{\text{LOAD}} \quad (5-14)$$

and

$$\Delta P_{\text{LOAD}} = P_2 - P_1$$

The energy required to compensate for the frequency variation during the load transient can also be approximated by finding the area of the time limited power profile which has a base of  $t_{\text{ES}}$  and a height of  $P_{\text{STATCOM}}$ .

$$E_{\text{REQUIRED\_MIN}} = \frac{P_{\text{STATCOM}} \times t_{\text{ES}}}{2} \quad (5-15)$$

The energy stored in the supercapacitor can be expressed as:

$$E_{\text{SUPERCAPACITOR}} = \frac{1}{2} C (V_{\text{SC-MAX}}^2 - V_{\text{SC-MIN}}^2) \quad (5-16)$$

Where  $V_{\text{SC-MAX}}$  and  $V_{\text{SC-MIN}}$  are allowable voltage of the supercapacitor

Therefore the capacity of the energy storage unit to be installed can be estimated using the value of the change in the load current and the time required for the prime mover output to match the new load condition as shown in Equation (5-15).

$$\frac{P_{\text{STATCOM}} \times t_{\text{ES}}}{2} < E_{\text{SUPERCAPACITOR}} \quad (5-17)$$

Alternatively, the knowledge of the kinetic energy across the rotational mass can be used to determine the minimum energy required.

$$E_{\text{REQUIRED\_MIN}} = E_{\text{Rotational-mass}} = \frac{1}{2} J \Delta \omega_{\text{MIN}}^2 \quad (5-18)$$

## Chapter 5: Frequency control improvement within a microgrid

Where  $J$  is the rotational inertia of the DG unit and  $\omega_{\text{MIN}}$  is the minimum speed /frequency determined by grid code standards.

The size of supercapacitor is dependent on the minimum energy required and the maximum allowed supercapacitor voltage as shown in Equation (5-19).

$$C_{\text{SC}} = \frac{2 \cdot E_{\text{REQUIRED-MIN}}}{V_{\text{SC-MAX}}^2} \quad (5-19)$$

System ratings such as generator power rating and converter rating are important factors to be considered when calculating the size of the energy storage to be employed in maintaining transient stability.

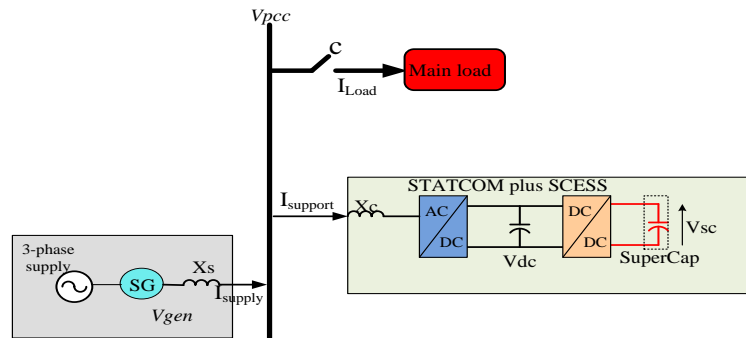


Figure 5-4: Single line diagram of a simplified microgrid set-up

Figure 5-4 relates the system ratings to the size of energy storage device to be installed in maintaining transient stability. In general, the value of the supercapacitor voltage ( $V_{\text{sc}}$ ) is dictated by the value of the DC-link voltage ( $V_{\text{dc}}$ ) as optimum energy is extracted from the supercapacitor when the duty cycle is 0.5. The value of the DC-link voltage ( $V_{\text{dc}}$ ) is dictated by the value of the generator voltage ( $V_{\text{gen}}$ ). This is because the generator voltage must be less than the DC-link voltage if the operation of the AC-DC inverter is to be maintained in the linear region. The value of the generator voltage ( $V_{\text{gen}}$ ) is dictated by the power rating of the generator and the current rating of the supply ( $L_s$ ) and coupling ( $L_c$ ) inductors. Details of the system ratings of the devices used in this work are described in Chapter 6.

In the next section, the control algorithms employed for the energy management scheme will be discussed in detail.

### 5.3 Open loop energy management scheme

In this section, the improvement to frequency control achieved by combining an open loop control action on the prime mover (diesel engine) and the combined STATCOM and SCESS is presented. To fully understand the open loop control energy management scheme, it is worthwhile reviewing the optimum response of a diesel engine to large load step transients introduced in chapter 4.

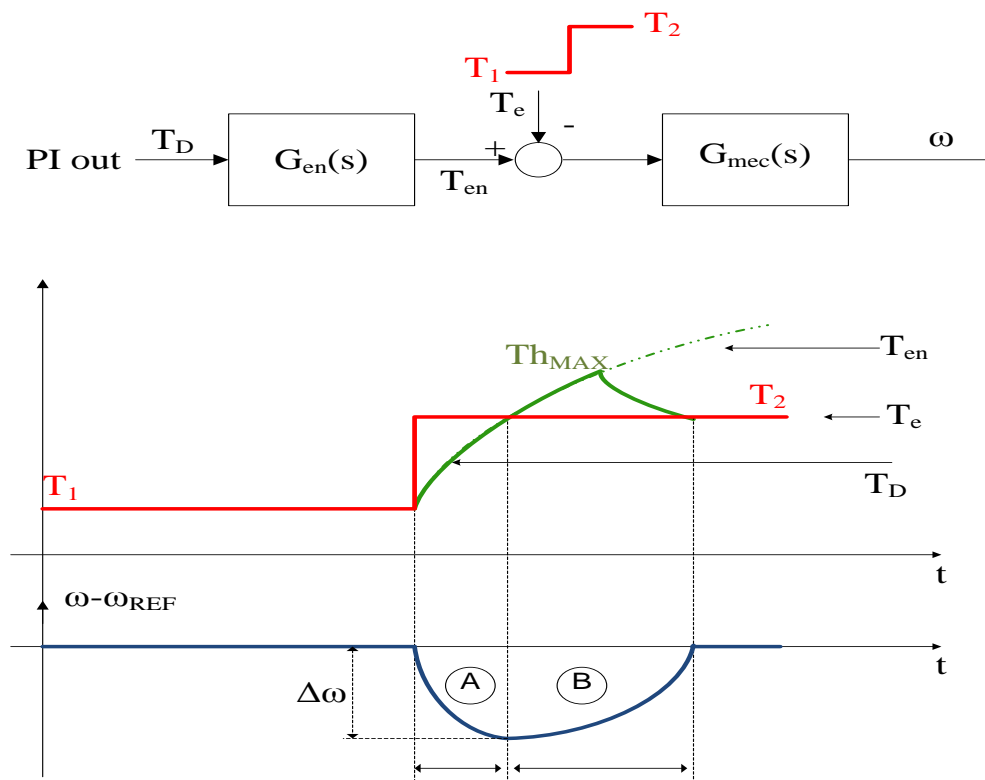


Figure 5-5: Response of the prime mover to a large load step transient

## Chapter 5: Frequency control improvement within a microgrid

A PI controller is used to provide the reference demand for the control of the prime mover as shown in Figure 5-2. The output of the PI controller is the throttle demand ( $T_D$ ). When an electrical load ( $T_e$ ) is detected, the generator will decelerate in response to the load demand as shown in Figure 5-5(A). The speed controller will increase the throttle demand to  $T_{hMAX}$  to accelerate the generator back to the set point speed and make sure the throttle demand matches the new load setting as shown in Figure 5-5(B).

As mentioned in chapter 3 and chapter 4, the real power capabilities of the combined STATCOM and SCESS can be exploited to provide frequency stability. The addition of the combined STATCOM modifies the prime mover's speed control loop shown in Figure 5-2 to the one shown in Figure 5-6.

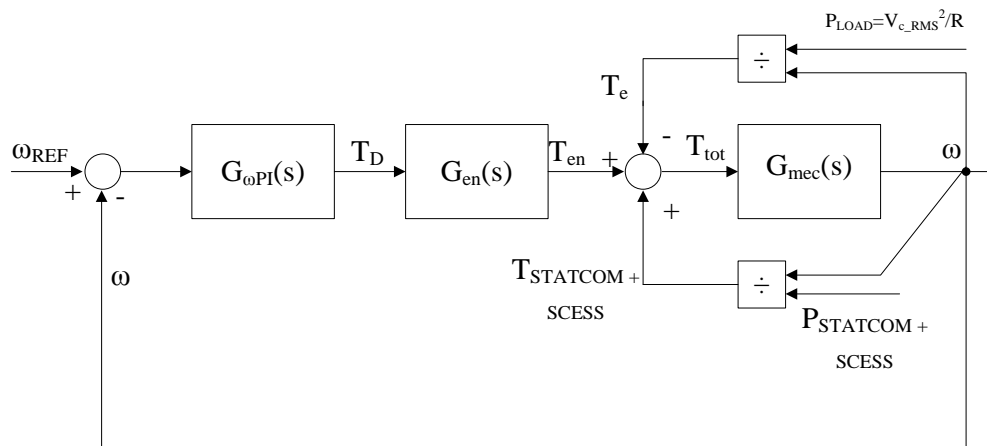


Figure 5-6: Modified speed control loop

From Figure 5-6, it can be observed that the speed can only be kept constant if the total torque ( $T_{tot}$ ) applied to the mechanical load is kept constant. In essence, the generated torque  $T_{gen} = T_{en} + T_{STATCOM+SCESS}$  has to instantaneously match the electrical load torque ( $T_e$ ). In this analysis, “load torque step” and “load power step” both mean a change of active power absorbed by the resistive load connected to the synchronous generator. The

## Chapter 5: Frequency control improvement within a microgrid

open loop action only takes place during the load transient, while before and after the load step, the control action is governed by the PI regulator.

The advantage of the open loop energy management scheme is its simplicity and its capability of minimizing the speed variation during all load power transients as shown in the simulation results presented in chapter 4.

The knowledge of the diesel engine transfer function and load currents are important requirements when implementing the open loop energy management scheme. As a result, the functionality of the open loop energy management is limited in scenarios where the load current measurement and diesel engine transfer function are unknown. In the next section, a proposed closed loop energy management scheme which addresses these limitations of the open loop energy management scheme is discussed in detail.

### **5.4 Proposed closed loop energy management scheme**

A closed loop control algorithm has been developed to overcome the limitations of the open loop energy management scheme discussed in the previous section. The closed loop control algorithm is based on a speed threshold which triggers the injection of real power by the combined STATCOM and SCESS during load transients. The proposed closed loop control architecture is effective in minimizing speed variation during load transients.

The closed loop control algorithm employ two control modes which are:

- a) Normal operation mode
- b) Transient operation mode

## Chapter 5: Frequency control improvement within a microgrid

During normal operation, the prime mover is controlled by a governor and the combined STATCOM and SCESS real power reference is set to zero. During the transient operation, the governor is driven to a maximum output to meet a new load demand as fast as possible. The combined STATCOM and SCESS real power reference required for the energy management scheme is derived from a high gain transient management controller which also acts as the speed controller during the load transient. A block diagram showing the two control modes employed is shown in Figure 5-7.

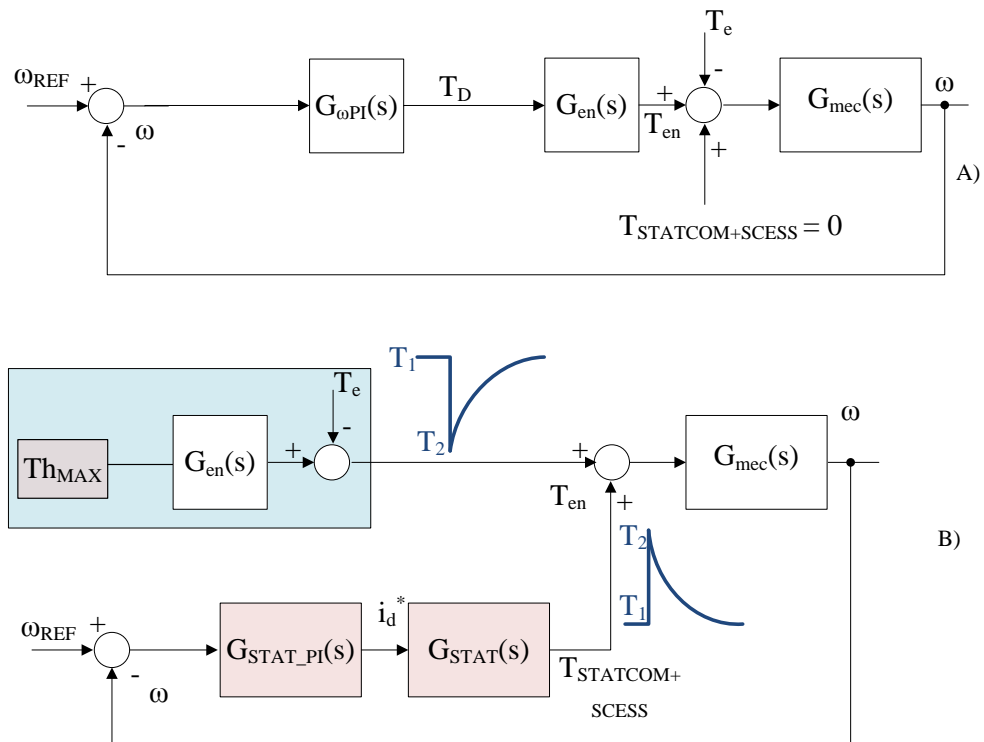


Figure 5-7: closed loop algorithm control block diagram

A block diagram of the proposed closed loop control architecture is shown in Figure 5-8

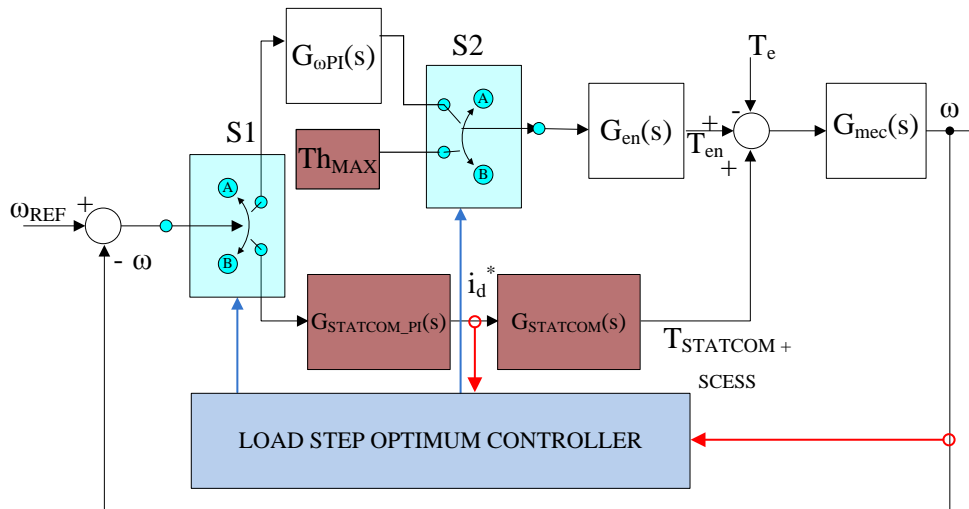


Figure 5-8: Proposed closed loop control architecture

$G_{\omega PI}(s)$  represents the governor speed controller.  $G_{STATCOM\_PI}(s)$  represents the STATCOM current controller. S1 and S2 represent the switches used to change operating modes.  $Th_{MAX}$  represents the maximum governor control input.  $G_{en}(s)$  represents the engine delay block.  $G_{mec}(s)$  represents the mechanical load block. An increase in the bandwidth of the speed loop will attenuate the effect of a load torque step transient. However, the bandwidth of the speed control loop cannot be increased because an increase in the bandwidth will result in an increase in the gains of the speed controller. High proportional gain values can cause instability and presence of high torque ripples. Since the mechanical load cannot be changed, zero speed variation can be achieved by modifying the speed loop during the load transient.

When the load change is detected, S1 and S2 switch from position A to position B.  $Th_{MAX}$  becomes the engine torque demand. The STATCOM can then be used temporarily for speed control by controlling the net electrical load added to the mechanical system when the electrical load is changed. The STATCOM speed control loop controls the speed and it also responds to an equivalent load torque transient equal to the difference between the load torque and the diesel engine torque as shown in Figure 5-7. The equivalent

Chapter 5: Frequency control improvement within a microgrid

torque corresponds to the STATCOM+SCESS torque reference that should be followed by the combined STATCOM and SCESS for the frequency compensation.

When operating in this mode (transient mode), the d-axis current of the STATCOM ( $i_d^*$ ) acts to control torque as shown in Figure 5-8. The reference current obtained from a transient management controller (STATCOM speed controller) has a faster dynamic response than the governor as it can release energy at a much faster rate than the diesel engine. The STATCOM speed control loop manages the power supplied by the combined STATCOM and SCESS whilst the prime mover power output is increased and therefore regulates the speed with little disturbance.

This control action will continue until the diesel engine generated torque matches the load torque. S1 and S2 will then switch from position B back to position A once the power matching has been achieved. A flow chart summarising how the power matching algorithm works is shown in Figure 5-9.

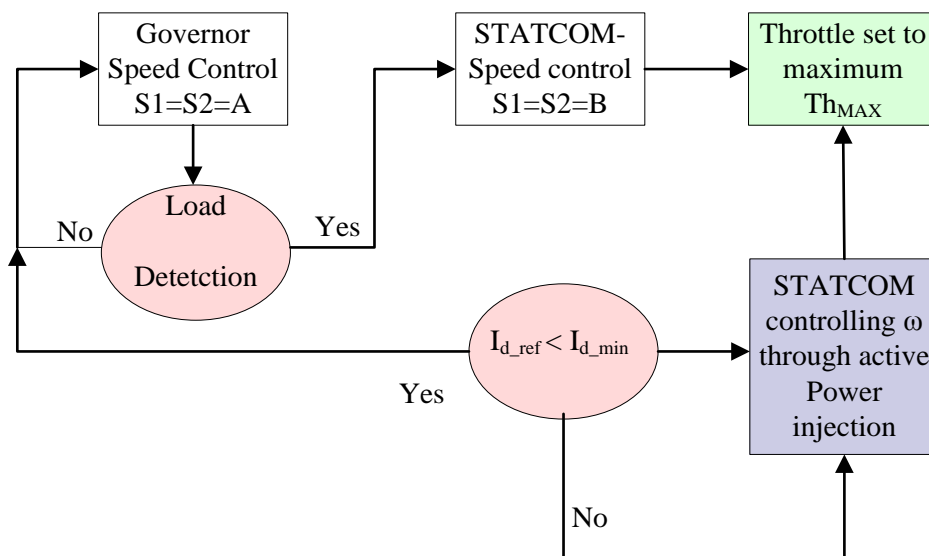


Figure 5-9: Flow chart describing the proposed closed loop algorithm

## Chapter 5: Frequency control improvement within a microgrid

Instantaneous torque match is achieved when the engine controller sets the throttle demand to its maximum value ( $T_{h_{MAX}}$ ) and this leads to the opening of the prime mover's speed loop. A time diagram depicting how the zero speed variation was achieved with the closed loop energy management scheme is shown in Figure 5-10.

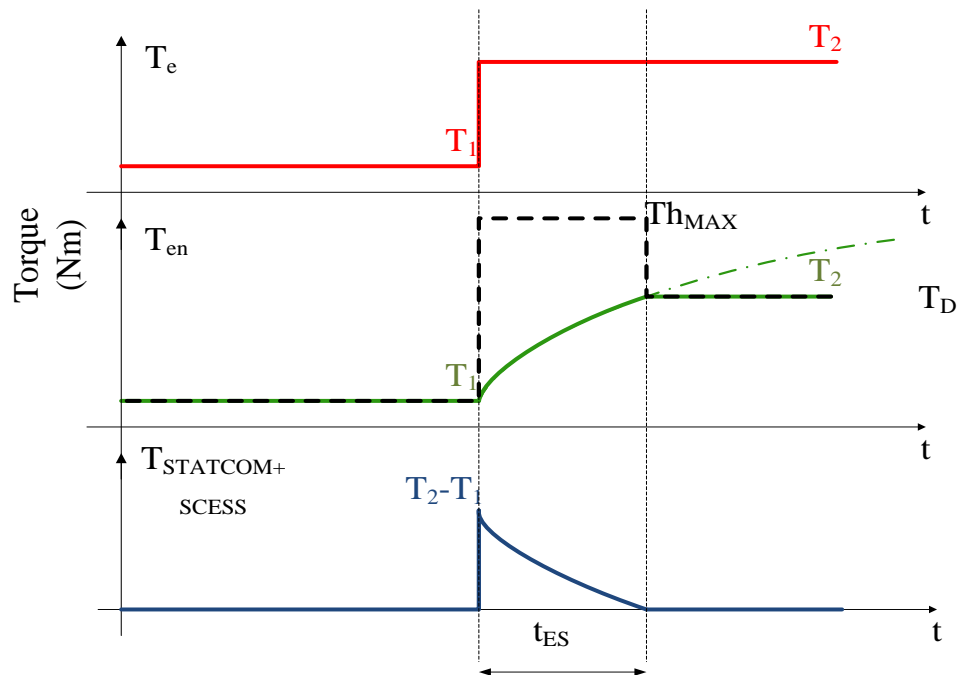


Figure 5-10: Time diagram depicting how minimum speed variation was achieved with the closed loop energy management scheme

From Figure 5-10, the load is represented by a step torque variation from  $T_1$  to  $T_2$ . Over the period  $t_{ES}$ , the PI output is set to  $T_{h_{MAX}}$  and the combined STATCOM and SCESS injects  $T_{STATCOM+SCESS} = T_e - T_{en}$ . This results in a zero speed variation as the total steady state torque is equal to zero. When the engine torque ( $T_{en}$ ) reaches the new load setting  $T_2$ , the PI controller takes over the control of the speed control loop.

Instantaneous detection and instantaneous response from both the STATCOM speed controller and current controller offers the possibility of the proposed

closed loop algorithm in providing zero speed variation during load transients. This is highlighted in the simulation studies carried out in the next section.

## 5.5 Simulation studies

A case study scenario with the power circuit diagram shown in Figure 5-11 is simulated to show how frequency control improvement can be achieved with the proposed closed loop energy management scheme described in the previous section.

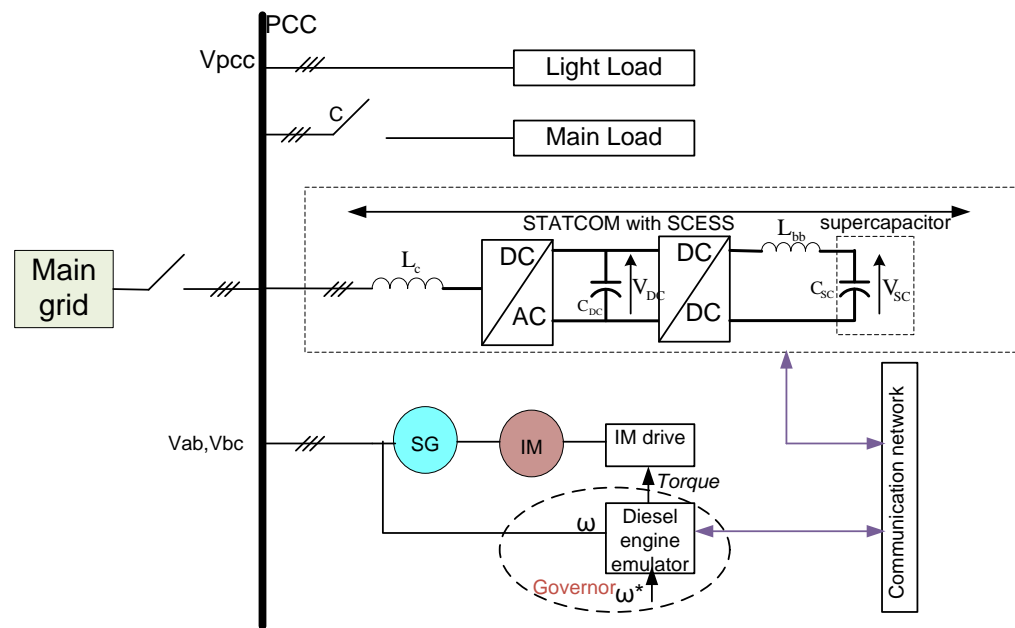


Figure 5-11: Power circuit diagram of the simulated system

The focus of the study is to verify that the proposed control algorithm can be used to achieve zero speed variation during load transients. A simulation based on the power circuit diagram shown in Figure 5-11 was devised using MATLAB/ Simulink simulation package and all the power circuit component models can be found in the sim power system blockset.

## Chapter 5: Frequency control improvement within a microgrid

The system consists of a diesel generating set supplying a load. The diesel generating set comprises of a prime mover (diesel engine) and a synchronous generator. The diesel engine was emulated with a vector controlled induction motor as described in chapter 4. The synchronous generator (SG) is equipped with a governor and an automatic voltage regulator (AVR) which combines to give it a slow dynamic response. The main components of a STATCOM with SCESS are the STATCOM and the supercapacitor based energy storage system (SCESS). A STATCOM consists of a coupling inductor ( $L_c$ ), a voltage source DC-AC inverter and a DC-link capacitor ( $C_{DC}$ ) usually an electrolytic capacitor. The SCESS consists of the supercapacitor ( $C_{SC}$ ), a buck-boost inductor ( $L_{bb}$ ) and a bi-directional DC-DC buck-boost converter. The light load represents the quiescent system load. The main load causes a sudden change in the demand for real power. The system also incorporates a communication network between the combined STATCOM and SCESS and the governor of the local generator. The proposed closed loop control algorithm is incorporated within the communication network. Coordinated communication helps to maintain requirements for power matching during transient events, for example a sudden change in the demand for real power.

When a load step is applied by closing the contactor (c) in Figure 5-11, if the load is of comparable rating to the generator, the sudden change in loading condition will not be matched by the output of the prime mover. The generator control, particularly the governor has a slow response so it will not be able to respond to the load change. The prime mover and the generator will initially slow down and the frequency of the system voltage will reduce. The requirements for power matching can be maintained by employing the real power capability of the combined STATCOM and SCESS described in chapter 3 and the closed loop control algorithm proposed in section 5.4.

## Chapter 5: Frequency control improvement within a microgrid

Table 5-1 summarizes the circuit parameters used in the simulation study.

Symbol	Description	Nominal value
$V_{SG}$	Generator voltage (RMS phase)	100V
LL	Light load	57 $\Omega$
ML	Main load	10 $\Omega$
Tstep	Main load step time	0.5s

Table 5-1: Simulation parameters

The simulation parameters for the combined STATCOM and SCESS and the diesel gen set emulator are the same as the ones used in the simulation study carried out in chapter 3 and chapter 4 respectively with the exception of the parameters shown in Table 5-1.

Four scenarios are considered in the simulation study. The first scenario is the simulation of the system without the proposed closed loop energy management scheme during load application. The second scenario is the simulation of the system with the proposed closed loop energy management scheme during load application. The third scenario is the simulation of the system without the proposed closed loop energy management scheme during load removal. The fourth scenario is the simulation of the system with the proposed closed loop energy management scheme during load removal.

### **5.5.1 Simulation without the proposed closed loop energy management scheme (load application)**

To demonstrate the benefit of the proposed closed loop algorithm, it is worthwhile carrying out a simulation of the power circuit diagram shown in Figure 5-11 as a generator supplying a system with an active power load demand without the proposed closed loop energy management scheme. The simulation results presented are as follows:

Figure 5-12 shows the 3-phase load currents, generator currents and STATCOM +SCESS currents without the closed loop energy management scheme.

Figure 5-13 shows the 3-phase voltages measured at the point of common coupling (PCC).

Figure 5-14 shows the real power current reference.

Figure 5-15 shows the diesel engine torque.

Figure 5-16 shows the speed response of the prime mover to the active power load demand.

Figure 5-17 shows the electrical frequency response to an active power load step demand.

## Chapter 5: Frequency control improvement within a microgrid

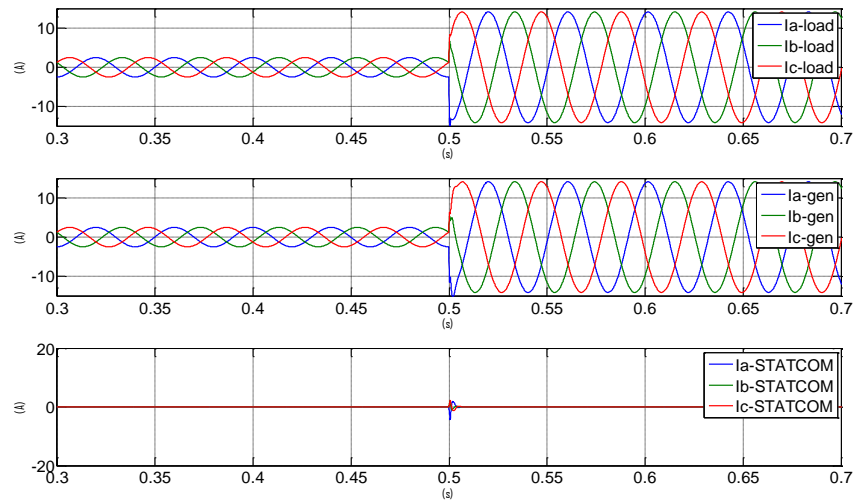


Figure 5-12: Load currents, generator currents and STATCOM+SCESS currents during simulation without the proposed closed loop algorithm

From the current waveforms shown in Figure 5-12, it can be seen that the main load is switched on at time  $t=0.5\text{s}$ . This resulted in a load step being imposed on the system. A sudden load current change from 2.5A (peak) to approximately 14A (peak) can be clearly seen in the top trace. This load demand will be supplied only by the generator. The sudden change in the generator current also appears in the middle trace with the same trend as of the load current. The bottom trace shows that in this operation mode there is no support current from the combined STATCOM and SCESS unit.

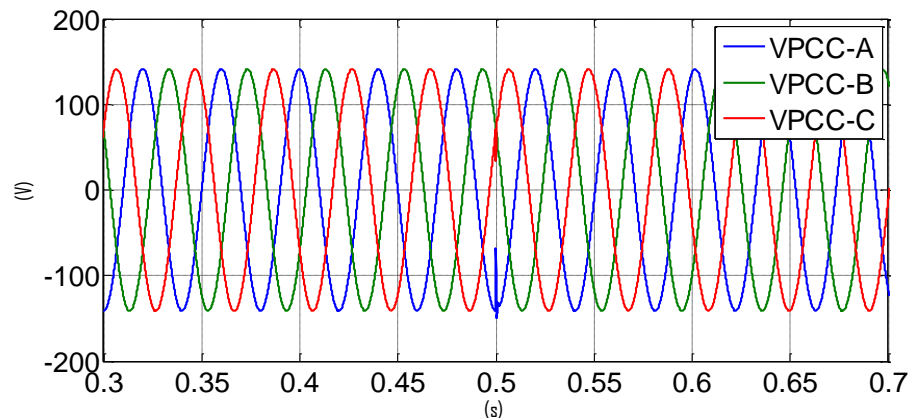


Figure 5-13: Voltage measured at the point of common coupling

## Chapter 5: Frequency control improvement within a microgrid

The voltage measured at the point of common coupling is shown in Figure 5-13. The generator internal impedance is assumed to be negligible in comparison to the main load. Hence, the voltage measured at the point of common coupling (PCC) is equal to the generator voltage regulated by the AVR ( $100\sqrt{2}$  peak voltage).

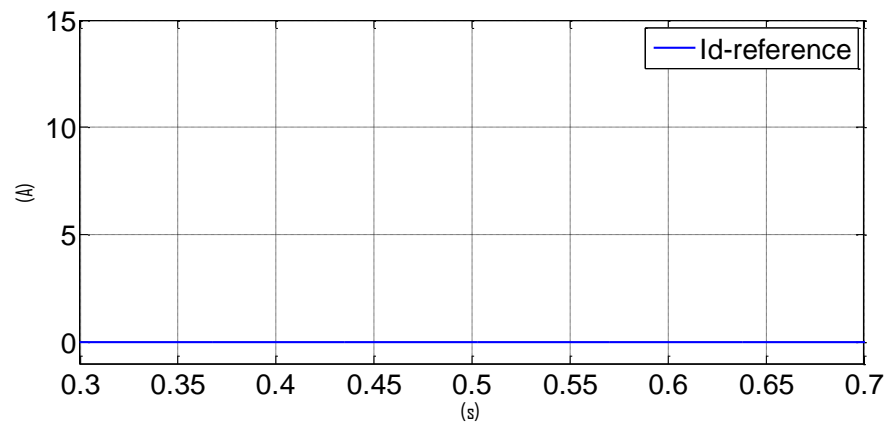


Figure 5-14: Real power current demand (without the proposed closed loop algorithm)

The real power current reference is shown in Figure 5-14. It can be clearly seen that the real power current reference is zero since the simulation was carried out without the proposed closed loop control algorithm.

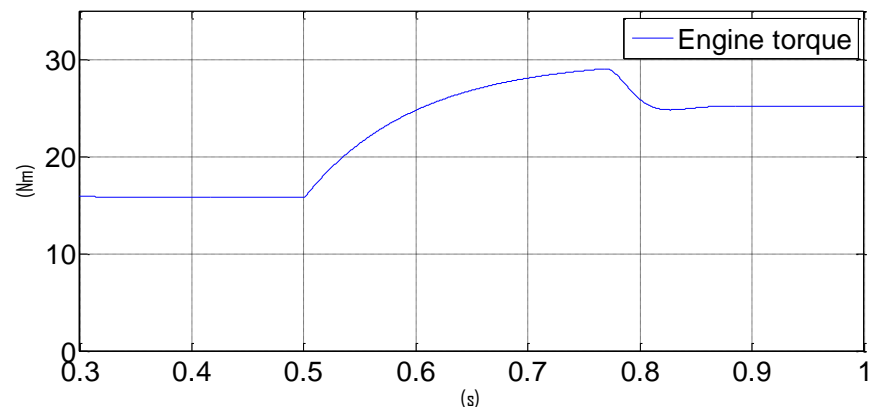


Figure 5-15: Engine torque output (without the proposed closed loop algorithm)

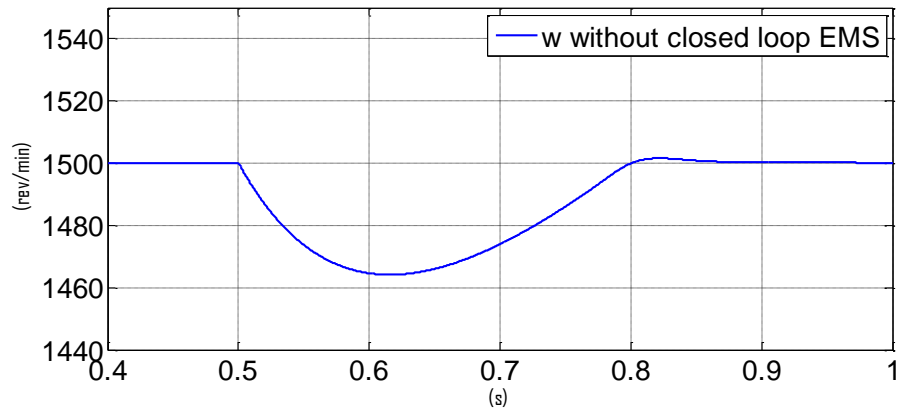


Figure 5-16: Speed response of the prime mover to an active power load step demand during simulation without the proposed control algorithm

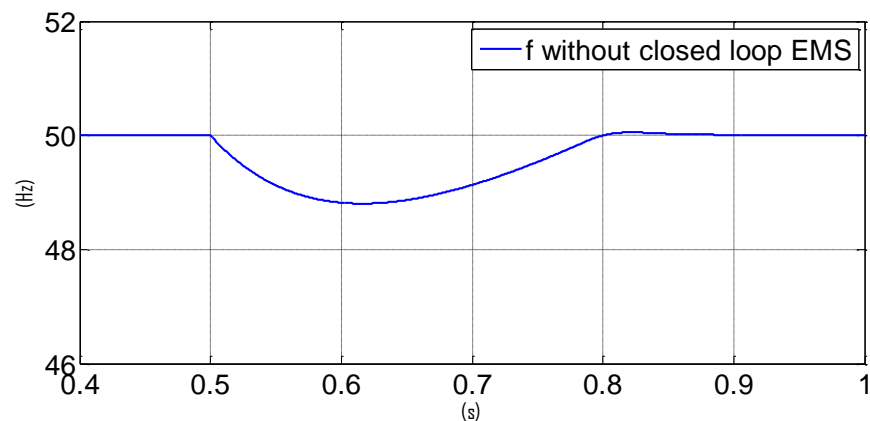


Figure 5-17: Electrical frequency response to an active power load step demand during simulation without the proposed control algorithm

When the load step is imposed, the generator can only respond to the power demand by slowing down and releasing only a small amount of stored kinetic energy as shown in Figure 5-16. The speed controller will increase the throttle demand to the maximum engine torque to accelerate the generator back to the set point speed and make sure the throttle demand matches the new load setting as shown in Figure 5-15. Before the load impact, there is no change in the generator's rotor speed. This implies that the generator's speed is constant at the synchronous speed. However, with the impact of the sudden load change as shown in Figure 5-16, the rotor speed deviates over the period  $t=0.5s$  and

$t=0.6s$ . This results in a speed drop of about 36RPM during that period. From  $t= 0.6s$  onward, the governor control responds to the change by modulating the appropriate mechanical input power to the generator in order to match the new load power. The speed of the prime mover then gradually increases until the mechanical and electrical power is matched (at approximately 0.8s). The electrical frequency response to the active power load demand is shown in Figure 5-17. A frequency drop of 1.2 Hz can be observed during the load transient.

## **5.5.2 Simulation with the proposed closed loop energy management scheme (load application)**

To demonstrate the capability of the proposed closed loop control algorithm in providing frequency control improvement within a microgrid, the power circuit diagram shown in Figure 5-11 is simulated with the proposed closed loop energy management scheme. The simulation results presented are as follows:

Figure 5-18 shows the active power load demand.

Figure 5-19 shows the 3-phase load currents, generator currents and STATCOM +SCESS currents with the closed loop energy management scheme.

Figure 5-20 shows the 3-phase voltages measured at the point of common coupling (PCC).

Figure 5-21 shows the real power current reference.

Figure 5-22 shows the diesel engine torque.

## Chapter 5: Frequency control improvement within a microgrid

Figure 5-23 shows the speed response of the prime mover to the active power load step demand

Figure 5-24 shows the electrical frequency response to an active power load step demand

An active power load demand step of 2.5kW imposed on the system is shown in Figure 5-18. The load step was imposed at time  $t=0.5$ s.

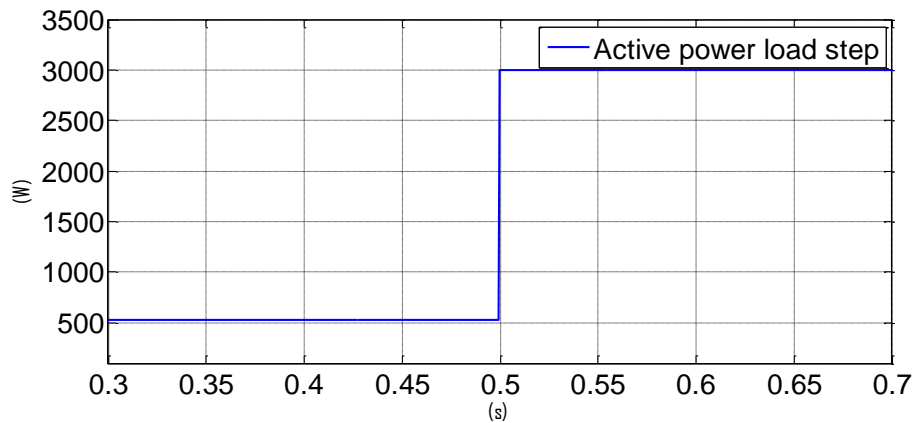


Figure 5-18: Active load power step

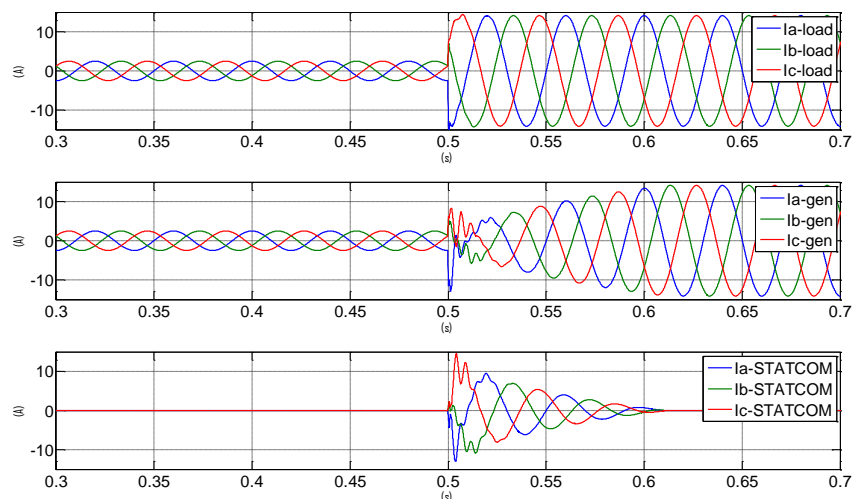


Figure 5-19: Load currents, generator currents and STATCOM+SCES currents during simulation with the proposed control algorithm

## Chapter 5: Frequency control improvement within a microgrid

From the current waveforms shown in Figure 5-19, it can be seen that the main load is switched on at time  $t=0.5s$ . The same sudden change in the main load current from 2.5A (peak) to 14A (peak) as described previously is seen in the top trace. To minimise the impact on the generator, at the beginning of this transient condition, the load is supplied partly by the rapid real power injection generated by the combined STATCOM and SCESS unit via the high gain transient management controller.

During normal operation, the prime mover is controlled by a governor and the combined STATCOM and SCESS real power reference is set to zero. During the load transient, the governor is driven to a maximum output to meet the new load demand as fast as possible. According to the limit in the amount of stored energy in the combined STATCOM and SCESS unit, the high gain transient management controller is designed to inject real power to the load with magnitude equal to the change in the load current at the detection of the load step ( $t=0.5s$ ) then reducing constantly to zero at  $t=0.6s$  as shown in the bottom trace of Figure 5-19. Consequently, at the beginning of the load impact, the generator current increases constantly with the support current from the combined STATCOM and SCESS unit until reaching the maximum current at time  $t=0.6s$  (when the combined STATCOM and SCESS current becomes zero) as shown in the middle trace of Figure 5-19. This control action will continue until the diesel engine generated torque matches the load torque

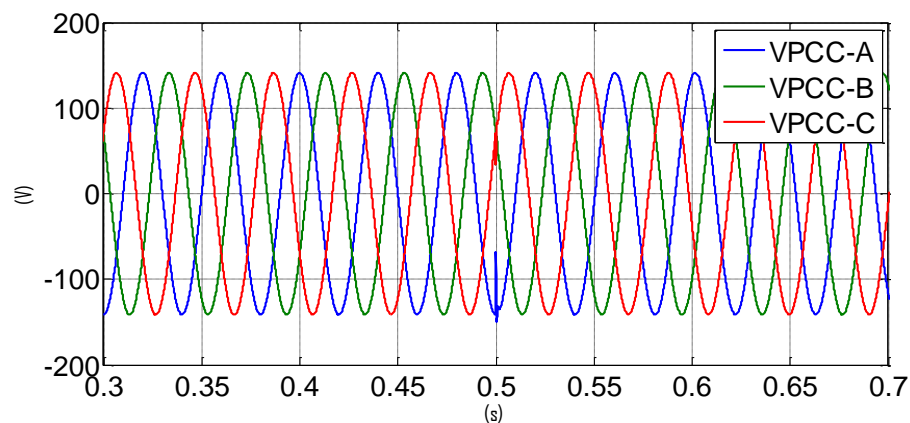


Figure 5-20: Phase voltage measured at the point of common coupling

## Chapter 5: Frequency control improvement within a microgrid

The voltage measured at the point of common coupling is shown in Figure 5-20. The voltage measured at the point of common coupling (PCC) is equal to the generator voltage regulated by the AVR ( $100\sqrt{2}$  peak voltage).

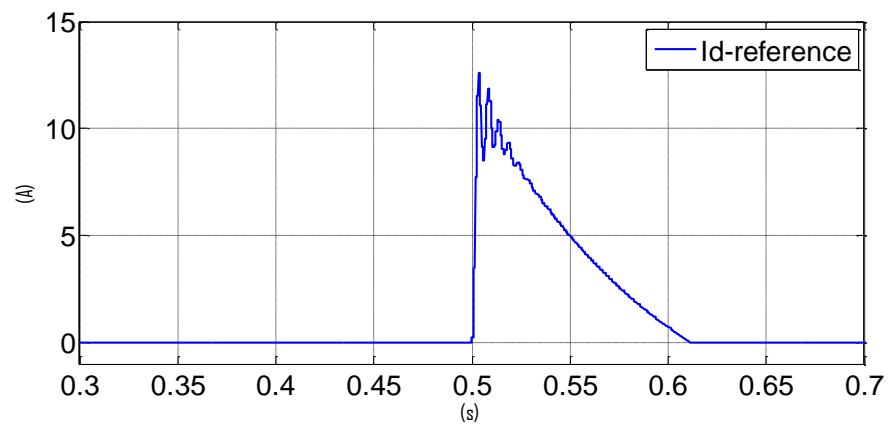


Figure 5-21: Real power current demand (with the proposed closed loop algorithm)

The real power current reference is shown in Figure 5-21. The real power current reference ( $\sim 12A$ ) is obtained from the high gain transient management controller and it is used to determine the amount of real power to be injected by the combined STATCOM and SCESS. The controller has a fast dynamic response which offers the possibility of releasing energy at a much faster rate than the prime mover.

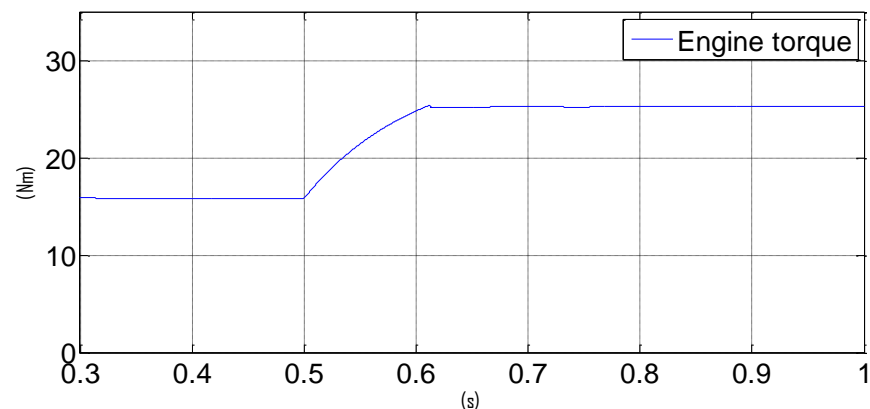


Figure 5-22: Engine torque output (with the proposed closed loop algorithm)

## Chapter 5: Frequency control improvement within a microgrid

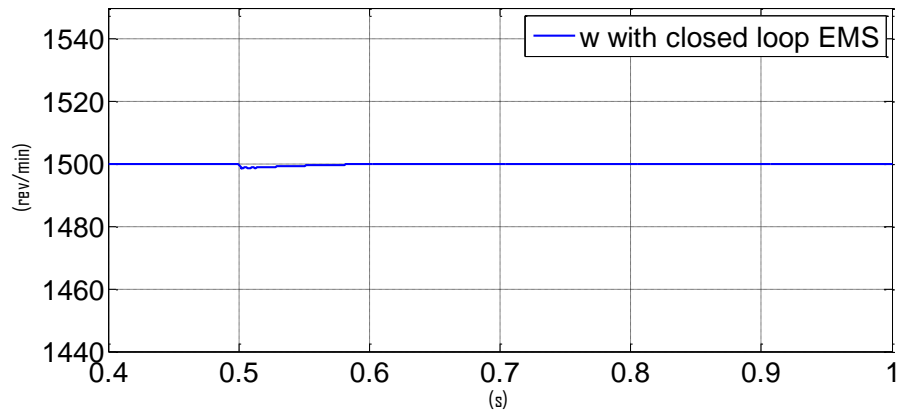


Figure 5-23: Speed response of the prime mover during the simulation with the proposed control algorithm

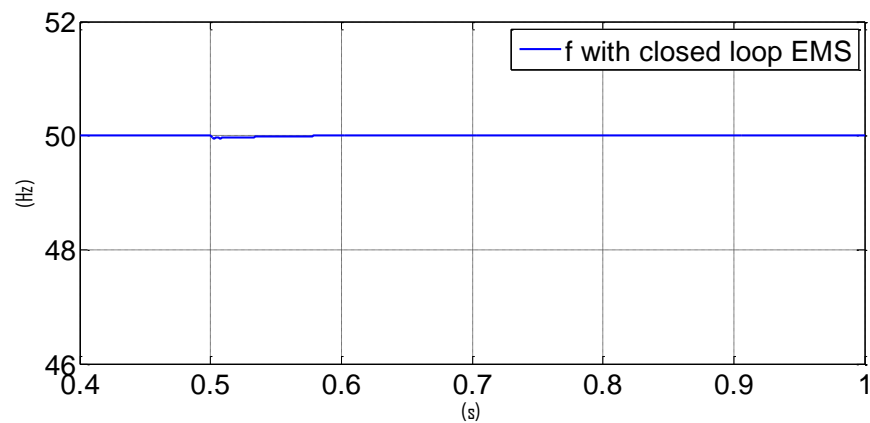


Figure 5-24: Electrical frequency response during the simulation with the proposed control algorithm

The transient management controller (STATCOM speed control) controls the speed and manages the power supplied by the combined STATCOM and SCESS whilst the prime mover power output is increased and therefore regulates the speed with little disturbance. The diesel engine torque output is shown in Figure 5-22. It can be seen that the new load setting is matched at time  $t=0.6s$  following the real power injection from the combined STATCOM and SCESS. Consequently, a minimised speed and frequency variation as shown in Figure 5-23 and Figure 5-24 respectively is achieved with the proposed closed loop algorithm.

## Chapter 5: Frequency control improvement within a microgrid

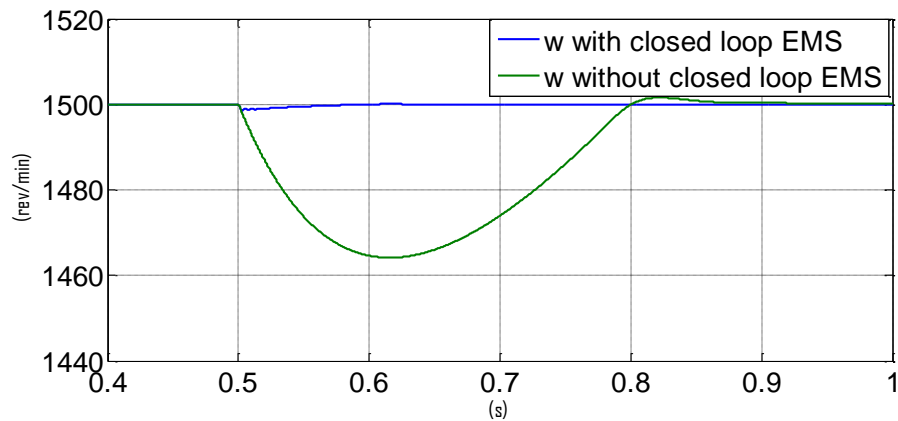


Figure 5-25: Zoomed response of the prime mover (without and with the proposed closed loop algorithm)

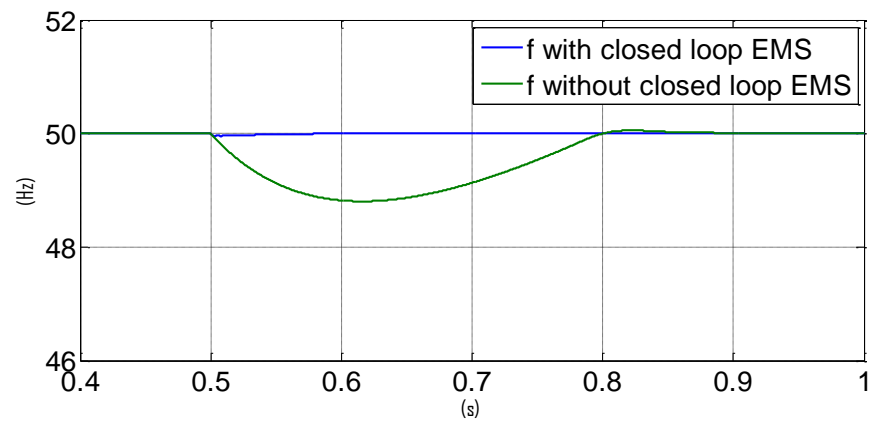


Figure 5-26: Zoomed electrical frequency response (without and with the proposed closed loop algorithm)

In order to highlight the effectiveness of the proposed closed loop control algorithm in providing frequency control improvement within a microgrid, the speed response of the prime mover and electrical frequency response during the simulation of the system without the closed loop algorithm is compared to the simulation of the system with the closed loop algorithm.

A zoomed response of the prime mover and electrical frequency response during the active power load transient is shown in Figure 5-25 and Figure 5-26 respectively. The green trace shows a speed deviation of 36 RPM during the simulation of the system without the proposed closed loop algorithm while the

blue trace shows a deviation of 2 RPM during the simulation of the system with the proposed closed loop algorithm. The blue trace shows an improvement of 94 % in the speed response of the prime mover.

The variation seen when the closed loop control algorithm was employed is attributed to a torque demand oscillation resulting from the crossover from the conventional PI controller used by the governor to the high gain STATCOM speed controller employed during the load transient.

### **5.5.3 Simulation without the proposed closed loop energy management scheme (load removal)**

To demonstrate the benefit of the proposed closed loop algorithm, it is worthwhile carrying out a simulation of the power circuit diagram shown in Figure 5-11 as a generator supplying a system with a sudden loss of active power load without the proposed closed loop energy management scheme. The simulation results presented are as follows:

Figure 5-27 shows the 3-phase load currents, generator currents and STATCOM +SCESS currents without the closed loop energy management scheme.

Figure 5-28 shows the real power current reference.

Figure 5-29 shows the diesel engine torque.

Figure 5-30 shows the speed response of the prime mover to the sudden loss of active power load

## Chapter 5: Frequency control improvement within a microgrid

Figure 5-31 shows the electrical frequency response to the sudden loss of active power load

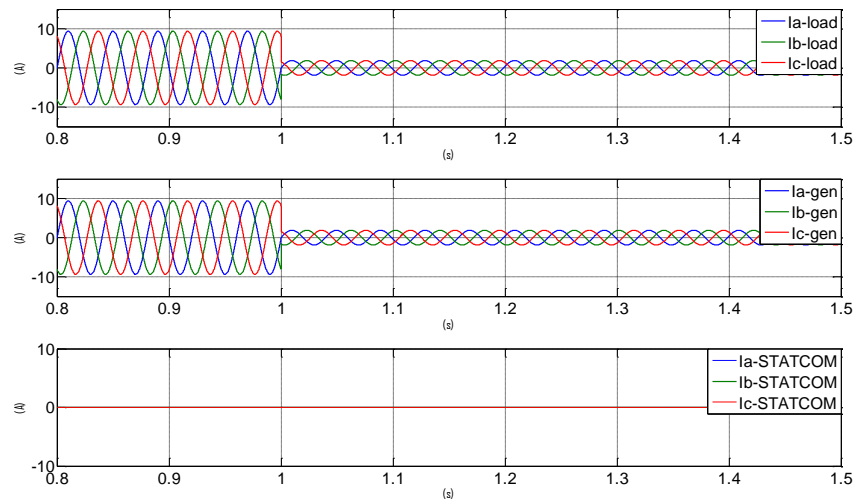


Figure 5-27: Load currents, generator currents and STATCOM+SCES currents during simulation without the proposed control algorithm

From the current waveforms shown in Figure 5-27, it can be seen that the main load is switched off at time  $t=1s$ . This resulted in a negative load step being imposed on the system. A sudden load current change from 10A (peak) to approximately 2A (peak) can be clearly seen in the top trace. This sudden load loss will be absorbed only by the generator. The sudden change in the generator current also appears in the middle trace with the same trend as of the load current. The bottom trace shows that in this operation mode there is no support current from the combined STATCOM and SCES unit.

## Chapter 5: Frequency control improvement within a microgrid

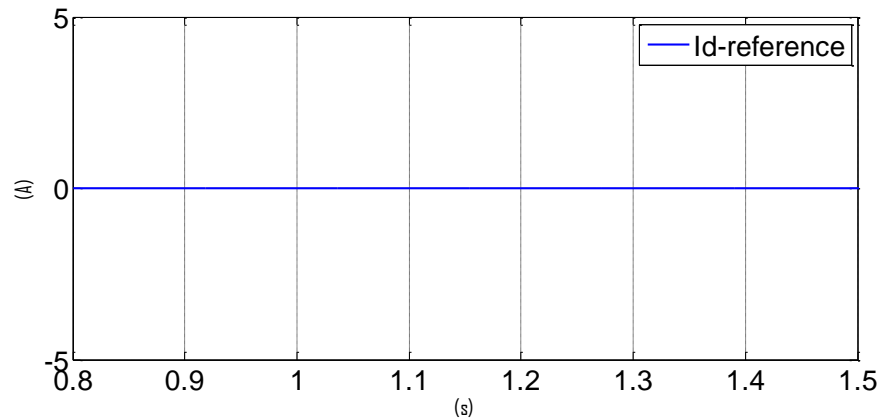


Figure 5-28: Real power current demand (without the proposed closed loop algorithm)

The real power current reference is shown in Figure 5-28. It can be clearly seen that the real power current reference is zero since the simulation was carried out without the proposed closed loop control algorithm.

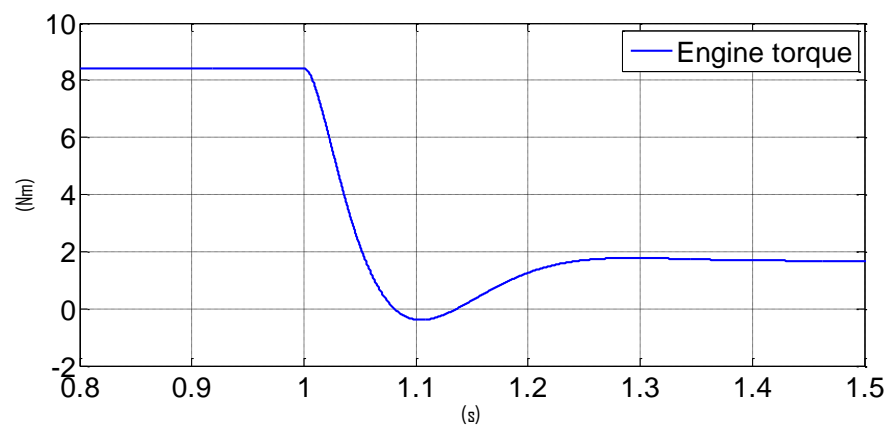


Figure 5-29: Engine torque output (without the proposed closed loop algorithm)

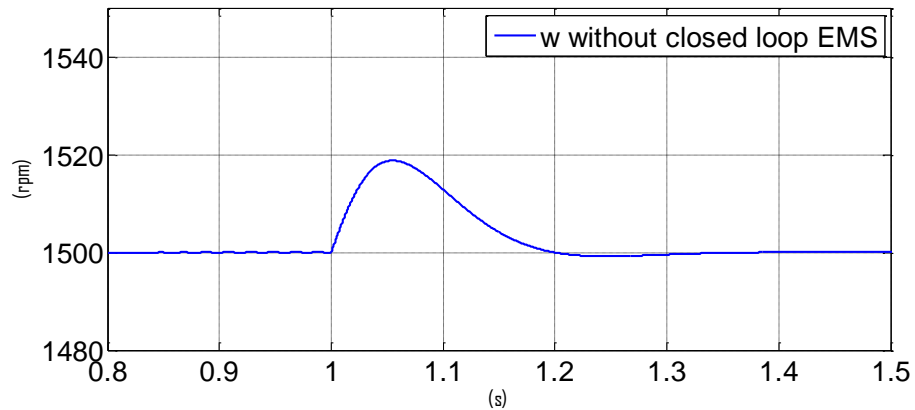


Figure 5-30: Speed response of the prime mover to an active power load step demand during simulation without the proposed control algorithm

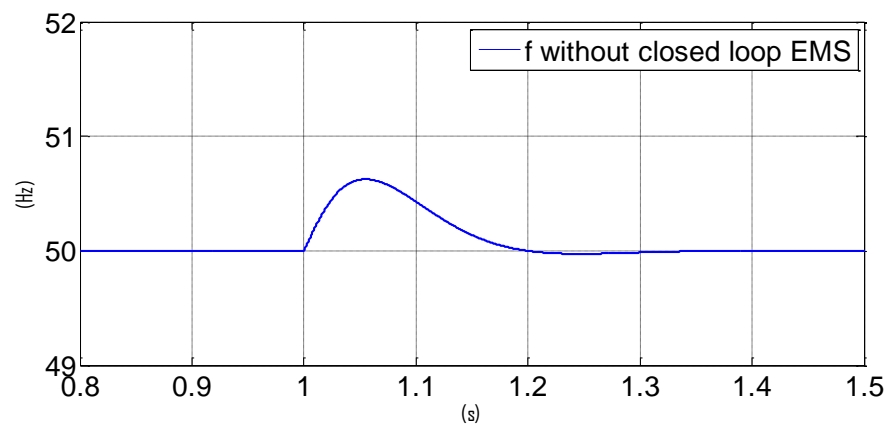


Figure 5-31: Electrical frequency response to an active power load step demand during simulation without the proposed control algorithm

When the load step is imposed, the generator can only respond to the sudden loss of active power load by increasing its speed and absorbing the excess kinetic energy across the rotating mass as shown in Figure 5-30. The speed controller will decrease the throttle demand to the minimum engine torque to decelerate the generator back to the set point speed and make sure the throttle demand matches the new load setting as shown in Figure 5-29. Before the load impact, there is no change in the generator's rotor speed. This implies that the generator's speed is constant at the synchronous speed. However, with the impact of the sudden load change as shown in Figure 5-30, the rotor speed

deviates over the period  $t=1\text{s}$  and  $t=1.05\text{s}$ . This results in a speed increase of about 20RPM during that period. From  $t= 1.05\text{s}$  onward, the governor control responds to the change by modulating the appropriate mechanical input power to the generator in order to match the new load power. The speed of the prime mover then gradually decreases until the mechanical and electrical power is matched (at approximately 1.2s). The electrical frequency response to the active power load demand is shown in Figure 5-31. A frequency drop of 0.67 Hz can be observed during the load transient.

#### **5.5.4 Simulation with the proposed closed loop energy management scheme (load removal)**

To demonstrate the benefit of the proposed closed loop algorithm, it is worthwhile carrying out a simulation of the power circuit diagram shown in Figure 5 11 as a generator supplying a system with a sudden loss of active power load with the proposed closed loop energy management scheme. The simulation results presented are as follows:

Figure 5-32 shows the 3-phase load currents, generator currents and STATCOM +SCESS currents without the closed loop energy management scheme.

Figure 5-33 shows the real power current reference.

Figure 5-34 shows the diesel engine torque.

Figure 5-35 shows the speed response of the prime mover to the sudden loss of active power load

## Chapter 5: Frequency control improvement within a microgrid

Figure 5-36 shows the electrical frequency response to the sudden loss of active power load

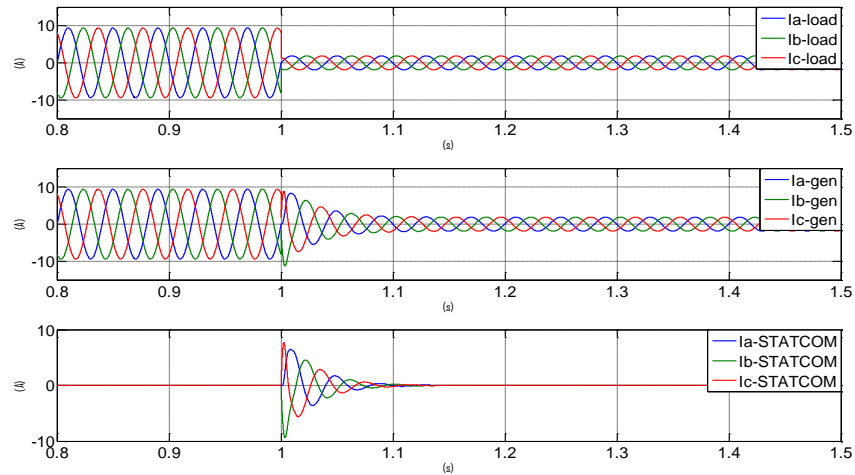


Figure 5-32: Load currents, generator currents and STATCOM+SCESS currents during simulation with the proposed control algorithm

From the current waveforms shown in Figure 5-32, it can be seen that the main load is switched off at time  $t=1s$ . The same sudden change in the main load current from 10A (peak) to 2A (peak) as described previously is seen in the top trace. To minimise the impact on the generator, at the beginning of this transient condition, the excess power is absorbed by the combined STATCOM and SCESS unit via the high gain transient management controller.

During normal operation, the prime mover is controlled by a governor and the combined STATCOM and SCESS real power reference is set to zero. During the load transient, the governor is driven to a minimum output to meet the new load demand as fast as possible. According to the limit in the amount of stored energy in the combined STATCOM and SCESS unit, the high gain transient management controller is designed to absorb real power from the load with magnitude equal to the change in the load current at the detection of the load

## Chapter 5: Frequency control improvement within a microgrid

step ( $t=1s$ ) then reducing constantly to zero at  $t=1.1s$  as shown in the bottom trace of Figure 5-32. Consequently, at the beginning of the load impact, the generator current decreases constantly with the support current from the combined STATCOM and SCESS unit until reaching the maximum current at time  $t=1.1s$  (when the combined STATCOM and SCESS current becomes zero) as shown in the middle trace of Figure 5-32. This control action will continue until the diesel engine generated torque matches the load torque

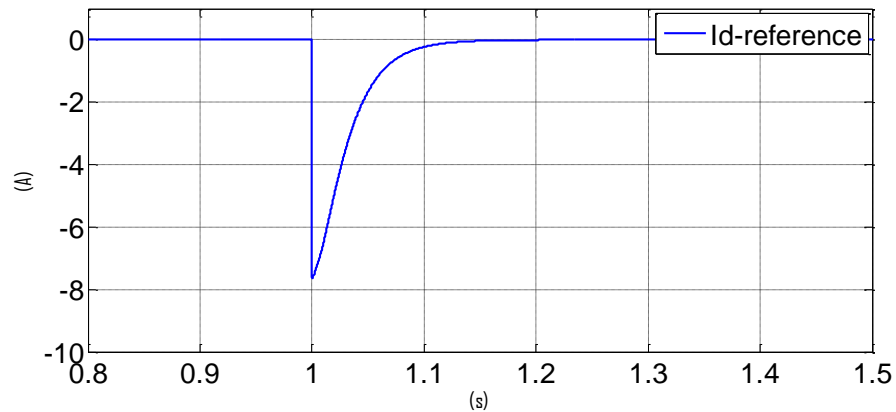


Figure 5-33: Real power current demand (with the proposed closed loop algorithm)

The real power current reference is shown in Figure 5-33. The real power current reference ( $\sim -8A$ ) is obtained from the high gain transient management controller and it is used to determine the amount of real power to be absorbed by the combined STATCOM and SCESS. The controller has a fast dynamic response which offers the possibility of absorbing energy at a much faster rate than the prime mover.

## Chapter 5: Frequency control improvement within a microgrid

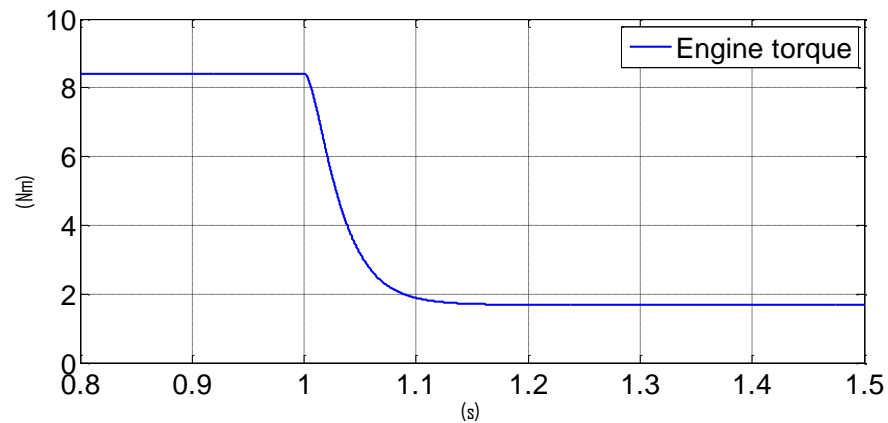


Figure 5-34: Engine torque output (with the proposed closed loop algorithm)

The transient management controller (STATCOM speed control) controls the speed and manages the power absorbed by the combined STATCOM and SCESS whilst the prime mover power output is decreased and therefore regulates the speed with little disturbance. The diesel engine torque output is shown in Figure 5-34. It can be seen that the new load setting is matched at time  $t=1.1s$  following the real power absorption from the combined STATCOM and SCESS. Consequently, a minimised speed and frequency variation as shown in Figure 5-35 and Figure 5-36 respectively is achieved with the proposed closed loop algorithm.

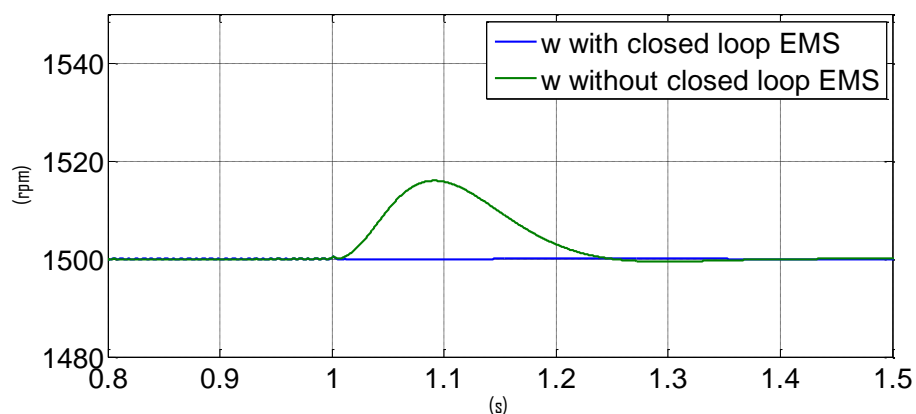


Figure 5-35: Speed response of the prime mover during the simulation with the proposed control algorithm

## Chapter 5: Frequency control improvement within a microgrid

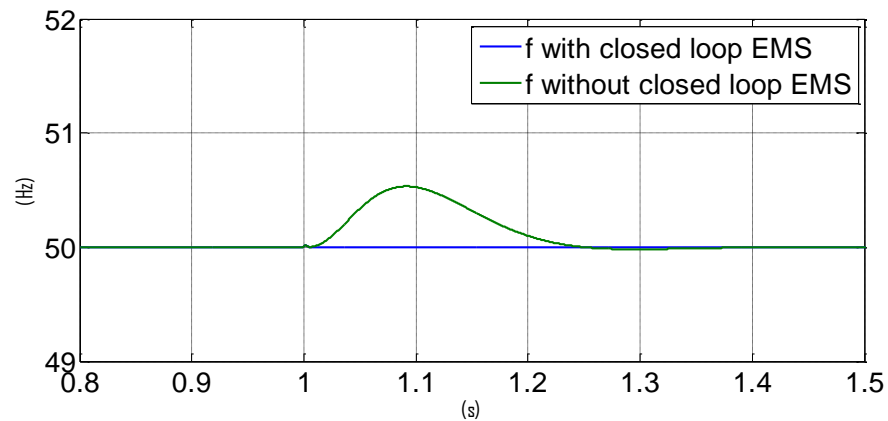


Figure 5-36: Electrical frequency response during the simulation with the proposed control algorithm

In order to highlight the effectiveness of the proposed closed loop control algorithm in providing frequency control improvement within a microgrid, the speed response of the prime mover and electrical frequency response during the simulation of the system without the closed loop algorithm is compared to the simulation of the system with the closed loop algorithm.

A zoomed response of the prime mover and electrical frequency response during the active power load transient is shown in Figure 5-35 and Figure 5-36 respectively. The green trace shows a speed deviation of 20 RPM during the simulation of the system without the proposed closed loop algorithm while the blue trace shows a deviation of 1.2 RPM during the simulation of the system with the proposed closed loop algorithm. The blue trace shows an improvement of 94 % in the speed response of the prime mover.

The variation seen when the closed loop control algorithm was employed is attributed to a torque demand oscillation resulting from the crossover from the conventional PI controller used by the governor to the high gain STATCOM speed controller employed during the load transient.

## **5.6 Conclusion**

In this chapter, energy management schemes that can provide improvements to frequency stability within a microgrid have been explained in detail. Although the open loop energy management scheme has the ability to minimize the variation in speed during load transients, its major drawback is the requirement for the knowledge of the load current and engine transfer function. An improved structure which addresses this drawback was proposed. The proposed closed loop energy management scheme has been described in detail. The closed loop algorithm triggers the combined STATCOM and SCESS to inject/absorb real power to match the new load whilst at the same time communicates with the governor requesting that it should apply full actuation to the prime mover. The performance of the proposed architecture has been investigated by simulation. Simulation results show the effectiveness of the proposed structure in providing frequency control improvements within a microgrid. Results from the simulation will be compared with the experimental results presented in chapter 7.

# Chapter 6

## Experimental layout

---

### 6.1 Introduction

This chapter describes the equipment that was employed to experimentally validate the energy management scheme proposed in chapters 4 and 5 using the real power capability of the enhanced STATCOM and SCESS discussed in chapter 3. For this research, an experimental facility was developed with the aim of:

- I. Demonstrating the real power capability of the combined STATCOM and SCESS under changing load conditions.
- II. Showing the response of an emulated diesel generating set under changing load conditions.

## Chapter 6: Experimental layout

- III. Validating the potential improvements to frequency control by using the proposed energy management scheme.
- IV. Comparing the experimental results with results from the simulation studies carried out in chapters 3, 4 and 5.

The STATCOM and SCESS used for this research was constructed by Phinit Srithorn Ph.D. for the project titled “Control of a STATCOM with Supercapacitor energy storage”[135].

In this chapter, an overview of the experimental rig is presented. Design considerations and details of the associated hardware and software devices used to implement the proposed energy management scheme are also described.

### **6.2 Experimental rig**

The overall layout of the experimental rig can be seen in Figure 6-1. Details of the experimental rig parameters and symbols are shown in Table 6-1. The experimental rig can be divided into two main parts which are the combined STATCOM and Supercapacitor energy storage system (SCESS) and the emulated diesel generating set.

The combined STATCOM and SCESS consist of three coupling reactors, a three phase voltage source inverter, an electrolytic DC-link capacitor, a bi-directional DC-DC converter and a supercapacitor unit. The emulated diesel generating set consist of an induction motor drive and an induction motor coupled to a synchronous generator. Both the combined STATCOM and SCESS and the emulated diesel generating set are controlled from a dSPACE control platform.

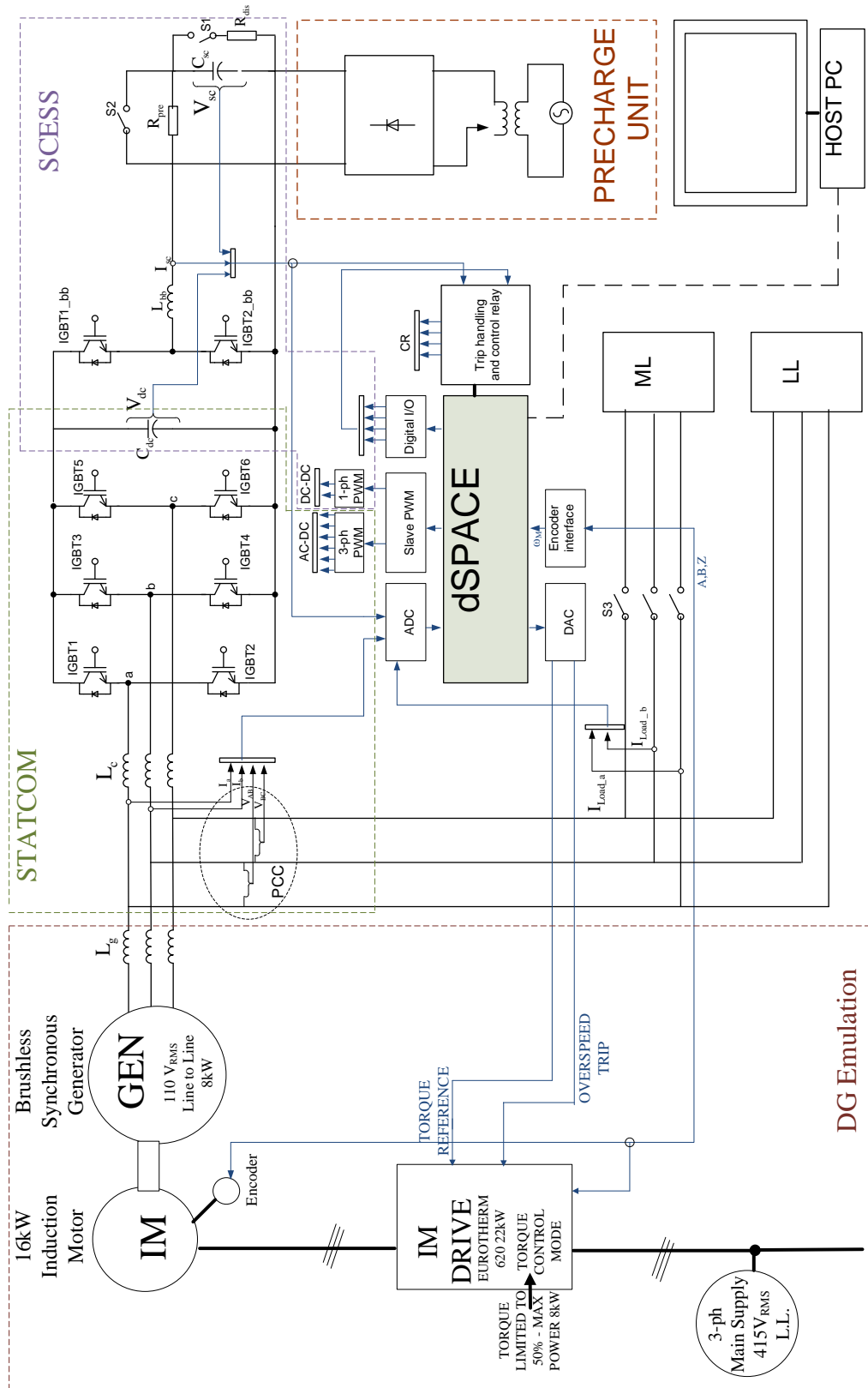


Figure 6-1: Overall layout of the experimental rig

## Chapter 6: Experimental layout

Parameter	Symbol	Value
AC/DC Inverter rating	IGBT <sub>1-6</sub>	10kVA
DC/DC Inverter rating	IGBT <sub>bb1-2</sub>	5kW
DC-link capacitor	C <sub>dc</sub>	1000 $\mu$ F,800V
Supercapacitor module	C <sub>sc</sub>	9.5F,200V
Coupling reactor	L <sub>c</sub>	10mH
DC/DC inductor	L <sub>bb</sub>	10mH
Generator equivalent inductors	L <sub>g</sub>	20mH
Synchronous generator	SG	10kVA@cos $\phi$ =0.8
Synchronous generator voltage	V <sub>SG</sub>	110V <sub>RMS</sub> line to line
Induction motor	IM	16kW
Induction motor drive	IM drive	22kW
Main load	ML	10 $\Omega$

## Chapter 6: Experimental layout

Light load	LL	57 $\Omega$
High power resistor	R <sub>pre</sub> , R <sub>dis</sub>	4kW
High power switch	S <sub>1</sub> ,S <sub>2</sub> ,S <sub>3</sub>	10kW
Control relays	CR	10A, 250V <sub>ac</sub>
DC-link voltage	V <sub>dc</sub>	V <sub>dc</sub> *= 400V
Supercapacitor voltage	V <sub>sc</sub>	V <sub>sc</sub> *=200V

Table 6-1: Experimental rig parameters

### 6.2.1 Design considerations

The synchronous generator is rated at 8kW and configured to generate a PCC voltage of 110V<sub>RMS</sub> line to line. The induction motor is rated at 16kW. It is obvious that the power rating of the induction motor is twice the power rating of the generator. As a result, the torque limit for the induction motor drive has been set to 50%, so that the maximum power generated is around the generator power rating.

As mentioned in chapter 3, the SCESS was integrated to the STATCOM to enhance its real power capability. The AC-DC inverter and the DC-DC converter in this project are designed for utilising and storing energy in the supercapacitor units. As a result, the supercapacitor terminal voltage (V<sub>sc</sub>) is considered as the dominant rating that defines the other voltage limitations. The maximum and minimum voltage ratings of the supercapacitor unit are V<sub>sc\_max</sub>=200V and V<sub>sc\_min</sub>=100V respectively.

## Chapter 6: Experimental layout

The bi-directional DC-DC converter was placed between the supercapacitor unit and the STATCOM to facilitate the exchange of power between the grid and the energy storage system. The converter is designed to keep the DC-link voltage constant at 400V by operating at a duty ratio of about 0.5- the optimum point where energy can be extracted from the supercapacitors by the DC-DC converter [136]. Since the DC-DC converter is interfaced to the STATCOM's DC-link capacitor, the DC-link capacitor is rated at 400V.

To ensure the operation of the STATCOM in the linear region, the three phase PWM voltage at the front-end of the STATCOM should have a higher magnitude than the three phase power supply voltage. With the DC-link voltage fixed at 400V, the generator has been configured to generate a PCC voltage of  $110V_{RMS}$  line to line.

### **6.2.2 STATCOM and SCESS**

The STATCOM comprises of three coupling inductors, three half bridge IGBT modules and a conventional DC-link capacitor as shown in Figure 6-1. The coupling inductors are sized to allow the system to be operated as a controlled current source. The high value of the coupling inductors helps to filter the switching frequency components in the line currents. However, the high value reduces the speed response of the current controller and the size of the current that can be controlled. In this research, a three-phase coupling inductor of 10mH was chosen as a compromise between reduction of switching harmonics and size of current that can be controlled. As mentioned in chapter 3, the value of the DC-link capacitor needs to be large enough to couple the STATCOM and SCESS and maintain a stable DC link voltage Two  $2000\mu F$  415V series connected capacitors were employed as the DC-link capacitor.

## Chapter 6: Experimental layout

The SCESS comprises a bi-directional power flow DC-DC converter rated at 5kW, an inductor and a supercapacitor unit as shown in Figure 6-1. The DC-DC consists of two IGBTs (one half bridge IGBT module). One end of the DC-DC converter is connected to the supercapacitor unit via an inductor and the other end is connected to the STATCOM's DC-link capacitor. The SCESS is designed to improve the performance of the STATCOM. The supercapacitor unit comprises of 10 modules of 95F, 20V supercapacitors connected in series. A 10mH inductor is used as the medium for energy transfer between the supercapacitor unit and the STATCOM's DC-link capacitor.

### **6.2.3 Emulated diesel generating set**

The emulated diesel generating set consist of an induction motor coupled to a synchronous generator and a commercial drive. The generator is a 10kVA, 8kW Leroy Somer LS 40 VS1 synchronous generator equipped with an automatic voltage regulator (AVR). The voltage amplitude is set through the AVR and the internal connections of the windings.

The diesel engine is emulated with a Magnetics MA 133K F1 16kW two pole pairs induction motor and a dedicated drive. The diesel engine emulation is achieved by incorporating a single delay into the speed control loop of the vector controlled induction motor as described in chapter 4. The induction motor is fitted with an on board incremental encoder to measure the rotor speed. The output signal of the encoder is sent to the dSPACE controller card which uses this speed measurement as part of the emulation algorithm. A block diagram showing how the emulation algorithm was achieved is shown in Figure 6-2.

## Chapter 6: Experimental layout

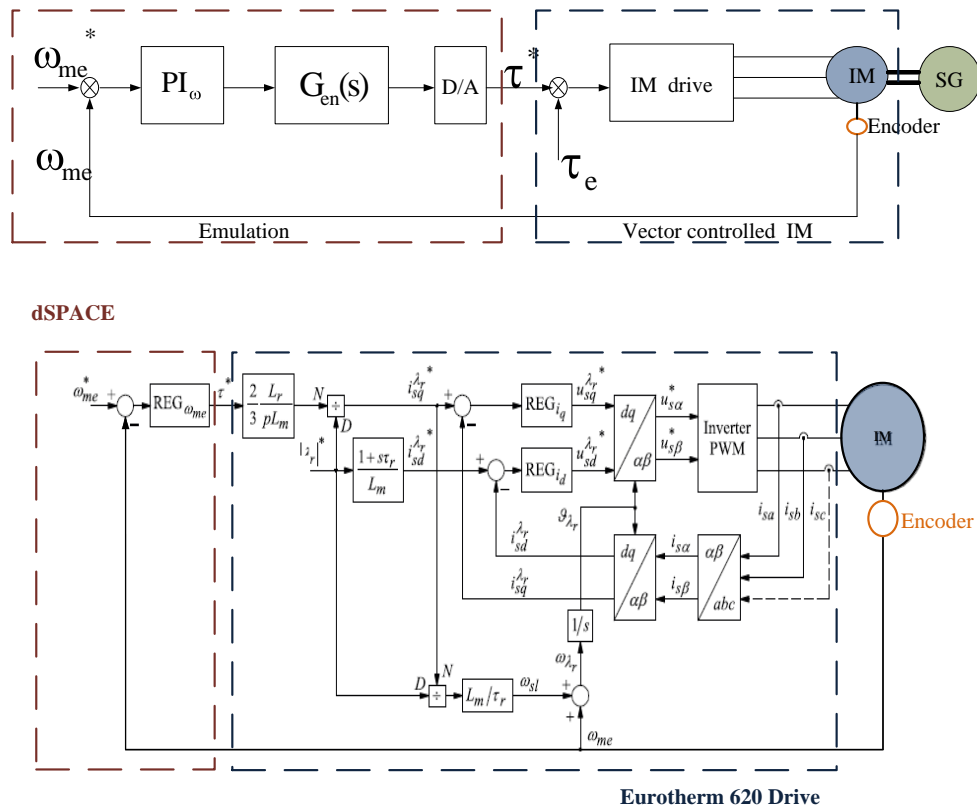


Figure 6-2: Control architecture of the emulated diesel generating set

As shown in Figure 6-2, the emulation algorithm was implemented in dSPACE. A single delay  $G_{en}(s)$  representing the delays inside the prime mover is incorporated in the speed control loop. The emulation algorithm output ( $\tau^*$ ) is then fed into the variable speed drive which drives the prime mover (IM). The emulation algorithm was designed such that when the main load (ML) shown in Figure 6-1 is switched, the generator will see a significant drop in frequency as the prime mover slowly reacts to the load change.

A commercial Eurotherm 620 vector series inverter was employed as the drive in this work. The commercial drive is rated at 22kW and it implements field oriented control (FOC) and space vector modulation (SVM) at a switching frequency of 3 kHz. The drive was considered ideal and the running operation was set by following the instructions in the datasheet. An auto tuning

## Chapter 6: Experimental layout

procedure defines the internal DQ current control parameters and the required magnetizing current reference. The drive is fully protected from overspeed, overcurrent and overvoltage and all the thresholds are configurable by the user. Interaction with the drive is done through the I/O ports. An input equivalent to the q current reference (a percentage of the nominal torque driven by the DAC) was connected to the internal torque reference by following the I/O maps in the data sheet. An external trip that permits the software synchronization between the STATCOM protection system and the drive protection system has also been set as an input signal.

The emulated diesel engine is connected to a synchronous generator, whose output feeds a set of resistive loads, representing a simplified micro grid.

Details of the synchronous generator and induction motors parameters can be found in [137] and [138] respectively.

### **6.2.4 Current mirror and Gate drive circuit**

The high frequency switching operation of both the AC-DC inverter and the DC-DC converter generates high switching frequency noise that can influence the performance of nearby digital electronic devices. Low voltage PWM signals are susceptible to noise problems in noisy environments especially if the PWM voltage signals are transmitted over a long distance.

The noise immunity of a PWM voltage signal transmitted over a long distance can be improved by converting the voltage signal into a current signal before sending the signal to a gate drive circuit which is usually mounted on the IGBT. Alternatively, an optical fibre can be employed but this approach adds cost to the system.

## Chapter 6: Experimental layout

A current mirror circuit based on a Wilson current source configuration [139] was used to convert the PWM voltage signals to current signals. The circuit diagram of the current mirror circuit is shown in Figure 6-3.

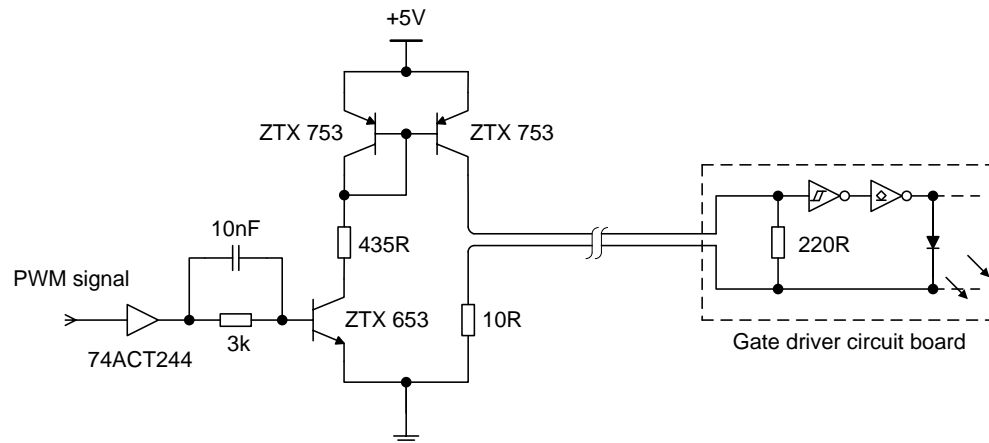


Figure 6-3: Current mirror circuit

The original PWM voltage signal is buffered using a 74ACT244 octal buffer to ensure that the signal will be at +5V and 0V. The buffer also prevents loading error from the control board if any abnormal condition occurred at the current mirror. The PWM voltage signal is converted to current signal with the Wilson current source which has the advantage of eliminating the base current mismatch of the conventional current mirror thereby ensuring that the output current flowing into the input of the optocoupler is almost equal to the input current. The output current signal is then transmitted to the gate drive circuit.

The current signal provided by the current mirror circuit is not capable of turning on and turning off the high power switching devices. Therefore, a gate driver circuit is required to adapt the low level PWM logic signal to a higher level signal that can gate the high power IGBT modules.

The gate driver circuit also provides the isolation between the control and the high power circuit. The gate driver circuit adapts the low level PWM logic signal into an adequate signal that can gate the IGBTs by providing +15V between the gate and emitter of the IGBTs to turn ON the device when the

## Chapter 6: Experimental layout

digital control signal is high and -15V between the gate and the emitter of the IGBTs to turn OFF the device when the digital control signal is low. The arrangement of the gate drive circuit is shown in Figure 6-4.

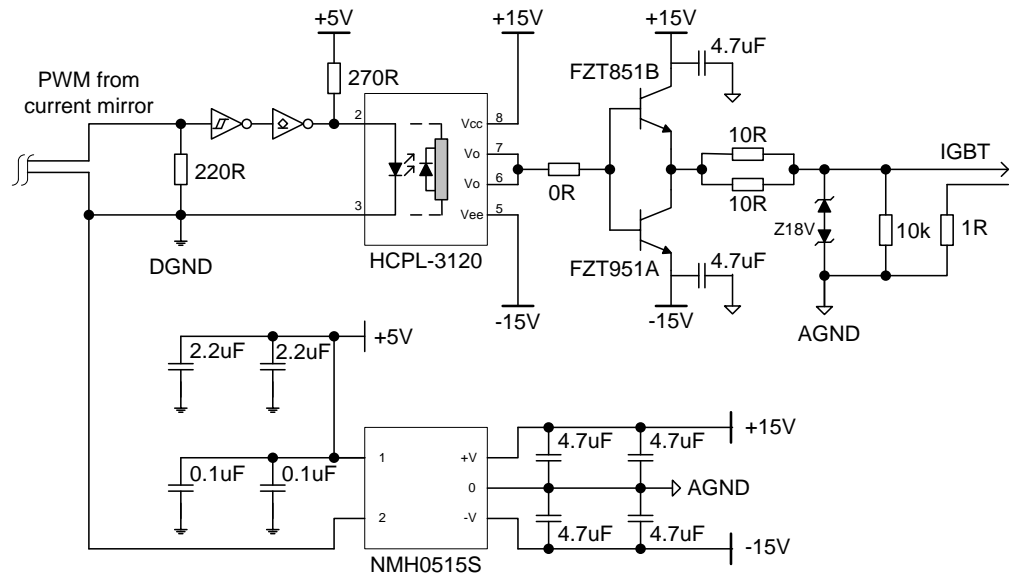


Figure 6-4: Gate drive circuit

As shown in Figure 6-4, the input of the gate drive circuit is the current signal coming from the current mirror and the output is the high level PWM voltage signal required to gate the IGBTs.

The PWM current signal from the current mirror is converted to a voltage signal through the 220R resistor. A voltage input is then presented at the input of the Schmitt trigger. The Schmitt trigger reduces the possible noise effects and provides a well-defined voltage signal to the open collector buffer which drives the Schmitt trigger output to the HPCL3120 in conjunction with the 270R pull up resistor. The HPCL 3120 is an optocoupler which provides galvanic isolation between the control signal and the IGBT connections. The HPCL 3120 drives a push pull configuration, used to increase the current available to drive the gate of the IGBTs. It is important to carefully choose the value of the gate resistance as it determines the turn on and off speed which is

dependent on the characteristics of the IGBT module. In this research, a GP200MHS12 half bridge IGBT module (one for each phase) manufactured by Dynex was used and a gate resistor of  $5\Omega$  (two  $10R$  resistor connected in parallel) was chosen.

### **6.3 Control platform**

The dSPACE system based on the DS1104 R&D Controller Board is employed as the control platform. The subsystems of the experimental rig are controlled from the PC via the DS1104 R&D Controlled board. The DS1104 R&D Controller Board can be plugged into a PCI slot of a PC. The DS1104 R&D Controller Board is a complete real time control system based on a 603 PowerPC floating-point processor running at 250MHz. The board also includes a slave-DSP subsystem based on the TMS320F240 DSP microcontroller which can be used for advanced I/O purposes [140].

The dSPACE system has a specific interface connector panel which provides easy access to all the input and output signals of the DS1104 R&D Controller Board. The connector panel provides easy-to-use connections between the DS1104 R&D Controller Board and the devices to be connected to it. Devices can be individually connected, disconnected or interchanged without soldering via BNC connectors and sub-D connectors. The dSPACE system also comes with the ControlDesk software package version 3.7.2, a graphical user interface which is used to monitor, automate and capture data during experiments [141].

The control operations performed by the dSPACE board can be programmed in MatLab/Simulink which is the same software package used for the simulation studies carried out in chapter 3, 4 and 5. The RTI blocks provided with the controller board are compatible with MatLab/Simulink and are used to build the simulation files to complete the connections to the hardware. The

## Chapter 6: Experimental layout

DS1104 R&D Controller Board can connect the variables of the simulation structure to all the necessary peripherals by generating code based on the simulation structure. The controller board also provides the control for the implementation process from simulation up to real time experiment. More details of how to program the dSPACE controller board can be found in [140].

### 6.4 Data acquisition

As mentioned earlier, the controller board comes with a connector panel which provides easy-to-use connections between the board and the devices to be connected to it. The connector panel consist of eight ADC channels, eight 16-bit DAC channels, a 20-bit master I/O unit, a slave I/O unit and an incremental encoder unit. A block diagram depicting how the data acquisition and pulse generation is achieved with the DS1104 R&D Controller Board is shown in Figure 6-5.

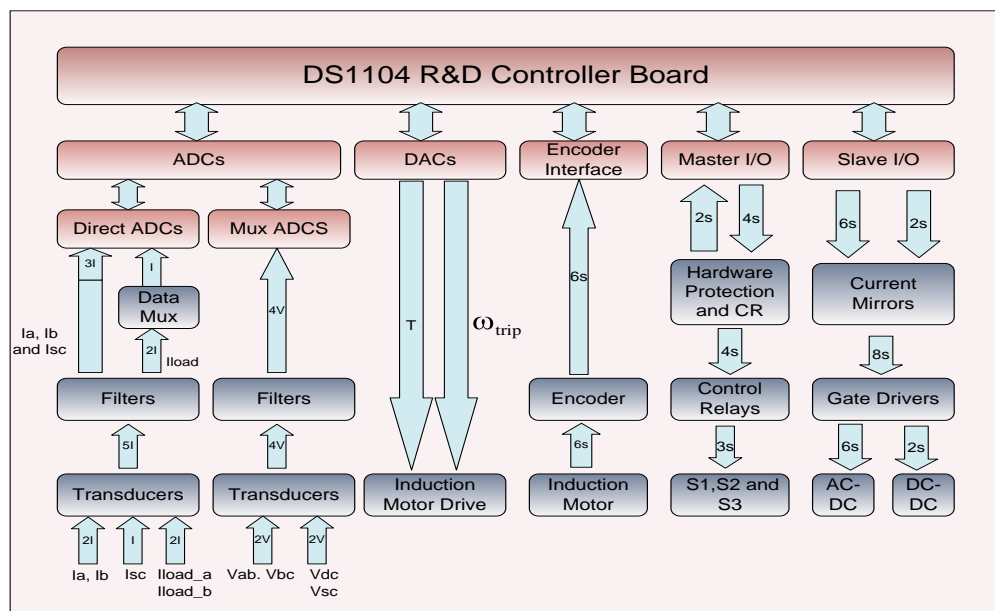


Figure 6-5: Functional block diagram of the data acquisition and pulse generation process

## Chapter 6: Experimental layout

In Figure 6-5, the connector panel provides four direct 12-bit ADC channels and four multiplex 16-bit ADC channels. In this research, the current controller is important when controlling the flow of power. To avoid the delay from the multiplexing process, the current signals from the transducers are all connected to the direct ADC channels and the voltage signals are connected to the multiplex ADC channels. The torque reference analogue input of the induction motor drive and the overspeed trip are generated through two of the DAC channels. The master I/O unit is used to generate the signals required to control the hardware protection and control relaying board. The slave I/O unit is used to generate the PWM pulses which are transmitted to the current mirror circuit. The current mirror is employed to improve the noise immunity of the transmitted PWM signals by converting the voltage PWM signals to current PWM signals. The current PWM signals are then sent to the gate drive circuits of both the AC-DC voltage source inverter and the DC-DC converter.

As shown in Figure 6-5, the input data required by the control platform are supplied from the measurement boards. These data include two line voltages at the point of common coupling ( $V_{ab}, V_{bc}$ ), DC-link voltage ( $V_{dc}$ ), Supercapacitor voltage ( $V_{sc}$ ), two line currents between the ac power grid and the voltage source inverter ( $I_a, I_b$ ), supercapacitor current ( $I_{sc}$ ), load currents ( $I_{load\_a}, I_{load\_b}$ ) and the encoder position signals used to obtain the induction motor speed ( $\omega$ ). Four voltage transducers, five current transducers and an encoder are used to measure the data required by the control platform. There are nine signals to be fed into ADC channel provided by the control board. However there are eight ADC input channels on the connector panel. The load currents were multiplexed as explained in section 6.4.3. Measurement of the data using the voltage transducers, current transducers and the encoder are detailed in section 6.4.1 and 6.4.2.

## 6.4.1 Voltage and Current measurements

LEM LV25-P voltage transducers were used to measure the DC-link voltage, supercapacitor voltage and the PCC voltages. A schematic diagram of the voltage measurement circuit is shown in Figure 6-6.

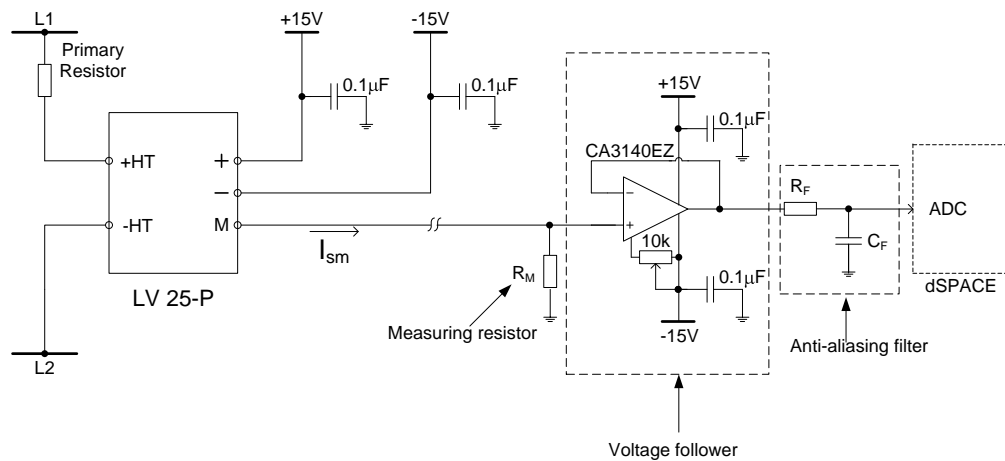


Figure 6-6: Voltage measurement circuit

The transducer is fed by a +15V and -15V power supply. The transducer primary side is connected in series with a primary resistor which limits the primary current to a maximum value of 10mA. At the secondary side, the transducer output current is passed through a measuring resistor ( $R_M$ ) that converts the output current into the original voltage seen on the primary side. The output voltage resulting from the secondary current flowing through the measuring resistor ( $R_M$ ) is then connected to an anti-aliasing filter through a voltage follower circuit. The voltage follower circuit is used as a buffer which prevents interference between the transducer output circuit and the anti-aliasing filter. Details of the design of the voltage measurement circuit can be found in [142].

LEM LA55-P current transducers were used to measure the line currents, load currents and the supercapacitor current. LA55-P current transducer has a

## Chapter 6: Experimental layout

maximum current capability of 50A, a conversion ratio of 1:1000 and a bandwidth of 200 kHz [143]. A schematic diagram of the current measurement circuit is shown in Figure 6-7.

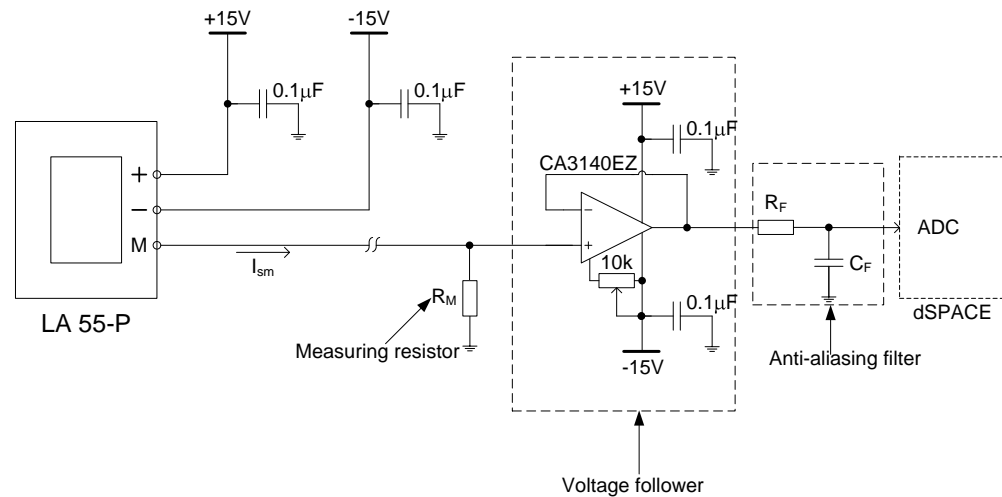


Figure 6-7: current measurement circuit

The transducer is fed by a +15V and -15V power supply. At the secondary side, the transducer primary current is converted to an equivalent voltage signal. The voltage follower circuit and the anti-aliasing filter are added to the transducer output circuit as shown in Figure 6-7. Details of the design of the current measurement circuit can be found in [143].

### 6.4.2 Speed measurement

The Eltra EH 80K 2048 Z 8/24 VLD incremental encoder is used to measure the speed of the induction motor. The maximum measurable frequency  $f_{MAX}$  is 1000 kHz and the resolution  $r = 2048$  impulses/turn, meaning that the maximum measurable speed  $\omega_{MAX} = (f_{MAX} * 60/r) = 2920$  RPM. The encoder is suitable for this work because the nominal speed of the induction motor employed is 1500RPM.

## Chapter 6: Experimental layout

The incremental encoder generates a pulse for each incremental step in its rotation. The encoder uses two output channels (A and B) to sense position. The two output channels are positioned  $90^\circ$  out of phase. A third output channel called the zero signal (Z) supplies a single pulse per revolution which is used for precise determination of a reference position. The encoder output signals A, B and Z were sent to the digital increment encoder interface of the controller board using sub-D connectors. A schematic diagram of the input circuitry of the incremental encoder is shown in Figure 6-8.

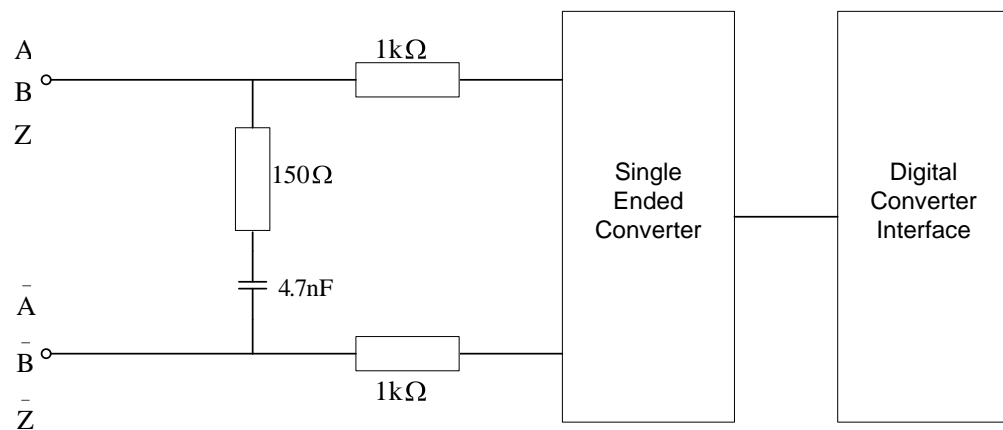


Figure 6-8: Input circuitry of the incremental encoder interface

The encoder is fed by an external 12V power supply. The encoder interface of the dSPACE system simply counts the number of edges of the encoder signals and identifies the position and direction of the induction motor by monitoring both the number of pulses and the relative phases of the encoder signals. The encoder resolution is quadrupled by counting all the edges of A and B and the total resolution is 8192 impulses/turn. The rotor speed can be obtained in the dSPACE controller board from the rate of change of the position signal.

### 6.4.3 Data multiplexer

A data multiplexer board was used to extend the availability of the ADC input channels. A circuit diagram of the data multiplexer is shown in Figure 6-9.

## Chapter 6: Experimental layout

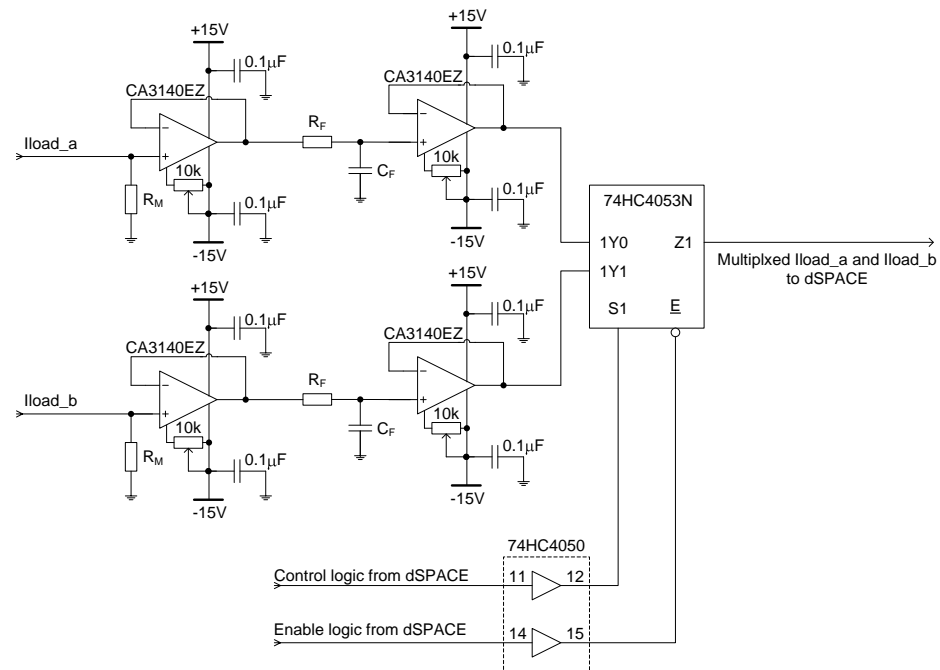


Figure 6-9: Data multiplexer circuit

At the inputs of the board, load currents from the current transducers are passed through the measuring resistors  $R_M$ , resulting in the equivalent voltage signals. These voltage signals are passed into two voltage follower circuits as described in section 6.4.1. The output of the voltage followers are fed into the 2-channel multiplexer device MM74HC4053. The control and enable logic signals are generated by the dSPACE controller board. These logic signals are sent via high-speed Si-gate CMOS non inverting buffers to prevent loading error between the multiplexer and the controller board.

The multiplexed load current is read from one of the ADC input channel of the connector panel and de-multiplexed by the control logic signal produced by a toggle and a flip-flop. The control logic signal is also used to synchronise the de-multiplexed output signal with the input load signal at the multiplexer board.

## **6.4.4 Trip Handling**

Both software and hardware protection schemes were implemented in this work. Hardware trips are faster than the software trips due to the limitations caused by the sampling delay in the latter. Hardware trips are thus more important. Varistors and semiconductor fuses were placed at the front end of the inverter to form over-voltage and over-current protection respectively for the STATCOM.

The hardware protection implemented compares the supercapacitor and DC-link voltage transducers output signal with an adjustable reference voltage. If the transducer output signal is greater than the reference voltage, the output of the comparator will be held as logic high by a D-latch until the reset switch is pushed. The output logic from the D-latch is sent to an optocoupler in order to turn on the control relay which is used to disconnect the power circuit from the power supply.

The software protection scheme is also designed to check if the experimental rig is operated within acceptable limits. If the experimental rig is operated beyond the acceptable limits, the protection scheme will trigger a trip signal that will stop the operation of the rig immediately. The STATCOM currents, supercapacitor currents and voltages, DC-link voltage and the speed of the induction motor are compared with the reference values. If any of the aforementioned signals is greater than the reference values, the output logic will be set to 1 and the output logic is held as 1 by a SR flip flop. The output logic signal is used as the stop logic for the functional built in block that is used to generate the PWM signals for the STATCOM and SCESS. A reset signal is used to refresh the protection scheme after the operating condition becomes normal.

## **6.5 Conclusion**

The experimental rig used to validate the proposed control scheme for frequency control improvement has been presented in this chapter. The rig was also used to validate the simulation studies investigated in chapters 3, 4 and 5. The layout of the experimental rig including all the hardware and software devices was described in detail.

In the next chapter, the experimental results obtained from the operation of the rig will be presented.

# Chapter 7

## Experimental results

---

### 7.1 Introduction

This chapter presents the results obtained from the experimental rig described in chapter 6. These results are presented in order to validate the simulation results described in chapter 5 where the frequency control capability of the combined STATCOM and SCESS was demonstrated.

The aim of this work is to develop control algorithms for frequency control within a microgrid. A single line diagram of the experimental test system is shown in Figure 7-1.

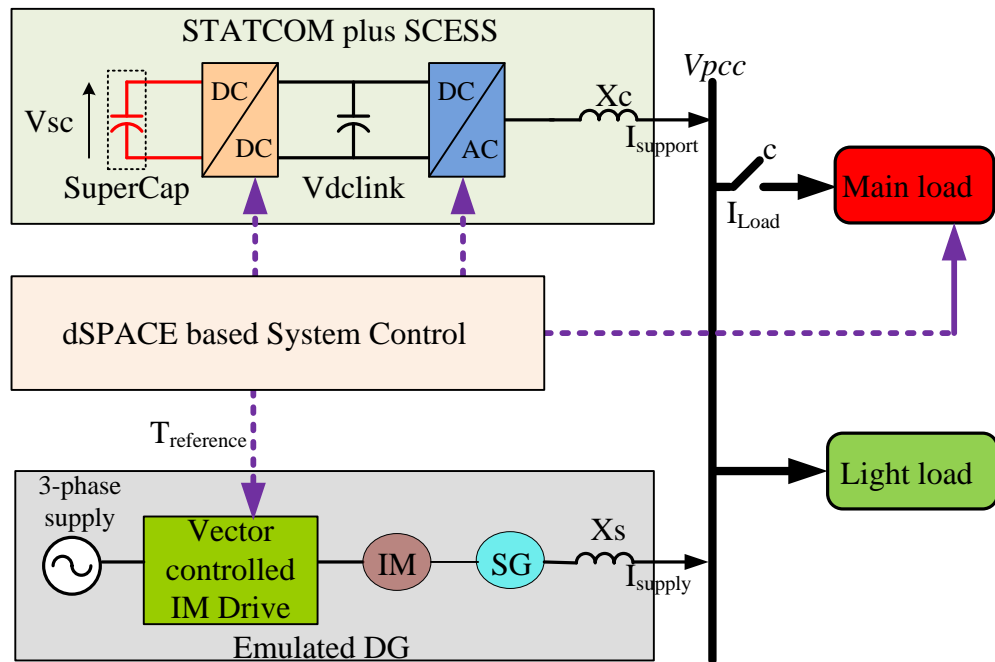


Figure 7-1: Single line diagram of the experimental rig

The results obtained from the experimental rig are presented in three sections. In the first section, the effects of load changes on a weak microgrid network based on the emulated diesel generating set described in chapter 4 are presented. In the second section, the results obtained from the operation of the combined STATCOM and SCESS described in chapter 3 are presented. In the third section, improvements to frequency control using the real power capability of the STATCOM and SCESS and the control algorithms proposed in chapter 5 are presented. The benefits of the proposed control algorithms are illustrated explicitly by comparing the results obtained with and without the proposed algorithm.

## 7.2 Effects of active power load change on a microgrid network

To demonstrate the benefits of the proposed control algorithms, it is worthwhile highlighting the behaviour of the microgrid network during active power load changes. As mentioned in chapters 4 and 6, the microgrid network is based on an emulated diesel generating set. The diesel engine emulation is achieved by incorporating a delay into the speed control loop of the vector controlled induction motor. The emulation algorithm was implemented in dSPACE and its output (torque reference) is fed into a vector controlled induction motor drive as shown in Figure 7-1. The speed control loop is verified experimentally with the response of the speed regulator to a step change in speed of 100RPM as shown in Figure 7-2.

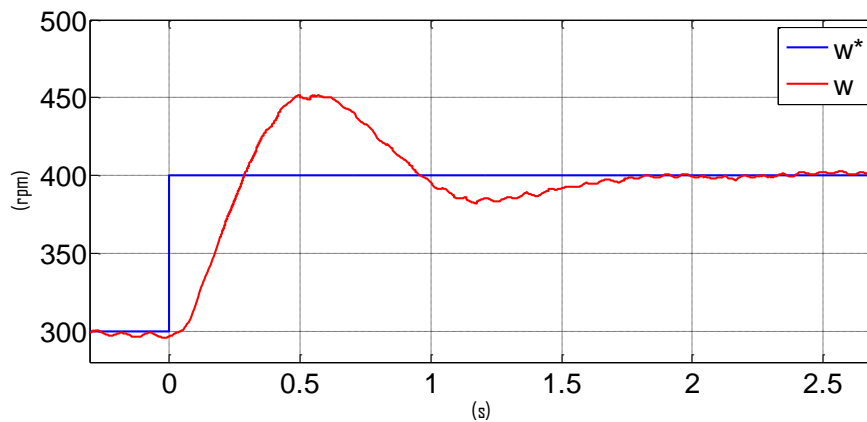


Figure 7-2: Response of the speed controller to a step change of 100 RPM

The response to a speed step change is close to the simulation results described in chapter 4. It can be clearly seen that actual speed (red line) and the reference speed (blue line) captured on the control board are the same at steady state. An overshoot of 12.5% is observed. In terms of the time constant, the rise time takes longer than the designed value. The rise time is about 0.18s (2ms longer than the design). The difference in time constants between the captured value and the design is possibly due to the sample and processing

## Chapter 7: Experimental results

delays associated with the commercial drive. The corresponding torque reference sent to the induction motor drive is shown in Figure 7-3.

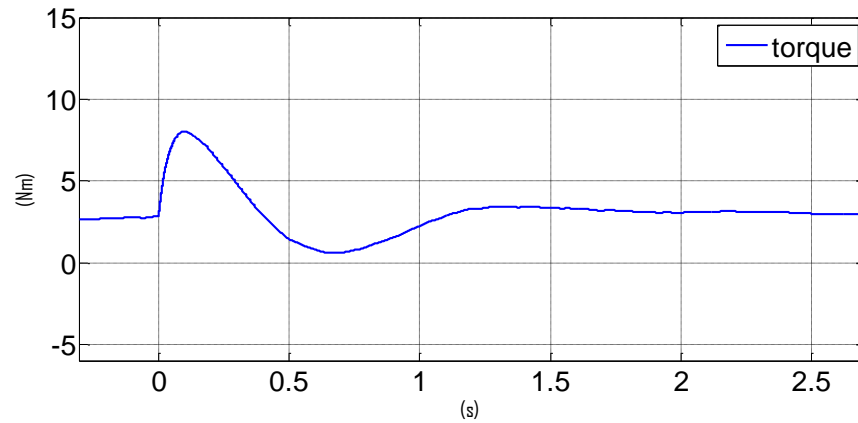


Figure 7-3: Torque reference during speed step change

The oscillations seen on the speed response and the torque reference originate from the quantization of the encoder outputs and the delay associated with the analogue input of the commercial drive.

The measured three-phase voltages generated by the Leroy-Somers synchronous generator when the prime mover (emulated diesel engine) is running at a steady state value of 1500 RPM (electrical frequency of 50Hz) and loaded with a light load of  $57\Omega$  (0.2kW) are shown in Figure 7-4.

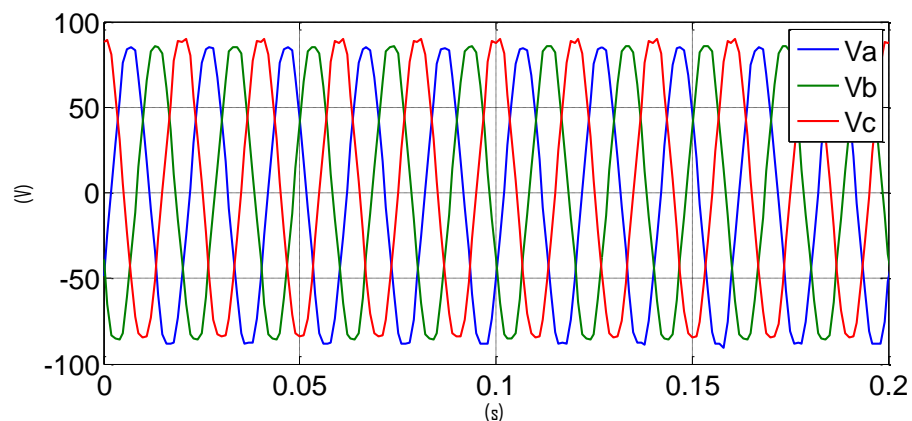


Figure 7-4: Generator 3-phase voltages whilst prime mover is rotating at 1500RPM

## Chapter 7: Experimental results

It is clear that the generator 3-phase voltages shown in Figure 7-4 are distorted. The distortion indicates that the generator voltages are not purely sinusoidal. The distortion is due to harmonic components which exist in the output voltages when generators with large impedance are operated at low voltages.

The currents absorbed by the three phase resistive load (light load) are shown in Figure 7-5 . 3-phase currents of 1.57A absorbed by the load were provided by the generator.

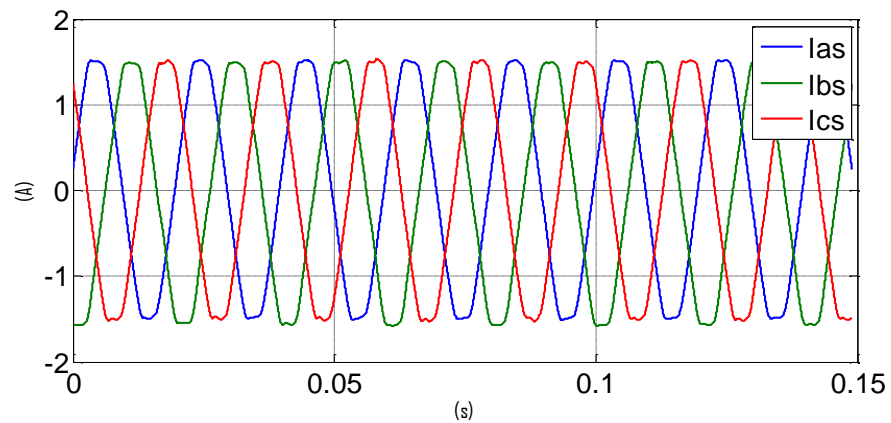


Figure 7-5: Current flowing across light load

The behaviour of the microgrid network to an active power load change is highlighted by imposing a sudden load step of 1kW (0.2kW to 1.2kW) on the generator. When contactor (c) as shown in Figure 7-1 is closed, the main load is switched on. Currents absorbed by the main load and the supply currents (generator currents) are shown in Figure 7-6 and Figure 7-7 respectively.

## Chapter 7: Experimental results

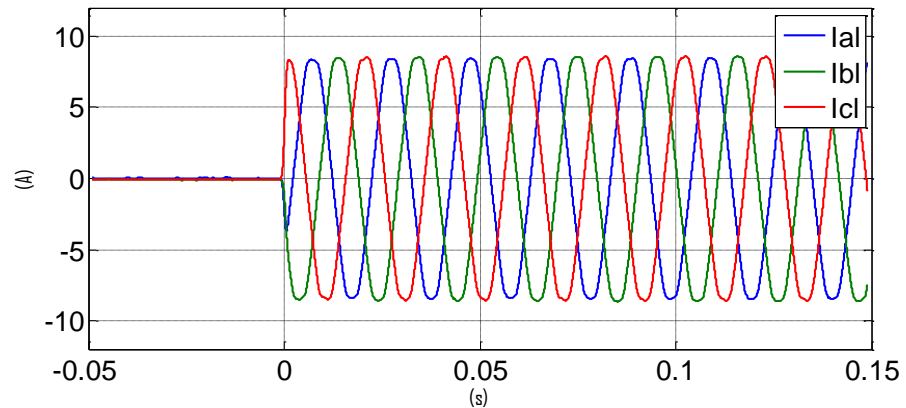


Figure 7-6: Main load currents during active power load change

From the load currents waveform shown in Figure 7-6, it can be seen that the main load was imposed on the generator at time  $t=0s$ . A sudden load current of approximately 8.5A was drawn by the main load when the load step was imposed.

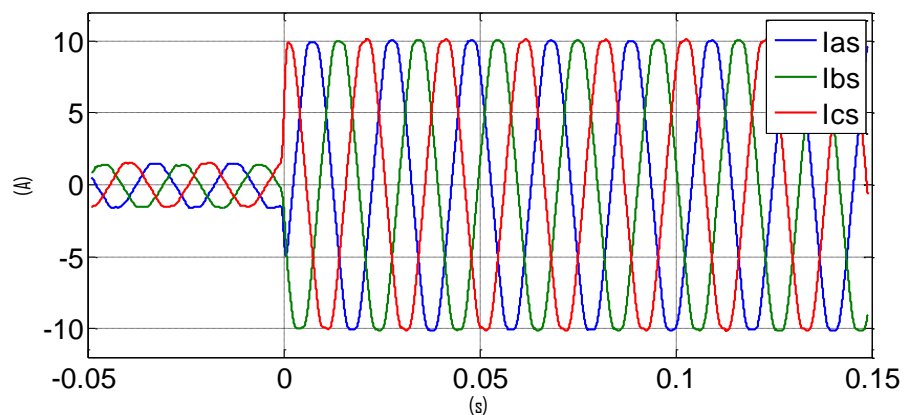


Figure 7-7: Generator currents during active power load change.

The load demand is supplied by the generator as shown in Figure 7-7. Before the main load was imposed on the generator (between time  $t=-0.05s$  and  $0s$ ), it can be seen that the generator supplied only the light load. At time  $t=0s$ , there is a sudden change in the generator current. A current of approximately 10A was supplied by the generator when the load step was imposed. At this instant, the generator provided active power to both the light load and main load.

## Chapter 7: Experimental results

When the load step is imposed, the generator can only respond to the active power demand by slowing down and releasing a small amount of stored kinetic energy across its rotating mass as shown in Figure 7-8.

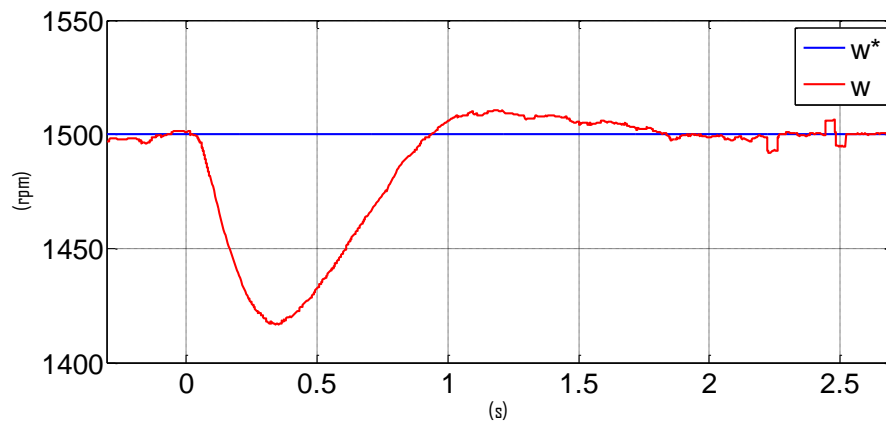


Figure 7-8: Mechanical speed response during active power load step

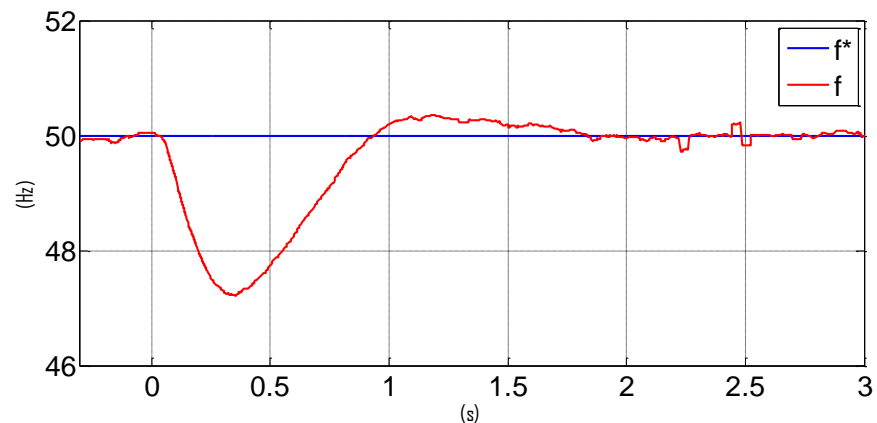


Figure 7-9: Electrical frequency response during active power load step

Before the load impact, there is no change in the generator's rotor speed. However, with the impact of the sudden load change, the rotor speed drops by 84RPM over the period  $t=0s$  and  $t=0.4s$  as shown in Figure 7-8. From  $t=0.4s$  onward, the speed controller responds to the load change by modulating the appropriate mechanical input power to the generator in order to match the new load power. It does this by increasing the throttle demand to the maximum engine torque. This accelerates the generator back to the set point speed and make sure the throttle demand matches the new load setting. The electrical

## Chapter 7: Experimental results

frequency response to an active power load demand is shown in Figure 7-9. A frequency drop of 2.8Hz can be observed during the transient period.

The torque response during the active power load step is shown in Figure 7-10

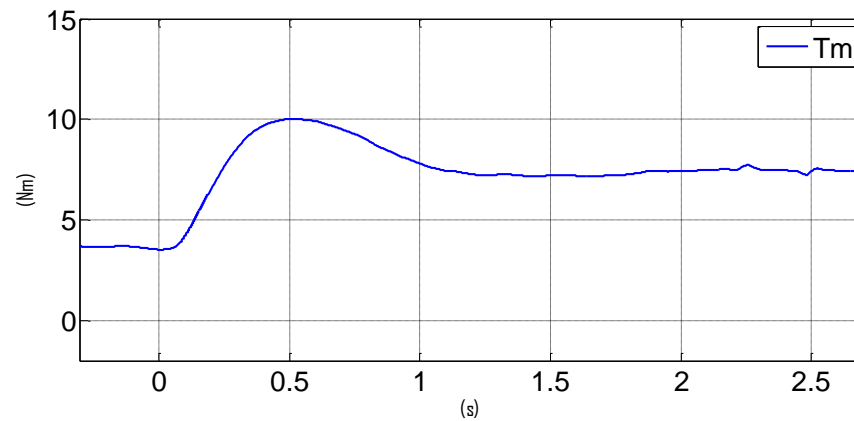


Figure 7-10: Torque response during active power load step

As mentioned in chapter 4, sudden load steps can cause instabilities such as frequency excursions beyond acceptable limits in a microgrid network. The immediate power imbalance between the generation and consumption caused by sudden load steps can cause unnecessary or nuisance tripping of generators by ROCOF relays. Frequency control can be improved by providing real power support to the generator during these load transients. A STATCOM integrated with SCESS is known to have real power capability. In the next section, experimental results describing the operation of a combined STATCOM and SCESS will be presented.

### 7.3 Operation of STATCOM and SCESS

As described in chapter 3, reactive and active power control can be achieved by controlling the q and d axis current components ( $I_q$  and  $I_d$ ) in the d-q reference frame respectively. The reactive and active power capabilities of the combined STATCOM and SCESS are dominated by the current reference tracking performance of the current control scheme. The current control is experimentally verified with the response of the current controllers to a step change in the q and d axis current reference. The response of the q and d- axis current controllers to a step change of 6A is shown in Figure 7-11 .

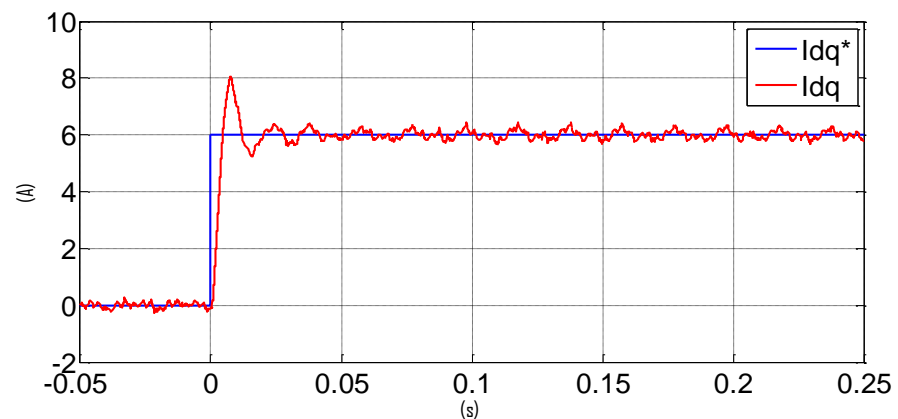


Figure 7-11: Response of the d-axis current controller to a step change of 6A

It can be clearly seen that actual current (red line) and the reference current (blue line) captured on the control board are the same at steady state. An overshoot of 33 % was observed. The rise time is about 5ms and the settling time is approximately 50ms. A comparison of the speed controller response shown in Figure 7-2 and the current controller response shown in Figure 7-11 confirm that the STATCOM and SCESS can be used for frequency compensation within a microgrid network due to its faster dynamics.

To demonstrate the reactive power capability of the STATCOM and SCESS, The STATCOM shown in Figure 7-1 is enabled. As a result, the dc-link voltage will be regulated at 400V as shown in the second trace of Figure 7-12.

## Chapter 7: Experimental results

A reactive power current of 6A is demanded at time  $t = 0$ s. The 3-phase STATCOM currents are shown on the bottom trace of Figure 7-12. During this period, a small drop in the DC-link voltage is seen as some energy in the DC-link capacitor is needed to supply losses in the system e.g. switching and conduction losses in the IGBT.

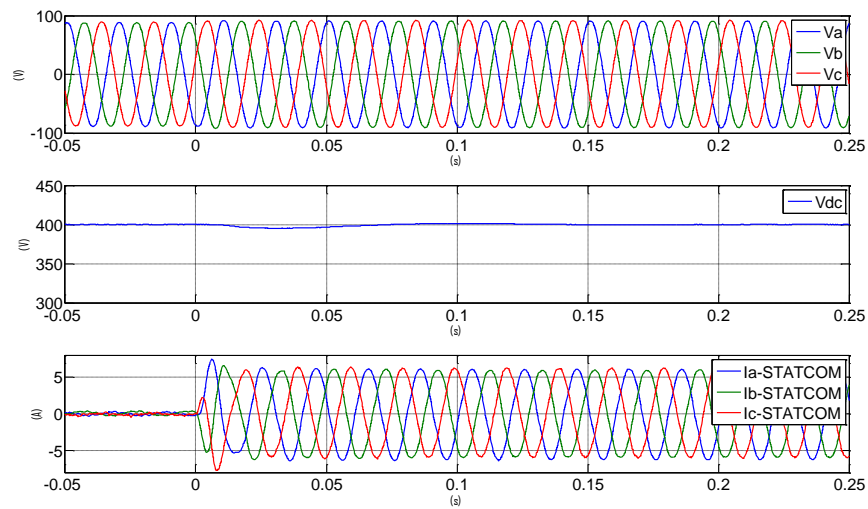


Figure 7-12:  $V_{pcc}$ ,  $V_{dc-link}$  and STATCOM support currents of the system when the STATCOM was energized

The ability to inject and absorb reactive power by the combined STATCOM and SCESS can be clearly described with the phase angle relationship of the STATCOM current and the voltage at the point of common coupling ( $V_{pcc}$ ). STATCOM injects reactive power to the ac grid when the phase current is  $90^\circ$  leading the phase voltage as shown in Figure 7-13 and Figure 7-14.

## Chapter 7: Experimental results

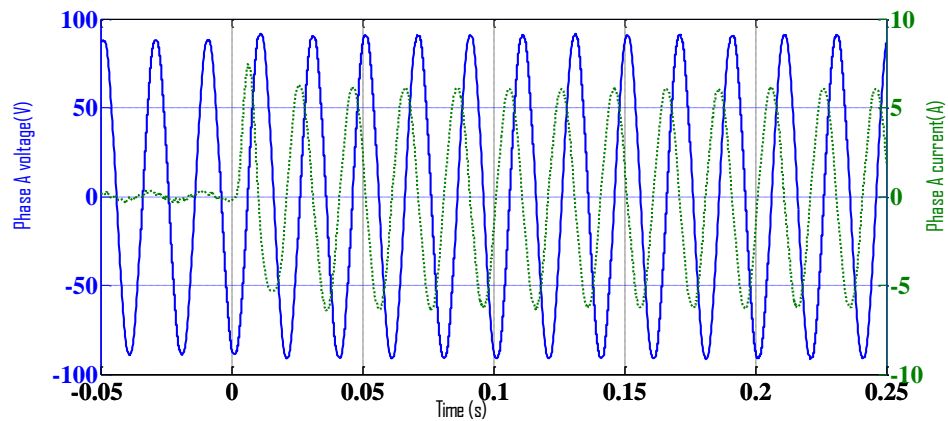


Figure 7-13: Phase “A” voltage and current when combined STATCOM and SCESS inject reactive power

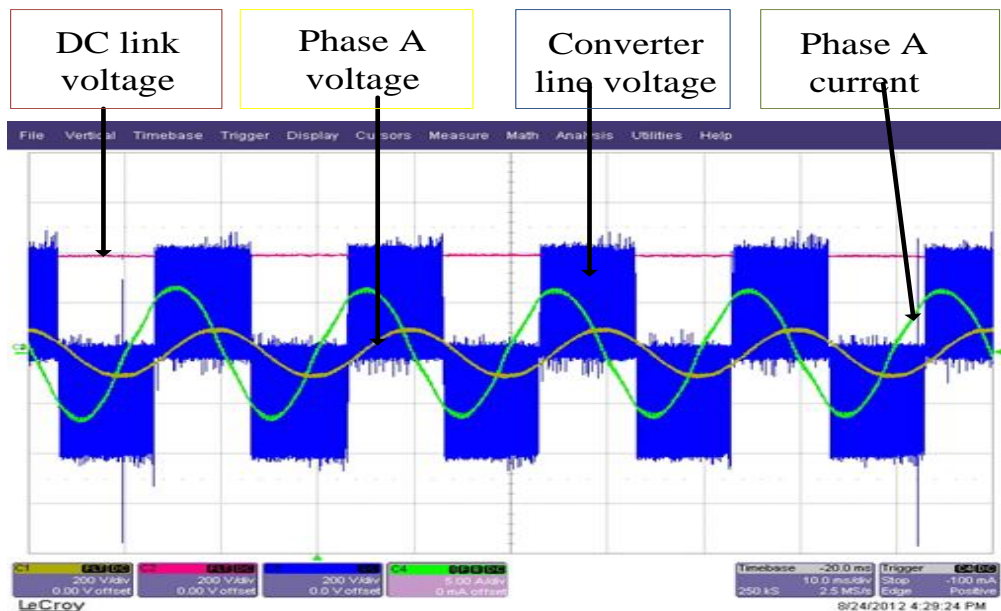


Figure7-14: Data Captured for STATCOM operating at 110Vrms, 400VDClink with an  $I_q$  demand of 6A (x-axis 10ms/div)

As mentioned in chapter 3, the real power capability of the STATCOM is improved by interfacing its DC side to an energy storage element. The SCESS regulates the DC-link voltage during the process of real power exchange between the STATCOM and the ac grid.

Figure 7-15 shows the results obtained during the period the STATCOM and SCESS injects real power to the grid. A negative  $I_d$  indicates the power boost

## Chapter 7: Experimental results

operation (injecting energy to the grid) while a positive  $I_d$  indicates the power buck operation (absorbing energy from the grid).

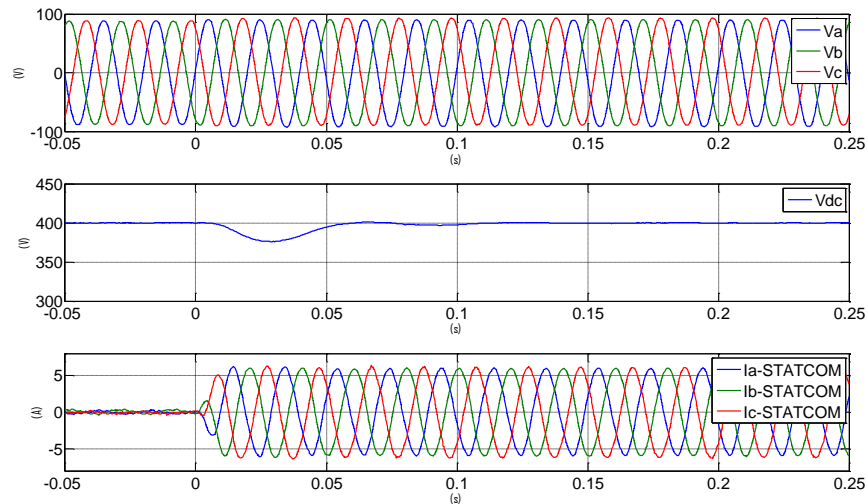


Figure 7-15:  $V_{pcc}$ ,  $V_{dc}$ -link and STATCOM support currents of the system during real power injection from STATCOM and SCESS to the ac grid

An injection of active power current of 6A is demanded at time  $t=0s$ . The 3-phase STATCOM currents are shown on the bottom trace of Figure 7-15. A noticeable drop (7%) appears on the DC-link voltage between  $t=0ms$  and  $t=50ms$ . During this period, the SCESS is not energized and energy is transferred from the STATCOM's DC-link capacitor to the ac grid. After time  $t=50ms$ , The DC-link voltage is regulated by the SCESS boost controller described in chapter 3. Stored energy is taken from the supercapacitor modules and fed to the DC-link capacitor in order to keep the DC-link voltage constant.

Conversely, when real power is demanded from the ac grid, energy is transferred from the ac grid to the STATCOM's dc side. The transfer of energy will cause the DC-link voltage to increase until the SCESS takes control.

The ability to inject and absorb real power by the combined STATCOM and SCESS can be clearly described with the phase angle relationship of the

## Chapter 7: Experimental results

STATCOM current and the voltage at the point of common coupling ( $V_{pcc}$ ). STATCOM injects real power to the ac grid when the phase current is  $180^\circ$  leading the phase voltage as shown in Figure 7-16 and Figure 7-17.

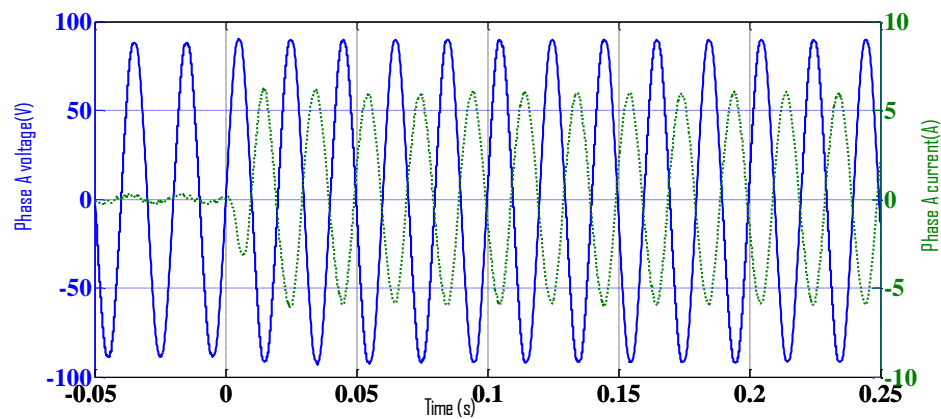


Figure 7-16: Phase “A” voltage and current when combined STATCOM and SCESS inject real power

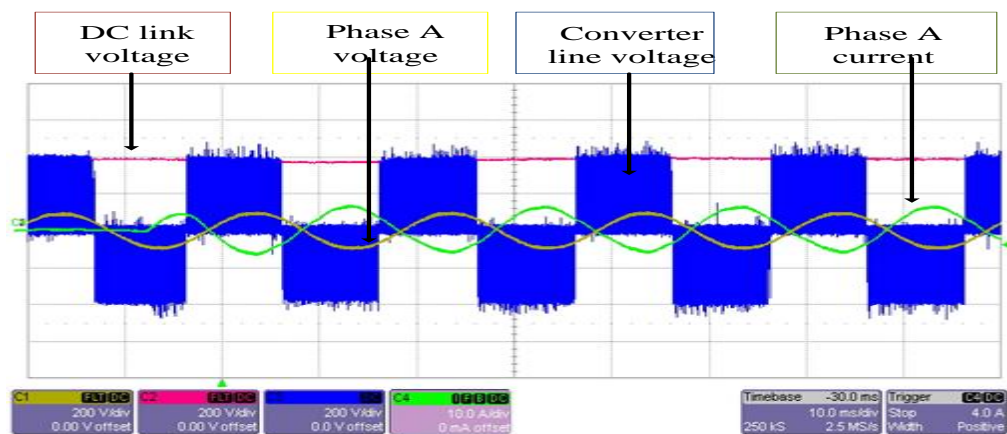


Figure 7-17: Data captured for STATCOM and SCESS operating at 110Vrms, 400VDClink, 140Vsc and Id demand of 6A (x-axis 10ms/div)

It can be clearly seen from the results that the STATCOM and SCESS have active and reactive power capabilities which can be used to improve transient stability of ac power systems. The active power capability of the STATCOM and SCESS can be used for frequency control in micro grids. In the next

section, results will be presented to validate the proposed algorithms described in chapter 5.

## **7.4 Frequency control improvement using the real power capability of STATCOM and SCESS**

To demonstrate the capability of the proposed closed loop control algorithm in providing frequency control improvement within a microgrid, the experimental test system shown in Figure 7-1 is operated with the proposed closed loop energy management scheme described in chapter 5. Experimental results supporting the performance of the proposed closed loop algorithm are presented as follows:

Figure 7-18 shows the real power current reference generated by the transient management controller during the closed loop energy management scheme.

Figure 7-19 shows 3-phase STATCOM +SCESS currents during the closed loop energy management scheme.

Figure 7-20 shows the mechanical speed response of the prime mover during the closed loop energy management scheme.

Figure 7-21 shows measured voltages at the point of common coupling and the DC-link voltage during the closed loop energy management scheme.

Figure 7-22 shows the comparison of the mechanical response of the prime mover with and without the closed loop energy management scheme.

Figure 7-23 shows the comparison of the electrical frequency response with and without the closed loop energy management scheme

## Chapter 7: Experimental results

As mentioned in chapter 4 and chapter 5, the load impact on the generator at the beginning of the load transient is minimised by rapid real power injection from the combined STATCOM and SCESS. The real power current reference is produced by a high gain controller for the energy management. During normal operation, the prime mover is controlled by a governor and the combined STATCOM and SCESS real power reference is zero. During the load transient, the governor is disabled and its output is driven to a maximum value to meet a new load demand as fast as possible. A speed threshold is used to trigger the operation of the transient management controller. The transient management controller regulates the speed in this operation mode and provides the reference for the real power current to be injected by the combined STATCOM and SCESS. The transient management controller is designed to inject real power to the load once the speed threshold is detected and then reduce constantly to zero once the governor is able to respond to the load transient. The transient management controller has a fast dynamic response which offers the possibility of releasing energy at a much faster rate than the prime mover during the load transient. Real power current reference of 12A generated by the transient management controller during an active power load step of 1kW is shown in Figure 7-18.

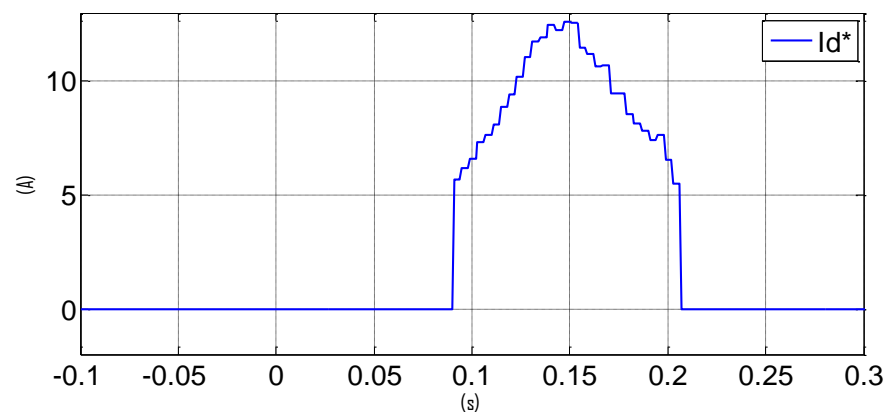


Figure 7-18: STATCOM D-axis current reference generated by the transient management controller during active power load step

## Chapter 7: Experimental results

The three phase current injected by the combined STATCOM and SCESS during the transient energy management scheme is shown in Figure 7-19.

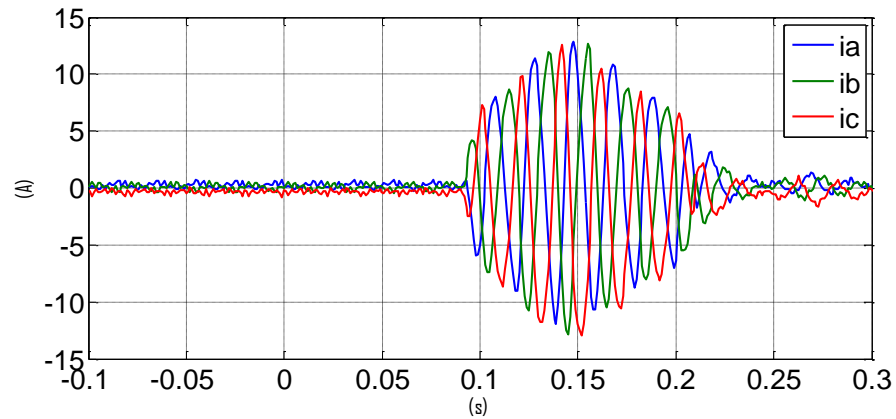


Figure 7-19: Three phase real power current injected by the combined STATCOM and SCESS during the active power load step

The transient management controller regulates the speed and manages the power supplied by the STATCOM and SCESS whilst the prime mover power output is increased. A minimised variation in the mechanical speed of the prime mover during the active power load step is shown in Figure 7-20.

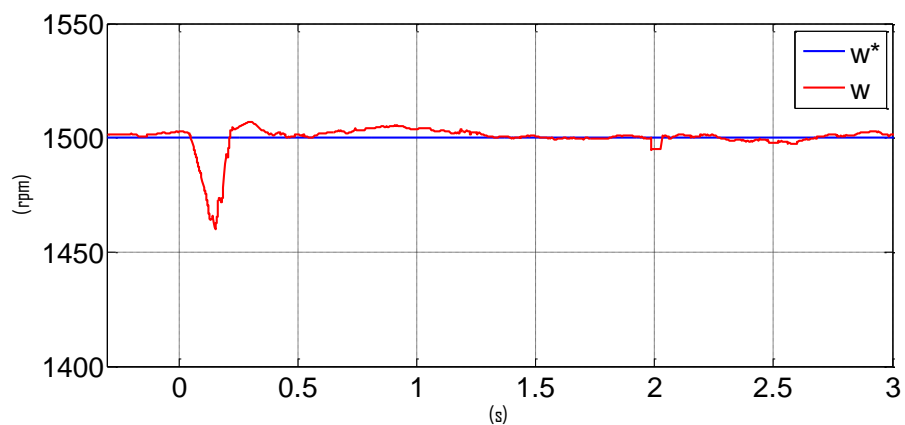


Figure 7-20: Mechanical speed response in RPM during active power load step with STATCOM -SCESS support

It can be observed from Figure 7-20 that there is a drop in the mechanical speed of the prime mover between time  $t=0.03s$  and  $t=0.15s$ . It is worth noting that the triggering of the transient management controller does not occur until

## Chapter 7: Experimental results

the speed threshold has been reached. A speed threshold of 1480 RPM was chosen for the closed loop transient energy management. The drop in the mechanical speed can also be attributed to the delay in the time it takes the boost converter of the SCESS to be energised during the real power injection. As mentioned in chapter 3, the DC-link voltage controller is disabled during the boost operation of the SCESS and the DC-link voltage is regulated by the boost controller. This is depicted by the drop in the DC-link voltage as shown in the bottom trace of Figure 7-21.

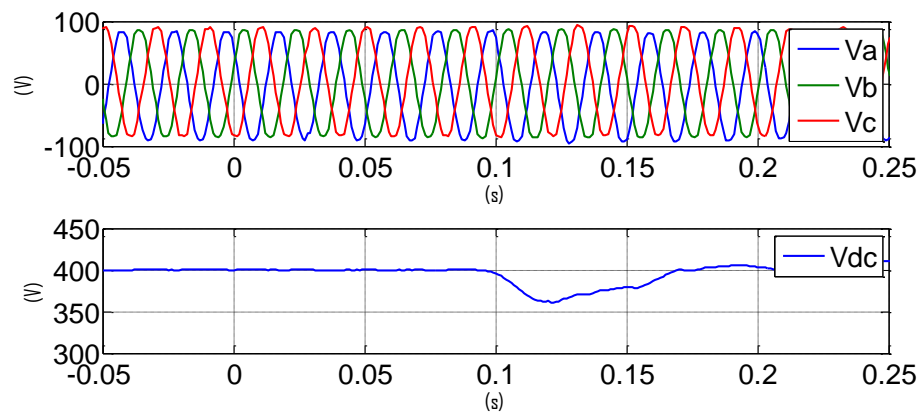


Figure 7-21:  $V_{pcc}$ ,  $V_{dc-link}$  measured during the active power load step

In order to highlight the effectiveness and benefits of the proposed closed loop transient energy management scheme in providing frequency control improvement within a microgrid, a comparison of the behaviour of the prime mover and electrical frequency response during sudden active power load change without and with the closed loop energy management scheme will be carried out.

Response of the prime mover and electrical frequency response to an active power load transient with and without the closed loop energy management is shown in Figure 7-22 and Figure 7-23 respectively. The blue trace shows a speed deviation of 84 RPM during the sudden active power load change without the proposed control algorithm while the red trace shows a deviation of 40 RPM during the sudden active power load change with the proposed algorithm. An improvement of 52% in the mechanical speed response of the

## Chapter 7: Experimental results

prime mover can be observed. An improvement to system stability in terms of the response time of the microgrid network during the sudden active power load change can also be seen.

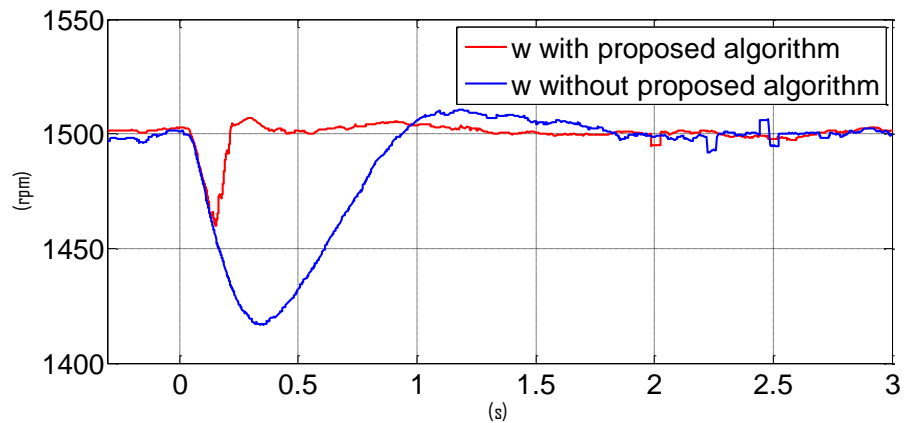


Figure 7-22: Comparison of the mechanical response of the prime mover with and without the closed loop energy management scheme.

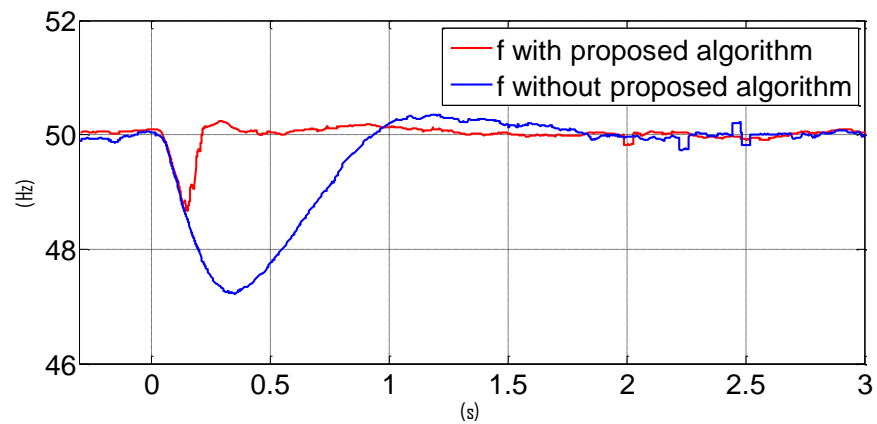


Figure 7-23: Comparison of the electrical frequency with and without the closed loop energy management scheme.

It is worth noting that the speed variation seen when the closed loop energy management scheme was employed can be attributed to the speed detection threshold and the delay period it takes for the boost converter to be energised.

## **7.5 Conclusion**

In this chapter, the results taken from the experimental rig developed has been presented. The effect of sudden load changes to the stability and performance of a microgrid network during active power load changes has been highlighted experimentally. These results are comparable with the simulation results under the same condition.

Reactive and active power capabilities of the combined STATCOM and SCESS have been validated experimentally. The combined STATCOM and SCESS can control current effectively in all four quadrants i.e. active and reactive power can flow in either direction at each end of the dc-link which make it an attractive choice for frequency control within a microgrid.

The application of the closed loop control algorithm proposed for frequency control resulted in significant improvement to frequency variation during active power load changes. The benefit of the proposed algorithm was highlighted by comparing the behaviour of the microgrid network with and without the closed loop algorithm during the disturbance. The disparity between the simulation results and the experimental results can be attributed to factors such as use of finite energy storage, speed resolution, processing delays within the commercial drive and system parameters of the induction motor and synchronous generator which were not accounted for in the simulation studies.

## Chapter 8

### Conclusions and future work

---

In recent times, new and interactive electricity grid structures which consist of interconnected generators, power electronic technologies and energy storage elements are being developed to meet the growing demand in provision of better quality electric power. A key feature of this new grid structure is distributed generation (DG). Distributed generation offers the potential to displace power supplied through centralized power generation (a common feature of the traditional grid structure) with localised power generation. The potential of DG can be realized by taking a system approach that views generation and associated loads as a microgrid.

Although microgrids are accepted as possible solutions to power quality and power stability issues in ac power systems, the uncertainty in the ability of microgrids to cope with severe fluctuating conditions is a major concern in the

## Chapter 8: Conclusions and Future work

operation of these new grid structures. The penetration of power electronic technologies and energy storage elements in power distribution systems has made it possible to expand their use to enable greater stability under severe fluctuating loads. A STATCOM integrated with supercapacitor energy storage offers a solution in allaying this uncertainty.

The aim of the work carried out in this research is to investigate and experimentally verify novel control algorithms to improve frequency control within a microgrid using a STATCOM integrated with supercapacitor energy storage. The work in this thesis looked at the operation and control of a STATCOM integrated with a supercapacitor energy storage system (SCESS). The STATCOM and the SCESS are integrated by interfacing a DC/DC converter between the DC-link capacitor and supercapacitor modules. Simulation and experimental results showing the active and reactive power capability of the combined STATCOM and SCESS were presented in chapter 3 and chapter 7 respectively. The combined STATCOM and SCESS can control current effectively in all four quadrants which makes it a popular choice for frequency control within a microgrid.

In chapter 4, the characteristics of an internal combustion engine driven synchronous generator was described and the key features which dominate the transient response were identified so that an emulation of a diesel generating set was achieved with a vector controlled induction motor driving a synchronous generator. The diesel engine emulation was achieved by incorporating a single delay into the speed control loop of the vector controlled induction motor. The emulation algorithm was designed such that when the real power load is applied on the network, the generator will see a significant drop in frequency as the prime mover slowly reacts to the load change. The instability of an ac power system that employs DG has been analysed. The dynamic response of the emulated diesel generating set has been investigated with a focus on the variation of the speed due to power imbalance during load transients. Potential improvement to stability within a modelled microgrid network was achieved with an ideal energy management scheme.

## Chapter 8: Conclusions and Future work

Instantaneous real power support provided by a STATCOM and energy storage system helped the generator to handle sudden power imbalance conditions within the microgrid network. A simulation study highlighting the potential improvement to system control was also discussed in full detail.

The concept of frequency control improvement within a microgrid was discussed in detail in chapter 5. Power imbalance between power supplied by the generator and power demanded during the load transient was minimized by implementing the energy management scheme introduced in chapter 4. The minimum amount of stored energy required for the stability of the microgrid has been derived. Frequency control improvement was initially achieved by combining an open loop control action on the prime mover speed loop and the combined STATCOM and SCESS. This involves the modification of the prime mover's speed loop such that the total torque applied to the mechanical load is kept constant and zero speed variation is achieved during the load transient. The advantage of the open loop control is its simplicity but the functionality of the control action is limited with the knowledge of the diesel engine transfer function and load current measurement being important requirements. A closed loop control scheme was employed to address the limitations of the open loop control action. Two control modes were employed in the closed loop control scheme. The closed loop control architecture employed a switch over mechanism based on load detection for the operation modes. In the normal operation mode, the prime mover's speed was regulated by a governor. In the transient operation mode, the governor was driven to a maximum output to meet the new load demand and the STATCOM and SCESS was temporarily used to regulate the speed. The STATCOM and SCESS speed controller provided the real power current reference required for the energy management scheme. The real power current reference acted to control torque while the prime mover output was increased and therefore regulated the speed with little disturbance. The transient operation mode lasted until the new load demand was matched. The performance of the proposed architecture has been investigated by simulation. Simulation results show the

## Chapter 8: Conclusions and Future work

effectiveness of the control algorithms in providing frequency control improvements within a microgrid.

In order to experimentally verify the proposed control algorithms for frequency control within a microgrid, an experimental rig as described in chapter 6 was developed. The experimental rig consist of an emulated diesel generating set, load banks and a STATCOM device integrated with supercapacitor energy storage. The control of the experimental rig is provided by the dSPACE DS 1104 controller card which is placed in the PCI slot of a computer. The DS1104 card works within MatLab/Simulink environment. Codes are generated based on the structures within the simulation environment and these codes provide the control for the implementation process from simulation up to real time experiment. The rig has been shown to operate successfully in providing frequency control for microgrids.

The results taken from the rig were presented in chapter 7. It is concluded that the proposed closed loop algorithm is very effective in minimizing frequency variation during load transients. In addition, the practical implementation of the control algorithm show that frequency control can be improved within a microgrid by employing a coordinated communication between the combined STATCOM and SCESS and the DG network.

### **8.1 Future work**

Frequency control within a microgrid using enhanced STATCOM and supercapacitor energy storage has been implemented successfully and the control algorithms employed in achieving frequency control has been validated on an experimental rig. Some of the areas in which further research can be undertaken based on the work carried out in this research are,

- The extension of control algorithms proposed to multiple generators to demonstrate improvement to stability within microgrids. More

## Chapter 8: Conclusions and Future work

thorough investigation into real and reactive power management for a generalised distribution system will be required.

- The extension of control algorithms proposed to microgrid fault ride through studies to demonstrate the capabilities of the STATCOM and SCESS.
- The investigation of other techniques that can detect sudden large load steps e.g. Active Impedance estimation.
- The investigation of other methods that can track frequency variation quickly e.g. advanced PLL.

## **8.2 Publications resulting from the project**

1. A. Agbedahunsi, M. Sumner, E. Christopher, A. Watson, A. Costabeber, and R. Parashar, "Frequency control improvement within a microgrid, using enhanced STATCOM with energy storage," in Power Electronics, Machines and Drives (PEMD 2012), 6th IET International Conference , 2012, pp. 1-6.

# Appendix A

## Coordinates Transformation

---

### A.1 Co-ordinates Transformation

The abc to dq transformation is a coordinate change from a stationary three phase system to a rotating two phase system. The transformation process can be divided into two stages. They are, (a) transformation from the stationary three phase abc reference frame to the stationary two phase  $\alpha\beta$  reference frame and (b) transformation from the stationary two phase  $\alpha\beta$  reference frame to the rotating two phase dq reference frame.

A set of three instantaneous phase variables that sum up to zero can be uniquely represented by a single point in a plane. The vector drawn from the origin to this point has a vertical projection onto each of three symmetrically disposed phase axes which corresponds to the instantaneous value of the

## Appendix A

associated phase variables [79]. As values of the phase variables change, the associated vector moves around the plane describing various trajectories. The vector representation can be extended by introducing an orthogonal co-ordinate system in which each vector is described by means of its  $\alpha$  and  $\beta$  components.

The phase vectors are represented as

$$\bar{X}_{abc}(t) = \begin{bmatrix} X_a(t) \\ X_b(t) \\ X_c(t) \end{bmatrix} \quad (\text{A.1})$$

The transformation from abc to  $\alpha\beta$  co-ordinates is as follows:

$$\bar{X}_{\alpha\beta 0}(t) = T_{abc/\alpha\beta 0} \bar{X}_{abc}(t) \quad (\text{A.2})$$

Where the matrix  $T_{abc/\alpha\beta 0}$  is defined as:

$$T_{abc/\alpha\beta 0} = \frac{2}{3} \begin{bmatrix} 1 & -\frac{1}{2} & -\frac{1}{2} \\ 0 & \frac{\sqrt{3}}{2} & -\frac{\sqrt{3}}{2} \\ \frac{1}{2} & \frac{1}{2} & \frac{1}{2} \end{bmatrix} \quad (\text{A.3})$$

Substituting Equation (A.1) and Equation (A.3) into Equation (A.2) gives the  $\alpha$  and  $\beta$  vector components.

$$\begin{aligned} X_\alpha(t) &= \frac{2}{3} \left( X_a(t) - \frac{1}{2} X_b(t) - \frac{1}{2} X_c(t) \right) \\ X_\beta(t) &= \frac{2}{3} \left( \frac{\sqrt{3}}{2} X_b(t) - \frac{\sqrt{3}}{2} X_c(t) \right) \\ X_0(t) &= \frac{2}{3} \left( \frac{1}{2} X_a(t) + X_b(t) + X_c(t) \right) \end{aligned} \quad (\text{A.4})$$

## Appendix A

Further manipulation of the  $\alpha\beta$  vector co-ordinate frame leads to the rotating dq frame. Figure A.1 shows the definition of the rotating reference frame

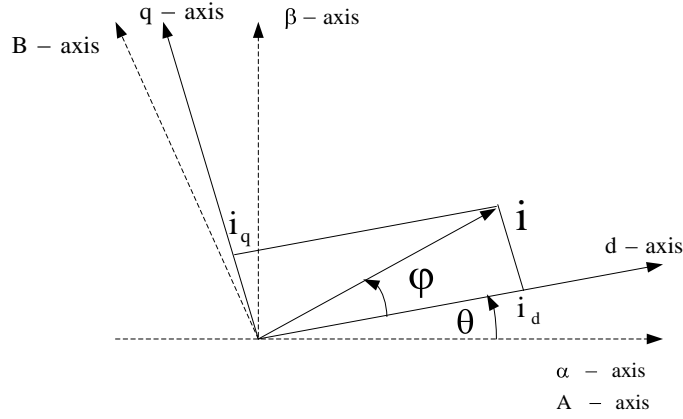


Figure A-1: Definition of rotating reference frame

The transformation from  $\alpha\beta$  co-ordinates to rotating dq coordinates is as follows:

$$\bar{X}_{dq0}(t) = T_{\alpha\beta0/dq0} \bar{X}_{\alpha\beta0}(t) \quad (\text{A.5})$$

Where the matrix  $T_{\alpha\beta0/dq0}$  is defined as:

$$T_{\text{abc}/dq0} = \frac{2}{3} \begin{bmatrix} \cos \theta & \cos\left(\theta - \frac{2\pi}{3}\right) & \cos\left(\theta - \frac{4\pi}{3}\right) \\ -\sin \theta & -\sin\left(\theta - \frac{2\pi}{3}\right) & -\sin\left(\theta - \frac{4\pi}{3}\right) \\ \frac{1}{2} & \frac{1}{2} & \frac{1}{2} \end{bmatrix}$$

$$\theta = \tan^{-1}\left(\frac{\beta}{\alpha}\right)$$

(A.6)

## Appendix A

Substituting Equation (A.4) and Equation (A.6) into Equation (A.5) gives the d and q vector components.

$$\begin{aligned} X_d(t) &= X_\alpha(t) \cos \theta + X_\beta(t) \sin \theta \\ X_q(t) &= -X_\alpha(t) \sin \theta + X_\beta(t) \cos \theta \end{aligned} \quad (\text{A.7})$$

The d and q axes are not stationary in the plane. They follow the trajectory of the voltage vector. Under balanced steady state conditions, the coordinates of the vectors in the rotating reference frame are constant quantities. This feature is useful for analysis and for decoupled control of the two current components.

# Appendix B

## Power flow control

---

### **B.1 Power flow control**

The power flow theory in AC power systems states that the flow of active power (P) and reactive power (Q) between two sources can be controlled by adjusting the power angle and the voltage magnitude of each system i.e. active power is mainly controlled by the power angle while the reactive power is controlled by voltage magnitude. The flows of active and reactive power are fairly independent of each other and are influenced by different control actions. Active power control is associated with frequency control while reactive power control is associated with voltage control.

## Appendix B

Analysis of load sharing control of paralleled power supplies gives a useful insight into power flow in AC power systems. Figure B-1 shows two power supplies represented by two controlled voltage sources ( $E_1$  and  $E_2$ ) connected to a load through line impedances represented by pure inductance  $L_1$  and  $L_2$ .

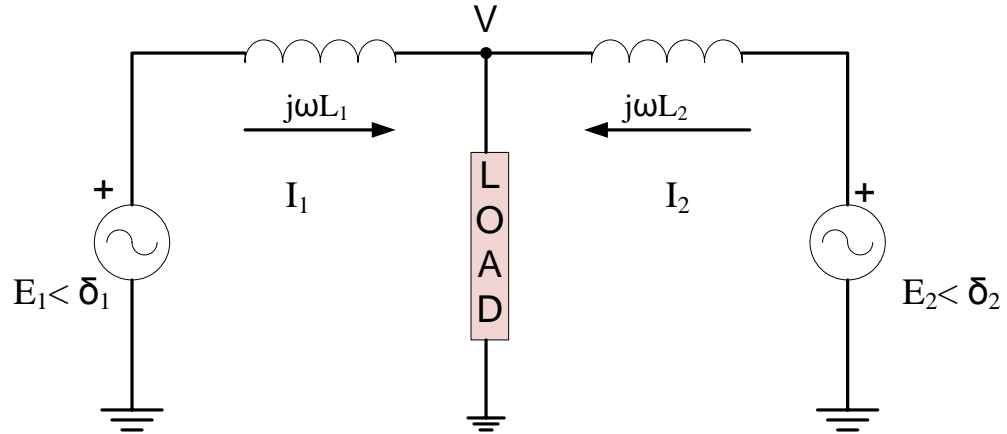


Figure B-1: Equivalent single phase power flow diagram

The complex power at the load due to the two power supplies is given by:

$$S_i = P_i + jQ_i = VI_i^* \quad (\text{B-1})$$

Where  $i=1, 2$  and  $I_i^*$  is the complex conjugate of the power supply current

Using Kirchoff's voltage rule,

$$\begin{aligned} E_i < \delta_i - j\omega L_i I_i - V &= 0 \\ E_i \cos \delta_i + jE_i \sin \delta_i - j\omega L_i I_i - V &= 0 \\ I_i &= \frac{E_i \cos \delta_i + jE_i \sin \delta_i - V}{j\omega L_i} \\ I_i &= \frac{-jE_i \cos \delta_i + E_i \sin \delta_i + jV}{\omega L_i} \end{aligned} \quad (\text{B-2})$$

The complex conjugate of the power supply current  $I_i^*$  is given by:

$$I_i^* = \frac{E_i \sin \delta_i + jE_i \cos \delta_i - jV}{\omega L_i} \quad (\text{B-3})$$

## Appendix B

Substitute Equation (B-3) into Equation (B-1) the final expression of the complex power can be obtained as:

$$S_i = V \left[ \frac{E_i \sin \delta_i + jE_i \cos \delta_i - jV}{\omega L_i} \right] \quad (\text{B-4})$$

From Equation (B-4) the active and reactive power flowing is given as:

$$P_i = \frac{VE_i \sin \delta_i}{\omega L_i} \quad (\text{B-5})$$

$$Q_i = \frac{VE_i \cos \delta_i - V^2}{\omega L_i} \quad (\text{B-6})$$

From Equation (B-5) and Equation (B-6), it can be seen that if  $\delta_1$  and  $\delta_2$  are small, the active power flow is influenced by the power angles  $\delta_1$  and  $\delta_2$  and the reactive power flow is dependent on the output voltages  $E_1$  and  $E_2$ . It can also be inferred that the active and reactive power flow can be controlled independently.

As constancy of frequency and voltage are important factors in determining the quality of power supply, the control of active power and reactive power is vital to the satisfactory performance of power systems.

The above control theory can be applied to the case considered in this work. The possible flows of power between the converter and the AC grid will be discussed. A single phase circuit diagram of the configuration with a 2-level converter is illustrated in Figure B-2 where  $V_{\text{GRID}}$  represents the grid voltage and  $V_{\text{CONV}}$  represents the converter voltage.  $V_L$  represents the voltage across the coupling reactor.  $I$  represents the current flowing through the coupling

## 8.2.1 Power flow between converter and grid

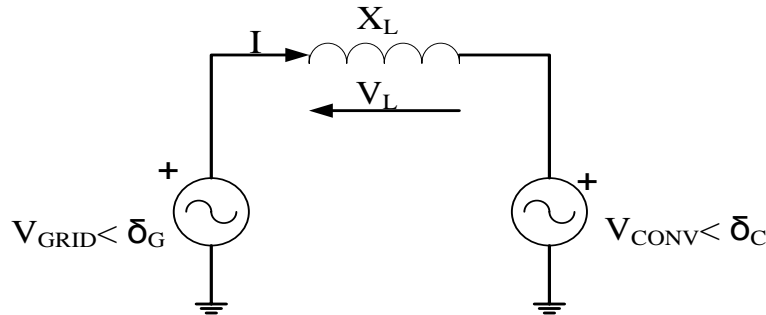


Figure B-2: Equivalent single phase circuit depicting power exchange between the grid and the converter

The active and reactive power can be expressed as

$$P = \frac{|V_{GRID}| |V_{CONV}|}{X_L} \sin \delta \quad (B-7)$$

$$Q = \frac{|V_{GRID}| |V_{CONV}|}{X_L} \left( \cos \delta - \frac{V_{CONV}}{V_{GRID}} \right) \quad (B-8)$$

Where  $\delta = \delta_G - \delta_C$

In the stationary a-b-c reference frame, the instantaneous active power (P) and reactive power (Q) at any point can be defined by using the instantaneous three phase voltages and currents. For control purposes, the synchronously rotating reference frame (d-q reference) is introduced. This entails the vector interpretation of the instantaneous three phase values using co-ordinate transformation. The stationary frame  $\alpha$ - $\beta$  transformation matrix transforms the associated instantaneous phase voltages and currents to the instantaneous voltage and current vectors. These vectors are further manipulated in the rotating d-q reference frame. Details of the transformation process can be found in Appendix A. In the d-q reference frame, the d and q axes follow the trajectory of the phase voltage vector with the rotating angle  $\theta$ . In general, the

## Appendix B

d-axis voltage vector is coincident with the instantaneous phase voltage vector of the ac power grid, thus the q-axis voltage is zero.

Instantaneous active and reactive power control can be achieved by controlling the d and q axes current components. The possible flow of power between the converter and the grid is illustrated in Figure B-3 where (P) is the active power, (Q) is the reactive power,  $V_{\text{GRID}}$  is the grid voltage,  $V_{\text{CONV}}$  is the controllable converter voltage and  $I_d$  and  $I_q$  are the d and q- axis current representing active and reactive power respectively .

## Appendix B

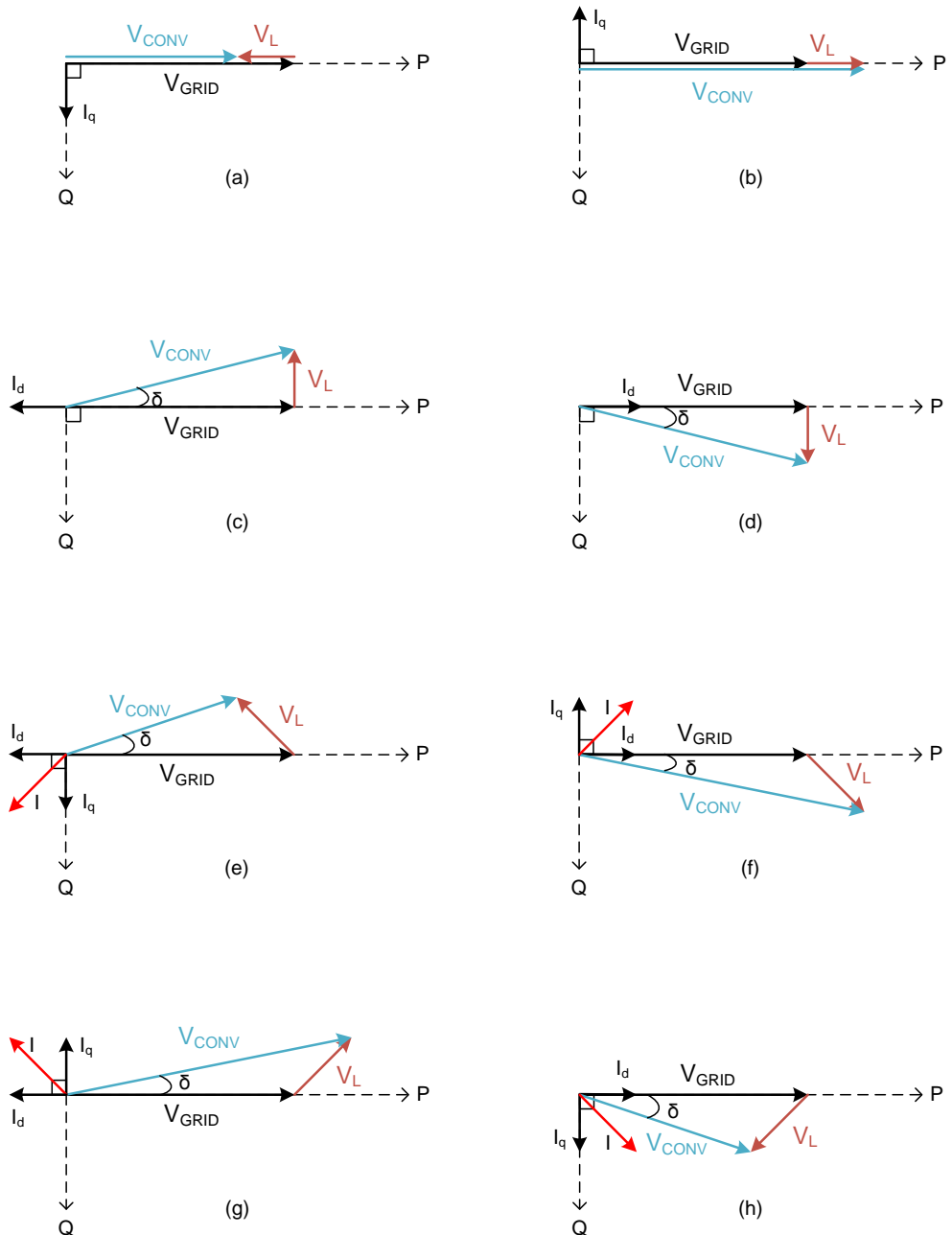


Figure B-3: The possible flow of power between the grid and the converter

Reactive power control can be achieved by controlling the magnitude of the converter output voltage. If the magnitude of  $V_{CONV}$  is greater than the magnitude of  $V_{GRID}$ , the converter will inject reactive power to the AC power grid indicated by 90 degree leading  $I_q$  as shown in Figure B-3 (b),(f) and (g). Conversely if the magnitude of  $V_{CONV}$  is lesser than the magnitude of  $V_{GRID}$ ,

## Appendix B

the converter will absorb reactive power from the AC power grid indicated by 90 degree lagging  $I_q$  as shown in Figure B-3 (a), (e) and (h).

Active power control can be achieved by controlling the phase displacement of the converter voltage. If  $V_{CONV}$  leads  $V_{GRID}$ , the converter will inject active power to the AC power grid indicated by  $I_d$  lagging  $V_{GRID}$  (negative  $I_d$ ) by 180 degree as shown in Figure B-3 (c), (e) and (g). Conversely If  $V_{CONV}$  lags  $V_{GRID}$ , the converter will absorb active power from the AC power grid indicated by  $I_d$  in phase with  $V_{GRID}$  (positive  $I_d$ ) as shown in Figure B-3(d), (f) and (h).

It can be seen from Figure B-3 that the exchange of power between the converter and the AC power grid corroborates the power flow theory discussed in the earlier part of this section.

## Appendix C

# State equations for the SCESS control

---

### C.1 Introduction

A power circuit diagram of the SCESS is shown in Figure C-1. As mentioned in chapter 3, the control of the inductor current ( $I_L$ ) dictates the control of the energy transferred between the two sides of the SCESS ( $V_{dclink}$  and  $V_{sc}$ ). The inductor current is directly related to the gating of the bi-directional DC-DC converter.

## Appendix C

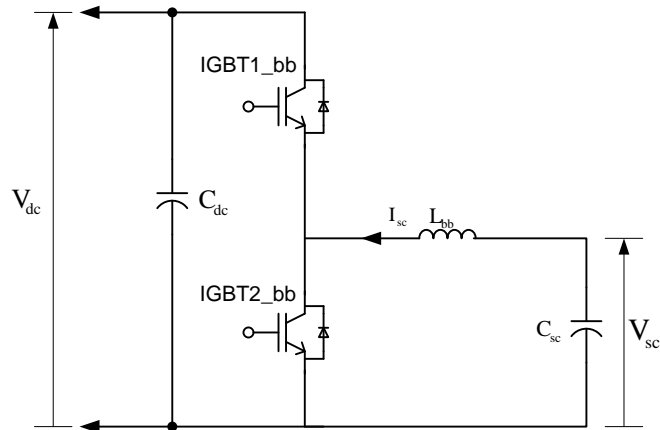


Figure C-1: The power circuit diagram of the SCESS

## C.2 State equation for buck mode equation

The buck mode circuit diagram is shown in Figure C-2. In the buck mode, only the gating of IGBT1\_bb is controlled under the DCM switching technique and IGBT2\_bb will be turned off at all times.

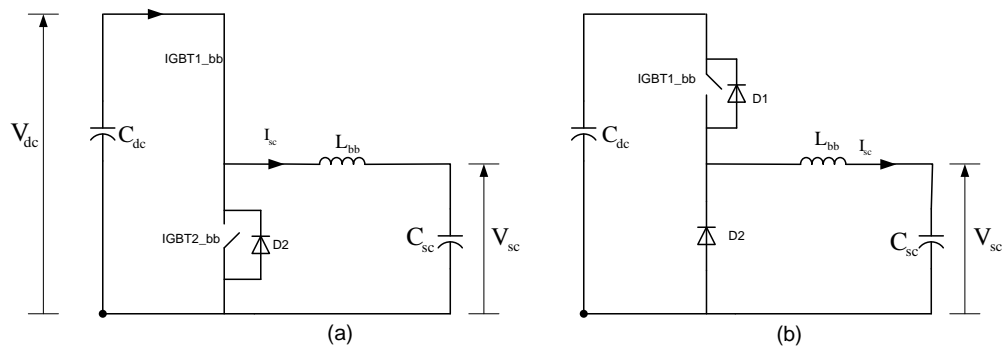


Figure C-2: SCESS buck mode circuit

The inductor current is the main control parameter for controlling the flow of the energy as energy is transferred from the DC-link side to the supercapacitor

## Appendix C

modules. The change in the inductor current during one sampling period is shown in Figure C-3.

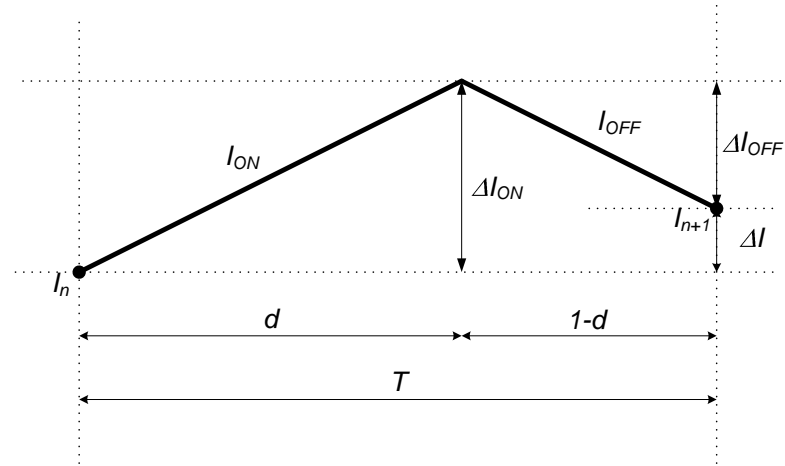


Figure C-3: Inductor current waveform during one sampling period

Where

$T$  is the sampling period, s.

' $d$ ' is the on-period during one switching time, s.

' $1-d$ ' is the off-period during one switching time, s.

$I_n$  is the inductor current at the beginning of the switching period, A.

$I_{n+1}$  is the inductor current at the end of the switching period, A.

$I_{ON}$  is the inductor current during on-period, A.

$I_{OFF}$  is the inductor current during off-period, A.

$\Delta I_{ON}$  is the change in the inductor current during on-period, A.

$\Delta I_{OFF}$  is the change in the inductor current during off-period, A.

$\Delta I$  is the change in the inductor current over one sampling period,

A and  $\Delta I = \Delta I_{ON} - \Delta I_{OFF}$ .

According to the control concept for buck mode operation described as in Figure 3-13 of chapter 3 which is shown again in Figure C-4, the inductor

## Appendix C

current is controlled by the reference current ( $I_{sc}^*$ ) produced from the supercapacitor voltage control loop.

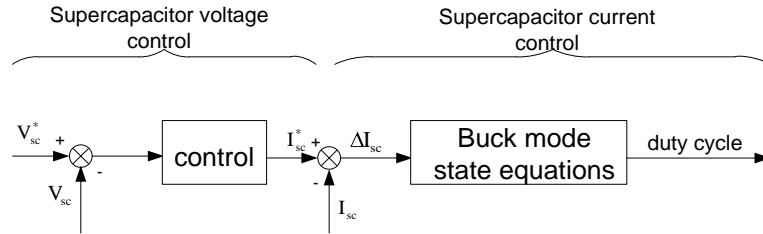


Figure C-4: Buck mode control block diagram

In Figure C-3 the supercapacitor current ( $I_{sc}$ ) equals the inductor current ( $I_L$ ). The change in the inductor current ( $\Delta I$ ) is related to the controlled reference current ( $I_{sc}^*$ ), and the inductor current will be controlled proportionally to the duty cycle according to the state equation derived below.

When the IGBT1\_bb is on (a), the voltage drop across the inductor is given as:

$$\begin{aligned} V_L &= V_{dclink} - V_{sc} \\ &= \frac{L\Delta I_{ON}}{\Delta t_{ON}} \end{aligned} \quad (C-1)$$

During on-period  $\Delta t_{ON}$ , the inductor current increases linearly without losses, the change in the inductor current during this period is defined as

$$\Delta I_{ON} = \frac{d V_{dclink} - V_{sc}}{L} \quad (C-2)$$

When IGBT1\_bb is off (b), the supercapacitor voltage ( $V_{sc}$ ) equals the inductor voltage ( $V_L$ ) as shown in Equation (C-3) due to the conduction of the diode.

## Appendix C

$$V_L = V_{sc} = \frac{L\Delta I_{OFF}}{\Delta t_{OFF}} \quad (C-3)$$

The change in the inductor current during off-period  $\Delta t_{OFF}$  is defined as

$$\Delta I_{OFF} = \frac{(1-d)V_{sc}}{L} \quad (C-4)$$

According to Figure C-3, the overall change in the inductor current during one sampling period ( $\Delta I$ ) is given.

$$\begin{aligned} \Delta I &= \Delta I_{ON} - \Delta I_{OFF} \\ &= \frac{d V_{dclink} - V_{sc}}{L} - \frac{1-d V_{sc}}{L} \end{aligned} \quad (C-5)$$

From Equation (C-5), the change in the inductor current over one sampling period under buck mode is given as

$$\Delta I = \frac{1}{L} dV_{dclink} - V_{sc} \quad (C-6)$$

The buck mode duty cycle is obtained as

$$d_{buck} = \frac{L\Delta I + V_{sc}}{V_{dclink}} \quad (C-7)$$

### **C.3 State equation for boost mode equation**

The boost mode circuit diagram is shown in Figure C-5. In the boost mode, only the gating of IGBT2\_bb is controlled under the DCM switching technique and IGBT1\_bb will be turned off at all times.

## Appendix C

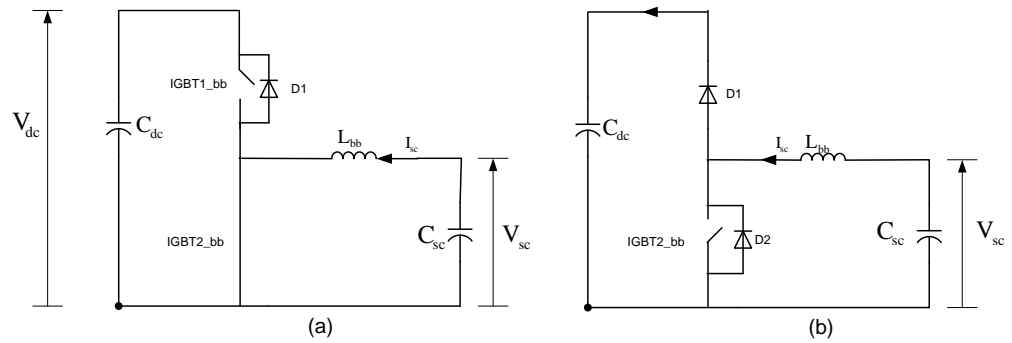


Figure C-5: SCESS boost mode circuit

According to the control concept for boost mode operation described as in Figure 3-14 of chapter 3 which is shown again in Figure C-6, the inductor current is controlled by the reference current ( $I_{sc}^*$ ) produced from DC-link voltage control loop.

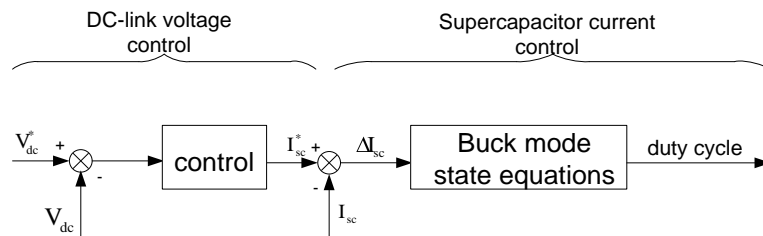


Figure C-6: Boost mode control block diagram

The same relationship described for the buck operation during one sampling period exists for the boost operation during one sampling period. As a result, the supercapacitor current ( $I_{sc}$ ) equals the inductor current ( $I_L$ ). The change in the inductor current ( $\Delta I$ ) is related to the controlled reference current ( $I_{sc}^*$ ), and the inductor current will be controlled proportionally to the duty cycle according to the state equation derived below.

When the IGBT2\_bb is on (a), the voltage across the inductor ( $V_L$ ) is equal to the voltage at the supercapacitor terminals ( $V_{sc}$ )

## Appendix C

$$V_L = V_{sc} = \frac{L\Delta I_{ON}}{\Delta t_{ON}} \quad (C-8)$$

During the on-period  $\Delta t_{ON}$ , the inductor current increases linearly without losses, the change in the inductor current during this period is defined as

$$\Delta I_{ON} = \frac{dV_{sc}}{L} \quad (C-9)$$

When IGBT2\_bb is off (b), the voltage across the inductor ( $V_L$ ) is given as

$$\begin{aligned} V_L &= V_{dclink} - V_{sc} \\ &= \frac{L\Delta I_{OFF}}{\Delta t_{OFF}} \end{aligned} \quad (C-10)$$

The period  $\Delta t_{OFF}$  is the off-period and equals to '1-d'. The change in the current during the off-period ( $\Delta I_{OFF}$ ) is

$$\Delta I_{OFF} = \frac{1-d}{L} (V_{dclink} - V_{sc}) \quad (C-11)$$

The change in the inductor current is given as

$$\begin{aligned} \Delta I &= \Delta I_{ON} - \Delta I_{OFF} \\ &= \frac{dV_{sc}}{L} - \frac{1-d}{L} (V_{dclink} - V_{sc}) \end{aligned} \quad (C-12)$$

From Equation (C-12), the change in the current over one sampling period is given as

## Appendix C

$$\Delta I = \frac{1}{L} d - 1 V_{dclink} + V_{sc} \quad (\text{C-13})$$

And the boost mode duty cycle is obtained as

$$d_{boost} = \frac{L\Delta I - V_{sc}}{V_{dclink}} + 1 \quad (\text{C-14})$$

## **Appendix D**

### **Graphic description of the experimental setup**

---

This appendix shows a graphic description of the equipment that was developed to validate the frequency control algorithms proposed in this work. The STATCOM and SCESS used for this research was constructed by Phinit Srithorn Ph.D. for the project titled “Control of a STATCOM with Supercapacitor energy storage”.

As mentioned in chapter 6, the experimental rig can be divided into two main parts which are the combined STATCOM and Supercapacitor energy storage system (SCESS) and the emulated diesel generating set. The combined STATCOM and SCESS consist of a three phase voltage source inverter, an electrolytic DC-link capacitor, a bi-directional DC-DC converter and a

## Appendix D

supercapacitor unit. The emulated diesel generating set consist of an induction motor drive (IM drive) and an induction motor coupled to a synchronous generator (IM+ SG).

The emulated diesel generating set consist of an induction motor coupled to a synchronous generator and a commercial drive. The generator is a 10kVA, 8kW Leroy somers LS 40 VS1 synchronous generator equipped with an automatic voltage regulator (AVR). The diesel engine is emulated with a Magnetics MA 133K F1 16kW two pole pairs induction motor and a dedicated drive. The AC-DC inverter and the DC-DC converter in this project are designed for utilising and storing energy in the supercapacitor units. The bi-directional DC-DC converter was placed between the supercapacitor unit and the STATCOM to facilitate the exchange of power between the grid and the energy storage system

Both the combined STATCOM and SCESS and the emulated diesel generating set are controlled from a dSPACE control platform.

The overall structure of the experimental test rig is shown in Figure D-1.

# Appendix D

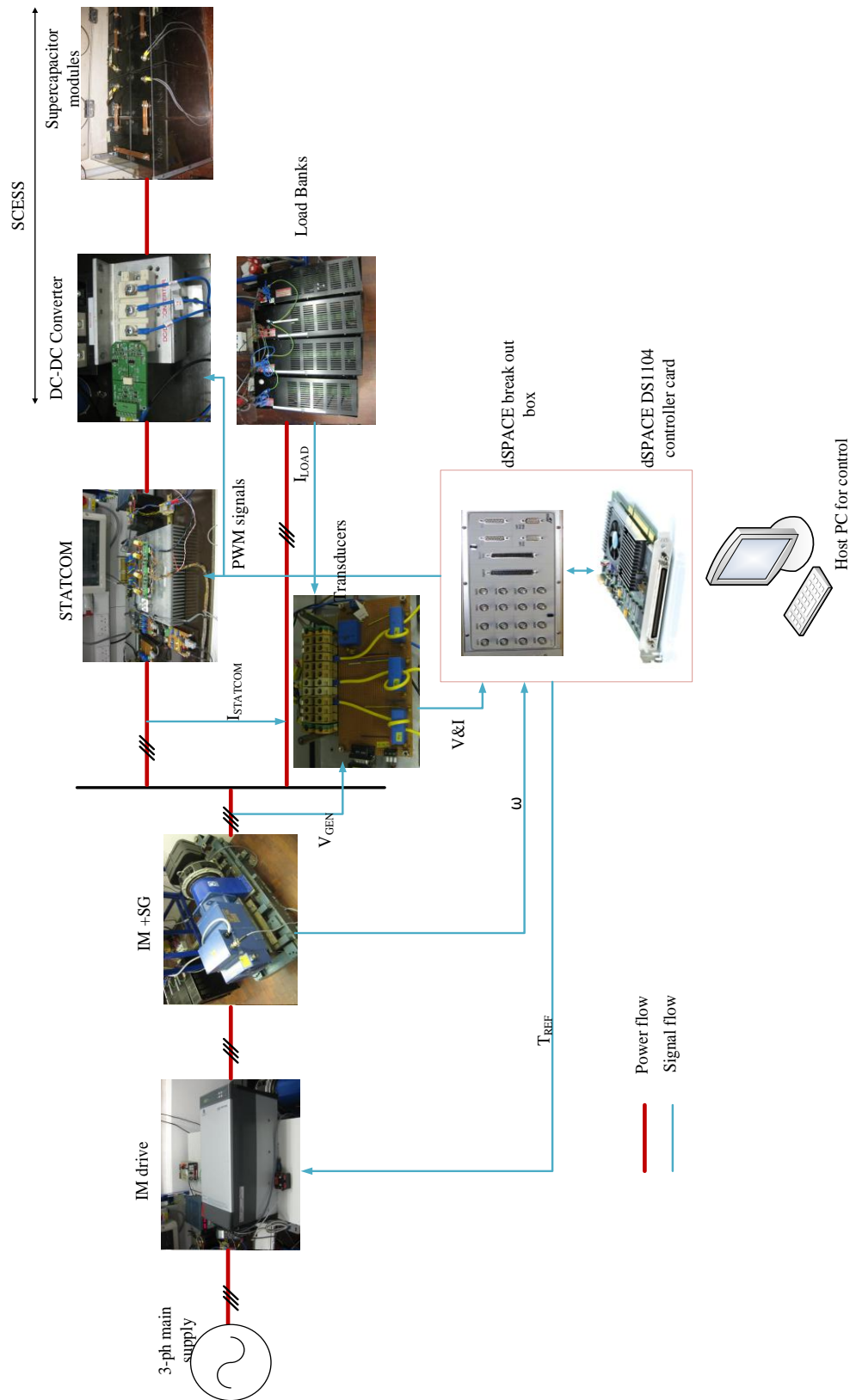


Figure D-1: Overall experimental rig structure

## Appendix D

Detailed descriptions of the sub-systems of the overall experimental rig are shown in Figures D-2- D-7.

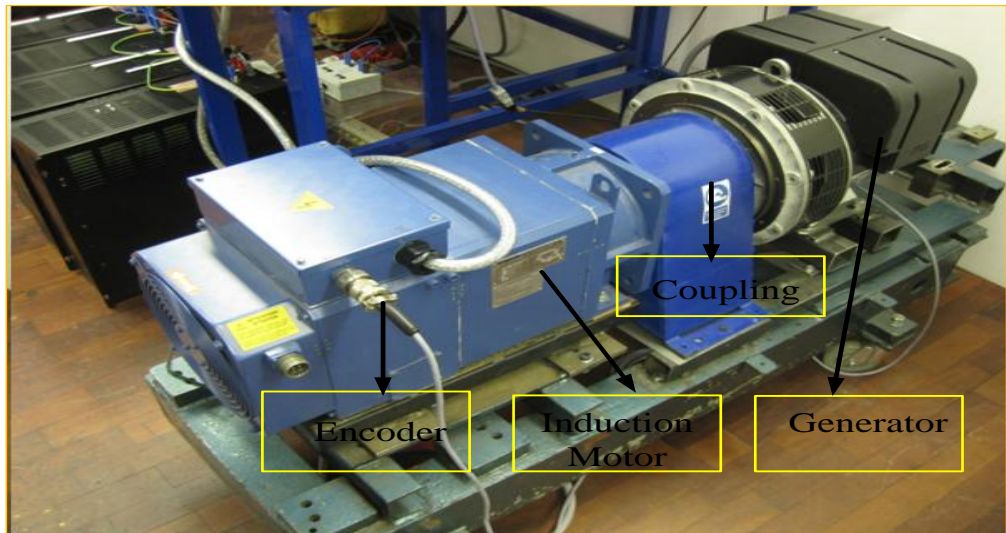


Figure D-2: Induction motor coupled to Synchronous generator

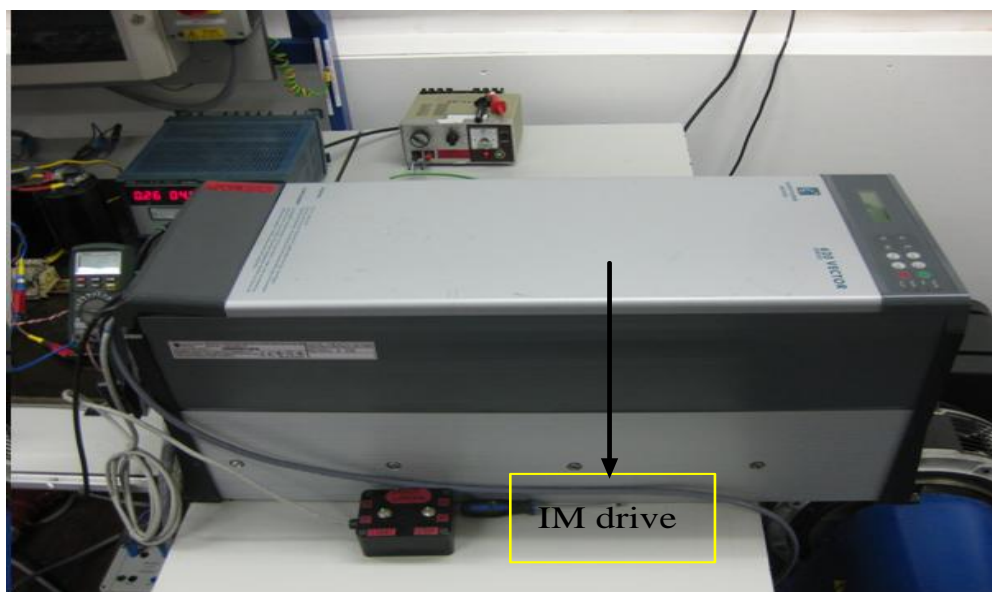


Figure D-3: Eurotherm 620 series drive used for the vector control operation of the induction motor

Appendix D

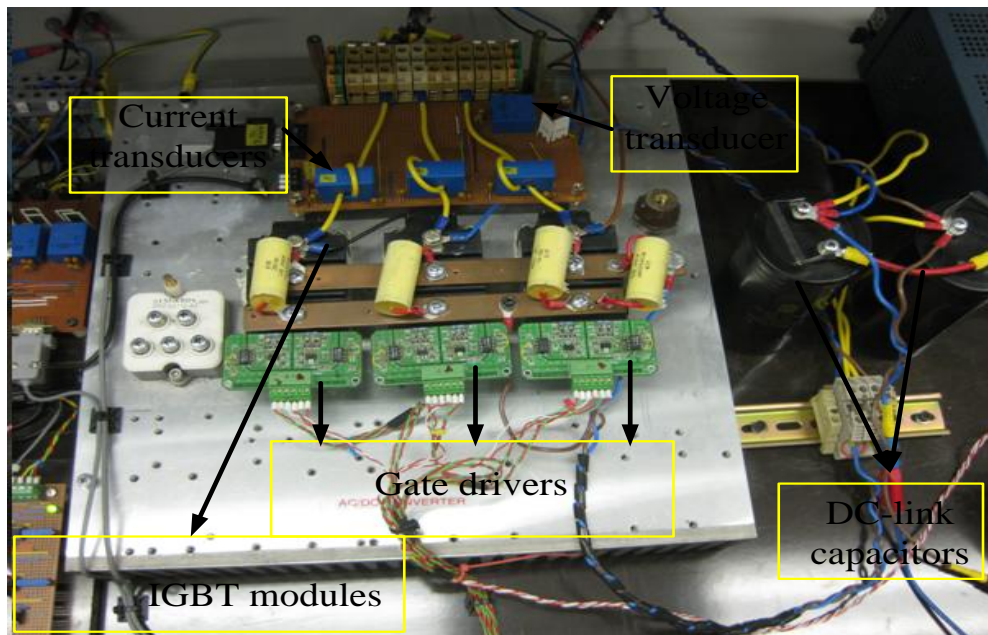


Figure D-4: DC/AC Inverter

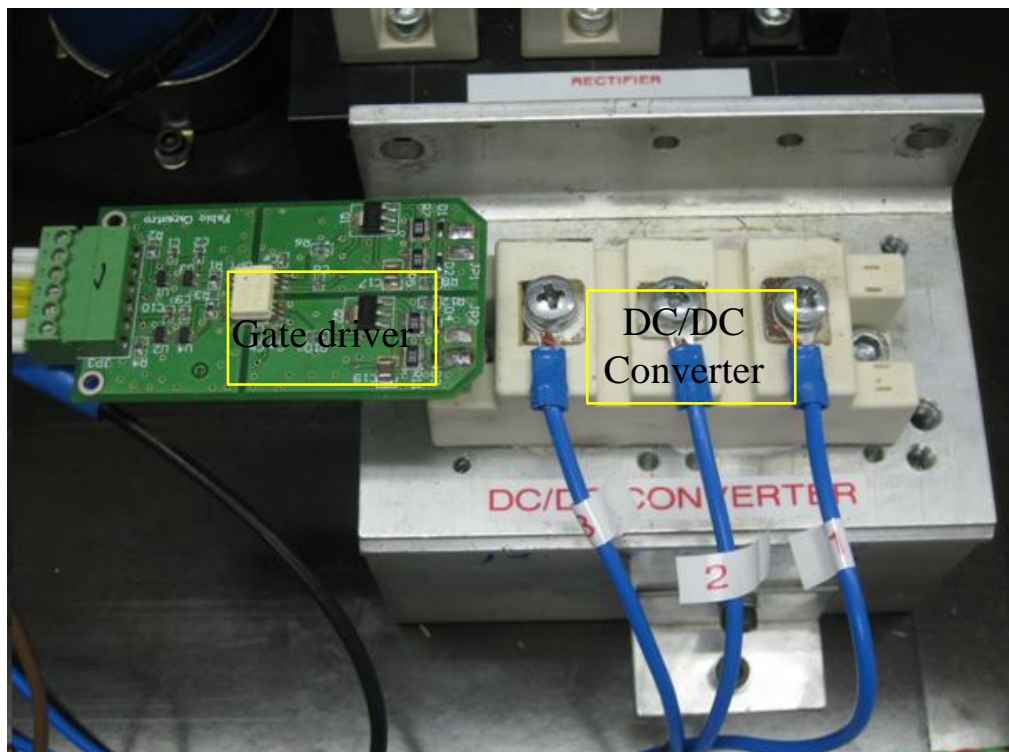


Figure D-5: DC/DC converter used as an interface between the DC-link and the Supercapacitor modules

Appendix D

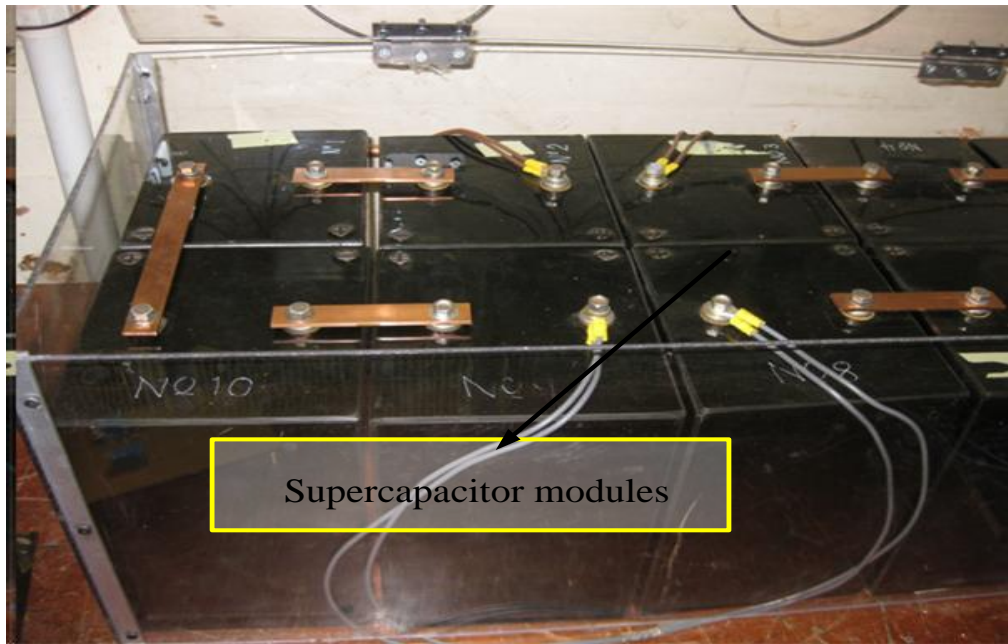


Figure D-6: Ten series connected Supercapacitor modules rated at 9.5 F, 20V

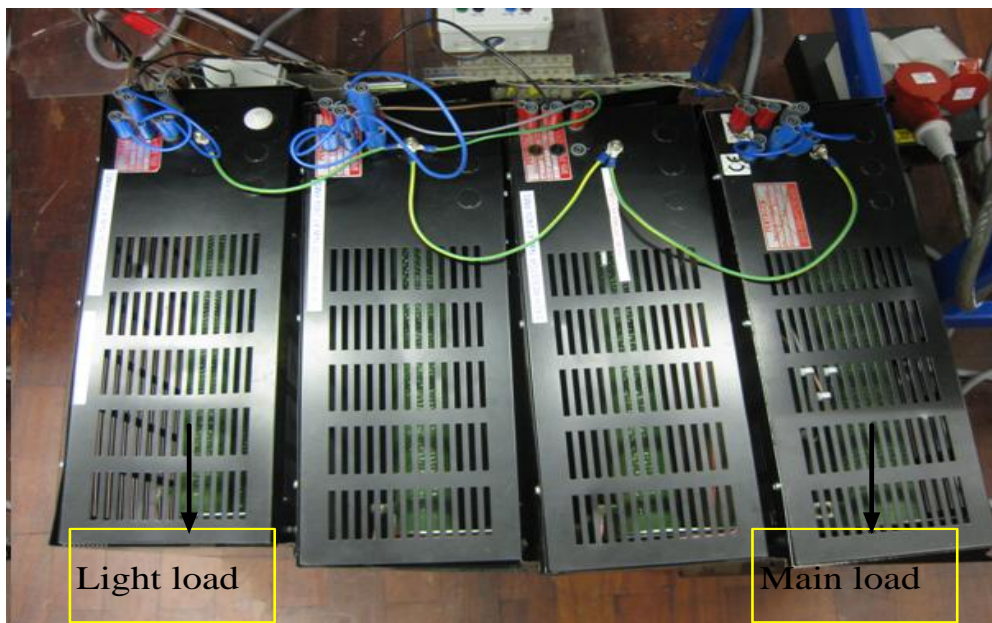


Figure D-7: Load Banks

## References

- [1] H. Farhangi, "The path of the smart grid," *Power and Energy Magazine, IEEE*, vol. 8, pp. 18-28, 2010.
- [2] R. H. Lasseter, "Smart Distribution: Coupled Microgrids," *Proceedings of the IEEE*, vol. 99, pp. 1074-1082, 2011.
- [3] H. B. Puttgen, P. R. MacGregor, and F. C. Lambert, "Distributed generation: Semantic Hype or the dawn of a new era," *IEEE Power and Energy Magazine*, vol. 1, pp. 22-29, Jan-Feb 2003.
- [4] The United Nation Framework Convention on Climate Change, November, 2005.
- [5] The EU'S Target for Renewable Energy: 20% by 2020, October, 2008.
- [6] Carbon Footprint of Electricity Generation, June, 2011.
- [7] Electricity in the U.K , Feb 2007.
- [8] R. H. Lasseter and P. Paigi, "Microgrid: a conceptual solution," in *Power Electronics Specialists Conference, 2004. PESC 04. 2004 IEEE 35th Annual, 2004*, pp. 4285-4290 Vol.6.
- [9] P. A. Daly and J. Morison, "Understanding the potential benefits of distributed generation on power delivery systems," in *IEEE Rural Electric Power Conference, 2001*, pp. A2/1-2/13.

## References

- [10] P. P. Barker and R. W. D. Mello, "Determining the impact of distributed generation on power systems. I. Radial distribution systems," in IEEE Power Engineering Society Summer Meeting, 2000, pp. 1645-1656.
- [11] P. M. Sotkiewicz and J. M. Vignolo, "Nodal pricing for distribution networks: efficient pricing for efficiency enhancing DG," IEEE Transactions on Power Systems, vol. 21, pp. 1013-1014, May 2006.
- [12] W. Y. Zhang, S. Z. Zhu, J. H. Zheng, and H. Zhang, "Impacts of Distributed Generation on Electric Grid and Selecting of Isolation Transformer," in IEEE Transmission and Distribution Conference and Exhibition: Asia and Pacific, 2005, pp. 1-7.
- [13] N. Jenkins, R. Allan, P. Crossley, D. Kirschen, and G. Strbac, Embedded generation: IEE, London, UK, 2000.
- [14] M. F. AlHajri and M.E.El-Hawary, "Improving the voltage profiles of distribution networks using multiple distribution generation sources," in IEEE Power Engineering - Large Engineering Systems Conference, 2007, pp. 295-299.
- [15] R. C. Dugan, M. F. McGranaghan, and H. W. Beaty, Electrical power systems quality. New York ; London: McGraw-Hill, 1996.
- [16] P. L. Villeneuve, "Concerns generated by islanding [electric power generation]," IEEE Power and Energy Magazine, vol. 2, pp. 49-53, May-Jun 2004.
- [17] J. Sung-II and K. Kwang-Ho, "An islanding detection method for distributed generations using voltage unbalance and total harmonic distortion of current," IEEE Transactions on Power Delivery, vol. 19, pp. 745 - 752, Apr 2004.

## References

- [18] H. H. Zeineldin and J. L. Kirtley, "A Simple Technique for Islanding Detection With Negligible Nondetection Zone," *IEEE Transactions on Power Delivery*, vol. 24, pp. 779 - 786, Apr 2009.
- [19] L. K. Kumpulainen and K. T. Kauhaniemi, "Analysis of the impact of distributed generation on automatic reclosing," in *IEEE Power System conference and Exposition*, 2004, pp. 603-608.
- [20] X. Ding and P. A. Crossley, "Islanding detection for distributed generation," in *IEEE Russia Power Tech Conference*, 2005, pp. 1-4.
- [21] M. Guillot, C. Collombet, P. Bertrand, and B. Gotzig, "Protection of embedded generation connected to a distribution network and loss of mains detection," in *IET CIRED 16th Electricity Distribution Conference*, 2001, p. 5.
- [22] M. Ezzi, M. I. Marei, M. A-Rahman, and M. M. Mansour, "A Hybrid strategy for distributed generators islanding detection," in *IEEE Power Engineering Society Conference and Exposition in Africa*, 2007, pp. 1-7.
- [23] J. M. Carrasco, E. Galvan, R. Portillo, L. G. Franquelo, and J. T. Bialasiewicz, "Power Electronic Systems for the Grid Integration of Wind Turbines," in *IEEE Industrial Electronics, IECON 2006 - 32nd Annual Conference on*, 2006, pp. 4182-4188.
- [24] P. Srithorn, M. Sumner, Y. Liangzhong, and R. Parashar, "The control of a STATCOM with supercapacitor energy storage for improved power quality," in *SmartGrids for Distribution*, 2008. IET-CIRED. CIRED Seminar, 2008, pp. 1-4.
- [25] P. Srithorn, M. Sumner, Y. Liangzhong, and R. Parashar, "Power System Stabilisation Using STATCOM with Supercapacitors," in

## References

- Industry Applications Society Annual Meeting, 2008. IAS '08. IEEE, 2008, pp. 1-8.
- [26] F. Iov, J. Clare, P. Wheeler, A. Rufer, and A. Hyde, "UNIFLEX-PM- A Key Enabling Technology for Future European Electricity Networks," *EPE Journal* vol. 19, December 2009 2009.
- [27] X. Zhaoxia, G. Manimaran, V. Vittal, A. G. Phadke, and V. Centeno, "An information architecture for future power systems and its reliability analysis," *Power Systems, IEEE Transactions on*, vol. 17, pp. 857-863, 2002.
- [28] S. Qiang, W. Jianzhong, Z. Yibin, N. Jenkins, and J. Ekanayake, "Comparison of the development of Smart Grids in China and the United Kingdom," in *Innovative Smart Grid Technologies Conference Europe (ISGT Europe)*, 2010 IEEE PES, 2010, pp. 1-6.
- [29] V. Loia and A. Vaccaro, "A decentralized architecture for voltage regulation in Smart Grids," in *Industrial Electronics (ISIE)*, 2011 IEEE International Symposium on, 2011, pp. 1679-1684.
- [30] B. Panajotovic, M. Jankovic, and B. Odadzic, "ICT and smart grid," in *Telecommunication in Modern Satellite Cable and Broadcasting Services (TELSIKS)*, 2011 10th International Conference on, 2011, pp. 118-121.
- [31] F. Iov, M. Ciobotaru, Y. Fan, S. Bifaretti, and P. Zanchetta, "Advanced Power Converters for Universal and Flexible Power Management in Future Electricity Network," *Aalborg University, Denmark and University of Nottingham, U.K* 2008.
- [32] R. H. Lasseter, "MicroGrids," in *Power Engineering Society Winter Meeting*, 2002. IEEE, 2002, pp. 305-308 vol.1.

## References

- [33] J. A. Pecas Lopes, C. L. Moreira, and A. G. Madureira, "Defining control strategies for analysing microgrids islanded operation," in *Power Tech, 2005 IEEE Russia*, 2005, pp. 1-7.
- [34] T. Tran-Quoc, N. Hadjsaid, G. Rami, L. Le-Thanh, L. Bernard, G. Verneau, J. L. Mertz, C. Corenwinder, P. Michalak, and M. Boll, "Dynamic analysis of an insulated distribution network," in *Power Systems Conference and Exposition, 2004. IEEE PES, 2004*, pp. 815-821 vol.2.
- [35] R. Caldon, F. Rossetto, and R. Turri, "Temporary islanded operation of dispersed generation on distribution networks," in *Universities Power Engineering Conference, 2004. UPEC 2004. 39th International, 2004*, pp. 987-991 vol. 2.
- [36] T. M. Masaud, L. Keun, and P. K. Sen, "An overview of energy storage technologies in electric power systems: What is the future?," in *North American Power Symposium (NAPS), 2010, 2010*, pp. 1-6.
- [37] P. F. Ribeiro, B. K. Johnson, M. L. Crow, A. Arsoy, and Y. Liu, "Energy storage systems for advanced power applications," *Proceedings of the IEEE*, vol. 89, pp. 1744-1756, 2001.
- [38] V. Babuska, S. M. Beatty, B. J. deBlonk, and J. L. Fausz, "A review of technology developments in flywheel attitude control and energy transmission systems," in *IEEE Aerospace conference proceedings, 2004*, pp. 2784-2800.
- [39] M. M. Flynn, P. McMullen, and O. Solis, "Saving energy using flywheels," *IEEE Industry Applications Magazine*, vol. 14, pp. 69-76, Nov-Dec 2008.

## References

- [40] R. Hebner, J. Beno, and A. Walls, "Flywheel batteries come around again," *IEEE spectrum*, vol. 39, pp. 46-51, Apr 2002.
- [41] T. Sels, C. Dragu, T. V. Craenenbroeck, and R. Belmans, "New energy storage devices for an improved load managing on distribution level," in *IEEE Power Tech Proceedings*, 2001, p. 6.
- [42] B. Yang, Y. Makarov, J. Desteese, V. Viswanathan, P. Nyeng, B. McManus, and J. Pease, "On the use of energy storage technologies for regulation services in electric power systems with significant penetration of wind energy," in *European Electricity Market - EEM 2008 Conference*, 2008, pp. 1-6.
- [43] H. Oman, "Batteries vs. alternatives for storing energy," *IEEE Aerospace and Electronic Systems Magazine*, vol. 11, pp. 37, 39, 41, 43, Aug 1996.
- [44] S. M. Schoenung and C. Burns, "Utility energy storage applications Studies," *IEEE Transactions on Energy Conversion*, vol. 11, pp. 658-665, Sep 1996.
- [45] S. Banerjee, S. Murad, and I. K. Puri, "Hydrogen Storage in Carbon Nanostructures: Possibilities and Challenges for Fundamental Molecular Simulations," *Proceedings of the IEEE*, vol. 94, pp. 1806-1814, 2006.
- [46] T. Gilchrist, "Fuel cells to the fore," *IEEE spectrum*, vol. 35, pp. 35-40, Nov 1998.
- [47] M. Kamibayashi and K. Tanaka, "Recent sodium sulfur battery applications," in *IEEE/PES Transmission and Distribution Conference and Exposition*, 2001, pp. 1169 - 1173.

## References

- [48] A. Schneuwly, "Charge ahead [ultracapacitor technology and applications]," *IET Power Engineering Journal*, vol. 19, pp. 34-37, Feb-Mar 2005.
- [49] V. V. N. Obreja, I. Iordache, D. Petroi, C. Ionescu, V. Golumbanu, and P. Svasta, "On the technology of the present-day of manufactured supercapacitors," in *IEEE Electronics Systemintegration Technology Conference*, 2006, pp. 307-312.
- [50] R. Lasseter and M. Erickson, "Integration of Battery-Based Energy Storage Element in the CERTS Microgrid," ed, 2009.
- [51] D. Rastler. (2008) New demand for energy storage. *Electric Perspectives*. pp 30-47.
- [52] H. K. Tyll, "FACTS technology for reactive power compensation and system control," in *Transmission and Distribution Conference and Exposition: Latin America*, 2004 IEEE/PES, 2004, pp. 976-980.
- [53] X. P. Zhang, L. Yao, B. Chong, C. Sasse, and K. R. Godfrey, "FACTS and HVDC technologies for the development of future power systems," in *Future Power Systems, 2005 International Conference on*, 2005, pp. 6 pp.-6.
- [54] X.-P. Zhang, B. Pal, and C. Rehtanz, *Flexible AC transmission systems: modelling and control*. Berlin: Springer, 2006.
- [55] C. C. Davidson and G. de Preville, "The future of high power electronics in Transmission and Distribution power systems," in *Power Electronics and Applications, 2009. EPE '09. 13th European Conference on*, 2009, pp. 1-14.

## References

- [56] N. G. Hingorani, "FACTS Technology - State of the Art, Current Challenges and the Future Prospects," in Power Engineering Society General Meeting, 2007. IEEE, 2007, pp. 1-4.
- [57] C. Oates and R. Bassett, "Future T&#x00026;D Technology," in Power Electronics and Motion Control Conference, 2006. EPE-PEMC 2006. 12th International, 2006, pp. 2144-2148.
- [58] J. Dorn, D. Ettrich, J. Lang, and D. Retzmann, "Benefits of Multilevel VSC Technologies for Power Transmission and System Enhancement," presented at the Electrical Networks of Russia, All - Russian Exhibition Centre (AREC), Moscow, 2007.
- [59] N. Flourentzou, V. G. Agelidis, and G. D. Demetriades, "VSC-Based HVDC Power Transmission Systems: An Overview," Power Electronics, IEEE Transactions on, vol. 24, pp. 592-602, 2009.
- [60] A. Lesnicar and R. Marquardt, "An innovative modular multilevel converter topology suitable for a wide power range," in Power Tech Conference Proceedings, 2003 IEEE Bologna, 2003, p. 6 pp. Vol.3.
- [61] L. Gyugyi, "Power electronics in electric utilities: static VAR compensators," IEEE Proceedings, vol. 76, pp. 483 - 494, Apr 1988.
- [62] H. L. Thanawala, D. J. Young, and M. H. Baker, Chapter 4 of Understanding FACTS : concepts and technology of flexible AC transmission systems. New York: IEEE Press, 2000.
- [63] N. Jenkins, Chapter 14 of Understanding FACTS : concepts and technology of flexible AC transmission systems. New York: IEEE Press, 2000.

## References

- [64] E. Acha, V. G. Agelidis, O. Anaya-Lara, and T. J. E. Miller, *Power Electronic Control in Electrical Systems*, 1st ed.: Newnes, 2002.
- [65] A. Ghosh and G. Ledwich, *Power quality enhancement using custom power devices*. Boston ; London, : Kluwer Academic, 2002.
- [66] E. V. Larsen, N. W. Miller, S. L. Nilsson, and S. R. Lindgren, "Benefits of GTO-based compensation systems for electric utility applications," *IEEE Transactions on Power Delivery* vol. 7, pp. 2056 - 2064, Oct 1992.
- [67] L. Gerin-Lajoie, G. Scott, S. Breault, E. V. Larsen, D. H. Baker, and A. F. Imece, "Hydro-Quebec multiple SVC application control stability study," *IEEE Transactions on Energy Conversion*, vol. 5, pp. 1543-1551, Jul 1990.
- [68] A. Yazdani and R. Iravani, *Voltage-Sourced Converters in Power Systems:Modelling ,Control and Applications*: John Wiley & Sons, Inc., 2010.
- [69] M. M. C. Merlin, T. C. Green, P. D. Mitcheson, D. R. Trainer, D. R. Critchley, and R. W. Crookes, "A new hybrid multi-level Voltage-Source Converter with DC fault blocking capability," in *AC and DC Power Transmission*, 2010. ACDC. 9th IET International Conference on, 2010, pp. 1-5.
- [70] R. Feldman, M. Tomasini, J. C. Clare, P. Wheeler, D. R. Trainer, and R. S. Whitehouse, "A hybrid voltage source converter arrangement for HVDC power transmission and reactive power compensation," in *Power Electronics, Machines and Drives (PEMD 2010)*, 5th IET International Conference on, 2010, pp. 1-6.

## References

- [71] J. Shen and N. Butterworth, "Analysis and design of a three-level PWM converter system for railway-traction applications," IEE Proceedings – Electric Power Applications, vol. 144, pp. 357-371, Sep 1997.
- [72] A. Nabae, I. Takahashi, and H. Akagi, "A new Neutral-Point-Clamped PWM Inverter," IEEE Transactions on Industry Applications, vol. 1A-17, pp. 518-523, Sep-Oct 1981.
- [73] C. Hochgraf, R. Lasseter, D. Divan, and T. A. Lipo, "Comparison of multilevel inverters for Static Var Compensation," in IEEE Industry Applications Society Annual Meeting, 1994, pp. 921-928.
- [74] F. Z. Peng, J. S. Lai, J. W. McKeever, and J. VanCoevering, "A multilevel voltage-source inverter with separate DC sources for static Var generation," IEEE Transactions on Industry Applications, vol. 32, pp. 1130-1138, Sep-Oct 1996.
- [75] J. S. Lai and F. Z. Peng, "Multilevel Converters – A new breed of power converters," IEEE Transactions on Industry Applications, vol. 32, pp. 509-517, May-Jun 1996.
- [76] P. Fang Zheng and L. Jih-Sheng, "Dynamic performance and control of a static VAR generator using cascade multilevel inverters," in Industry Applications Conference, 1996. Thirty-First IAS Annual Meeting, IAS '96., Conference Record of the 1996 IEEE, 1996, pp. 1009-1015 vol.2.
- [77] Y. S. Lai and F. S. Shyu, "New topology for hybrid multilevel inverter," in Power Electronics, Machines and Drives, 2002. International Conference on (Conf. Publ. No. 487), 2002, pp. 211-216.

## References

- [78] R. Teodorescu, M. Liserre, and P. Rodríguez *Grid Converters for Photovoltaic and Wind Power Systems* Wiley-IEEE Press, 2011.
- [79] C. Schauder and H. Mehta, "Vector analysis and control of advanced static VAR compensators," *IEE Proceedings – Generation, Transmission and Distribution*, vol. 140, pp. 299-306, Jul 1993.
- [80] A. B. Arsoy, Y. Liu, P. F. Ribeiro, and F. Wang, "StatCom-SMES," *IEEE Industry Applications Magazine*, vol. 9, pp. 21-28, Mar-Apr 2003.
- [81] M. A. Rahman, T. S. Radwan, A. M. Osheiba, and A. E. Lashine, "Analysis of current controllers for voltage-source inverter," *IEEE Transactions on Industrial Electronics*, vol. 44, pp. 477-485, Aug 1997.
- [82] C. Wei-Neng and Y. Kuan-Dih, "Design of D-STATCOM for fast load compensation of unbalanced distribution systems," *IEEE Power Electronics and Drive Systems Conference*, vol. 2, pp. 801-806, Oct 2001.
- [83] H. Chong, A. Q. Huang, M. E. Baren, S. Bhattacharya, W. Litzemberger, L. Anderson, A. L. Johnson, and A. A. Edris, "STATCOM Impact Study on the Integration of a Large Wind Farm into a Weak Loop Power System," *IEEE Transactions on Energy Conversion*, vol. 23, pp. 226-233, Mar 2008.
- [84] A. Jain, K. Joshi, A. Behal, and N. Mohan, "Voltage regulation with STATCOMs: modeling, control and results," *IEEE Transactions on Power Delivery*, vol. 21, pp. 726-735, Apr 2006.
- [85] H. Gaztanaga, I. Etxeberria-Otadui, D. Ocnasu, and S. Bacha, "Real-Time Analysis of the Transient Response Improvement of Fixed-Speed

## References

- Wind Farms by Using a Reduced-Scale STATCOM Prototype," *IEEE Transactions on Power Systems*, vol. 22, pp. 658-666, May 2007.
- [86] A. Arulampalam, J. B. Ekanayake, and N. Jenkins, "Application study of a STATCOM with energy storage," *IEE Proceedings -Generation, Transmission and Distribution*, vol. 150, pp. 373-384, May 2003.
- [87] A. Arulampalam, M. Barnes, N. Jenkins, and J. B. Ekanayake, "Power quality and stability improvement of a wind farm using STATCOM supported with hybrid battery energy storage," *IEE Proceedings - Generation, Transmission and Distribution*, vol. 153, pp. 701-710, Nov 2006.
- [88] Z. Yang, C. Shen, L. Zhang, M. L. Crow, and S. Atcitty, "Integration of a StatCom and battery energy storage," *IEEE Transactions on Power Systems*, vol. 16, pp. 254-260, May 2001.
- [89] Y. Cheng, C. Qian, M. L. Crow, S. Pekarek, and S. Atcitty, "A Comparison of Diode-Clamped and Cascaded Multilevel Converters for a STATCOM With Energy Storage," *IEEE Transactions on Industrial Electronics*, vol. 53, pp. 1512-1521, Oct 2006.
- [90] Y. Q. Zhan, S. S. Choi, and D. M. Vilathgamuwa, "A voltage-sag compensation scheme based on the concept of power quality control center," *IEEE Transactions on Power Delivery*, vol. 21, pp. 296-304, Jan 2006.
- [91] M. Kazmierkowski, R. Krishnan, and F. Blaabjerg, *Control in power electronics*: Academic press, 2002.
- [92] A. V. Timbus, R. Teodorescu, F. Blaabjerg, M. Liserre, and P. Rodriguez, "Linear and Nonlinear Control of Distributed Power Generation Systems," in *Industry Applications Conference, 2006. 41st*

## References

- IAS Annual Meeting. Conference Record of the 2006 IEEE, 2006, pp. 1015-1023.
- [93] F. Blaabjerg, R. Teodorescu, M. Liserre, and A. V. Timbus, "Overview of Control and Grid Synchronization for Distributed Power Generation Systems," *Industrial Electronics, IEEE Transactions on*, vol. 53, pp. 1398-1409, 2006.
- [94] T. Kawabata, T. Miyashita, and Y. Yamamoto, "Dead beat control of three phase PWM inverter," *Power Electronics, IEEE Transactions on*, vol. 5, pp. 21-28, 1990.
- [95] D. G. Holmes and D. A. Martin, "Implementation of a direct digital predictive current controller for single and three phase voltage source inverters," in *Industry Applications Conference, 1996. Thirty-First IAS Annual Meeting, IAS '96.*, Conference Record of the 1996 IEEE, 1996, pp. 906-913 vol.2.
- [96] Y. A. R. I. Mohamed and E. F. El-Saadany, "An Improved Deadbeat Current Control Scheme With a Novel Adaptive Self-Tuning Load Model for a Three-Phase PWM Voltage-Source Inverter," *Industrial Electronics, IEEE Transactions on*, vol. 54, pp. 747-759, 2007.
- [97] J. C. Moreno, J. M. E. Huerta, R. G. Gil, and S. A. Gonzalez, "A Robust Predictive Current Control for Three-Phase Grid-Connected Inverters," *Industrial Electronics, IEEE Transactions on*, vol. 56, pp. 1993-2004, 2009.
- [98] Z. Qingrong and C. Liuchen, "Study of advanced current control strategies for three-phase grid-connected pwm inverters for distributed generation," in *Control Applications, 2005. CCA 2005. Proceedings of 2005 IEEE Conference on*, 2005, pp. 1311-1316.

## References

- [99] A. Timbus, M. Liserre, R. Teodorescu, P. Rodriguez, and F. Blaabjerg, "Evaluation of Current Controllers for Distributed Power Generation Systems," *Power Electronics, IEEE Transactions on*, vol. 24, pp. 654-664, 2009.
- [100] E. Aldabas, L. Romeral, A. Arias, and M. G. Jayne, "Software-based digital hysteresis-band current controller," *Electric Power Applications, IEE Proceedings -*, vol. 153, pp. 184-190, 2006.
- [101] Krismadinata, N. A. Rahim, and J. Selvaraj, "Implementation of Hysteresis Current Control for Single-Phase Grid Connected Inverter," in *Power Electronics and Drive Systems, 2007. PEDS '07. 7th International Conference on*, 2007, pp. 1097-1101.
- [102] T. Kawagoshi, A. Kumamoto, T. Hikihara, Y. Hirane, K. Oku, O. Nakamura, S. Tada, K. Mizuki, and Y. Inoue, "Harmonic voltage suppression by active filter with neural network controller," in *Neural Networks to Power Systems, 1993. ANNPS '93., Proceedings of the Second International Forum on Applications of*, 1993, pp. 93-98.
- [103] S. K. Jain, P. Agrawal, and H. O. Gupta, "Fuzzy logic controlled shunt active power filter for power quality improvement," *Electric Power Applications, IEE Proceedings -*, vol. 149, pp. 317-328, 2002.
- [104] C. Chiarelli, L. Malesani, S. Pirondini, and P. Tomasin, "Single-phase, three-level, constant frequency current hysteresis control for UPS applications," in *Power Electronics and Applications, 1993., Fifth European Conference on*, 1993, pp. 180-185 vol.4.
- [105] Q. Yao and D. G. Holmes, "A simple, novel method for variable-hysteresis-band current control of a three phase inverter with constant switching frequency," in *Industry Applications Society Annual*

## References

- Meeting, 1993., Conference Record of the 1993 IEEE, 1993, pp. 1122-1129 vol.2.
- [106] L. Malesani, P. Mattavelli, and P. Tomasin, "High-performance hysteresis modulation technique for active filters," in Applied Power Electronics Conference and Exposition, 1996. APEC '96. Conference Proceedings 1996., Eleventh Annual, 1996, pp. 939-946 vol.2.
- [107] L. Sonaglioni, "Predictive digital hysteresis current control," in Industry Applications Conference, 1995. Thirtieth IAS Annual Meeting, IAS '95., Conference Record of the 1995 IEEE, 1995, pp. 1879-1886 vol.3.
- [108] D. J. Hanson, M. L. Woodhouse, C. Horwill, D. R. Monkhouse, and M. M. Osborne, "STATCOM: a new era of reactive compensation," *Power Engineering Journal*, vol. 16, pp. 151-160, 2002.
- [109] M. H. Haque and P. Kumkratug, "Application of Lyapunov stability criterion to determine the control strategy of a STATCOM," *Generation, Transmission and Distribution, IEE Proceedings-*, vol. 151, pp. 415-420, 2004.
- [110] B. Singh, S. S. Murthy, and S. Gupta, "Analysis and design of STATCOM-based voltage regulator for self-excited induction generators," *Energy Conversion, IEEE Transactions on*, vol. 19, pp. 783-790, 2004.
- [111] H. Chong, A. Huang, M. Baran, S. Bhattacharya, W. Litzemberger, L. Anderson, A. Johnson, and A. A. Edris, "STATCOM Impact Study on the Integration of a Large Wind Farm into a Weak Loop Power System," in *Power Engineering Society General Meeting, 2007. IEEE, 2007*, pp. 1-1.

## References

- [112] D. Butt, "An Investigation of harmonic correction techniques using active filtering," Ph.D thesis, University of Nottingham, August 1999.
- [113] G. W. Scott, V. F. Wilreker, and R. K. Shaltens, "Wind Turbine Generator Interaction With Diesel Generators on an Isolated Power System," *Power Engineering Review, IEEE*, vol. PER-4, pp. 28-29, 1984.
- [114] A. R. Cooper, D. J. Morrow, and K. D. R. Chambers, "A turbocharged diesel generator set model," in *Universities Power Engineering Conference (UPEC), 2009 Proceedings of the 44th International, 2009*, pp. 1-5.
- [115] A. Asmus and B. Wellington, *Diesel Engine and Fuel Systems*, 3rd ed., 1992.
- [116] J. B. Heywood, *Internal Combustion Engine Fundamentals: McGraw - Hill*, 1988.
- [117] Y. Hu, M. Cirstea, M. McCormick, and L. Haydock, "Modelling and simulation of a variable speed stand-alone generator system," in *Power Electronics and Variable Speed Drives, 2000. Eighth International Conference on (IEE Conf. Publ. No. 475), 2000*, pp. 372-377.
- [118] G. S. Stavrakakis and G. N. Kariniotakis, "A general simulation algorithm for the accurate assessment of isolated diesel-wind turbines systems interaction. I. A general multimachine power system model," *Energy Conversion, IEEE Transactions on*, vol. 10, pp. 577-583, 1995.
- [119] S. Roy, O. P. Malik, and G. S. Hope, "An adaptive control scheme for speed control of diesel driven power-plants," *Energy Conversion, IEEE Transactions on*, vol. 6, pp. 605-611, 1991.

## References

- [120] K. Bo, W. Youyi, and T. Yoke Lin, "An  $H_{\infty}$  controller design for diesel engine systems," in Power System Technology, 2000. Proceedings. PowerCon 2000. International Conference on, 2000, pp. 61-66 vol.1.
- [121] S. Roy, O. P. Malik, and G. S. Hope, "A least-squares based model-fitting identification technique for diesel prime-movers with unknown dead-time," Energy Conversion, IEEE Transactions on, vol. 6, pp. 251-256, 1991.
- [122] G.Asher, "Advanced AC Drives," ed. University of Nottingham, 2011.
- [123] A. M. Trzynadlowsky, Control of Induction Motors. London, United Kingdom: Academic Press, 2001.
- [124] M. Sumner and G. M. Asher, "Self-commissioning for voltage-referenced voltage fed vector controlled induction motor drives," in Power Electronics Specialists Conference, 1992. PESC '92 Record., 23rd Annual IEEE, 1992, pp. 139-144 vol.1.
- [125] L. Yen-Shin, "Machine modeling and universal controller for vector-controlled induction motor drives," Energy Conversion, IEEE Transactions on, vol. 18, pp. 23-32, 2003.
- [126] Y.H.Zweiri, J.F.Whidborne, L.D.Senevirante, and K. Althoefer. (2002). A Comparison of Dynamic Models of Various Complexity for Diesel Engines ;Mathematical and Computer Modelling of Dynamical Systems. 8.
- [127] S.C.Kong, Y.Ra, and R.D.Reitz, "Performance of multi-dimensional models for simulating diesel premixed charge compression ignition engine combustion using low and high pressure injectors," International journal for engine research, vol. 6, pp. 475-486, 2005.

## References

- [128] MATLAB7, "Simulink 6.0 / SimPowerSystems," ed: The MathWorks Inc., 1986-2004.
- [129] P. M. Anderson and A. A. Fouad, Power system control and stability, Second ed.: John Wiley & Sons, Inc., 2003.
- [130] P. Kundur, Power system stability and control: McGraw-Hill, Inc., 1994.
- [131] D. J. McGowan, D. J. Morrow, and M. McArdle, "A digital PID speed controller for a diesel generating set," in Power Engineering Society General Meeting, 2003, IEEE, 2003, p. 1477 Vol. 3.
- [132] W. Christiansen and D. Johnson, "Analysis of requirement in selected grid codes," 2006.
- [133] Magueed.F and Awad.H, "Voltage Compensation in Weak Grids Using Distributed Generation with Voltage Source Converter as a Front End," presented at the Power Electronics and Drives Systems, 2005.
- [134] "IEEE Application Guide for IEEE Std 1547, IEEE Standard for Interconnecting Distributed Resources with Electric Power Systems," IEEE Std 1547.2-2008, pp. 1-207, 2009.
- [135] P. Srithorn, "Control of a STATCOM with supercapacitor energy storage," Ph.D thesis, University of Nottingham, August 2009.
- [136] N. Mohan, T. M. Undeland, and W. P. Robbins, Power electronics : converters, applications, and design, 3rd ed. Hoboken, NJ: John Wiley & Sons, 2003.

## References

- [137] L. Wang and J.-Y. Liou, "Simulations of a Commercial Wind Power Generation System with Four Wind-Turbine Induction Generators," presented at the IEEE Power Engineering Society General Meeting 2007, 2007.
- [138] J. M. Guerrero, J. Matas, V. Luis Garcia de, M. Castilla, and J. Miret, "Decentralized Control for Parallel Operation of Distributed Generation Inverters Using Resistive Output Impedance," *Industrial Electronics, IEEE Transactions on*, vol. 54, pp. 994-1004, 2007.
- [139] A. S. Sedra and K. C. Smith, *Microelectronic Circuits*, 5 ed.: Oxford University Press, 2004.
- [140] dSPACE-GmbH, "Hardware Installation and Configuration for dSPACE R&D Digital Controller Board (User Manual)," ed: Germany, 2001-2011.
- [141] dSPACE-GmbH, "Installation Manual for ControlDesk Developer Version 3.7.2 Standard (User Manual)," ed. Germany, 2001-2011.
- [142] LEM, "Voltage Transducer LV 25-P ", ed: LEM Components Datasheet.
- [143] LEM, "Current Transducer LA 55-P ", ed: LEM Components Datasheet